Supramolecular Assembly and Nanoscale Morphologies for Organic Photovoltaic Devices

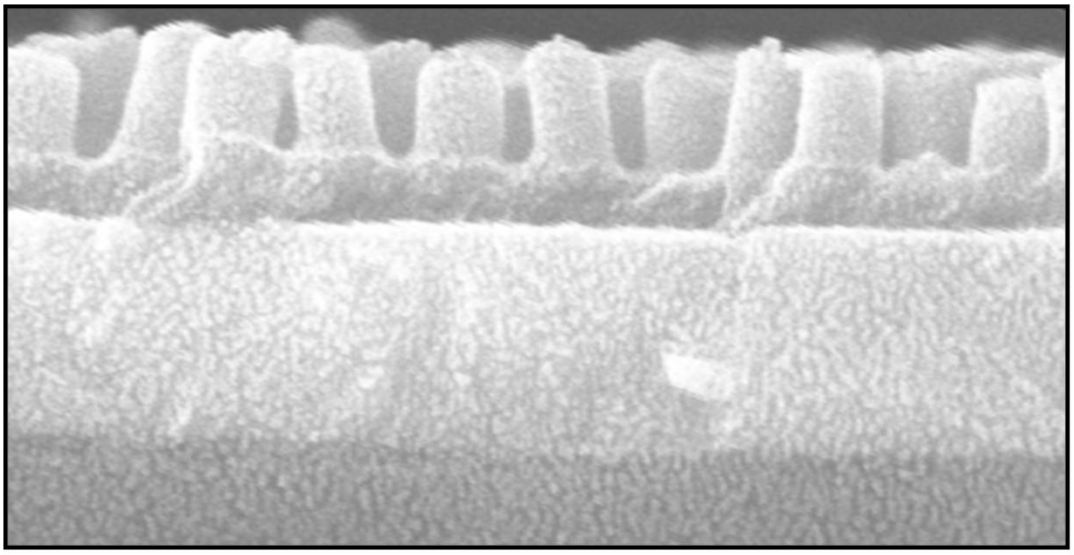

Dissertation

vorgelegt von

Holger C. Hesse

angefertigt in der Arbeitsgruppe
Hybrid Nanostructures
Prof. Dr. L. Schmidt-Mende

Fakultät für Physik
Ludwig-Maximilians-Universität München

January 25, 2012

Erstgutachter:	Prof. Dr. Lukas Schmidt-Mende
Zweitgutachter:	PD Dr. Bert Nickel
Prüfungsvorsitz:	Prof. Dr. Dieter Braun
Weiterer Prüfer:	Prof. Dr. Ulrich Gerland
Datum der mündlichen Prüfung:	5.12.2011

Contents

Abstract

Organic photovoltaics is a field of rapidly growing activity in both research and industry. Flexibility, light-weight, and low-cost render this technique an appealing alternative to silicon based devices for solar energy power conversion.
Recently, several donor-acceptor systems have been investigated as active materials for organic photovoltaic devices and it has been shown that the morphology of these heterojunction systems has a severe impact on the device performance.
This work focuses on the correlation of nanoscale morphologies of organic donor-acceptor systems with resulting spectroscopic and electronic properties of organic photovoltaic devices. Discotic molecules are used in the active layer of the devices exhibiting a number of properties highly desired for the application in organic photovoltaic devices: The planar core shape of this class of materials allows an assembly to 1-D molecular wires showing anisotropic and exceptionally high charge carrier mobility.It is the aim to establish supramolecular assemblies of the discotic molecules and to realize nanoscale interface morphologies between donor and acceptor compounds in order to optimize the photovoltaic performance of the resulting devices.
The impact of residue modifications attached to the disc shaped molecules on morphology, current generation and recombination is analyzed and design rules for these solution processable small molecule blend mixtures are derived. Vacuum sublimation is discussed as an alternative processing route facilitating the fabrication of devices with mixed but also bi-layered active material stacking.
Using a dye sensitization method the exciton harvesting and photovoltaic performance can be significantly increased in these thin film devices. A highly ordered nanoscale morphology at the donor-acceptor interface, demonstrated using a template assisted imprinting approach, offers high potential towards photovoltaic devices with interdigitated interfaces and superior power conversion efficiency.

Zusammenfassung

Die organische Photovoltaik ist ein extrem schnell wachsendes Gebiet, das von einem großen Interesse in Forschung und Industrie profitiert. Die mechanische Flexibilität, das geringere Gewicht und die potentiell niedrigeren Produktionskosten gegenüber herkömmlicher Silizium-basierter Photovoltaik lassen diese Technik als attraktive Alternative für Solar-Stromerzeugung erscheinen.
In letzter Zeit wurde eine Vielzahl von Donor-Akzeptor Systemen als aktive Schicht in organischen Solarzellen getestet und es konnte belegt werden, dass die Morphologie einen erheblichen Einfluss auf die resultierende Stromerzeugungs-Effizienz haben kann. Der Schwerpunkt dieser Arbeit liegt auf der Gegenüberstellung verschiedener Donor-Akzeptor Morphologien und den daraus resultierenden spektroskopischen und elektronischen Eigenschaften von organischen Solarzellen. Die hier verwendeten diskotischen Moleküle sind attraktive Kandidaten für die Anwendung in organischer Elektronik: Die planare Struktur dieser Klasse von Molekülen erlaubt eine Stapelung in eindimensionale molekulare Drähte mit anisotroper und ungewöhnlich hoher Ladungsträgermobilität. Ziel ist es eine supramolekulare Stapellung der diskotischen Moleküle zu erzielen und eine Strukturierung des Interfaces zwischen Donor und Akkzeptor Materialien zu erreichen um die Effizienz der resultierenden Solarzellen zu optimieren.
Der Einfluss verschiedener an die scheibenförmigen Moleküle angebundenen Seitenketten auf Morphologie, Stromerzeugung und Ladungsträger-Rekombination wurde analysiert und daraus ein Konzept für die Herstellung von löslichen Mischungen dieser kleinen Moleküle abgeleitet. Die Verdampfungs-Technik dient als alternative Variante um Bauelemente mit vermischter oder aber zweilagig getrennter aktiver Schicht zu realisieren. Eine Methodik zur Farbstoff-Sensibilisierung dieser dünnschichtigen organischen Solarzellen erlaubt es eine höhere Ausbeute an Exzitonen und dadurch eine deutliche Leistungssteigerung zu erzielen. Mittels "Schablonen-Druck" wurde eine Nanometer-Strukturierung der Donor-Akzeptor Grenzfläche realisiert, die ein großes Potential für eine Anwendung in Solarzellen mit verzahnter Interface Geometrie und stark erhöhter Leistungs-Wandlungseffizienz zeigt.

List of Abbreviations

η	Power conversion efficiency
Ag	Silver
Al	Aluminum
Al_2O_3	Aluminum oxide
Au	Gold
CBZ	Chlorobenzene
$CHCl_3$	Chloroform
EtOH	Ethanol
EQE	External quantum efficiency
FF	Fill factor
FRET	Fluorescence resonance energy transfer
H_2O	Water
H_3PO_4	Phosphoric acid
HBC	Hexa-*peri*-hexabenzocoronene
HOMO	Highest occupied molecular orbital
IPCE	Incident photon to current conversion efficiency
I_{SC}	Short circuit current density
L_D	Exciton diffusion length
LUMO	Lowest unoccupied molecular orbital
MDMO-PPV	(Poly-[2-(3,7-dimethyloctyloxy)-5-methyloxy]-para-phenylene-vinylene)
MPP	Maximum power point
N_2	Nitrogen
OFET	Organic field effect transistor
OPV	Organic photovoltaic device
O_2	Oxygen
PAH	Polycyclic aromatic hydrocarbon
POM	Polarized optical microscopy
P3HT	Poly-(3-hexylthiophene)
P4VP	Poly-(4-vinylphenol)
$PC_{61}BM$	[6,6]-Phenyl-C_{61}-butyric acid methyl ester
$PC_{71}BM$	[6,6]-Phenyl-C_{71}-butyric acid methyl ester
PCD	Photocurrent decay

PCPDTBT	Poly[2,1,3-benzothiadiazole-4,7-diyl[4,4-bis(2-ethylhexyl) -4H-cyclopenta[2,1-b:3,4-b']dithiophene-2,6-diyl]]
PDI	Perylene-diimide
PL	Photoluminescence
PVD	Photovoltage decay
RMS	root mean square
R_s	Series resistance
R_{sh}	Shunt resistance
TAS	Transient absorption spectroscopy
TiO_2	Titanium dioxide
V_{OC}	Open circuit voltage
WO_3	Tungsten oxide

1 Introduction

One of the major challenges of the 21st century is the development and use of sustainable power sources to supply the energy needs of a highly industrialized society. The extensive use of fossil resources such as coal, gas, oil and uranium for transportation as well as industrial and domestic power supply in the industrialized world has led to severe concerns about environmental and social consequences. Increasing carbon dioxide concentration in the atmosphere is said to be one of the the major reasons for the ongoing climate change [1, p.10f]. Furthermore, recent incidents in nuclear power plants have once more highlighted the unforeseeable risk of this fossil energy source [2]. Sustainable power generation is highly desired to feed the energy needs of a growing and strongly demanding world society. There is an ever increasing need for novel techniques that have the potential to supply mankind with abundant and carbon neutral power at low cost.

At present high investment prices still delimit the distributed application of renewable energy sources such as wind, solar and biomass for power generation. However, several long-term studies suggest that renewable sources are likely to provide a much greater proportion of the world energy supply in the second half of the twenty-first century due to both increasing cost of fossil fuels and reduced investment cost for sustainable energy sources [1, p. 14].

Organic photovoltaic devices do not only provide solar energy conversion at a potentially very low cost, but also provide other advantages such as mechanical flexibility and variability in color and design. This renders the technology especially interesting for novel fields of application such as off-grid power supply for small electronic devices, sophisticated architectural concepts and wearable electronic products.

1.1 Organic electronics

The field of *organic electronics* deals with the use of carbon-based chemical compounds as active materials in electronic circuits. Only recently the field emerged and has gained very high scientific as well as commercial interest. Alan J. Heeger, Alan G. MacDiarmid

and Hideki Shirakawa won the nobel prize in chemistry in the year 2000 for the synthesis and investigation of conducting polymers - a fact that emphasizes the scientific importance and the commercial relevance of this new type of materials [3]. Organic light emitting devices (OLEDs), organic field effect transistors (OFETs), printable organic circuits and organic photovoltaic devices (OPVs) are possible applications for conductive organic materials. First products reached the consumer market and an enormous growth potential is predicted for these emerging technologies in the near future [4].
However, still much progress has to be made to achieve improved electrical and photophysical properties when using organic materials. Researchers all over the world are currently working on the simulation and synthesis of new organic compounds. The molecular assembly and photophysical properties are studied for selected materials out of this vast pool of novel conducting materials. Charge transport capabilities and other suitable properties for the application in organic electronic devices have been found not only for polymers but a variety of highly π-conjugated materials including small molecules and oligomeric compounds all showing specific attractive properties for electronic applications.

1.2 Organic photovoltaics

The possibility to process organic materials at low temperatures and the potential to fabricate devices using roll-to-roll printing techniques has attracted a strong commercial interest in OPV devices. Furthermore, devices can be extremely thin, flexible, light-weight and manufactured in a variety of different colors making this technique an appealing alternative to conventional photovoltaics based on inorganic semiconductors like silicon.
To date the record efficiency of laboratory devices has reached over 8% [5, 6] and a variety of studies have highlighted the potential benefits of organic photovoltaics, e.g. semi-transparency [7], flexibility [8] and vacuum free processing [9]. A commercial breakthrough for this novel techniques with large scale and profitable production is predicted for devices with efficiencies above 15% [10]. Therefore, the main challenge in the field of OPV remains to further increase the power conversion efficiency. But also device stability and lifetime are extremely important for a widespread consumer usage. In order to achieving these goals it is indispensable to analyze the working principle of OPV devices including light absorption, charge carrier generation and extraction in detail.

1.3 Device working mechanism

In organic photovoltaics several requirements have to be addressed and challenges to be mastered. Photon absorption in the highly delocalized π-conjugated electron systems of organic semiconductors can lead to the formation of excitons. Unfortunately the binding energy of these excited states is commonly very strong in organic materials, mainly due to their low dielectric constants when compared to inorganic semiconductors. In order to efficiently separate the bound electron-hole pairs into free charges a *heterojunction* is necessary: the binding energy of the excited state is overcome by a potential drop at the interface between an organic donor and an organic acceptor material. Electrons and holes may be generated in the acceptor and donor materials, respectively. The schematic representation in Figure 1.1 summarizes the main processes of charge generation in an organic heterojunction solar cell.
An exact tuning of the energy levels of both organic compounds is necessary to minimize the potential drop at the interface and yield a maximum device voltage [11]. On the other hand photon absorption should be maximized to allow abundant exciton generation under solar illumination and a potential drop at the heterojunction is necessary to drive the separation of these excited states into free charges. Furthermore, the intrinsic conductivity of organic materials is typically low, commonly below 10^{-1} cm^2/Vs [12] delimiting the extraction of the charge carriers generated. Therefore, the photo-active materials of the devices are confined to a very thin layer sandwiched between the contact electrodes. It remains a challenge to further improve the charge carrier mobility in organic films allowing for solar light harvesting in devices with an increased thickness. The low charge carrier mobility is only in part balanced by organic materials which exhibit a very high absorbance, making comprehensive light harvesting feasible within the range of a few hundreds of nanometers.

1.4 Donor-acceptor morphology

In order to optimize the solar cell efficiency it is not only necessary to optimize the electrical properties of the pristine organic compounds but also to analyze their interplay in herterojunction devices. Exciton diffusion lengths are commonly very low in organic semicunductors, rarely exceeding 20 nm [13]. Excitons generated at a larger distance away from the organic heterojunction will recombine before reaching the interface and cannot contribute to charge generation. On the other hand, an organic layer thickness in the range of hundreds of nanometers is necessary for comprehensive light harvesting

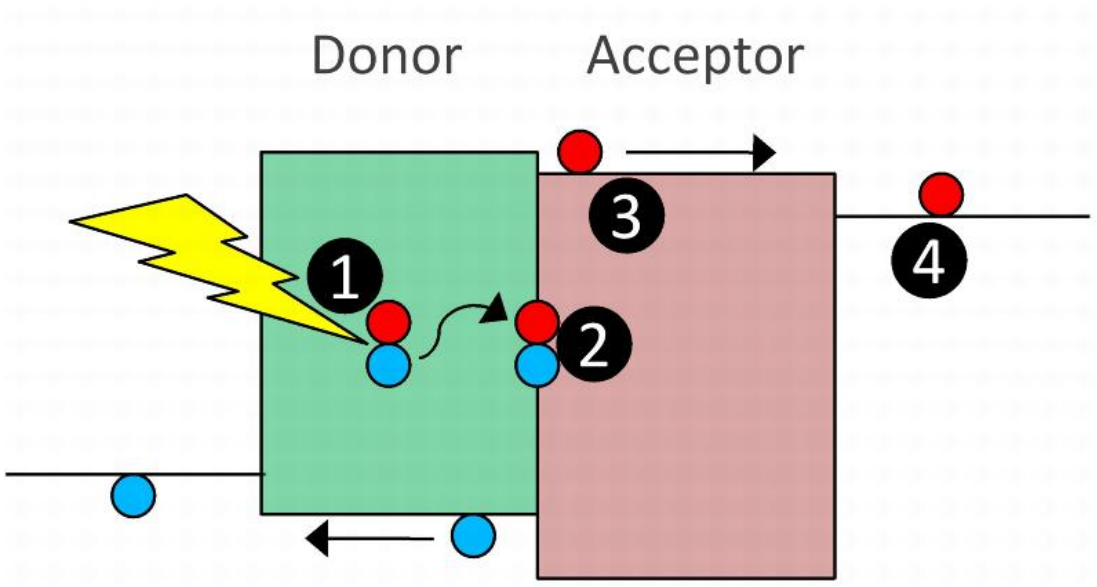

Figure 1.1: Schematic view of an organic photovoltaic device. Solar light absorption takes place in the donor or acceptor material generating excitons (1). After diffusion to the donor-acceptor interface (2) the excited states can be split to free charges (3) which may be extracted at the external contacts (4).

in strongly absorbing organic materials [14]. This "exciton diffusion bottleneck" [15] has motivated the use of intermixed donor-acceptor morphologies. The *bulk-heterojunction* concept allows exciton separation throughout the active layer of an OPV devcie [16]. The interfacial area of donor and acceptor is strongly increased when processing blends of active materials compared to a flat bi-layered junction. On the other hand, charge extraction may become more sophisticated in such mixed morphologies - cristallinity and charge carrier mobility might be limited, charges may become trapped and bi-molecular recombination is likely to be increased (as further described in Section 2.3).
Interpenetrating donor-acceptor networks with direct percolation pathways to the respective electrodes are necessary. Choosing specific organic materials, precisely defined processing conditions or more elaborate patterning and layer-by-layer production might offer a suitable approach to achieve this morphology. Establishing these ordered networks and optimizing their dimensions for optimum photon to electron conversion efficiency is of great interest for the entire OPV community.
In contrast to devices with a randomly intermixed donor-acceptor morphology this interdigitated interface geometry of the active materials ensures direct percolation path-

ways to the respective electrodes. Furthermore, favorable properties such as the high exciton diffusion lengths of pristine materials may remain accessible in the heterojunction structure. Studying the physics of exciton separation and charge generation at the interdigitated interface of the photovoltaic devices might pave the way to develop organic photovoltaic devices with a superior efficiency. It is the aim of this thesis to realize different nanoscale morphologies for donor-acceptor systems while maintaining a suitable supramolecular assembly of the individual compounds and to investigate the morphological properties with respect to the photovoltaic performance.

1.5 Supramolecular assembly

A bottom up approach relying on the self-assembly of organic molecules seems an appealing and cost effective way to achieve desired morphologies for OPV devices. The organization and assembly of the organic donor and acceptor molecules is strongly influenced by entropic and steric interactions of the molecules. Both molecular core and side chains attached at the periphery may have a severe impact on the stacking [17]. For systems with multiple building blocks, e.g. blended donor and acceptor molecules or block-copolymers these considerations may become very complex [18, 19]. Additionally, phase transitions, surface interactions and demixing at elevated temperatures should also be considered as they can strongly affect the molecular assembly.
In combination with a highly ordered stacking of the pristine material domains ideal exciton separation and charge transport might become feasible when a nanoscale phase separation is established. However, in the bulk and mixed phase the crystalline growth of materials is often disturbed by impurities and grain boundaries. Macroscopic charge transport can be drastically reduced due to trapping of charges at these boundaries. Materials with liquid crystalline (LC) properties hold great promise to allow for the growth of macroscopic domains with crystalline order and a suitable supramolecular assembly [17] (as is further discussed in Section 2.3.3).
Based on this concept a series of hexa-*peri*-hexabenzocoronenes (HBC) are investigated in organic photovoltaic devices. The core of this large polycyclic aromatic hydrocarbon consists of thirteen fused benzene rings. Very high charge carrier mobility and long exciton diffusion length could be evidenced for this discotic small molecule. The molecules tend to stack into one dimensional molecular wires exhibiting excellent charge conduction properties [20]. Furthermore, some of the solution processable derivatives show LC phases [17, 21]. Bulk and surface alignment of this class of organic compounds can be influenced by altering processing conditions and by residue modifications at the

periphery of the molecular core. Depending on the electronic character of the residues both p- and n-type semi-conducting properties can be accessed. However, one of the major drawbacks of HBC is its relatively limited absorption of sunlight due to its large optical bandgap. As such, for comprehensive photon harvesting visible light absorption must be accomplished in the acceptor molecules.
In combination with a strongly absorbing perylene-diimide (PDI) acceptor HBC has already proven its potential in bulk heterojunction photovoltaics [22]. Based on these results solution processed devices consisting of HBC and PDI are studied in OPV devices. Self assembly and morphology are related to the power generation efficiency. Complementary, the major loss channels and recombination mechanisms are investigated and combined with morphological considerations. Electronic properties and power conversion efficiency are also analyzed for vacuum sublimated photovoltaic devices consisting of n- and p- type semiconducting HBC derivatives.

1.6 Nanoscale morphologies

In contrast to the self assembly based bottom up approach described above independent and precise control of nanostructure dimensions and molecular packing can be gained by top down methods [23]: Hard templates with structures in the nanometer scale and very well defined dimensions can be produced using various methods like electron beam lithography or electrochemical anodization processes. The nanostructured templates can be subsequently filled with organic material by various techniques e.g. spin coating or electrophoretic deposition and subsequently removed leaving a nano-patterned organic film behind [24, 25]. Alternatively, the nanostructured template can be used as a stamp and used to imprint the organic material [26, 27]. When looking at the fabrication of these template assisted nano-patterned devices production time and cost should also be considered: electron beam lithography for nanometer-sized structuring does not seem to be appropriate for a large scale application.
Anodized aluminum oxide (AAO) membranes are used here to pattern organic compounds. This approach relies on self organization and may be scaled to large surface areas. The templates are subsequently used to structure both n- and p-type organic materials and the resulting organic layers are investigated for application in solar cells. The nanostructured organic layers show a strongly increased interfacial area when compared to non-structured bi-layered devices. On the other hand intermixing and perturbation of the pristine material properties - as are likely for blended compounds - can be avoided effectively. The approach allows precisely defining the donor-acceptor interface area and

geometry which can be exactly adapted to the desired dimensions. Furthermore, the well ordered nanoscale morphologies realized here can be used for light trapping schemes as shown for nanostructured metal-organic interfaces.

1.7 Summary of chapters

In this thesis the supramolecular assembly of discotic molecules is studied as well as nanoscale morphologies are analyzed for OPV devices. Several device morphologies are analyzed and optimized for the fabrication of heterojunction photovoltaic devices.
In the following section (Chapter 2) the device principle of organic solar cells is summarized and an overview to the current status of research in the field is given.
The experimental methods used for the electrical and optical characterization as well as the investigation of morphology and device performance are briefly described in Chapter 3.
The supramolecular assembly of solution processable and evaporated discotic molecules is investigated in Chapter 4. Blend mixtures of the molecules HBC and PDI are used as active materials for solution based OPV devices. Different side chains have been attached to the molecular cores of the donor molecule and the resulting molecular assembly is related to the photovoltaic performance. Charge carrier trapping at grain boundaries and unfavorable morphologies of the donor-acceptor blends are attributed to cause high recombination losses and delimit the power conversion efficiency. Pristine layers of HBC grown using vacuum sublimation techniques instead reveal the potential of this material as organic semiconductor showing an exceptionally long exciton diffusion length and remarkable efficiencies in bi-layered devices.
In chapter 5 a dye sensitization concept is presented allowing to increase the exciton harvesting yield and power conversion efficiency of the OPV devices. A blend mixture consisting of strongly absorbing PDI and a solution processable buckminsterfullerene derivative with excellent electron conduction properties is used in the acceptor phase of the heterojunction devices. Increased efficiency is shown not only in conjunction with the small molecular weight donor molecule HBC - absorbing strongly UV spectral region - but also in combination with a near-IR absorbing donor polymer. Detailed photophysical measurements reveal, that both energy and charge transfer mechanisms occur in the sensitized devices.
In chapter 6 a method is shown to transfer nanoscale morphologies realized in anodized alumina oxide templates into organic semiconducting materials. This approach facilitates the assembly of fully organic heterojunction solar cells with interdigitated in-

terfaces. Furthermore, the well ordered nanoscale morphologies realized here are shown to be suitable for additional light harvesting concepts based on plasmonic effects.
The conclusion (Chapter 7) summarizes the findings of this work and gives an outlook to possible future research directions.

2 Fundamental Concepts and State of the Art Devices

In this chapter a general overview including latest research results in the field of organic solar cells is given. Advantages and drawbacks of the third generation photovoltaic devices are highlighted and limitations discussed. Different conceptual approaches are presented and the physics of devices is analyzed.

2.1 An overview to excitonic and dye sensitized solar cells

Three different types of photovoltaic devices based on organic materialscan be distinguished: dye-sensitized, organic and hybrid solar cells. In all these novel photovoltaic devices a major fraction of the photon absorption occurs in strongly absorbing organic materials. The potentially low production cost due to reduced processing temperatures [28], mechanical flexibility [8] and almost free choice of color [29] are the most prominent advantages when compared to conventional inorganic photovoltaic solar cells. Despite efficiencies are still low to date and device stability in ambient conditions may be an issue first companies have started to produce solar cells based on these emerging technologies. For example, *Dyesol* [30] is currently having the greatest market share for dye-sensitized solar cells, *Konarka* [6] focuses mainly on the development of solution cast bulk heterojunction solar cells and *Heliatek* [5] develops high throughput fabrication tools of evaporated OPV devices.
Significant progress has been achieved in the last few years in device efficiency for all these emerging device technologies with OPV growing fastest as is shown in Figure 2.1.

2.1.1 Dye-sensitized solar cells

About twenty years ago Michael Grätzel published the first report on a 'dye-sensitized solar cell' (DSSC) drawing enormous attention [32]. As schematically shown in Fig-

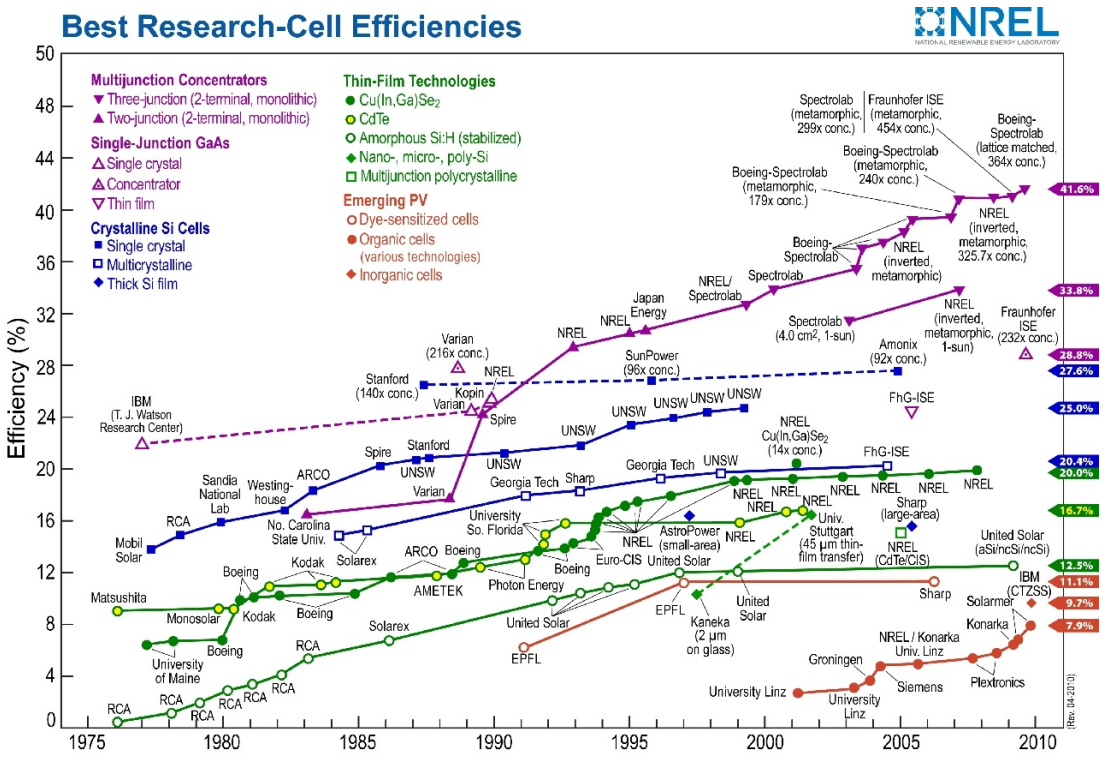

Figure 2.1: NREL research solar cell efficiency chart from [31]. The graph shows a dramatic performance increase of excitonic solar cells since their invention in the early 1990's.

ure 2.2 dye molecules with a high extinction coefficient are in contact with a mesoporous metal oxide surrounded by electrolyte solution. Upon illumination excitons are generated at the dye molecules, separated at the interface to a metal oxide semiconductor and electrons transported to a transparent conducting oxide (TCO) electrode. The regeneration of the dye cation is accomplished by the electrolyte solution which is in contact with a metal back-electrode. Typically dye molecules are grafted to TiO_2 nanoparticles to allow for highly efficient electron injection upon excitation. The nanoparticles are sintered to fluorine doped tin oxide (FTO) and an iodide/triiodide redox system is used as electrolyte [33].

Despite much effort has been made in optimizing efficiency and lifetime of DSSCs there are still a number off issues to be adressed for widespread device application: First, the use of a liquid elecrotlyte might be problematic in outdoor applications. Durable encapsulation is necessary and especially toxic iodine containing liquids must be recycled or disposed of properly. Furthermore, a higher power conversion efficiency would be desired for rooftop and facade integration of DSSC modules. After an initial boost

in performance reaching over 10% already in the year 2001 [34] efficiency records have been reported less frequent in the last decade.
One approach for optimization is to substitute the mesoporous TiO_2 layer by ordered metal oxide nanostructures providing increased electron mobility, a more directed charge transport and better properties for hole conductor infiltration [35]. This concept seems to be a promising route to further increase the efficiency of DSSCs. In the last decade, most progress has been achieved in addressing problems concerning the liquid electrolytes: the toxic and volatile electrolytes can be replaced by organic hole conducting materials. These solid-state dye-sensitized solar cells do not demand elaborate encapsulation [36]. However, hole conductor infiltration might be problematic and efficiencies of these devices cannot compete with the liquid electrolyte cells at present [29].

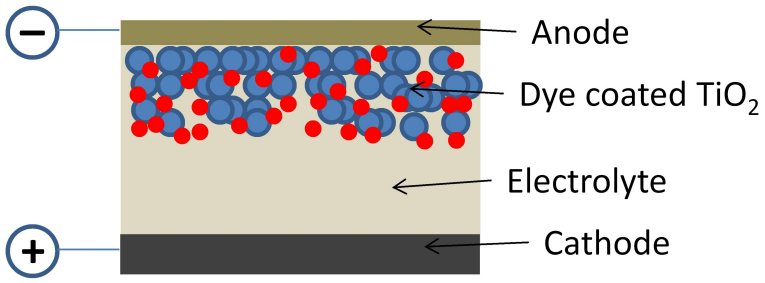

Figure 2.2: Schematic view of a typical dye sensitized solar cell. TiO_2 nanoparticles coated with strongly absorbing dye molecules are sintered on a transparent electrode and surrounded by a liquid electrolyte or solid state hole conducting media. A reflecting back contact serves as cathode.

2.1.2 Hybrid solar cells

Hybrid solar cells are excitonic devices and typically consist of at least one absorbing material (e.g. a dye) and a metal oxide with a large surface area [37]. Instead of relying only on a sensitizer molecule for light absorption, as is the case in DSSCs, light absorption and exciton generation can also take place in the organic hole conductor or a blend of hole and electron conductors infiltrated into the scaffold formed my nanostructured metal oxides [38, 39]. Using regular metal oxide structures the donor-acceptor interface and percolation pathways can be precisely controlled in hybrid nanostructures. Furthermore, the nanometer sized scaffold of the metal-oxide can induce a favorable stacking of the organic material. The interface between the organic and inorganic materials plays a crucial role for the charge separation. Interface modifiers may help to reduce recombination and have a strong influence on the open circuit potential [40].

At present the infiltration of the hole conductors into the metal-oxide scaffold remains a challenge and recombination issues still delimit the performance of hybrid solar cells [37].

2.1.3 Organic solar cells

The first fully organic solar cells were based on one organic compound sandwiched between metal and transparent electrodes achieving only poor efficiencies of far below one percent [28]. In 1986 Tang et al. were able for the first time to show a significantly increased efficiency when introducing a novel concept: A bi-layered sandwich structure consisting of donor and acceptor organic materials was used as active layer and it was shown, that photo-generated excitons are separated efficiently at the interface of this heterojunction device [41].
Since this cornerstone research activity and number of publications in the field has increased dramatically as is shown in Figure 2.3.

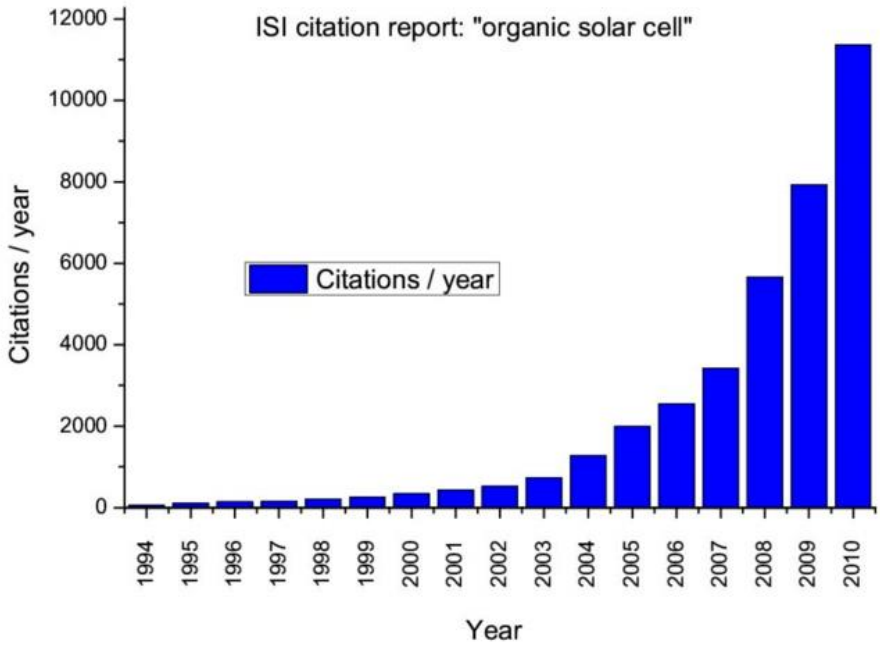

Figure 2.3: Number of citations found for the search phrase "organic solar cell". Citation report generated in August 2011 via ISI web of knowledge [42].

To date record devices allow an 8.3% power conversion efficiency with an active area of about 1 cm^2. This record value has been achieved both for tandem solar cells based

on evaporated small molecules and similarly for solution processed polymer-fullerene blends based on the bulk heterojunction principle [5, 6]. The different processing techniques for these devices and their individual advantages will be discussed further at a later point (Section 2.6).
One of the common challenges for all these devices still remains to increase the exciton harvesting and charge extraction yield while maintaining a high bias potential at the organic heterojunction. The following sections will give a short overview to the individual processes, physics and concepts necessary for the development of efficient organic photovoltaic devices.

2.2 Device working mechanism

2.2.1 Semiconducting properties of organic materials

The semiconducting properties of organic compounds are based on highly de-localized electron systems: alternating single-double bond structures in alkyl chains and highly conjugated aromatic systems (such as benzene and thiophene) in polymers and polycyclic aromatic hydrocarbons (PAHs) are common examples. In these large sp^2-hybridized organic systems the π-conjugated electrons are highly delocalized. Davidov splitting and Peierls instability lead to the splitting of the half filled p_z band into a bonding π and an anti-bonding π^* band [43]. The optical excitation of an electron hole pair between this ionization potential (highest occupied molecular orbital, HOMO) and the electron affinity (lowest unoccupied molecular orbital, LUMO) becomes possible. The energy gap between these two orbitals also strongly influences the optical absorption onset of the organic semiconductor similar to the situation in inorganic semiconductors. However, local deformations in the organic lattice upon excitation lead to the formation of polaronic states [44]. These polaronic states show a strong electronic coupling to the lattice resulting in low dielectric constants. Furthermore, these states have to be considered for the hopping mediated charge transport in the organic media and the energy level alignment at organic interfaces.

2.2.2 Charge generation

When analyzing the current generation in an OPV device under illumination four separate processes can be defined. The maximum current generation of the device is achieved when the product of these individual contributing terms is maximized [15]. We can separate the charge generation into:

- photon absorption
- exciton diffusion
- exciton separation and charge transfer
- charge carrier collection and extraction

In order to determine the efficiency of the devices fill factor (FF) and open circuit voltage (V_{OC}) have to be taken into account, also. These and other characteristic parameters of photovoltaic devices will be explained in detail separately (Section 2.4). The following paragraphs will focus on constraints and limitations for the current generation in OPV devices.

Solar light harvesting in organic photovoltaic devices

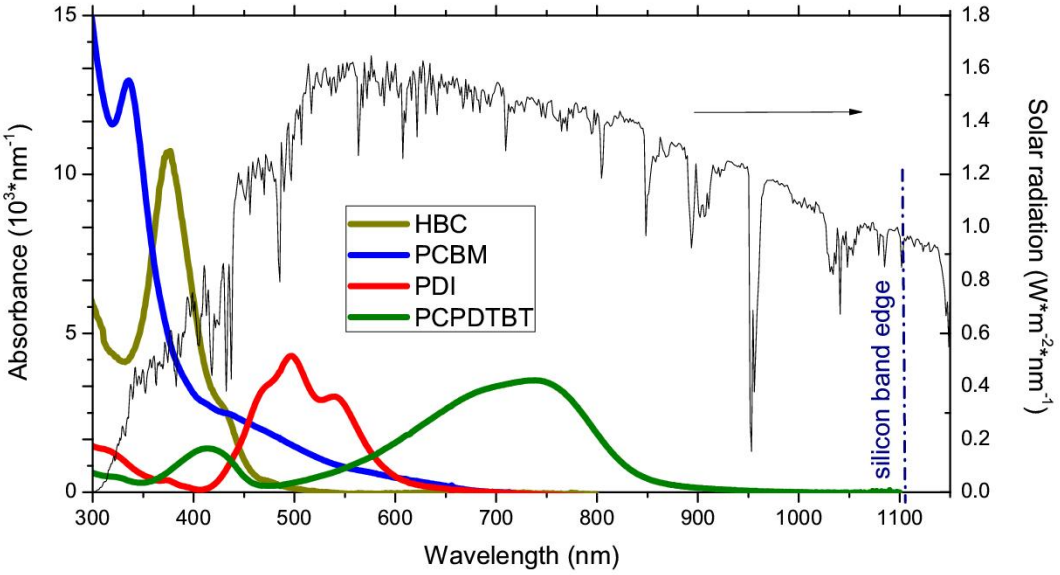

Figure 2.4: Organic material absorption spectra and spectrum of solar air mass 1.5 global radiation. The solar irradiance data is obtained from NREL [45]. Along with the radiation profile the absorption spectra of some common organic molecules and the band edge of silicon are shown for comparison.

The spectral distribution and power density of solar light incident on the earth surface depends strongly on the pathlength of the radiation in the atmosphere. For comparison purpose a standard power flux of 100 mW/cm^2 and reference spectrum have been defined assuming radiation of direct and scattered diffuse light at an incident angle of

48°. Figure 2.4 shows the global air mass 1.5 (AM1.5g) power distribution spectrum along with the band edge of silicon (strongly correlated with the absorption onset in this inorganic semiconductor) and spectra of several organic compounds. In a thick layer of silicon almost all photons with an energy higher than its band-gap of 1.1 eV ($\approx$ 1100 nm) can be absorbed [43]. As has been mentioned already (Section 2.2.1) the absorption of organic semiconductors depends strongly on the "optical bandgap" between occupied and non-occupied molecular orbitals. One of the methods to increase current generation in OPV devices is narrowing this optical bandgap.
It is worth mentioning here, that for common OPV devices with a thin active layer ($d \approx 100$ nm) commonly not all photons with an energy exceeding the energetic barrier of HOMO and LUMO level can be harvested. Furthermore, the open circuit voltage may also become affected when energy levels of the molecular orbitals are altered (as is further discussed in Section 2.4.2).

Exciton diffusion to the organic interface

Upon photon absorption excitons are formed in the organic layer with a certain lifetime (about 100 ps - 1 ns) [46, 47]. If these uncharged excited states diffuse to an interface between donor and acceptor materials excitons may become separated. Lunt et al. have recently elucidated how the exciton diffusion length L_D depends on material cristallinity, transition dipoles and hopping probabilities [13, 48]. The exciton diffusion length L_D is commonly much lower than the optical absorption length of organic materials $1/\alpha$ [15]. In devices using a sandwich type planar bi-layer structure (see Section 2.3.1) photon absorption and exciton separation yield can commonly not be maximized at the same time.
Several approaches have been proposed and investigated to overcome or at least reduce this exciton diffusion bottleneck:

- Synthesize and process materials with high purity and cristallinity exhibiting a long range order and thus high L_D values.
- Include very strong absorbing building blocks into the active materials reducing the optical absorption length $1/\alpha$.
- Introduce more sophisticated morphologies such as blend mixtures, interdigitated interfaces and multilayer stacks.
- Use advanced concepts such as sensitization and light trapping schemes.

All the above mentioned concepts will be discussed in more detail in this thesis. Materials with a tendency for supramolecular stacking and long exciton diffusion lengths

L_D have been processed and are used for the experimental studies (Chapter 4). Bilayered geometries, blend mixtures and interdigitated interfaces are realized for donor and acceptor compounds and analyzed for photovoltaic devices (Chapters 4, 5 and 6). Using a sensitization method a concept for the decoupling of photon absorption and charge carrier generation is presented in Chapter 5. Plasmonic effects occurring in the nanostructured organic films presented here may also allow increasing the photon absorption in thin organic layers (Chapter 6).

Exciton separation and charge transfer

The Onsager theory which was originally developed for charges in a liquid electrolyte can be also used to estimate the escape probability for coulombically bound excitons in an organic semiconductor [49, 50]. The coulomb binding energy (Equation 2.1) is typically large in organic semiconductors due to their low dielectric constants of $\epsilon_r \approx 3-4$ compared to $\epsilon_r \approx 12$ for silicon.

$$E_{coulomb} = \frac{e^2}{4\pi\epsilon\epsilon_0} \tag{2.1}$$

As such, excitons created in organic materials have a strong binding energy of about $0.1 - 1eV$ and can commonly not be dissociated by the thermal activation energy at room temperature ($k_BT \approx 0.025$ eV) alone. As has been mentioned already in the introduction of this thesis a heterojunction interface between donor and acceptor organic materials is necessary to separate these strongly bound excited states into free charges: The potential drop at the heterojunction compensates for the binding energy of the bound state. However, a more detailed analysis is necessary to correctly describe the separation process of the excitons: charge transfer states and polaron pairs are intermediate states that may be formed before free electrons and holes are generated in the acceptor and donor materials, respectively [51, 52]. The mechanisms involved in the charge separation process at heterojunction interfaces are still under discussion and not clearly understood at present.

Charge carrier migration and collection

Once excitons are separated into free charges holes and electrons have to be extracted to the external contacts of the device. Direct percolation pathways to the respective electrodes are a prerequisite for the efficient charge extraction. Especially for solution

cast blend and other mixed morphologies the formation of these direct pathways might be critical (Section 2.3.2). Furthermore, high charge carrier mobility is necessary for an efficient charge extraction also at low electric fields. Hopping of charges at local defects and charge trapping may result in a drastically lowered fill factor and thus affects the performance of the devices [53, 54].

2.3 Donor-acceptor morphology concepts

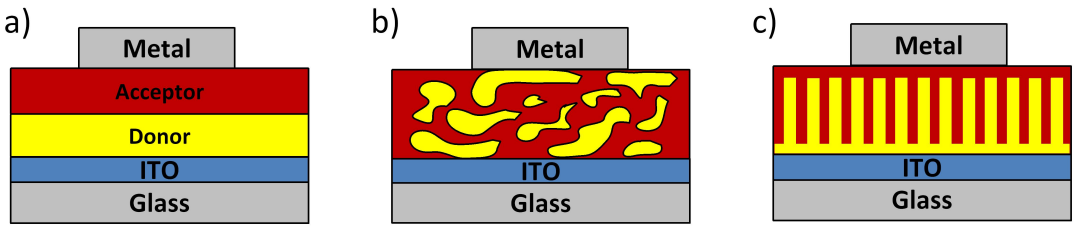

Figure 2.5: Morphology concepts for organic photovoltaic devices. For simplicity the devices are shown in a *normal device geometry* with no exciton, hole or electron blocking layers. Planar bi-layer **(a)**, blend mixture **(b)** and interdigitated interfaces **(c)** are distinguished.

One of the main challenges in the field of organic photovoltaics is achieving complete exciton harvesting while maintaining minimal losses due to the recombination of excitons and separated charge carriers (as mentioned previously in Section 2.2.2). The exciton diffusion length (L_D) in organic semiconductors is typically short, often below 10 nm. In order to achieve comprehensive harvesting of the excited states generated in the active layer of a bi-layered OPV device with a planar interface the thickness of the donor and acceptor layers must not exceed this characteristic length scale. For bulk-heterojunction devices with intermixed donor and acceptor materials the domain size should remain at or below this spacing to efficiently harvest generated excitons [19]. At the same time direct percolation pathways to the respective electrodes are necessary to suppress trapping and recombination of generated charge carriers. The influence of the nanoscale morphology on exciton separation and charge carrier transport has been studied intensively in the past [55–57].
Increasing charge carrier mobility and lifetime in the respective phases may help to reduce these recombination issues as can be visualized in simulated IV-curves shown by Street et al. (Figure 2.6) [58]. As such, architectures allowing the growth of crystalline and ordered materials with intimate contact of donor and acceptor on the nanometer length scale are desired for an improved efficiency [59, 60]. The synthesis of highly

π-conjugated molecules with functional groups fostering self assembly into mesoscopic and macroscopic architectures is a versatile tool to achieve this goal. Exciton harvesting, charge carrier generation and extraction pathways have to be optimized and loss mechanisms such as charge recombination and decrease in potential carefully analyzed.

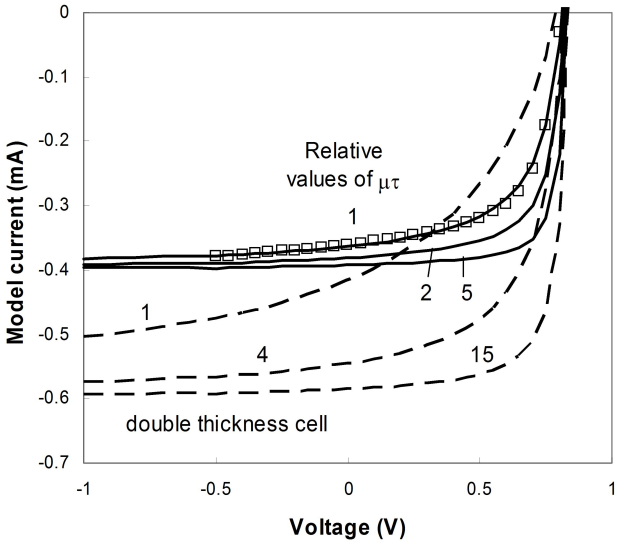

Figure 2.6: IV characteristics of OPV devices. The graph shows experimental data (dots) and modeled IV characteristics for a photoactive blend depending on the mobility-lifetime product and active layer thickness. When increasing the thickness of the active layer for the presented system a performance increase can be achieved only if the mobility-lifetime product is also enhanced. Reprinted with permission from [58]. Copyright 2010 by the American Physical Society and the author, Dr. Bob Street.

2.3.1 Planar Heterojunctions

The most straightforward architecture with a donor-acceptor interface is a planar heterostructure (shown schematically in Figure 2.5 **(a)**). Since the first devices were assembled using this sandwich-type geometry [41], many researchers have tried to optimize charge generation and extraction by proper choice of materials and processing conditions. To date best devices based on this planar heterojunction concept achieve 3- 4 % power conversion efficiency [61, 62]. In order to facilitate such a good performance it is a prerequisite to use materials with an exceptionally high L_D: The separation of photo-generated excitons and therefore the thickness of the photoactive layer con-

tributing to the current generation will be limited to this path length in the respective materials. On the other hand this simple device architecture provides ideal extraction pathways for the charges generated allowing the fabrication of devices with high fill factors. Furthermore, modeling and simulation of this type of OPV devices provides good agreement to experimental findings and may help to derive fundamental design rules [62, 63].
This device geometry also allows the arrangement of multiple active layers into tandem and multi-layered stacks [64], where an efficient recombination interlayer has to be introduced and series and parallel connection of sub-cells may be considered [65].

2.3.2 Blend mixtures

In 1995 the first solution processed bulk heterojunction solar cell was reported [66]. Blending the donor and acceptor organic materials offers the great advantage to facilitate photon harvesting at a strongly increased active layer thickness (Figure 2.5 **b**). The inter-penetrated networks of donor and acceptor materials allow the separation of excitons throughout the active area.
Polymer-fullerene blends are probably the most well studied system for the active layer of OPV devices [43]. However, solution processed or evaporated mixtures of small molecules and oligomers have drawn an increasing attention in the past and efficiencies of well above 5% have been similarly achieved for all these mixed heterojunction systems [67–69].
When blending the donor and acceptor materials a special focus lies in the nano-morphology of the active layer. Yielding high performance requirtes a domain size in the order of L_D and a structure that allows unhampered extraction of the generated charges to the external electrodes. In many recent publications thermal or solvent annealing, addition of additives or application of external fields has been shown to allow an increased device performance which is attributed mainly to morphological changes in the photoactive layer [70–72]. Precise control of processing parameters and sometimes post-production treatments are necessary to achieve suitable inter-penetrated donor and acceptor structures as is further explained in Section 2.6.3.
However, full control over the nano-morphology cannot be achieved by these bulk treatments and unwanted morphologies like insulated islands of donor and acceptor in the surrounding matrix of the organic counterpart can often not be avoided. This may lead to charge carrier trapping, space charge formation and strong bimolecular recombination. Limited current generation, especially at high illumination intensities, and low fill factors are a result as will be discussed separately (Section 2.7.1).

The extraction of the photo-generated charges in the donor and acceptor materials at the external contacts is also more sophisticated in this type of device - the charge extraction pathways are not intrinsically defined as it is the case for the bi-layered devices. In this context also the use of electron and hole selective contact materials is detrimental (further described in 3.1.4). Charge recombination at bottom or top electrodes can be suppressed by applying blocking layers as are presented in Section 3.1.5.
Furthermore, the morphology of these blended mixtures may be very sensitive to aging or the influence of external mechanical stress and heat. Thus long term stability and applicability for outdoor installations have to be carefully analyzed for each material combination separately.
Most importantly the desired photophysical properties of the organic semiconductors like elevated charge carrier mobility and long L_D that may be obtained in highly pristine compounds are often strongly affected when the supramolecular order is perturbed by intermixing of the active materials. An idealized heterojunction structure with pristine material phases that guarantees continuous percolation pathways but is intermixed on the nanometer length scale is therefore highly desired.

2.3.3 Interdigitated interfaces

Several approaches have been made to combine the desired properties of pristine materials as found in planar bi-layered devices with the exciton harvesting yield that can be achieved in an active layer of blended materials.
Interdigitated interfaces on the nanometer length scale ideally allow to combine these benefits and avoid their shortcomings: In this morphology donor and acceptor materials are well separated and in direct contact to their respective electrodes as it is the case for bi-layered devices (a schematic view is given in Figure 2.5 **(c)**). Charge carrier transport properties of pristine materials can be combined with an increased exciton harvesting. The comb like structure at the donor-acceptor interface provides a strongly increased interfacial area compared to bi-layered structures while maintaining direct percolation pathways to the electrodes. Similarly to blend devices an efficient exciton separation may be obtained throughout the active layer of the device without increasing the risk of charge recombination in insulated material phases. Ideally exciton harvesting and photon absorption will become decoupled and the exciton separation bottleneck (Section 2.2.2) can be overcome. Another important aspect, that should be considered are possible beneficial effect of nano-patterning of the organic materials on the molecular alignment [73].
In recent, theoretical calculations have shown that such an idealized heterojunction

structure could result in a strongly improved charge extraction and overall efficiencies twice as high as can be achieved for blend devices [74].
In the following paragraphs promising experimental approaches towards the realization of such an ideal morphology for the OPV device will be presented.

Polymer brush

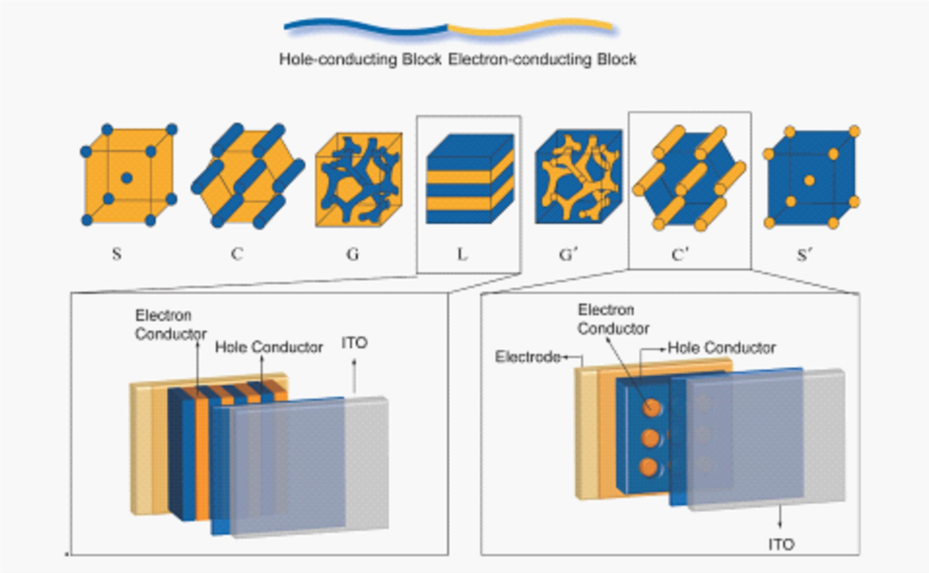

Figure 2.7: Schematic assembly of block-copolymers. Different morphologies can be realized by tuning the di-block co-polymer mixing ratio. Reprinted with permission from [19] Copyright 2010 American Chemical Society.

Using di-block copolymers is a promising method to achieving controlled architectures on the nanometer length scale: tuning length and composition of subunits incorporated in a polymer chain allows directly influencing the distribution and stacking of sub-domains from solution cast films (Figure 2.7). This self-assembly approach has can also be used to pattern the active layer of OPV devices: Repeat units of donor and acceptor can be covalently bound to each other. Upon solvent evaporation self assembly of the building blocks drives the formation of ordered architectures on a nanometer length scale. The size and type of linker units between donor and acceptor oligomers and their respective weight fraction determines the phase formation and thus the resulting nano-architecture. This direct morphology control is a clear advantage compared to the polymer-fullerene systems discussed. The self-assembly of block-copolymers has been studied intensively and ordered nanostructures with various different shapes have been

realized following this conceptual approach (depicted in Figure 2.7) [19].
Since the first successful application of this concept for OPV devices by S. Sun [60] using semiconducting di-block co-polymers a variety of different donor and acceptor moieties have been tested with high intrinsic absorption and mobility. However, up to date the efficiency of these devices remains still far below 1% which is mainly attributed to high series resistance and significant recombination losses [75]. Despite high exciton separation yield indicated by significant photoluminescence quenching, strong recombination losses at covalent bonding sites of the polymer backbone delimit the overall performance.
Further optimization of the molecular alignment yielding the formation of wire-like structures perpendicular to the substrate plane and the introduction of insulating spacer units may help to facilitate better charge extraction and a reduced recombination allowing to improve the efficiency of these devices. It should also be noted that the synthesis of these highly complex macromolecules with a minimal poly-dispersity and high yield remains a challenging task.
Block copolymer approaches can be used also in the context of a "soft-template" providing a scaffold for subsequent replacement with photoactive materials, similar to the methods discussed in Section 2.3.3. For these approaches a specific block of the copolymer is removed by reactive ion etching, mild base treatment or UV-light irradiation [76].

Liquid crystalline materials and supramolecular organization

Defect free and long range ordering of molecules is necessary to achieve high mobilities in organic compounds. However, typical thin films of pristine materials exhibit polycrystalline phases which allow highly ordered stacking and thus high mobility values only within the crystallite domain size [77]. On a macroscopic scale instead, the charge carrier mobility is often limited severely by grain-boundaries between the individual crystallites. On the other hand, charge transport in amorphous layers is commonly low due to an insufficient π-orbital overlap of the individual molecules. Uniformly aligning the molecular building blocks in a bulk material remains a very challenging task.
Liquid crystalline (LC) materials have been shown to hold great promise in order to span the molecular organization from the microscopic to mesoscopic or even macroscopic length scales [70, 78]. Molecules in a LC phase show an intermediate degree of order between the isotropic (amorphous) and crystalline states and may become aligned in the bulk phase.

Alignment of LC materials Self-assembly processes and supramolecular organization schemes are necessary to access the potential of LC materials: Using external stimuli macroscopic quantities of molecules may become simultaneously aligned. The organization and thus also electrical and photophysical behavior of the bulk material can be strongly influenced [79]. When heated to the isotropic state, electric or magnetic fields can induce long range orientation of the molecules which may be retained in the LC and sometimes also in the solid phase [80, 81]. Significant π-orbital overlap of neighboring molecules can be accomplished without introducing defects on the mesoscopic to macroscopic length scales. As such, this "bottom up" strategy allows directly influencing the material properties on a bulk scale, e.g. molecular orientation and resulting charge carrier mobility [17, 82]. Furthermore, local distortions in the supramolecular organization can be overcome by a self-healing procedure: structural and electronic defects may become eliminated spontaneously or via an annealing treatment [83].
Surface interactions and geometrical confinement may also have a severe impact on the resulting alignment and have to be precisely analyzed to facilitate the desired molecular stacking [84].
A variety of different molecules have been found with LC properties, often showing multiple phase transitions and having phases with different levels of supra-molecular organization. Common *mesogens* (i.e. molecules with a LC ordering) consist of flexible side chains covalently linked to a rigid molecular core unit exhibiting a high degree of anisotropy. A variety of LCs with disc-like ("discotic") and rod-shaped core units have been reported in the past.

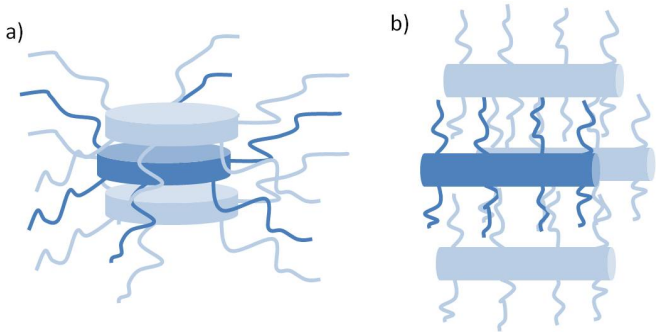

Figure 2.8: Schematic representation of common mesogens. Disc-shaped **a)** and rod shaped **b)** molecules are distinguished which may stack in quasi 1-D and quasi 2-D morphologies, respectively.

Discotic LC materials for organic photovoltaics Rod-shaped LC molecules show a high commercial relevance particularly in switchable thin film display technologies due

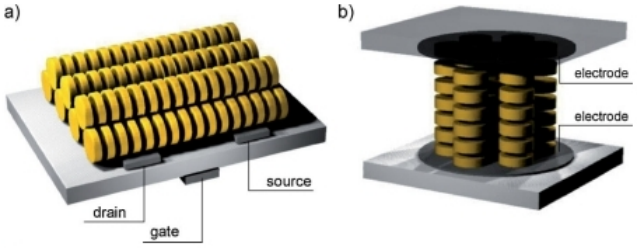

Figure 2.9: Alignment of discotic liquid crystals on a substrate. a) Egde-on orientation; Molecular cores are standing upright on the surface resulting in molecular stacks parallel to the substrate plane. **b)** Face-on or homeotrophic alignment; the molecular cores are lying on the surface, the stacks are standing upright. Reprinted with permission from [17]. Copyright 2009 Wiley-VCH.

to their high anisotropy resulting in birefringence effects.
Discotic LCs seem extremely appealing for applications where unidirectional charge transport is desired. The disc shaped molecules can form quasi 1-D patterns, which may display high charge carrier mobility along the nanowire axis [20].
In the case of planar[1] alignment, charge migration is favored along the substrate plane. This is especially important for the assembly of OFETs (Figure 2.9 **a**) [70].
For the application in photovoltaic devices instead a homeotrophic alignment[2] of the molecules is favored, as it may provide direct charge extraction pathways to the respective electrodes (Figure 2.9 **b**).
The supramolecular interactions in LC-phases allows a better organization on the molecular scale when compared to the isotropic state [17]. Furthermore, due to the avoidance of grain boundaries commonly found in crystalline packing an unhampered charge carrier transport can be provided also in the bulk material. These materials therefore very well meet the requirements as active layers in OPV devices. The self-healing capabilities of LC materials (Section 2.3.3) provide another aspect possibly allowing for an increased device lifetime [85].
At present, only a limited amount of studies have shown the application of LC materials as active media in OPV devices: Schmidt-Mende et al. investigated a solution processable HBC derivative combined with a strongly absorbing acceptor molecule resulting in a remarkable solar cell efficiency of 1.95 % at low light intensities and under monochromatic illumination [22]. Other studies show that the photovoltaic performance of such blend mixtures of liquid crystalline materials is extremely sensitive to the morphology [86, 87]. It is also known, that different types of supramolecular order can occur

[1] also reffed to as "edge on" stacking
[2] i.e. "face-on" alignment

in blend mixtures of LC materials [18]. Further detailed studies relating both morphology and resulting device performance are necessary on OPV devices based on liquid crystalline materials in order to derive design concepts for a superior power conversion efficiency.

Nano-patterning of organic materials

In order to access sophisticated interface architectures the pre-orientation of either donor or acceptor material and subsequent infiltration of the organic counterpart is a natural approach. In hybrid photovoltaic devices commonly a nanostructured metal-oxide template is grown on ITO support followed by infiltration of the organic material. The structuring of the metal-oxide is often accomplished by either self organized nano-pore formation or growth of nanometer sized architectures from the vapor phase [37].
For the fabrication of fully organic photovoltaic devices instead a structuring of the organic material requires template assisted methods. Nano-imprint lithography has shown to hold great promise [27, 88]. The nano-patterns are transferred from a master stamp to the substrate. In contrast to hybrid devices, the infiltration of the organic counterpart may become more challenging for fully organic nanostructured devices. Spin coating of the secondary material onto a solution processed structured support material does not seem an appropriate method. Very high surface interaction will disrupt the nanostructured interface during the spin coating procedure also when orthogonal solvents are used. Furthermore, inter-diffusion of the organic materials at the interface cannot be strictly avoided. As such, polymerization of the structured organic compound, vacuum deposition of the secondary organic layer or more sophisticated techniques seem more appropriate. For example, a solvent assisted two-step imprinting approach has been presented recently allowing precise interface structuring on the nanometer length scale [89].
Electron beam lithography and scanning probe lithography techniques do not seem to be appropriate for the patterning of the organic materials in OPV devices for the commercial market: high cost and low throughput will hinder their widespread application. Nanometer sized patterns generated by self assembly processes seem more appealing as will be discussed and demonstrated in Chapter 6.

2.4 Device operation

In the following section a brief overview to the operation mechanisms and the electrical characterization of OPV devices is given.

2.4.1 Ideal diode equation for an organic heterojunction

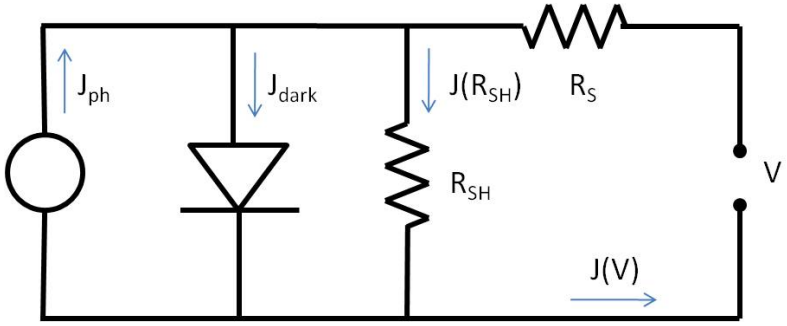

Figure 2.10: An equivalent circuit model often used for the description of an organic photovoltaic device.

Using an equivalent circuit model as shown in Figure 2.10 one can derive the current-voltage characteristics of an inorganic p-n junction [90]. The generalized Shockley equation describes the the current flow $J(V)$ of the device in this equivalent circuit model [91]:

$$\mathrm{J(V)} = \frac{\mathrm{R_{sh}}}{\mathrm{R_s + R_{sh}}} \times \left\{ \left[\mathrm{J_S} \left\{ \exp\left(\frac{\mathrm{q(V - IR_s)}}{\mathrm{nk_B T}} \right) - 1 \right\} + \frac{\mathrm{V}}{\mathrm{R_{sh}}} \right] - \mathrm{J_{ph}(V)} \right\} \tag{2.2}$$

With the photocurrent J_{ph} opponent to the dark current influenced by series and parallel resistance $\mathrm{R_s}$ and $\mathrm{R_{sh}}$. n denotes the diode ideality factor, q the elementary charge and J_S the reverse saturation current.
It has been shown by Rand et al., that this model originally derived for inorganic p-n junctions can also be applied to describe organic photovoltaic devices at normal working conditions [67]. In this case the reverse saturation current has an exponential dependence on the energy gap $\Delta \mathrm{E_{DA}}$between electron affinity of the acceptor (EA_A) and the ionization potential of the donor (IP_A):

$$\mathrm{J_S} \propto \exp(-\mathrm{E_{DA}}/2\mathrm{nk_B T}) \tag{2.3}$$

Using this empirical model the impact of changes in the energy gap ΔE_{DA} and device temperature on the charge generation in the photovoltaic device can be predicted.
It is worth mentioning, that only recently a diode equation based on the formation of polaron pairs has been derived specifically for OPV devices and shown good accordance to experimental data obtained from bi-layered devices [92].

2.4.2 Energy level alignment and open circuit voltage

Predicting and optimizing the open circuit voltage (V_{OC}) of heterojunction solar cells is of fundamental importance to achieve an increased solar cell efficiency. It is known, that the V_{OC} is strongly influenced by the energy gap of the donor-acceptor interface $\Delta E_{DA} = HOMO_{Donor} - LUMO_{Acceptor}$ [11].
Tuning ΔE_{DA} by increasing the LUMO energy level of the acceptor or decreasing the level of the HOMO of the donor should therefore result in a higher V_{OC}. On the other hand, as discussed in Section 2.2.2, a certain offset in HOMO and LUMO energy levels is necessary to facilitate efficient exciton separation at the heterojunction interface. Furthermore, the exciton generation yield is limited by the lowest optical bandgap of donor and acceptor compounds. A compromise has to be found between comprehensive light harvesting, driving force for efficient charge separation and a high open circuit voltage.
The influence of the external contacts of the device on the V_{OC} has also been studied intensively [93]. Given certain requirements for the level alignment at the organic/inorganic interface, doping of the organic layer (integer charge transfer) may occur leading to Fermi-level pinning of the conducting substrates thus yielding ohmic contacts - An only marginal influence of the electrode work function on the V_{OC} of the devices is observed [44, 93].
Light intensity and operation temperature are other factors that are known to influence the V_{OC} of the photovoltaic devices [90]. Recently theoretical models have been proposed and discussed for the determination of the open circuit voltage, taking not only energy level alignment but also recombination probabilities at the heterojunction interface into account. Equation 2.4 derived by Perez et al. is based on the generalized Shockley equation (Equation 2.2) and seems to hold for multiple organic heterojunction systems [94].

$$V_{OC} = \frac{nkT}{q} \ln \frac{I_{SC}}{I_{SO}} + \frac{\Delta E_{DA}}{2q} \tag{2.4}$$

where ΔE_{DA} is the donor acceptor energy difference and I_{SO} a temperature independent pre-factor. Combining equations (2.3) and (2.4) one can show, that $V_{OC} \propto ln(P_0)$ which

holds approximately for light intensities $P_0 \leq 100\,\mathrm{mW/cm^2}$. It is important to note that at these low to moderate light intensities $V_{\mathrm{OC}} \propto T^{-1}$ as $J_S(T)$ shows an only marginal influence on the temperature dependence of $\mathrm{V_{OC}}$ (Equation 2.3 and Equation 2.4).
Instead, at very high illumination intensities or very low temperatures a maximum $\mathrm{V_{OC}}$ (V_{OC}^{max}) will be achieved:

$$\mathrm{qV_{OC}^{max} = IP_D - EA_A - E_{EB}} \tag{2.5}$$

with E_EB being the exciton binding energy.

2.4.3 Current-voltage characteristics

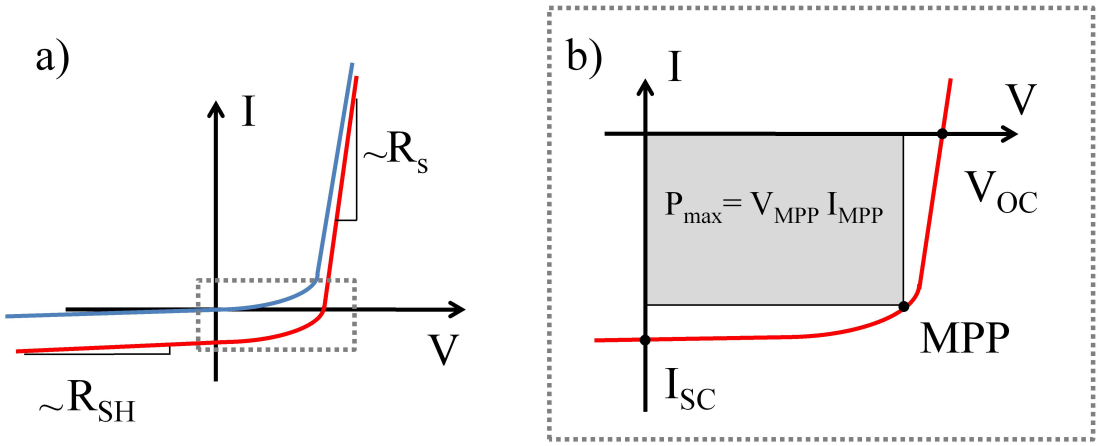

Figure 2.11: Typical IV-curves of a photovoltaic device. a) Blue and red lines show the device characteristics in the dark and under illumination, respectively. Series and shunt resistance can be roughly estimated from the slope at high reverse and forward bias voltage. The enlargement (**b**) shows characteristic parameters of the device under illumination.

Measuring current-voltage (IV) curves is one of the most important characterization methods when analyzing the electronic properties of photovoltaic devices. Measurements are commonly performed both in the dark and under constant white-light illumination at standard test conditions (AM 1.5 global, $100\,\mathrm{mW/cm^2}$) [95].
The device parameters open circuit voltage ($\mathrm{V_{OC}}$), short circuit current ($\mathrm{I_{SC}}$) and maximum power point (MPP) of the photovoltaic devices can be extracted directly from the IV characteristics as is shown in Figure 2.11: At the MPP the power output of the device $P = I * V$ reaches its maximum which is indicated also by the shaded rectangle in Figure 2.11. According values of current and voltage are abbreviated as V_{MPP} and

I_{MPP}. Using these characteristic device parameters one can derive the fill factor (FF) and power conversion efficiency (η) of the device as follows:

$$FF = \frac{V_{MPP} * I_{MPP}}{V_{OC} * I_{SC}} \tag{2.6}$$

$$\eta = \frac{V_{OC} * I_{SC} * FF}{P_0} \tag{2.7}$$

where P_0 is the incident light intensity.

2.4.4 Intensity and temperature dependence of IV-characteristics

As has been discussed in Section 2.2.2 and Section 2.4.2 current generation and open circuit voltage strongly depend on the exciton separation probability and exciton binding energy. As such, operation of devices at different temperatures and incident light intensities strongly alters the shape of resulting IV-curves and their analysis may reveal additional information on the physical properties of the photovoltaic device.
In recent, several models have been proposed to describe intensity and temperature dependence of IV-curves of organic devices. The generalized Shockley model (as discussed in Section 2.4.1) is strictly valid only for inorganic devices. However, the model has been applied for organic bi-layered and also bulk heterojunction devices with good agreement to the experimental data [90, 96]. It is worth mentioning, that especially at low temperatures significant deviation of experimental data from the generalized Shockley model is frequently observed. Light intensity modulations directly affect the short circuit current generation of the photovoltaic devices and give insight to the recombination mechanisms present in the devices: for a strictly mono-molecular recombination a linear dependence of I_{SC} with P_{inc} is commonly observed [97]. Instead, if non-geminate recombination plays a significant role in the devices under investigation a sub-linear increase of I_{SC} with rising illumination intensity is apparent.

2.5 Organic materials

The use of conjugated carbon based compounds as active materials in photovoltaic devices opened up a vast pool of compounds that might potentially be used for photon absorption and charge extraction. However, organic materials have to meet several specific properties to be considered as candidates for efficient power conversion in OPV

Material	HOMO [eV]	LUMO [eV]	Reference
$PC_{61}BM$	-6.0	-4.3	[11]
P3HT	-5.1	-3.2	[98]
PCPDTBT	-4.9	-3.5	[98]
PDI	-6.1	-3.9	[99]
HBC	-5.4	-2.7	[99]
CuPc	-5.2	-3.5	[100]

Table 2.1: Energy levels of organic materials used for solar cell fabrication. HOMO and LUMO levels are summarized a reported in the literature reference.

devices. High molecular extinction, good charge conduction properties and suitable energy levels are important factors.
A selection of some semiconducting organic compounds used for OPV are listed in Table (2.1) and in the following paragraphs.

2.5.1 Polymers

Polymers can exhibit high conjugation lengths, a strong molecular absorption and also very good solubility making these compounds specially attractive for the application in solution processed devices. The molecular structure of common polymers used for photovoltaic applications exhibits an elongated, highly conjugated backbone with short alkylic side chains attached.
Poly-3-hexothiophene (P3HT) with the chemical formula shown in Figure 2.12 is probably the most studied donor-compound in the field of organic photovoltaic devices: The planar structure of the adjacent thiophene units in the backbone facilitates highly ordered packing into lamella sheets with high cristallinity. The anisotropy of this elongated molecular structure also strongly influences the resulting electronic properties observed in the solid state [73].
The degree of poly-dispersity in molecular weight and coupling of the monomers into regio-regular or regio-random structures have been shown to have a very strong influence on molecular packing and resulting electronic properties [59, 101]. Efficiencies above 5% have been achieved in organic devices for the first time using a regio-regular P3HT in conjunction with a fullerene based acceptor and the molecule has become a standard acceptor material for OPV (see also Section 2.8.1) [102]. However, current generation in this donor-acceptor system is confined by the relatively large optical bandgap of P3HT ($\Delta E_{DA} \approx 1.9$ eV).
Recently push-pull donor polymers exhibiting a reduced optical bandgap have drawn

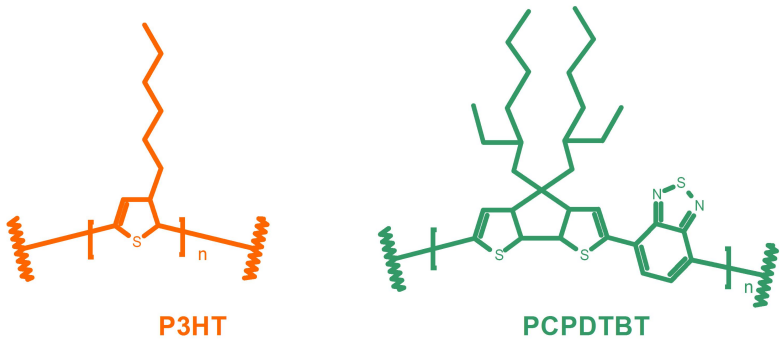

Figure 2.12: Molecular structure of P3HT and PCPDTBT Two common donor polymers used in OPV devices

much attention (as already mentioned in Section 2.2.2). For example, Poly[2,1,3-benzothiadiazole-4,7-diyl[4,4-bis(2-ethylhexyl) (PCPDTBT) has an absorption onset at around 900 nm and has been studied intensively in photovoltaic devices [98, 103, 104]. Charge generation rates of over 15 mA/cm^2 have been achieved for blends of this polymer with fullerene derivatives [103]. However, the nano-morphology of this solution cast blend is found to be non-ideal and post production treatments like solvent or thermal annealing are detrimental to achieve interpenetrating networks on the nanometer scale suitable for charge extraction (as further discussed in Section 2.6.3).

2.5.2 Small molecules and oligomers

Despite often being considered as "Polymer solar cells" by far not all OPV devices use solely polymerized compounds in the active layer. Instead, in a vast majority of devices fullerenes and solution processable derivatives (see Section 2.5.3) are applied as electron acceptors.

On of the major advantages of small molecules with respect to polymers is their monodispersity. This makes synthesis with high purity and batch-to-batch reproducibility feasible which also facilitates a more valuable comparison of experimental results [22, 105]. Similar to polymers, small molecules can be functionalized in order to ensure high solubility for solution processing. On the other hand, small molecules offer the advantage of deposition *via* vacuum sublimation [106, 107]. The evaporation of organic compounds allows the growth of highly crystalline structures providing exceptionally high charge carrier mobility and long exciton diffusion lengths [108, 109].

It is worth mentioning that oligomers and dendrimers have recently drawn remarkable

attention for the application in OPV devices bridging the properties and advantages of both small molecules and polymers.

2.5.3 Fullerenes

The by far most widely used acceptor materials in OPV devices are based on fullerenes. This holds true for both evaporated and solution processing of the active material where the unmodified buckminsterfullerene C_{60} and solution processable derivatives like [6,6]-Phenyl-C_{61}-butyric acid methyl ester ($PC_{61}BM$) are frequently used, respectively. Fullerenes have a very strong electron affinity, show excellent electron conduction properties and exhibit remarkably high exciton diffusion lengths of over 40 nm [11, 110, 111]. Unfortunately evaporated C_{60} is very sensitive to exposure on oxygen, hindering device fabrication and testing in ambient atmosphere. The solution processable $PC_{61}BM$ (Figure 2.13) instead has shown an increased air stability when blended with P3HT [112]. One of the drawbacks of fullerenes is their relatively low optical absorption when com-

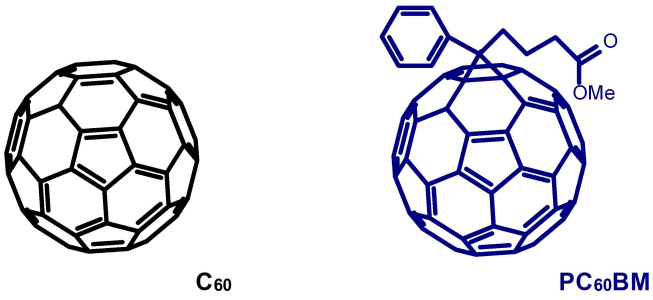

Figure 2.13: Molecular structure of Buckminster-fullerene derivatives. C_{60} and $PC_{61}BM$ are commonly processed from vacuum and solution phase, respectively.

pared to polymers and small molecular weight molecules with high extinction coefficients. Therefore, most photon harvesting has to take place in the donor phase used in combination with the fullerene molecules as photoactive layer.

2.5.4 Discotic materials

As already mentioned in Section 2.2 exciton diffusion length and charge carrier transport in organic compounds depend crucially on crystallinity and molecular packing. Macroscopically ordered stacking of molecules is desired for an unperturbed charge carrier transport resulting in high charge carrier mobility [48].

Discotic materials have a highly anisotropic and planar core. Based on π-π interactions of neighboring core molecules these disc shaped molecules have a tendency to align into supramolecular stacks [17, 70]. This renders discotic molecules very appealing for the application in organic electronic devices: Very high charge carrier mobility along the stacking axis and suitable energy levels for application in photovoltaic devices have been evidenced for several representatives.
Prominent examples of discotic molecular core units are shown in Figure 2.14. In the following some discotics are briefly discussed in the context of active materials for photovoltaic devices.

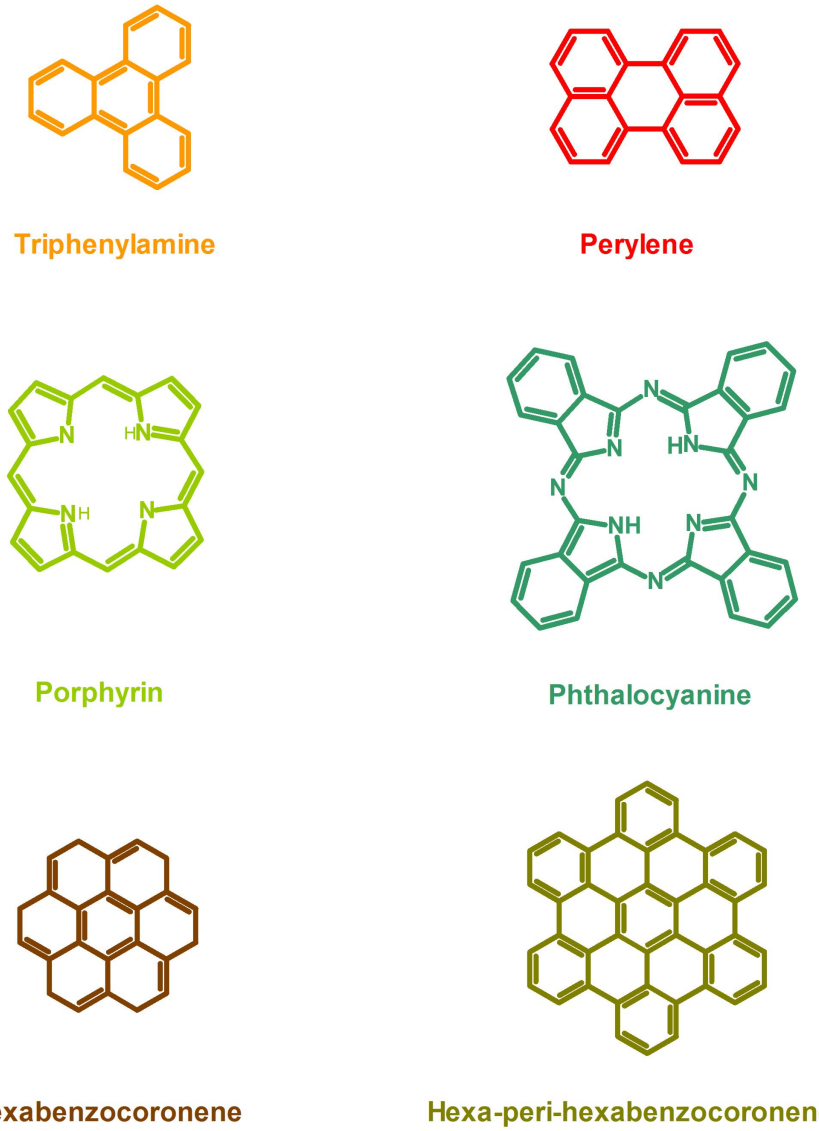

Figure 2.14: A selection of discotic molecules. The disk-shaped core of the compounds supports the assembly into columnar stacks and allows for high charge carrier mobility along the stacking axis.

Perylenes are very photo-stable dye molecules and various derivatives have been used both in dye-sensitized solar cells as well as in bulk heterojunction OPV devices [71, 113–115]. Perylene diimide (PDI) with the chemical formula 2,9-Di(pent-3-yl)-anthra[2,1,9-def:6,5,10-d'e'f']diisoquinoline-1,3,8,10-tetrone is a highly absorbing perylene derivative with short and symmetric dove-tailed side chains as shown in Figure 2.15. The molecule exhibits a strong tendency to form H-aggregate stacks [116] - Adjacent molecules sta-

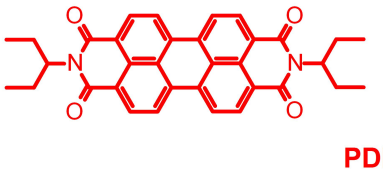

Figure 2.15: Molecular structure of a Perylene-diimide The molecular core allows strong photon absorption and high photo-stability.

ple on top of each other with a twist angle allowing for tight packing of the molecular cores and up to several micrometer long crystals may be formed [117]. PDI has been shown to be a very good electron acceptor with high electron mobilities of up to 0.12 $cm^2\ V^{-1}\ s^{-1}$ [22, 118].

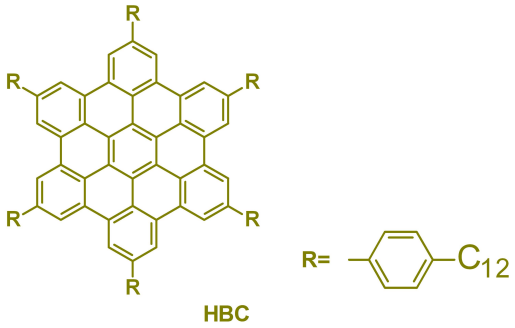

Figure 2.16: Molecular structure of hexa-*peri*-hexabenzocoronene. The molecule shows a strong tendency to stack into 1-D molecular wires and has shown application as donor material in OPV.

Hexa-*peri*-hexabenzocoronenes (HBCs) are very well studied large polycyclic aromatic hydrocarbons [70, 119]. The molecular core consists of thirteen fused benzene rings forming an hexagonally shaped planar structure. Side chains may be attached to the six peripheral bond sites of this highly symmetric shaped "mini-graphene" molecule which can strongly influence solubility, phase transitions and the photophysical behavior of the molecule [17, 120]. An outstandingly high charge carrier mobility of up to 1.1 $cm^2\ V^{-1}\ s^{-1}$ has been found for solution processable derivatives rendering this class of molecules exceptionally appealing for application in field effect transistors and photovoltaic devices [20, 87, 121].
HBC-Ph-C_{12} is a p-type discotic molecule which is liquid crystalline at room temperature (Figure 2.16). For this HBC derivative, charge carrier mobilities of 0.22 $cm^2\ V^{-1}\ s^{-1}$

have been evidenced from pulse-radiolysis time-resolved microwave conductivity measurements [20]. Furthermore, the molecule has already been intensively studied as electron donor for OPV devices [22, 86].

Phthalocyanines are organic compounds closely related to porphyrins. The molecule forms coordination complexes with many metal atoms like copper (CuPc) or zinc (ZnPc). CuPc shows a very good stability even at high temperatures and shown its potential as a strongly absorbing donor molecule mainly in sublimated heterojunction photovoltaic devices [62].

2.6 Processing techniques for OPV devices

Two different concepts have been applied for the processing of organic materials. Both vacuum-sublimation and solution deposition are well established methods for the active layer deposition. Recently, there is also an increasing interest in a combination of both these processing techniques for the application of donor and acceptor molecules allowing to combine some of the individual advantages of both processing.

2.6.1 Vacuum sublimation

Vacuum sublimation of organic materials is a well established techniques known from light emitting OLED devices. Processing the active materials from the vapor phase allows the deposition of pristine, mixed and also multi-layered stacks with a precise control over individual composition and thickness of each layer. Commonly low atmospheric pressure and slow evaporation rates allow highly pure and ordered material deposition resulting in the growth of near defect free crystallites with high intrinsic charge carrier mobility [48]. Control over molecular stacking and film morphology can be gained by individually tuning deposition rate, substrate temperature and process pressure as well as by using more advanced vapor deposition schemes [12, 122].
Unfortunately, evaporation techniques are limited to small molecular weight and oligomeric compounds which can be sublimed and deposited from the vapor phase. Furthermore, the necessity of evacuation steps during the processing of the active materials may also delimit the throughput capabilities during device manufacture when compared to roll-to-roll fabrication schemes which are applicable for all solution deposited devices [9].

2.6.2 Solution processing

The possibility to process materials at atmospheric pressure and therefore with potentially very high throughput is probably one of the main advantages of solution deposition methods over the sublimation techniques mentioned above. Polymers, oligomeric compounds and small molecules which are soluble in organic solvents can be considered for solution deposition. On small laboratory scale commonly rotatory spin-coating techniques are used for the controlled layer deposition. For large scale application spray coating, dip-coating or doctor blading of the photoactive materials seems more appropriate. The morphology of a bulk heterojunction layer can be strongly influenced by choice of solvent, mixing ratio and concentration of the blended donor and acceptor materials [28].
Despite morphologically optimized and efficient donor-acceptor BHJ devices have already been manufactured using the above mentioned methods (see Section 2.8.1) the solution deposition of blend materials lacks direct and precise influence on molecular ordering and blend morphology. Post production annealing treatments, as discussed in the following (Section 2.6.3) are frequently used to influence and improve the morphology of blend devices.
Device architectures with a multi-layered stacking appear more challenging for active materials processed from the solution phase: a subsequent deposition of the active materials from orthogonal solvents has been used frequently [27, 123]. However, this application method commonly yields "stratified" and partly inter-penetrated morphologies rather than strictly bi-layered interfaces [123].
A drawback of several efficient laboratory OPV devices processed from the solution phase are their often low active layer thicknesses of $80 - 100$ nm - instead thicknesses of around 200 nm are necessary to guarantee defect free production in roll-to-roll coating techniques. Furthermore, ideal morphology and efficiency of many blend devices is presented using a deposition of materials *via* non-scalable techniques like rotatory spin-coating - an application technique unsuitable for large scale device manufacture.

2.6.3 Post-processing: demixing and molecular rearrangement

Most solution processed and some vapor deposited blend devices require post-processing treatments or the deposition at elevated substrate temperatures to yield best power conversion efficiency [124, 125]. The annealing treatment allows for the rearrangement of the organic blend materials after the solid phase has been formed. Several methods of thermal and solvent annealing have been discussed in the past and changes in

the blend morphology can be analyzed at different stages of this optimization procedure [102, 126, 127].
However, for a given donor-acceptor couple, the influence of such post production treatments on morphology is limited: One lacks a method to directly and precisely tune the size of the individual domains in the blended structure and also the intermixing at a molecular level can commonly not be altered [19]. Furthermore, the formation of isolated islands of donor or acceptor material can sometimes not be avoided [128]. As one lacks precise and direct influence, it also remains very difficult to study the impact of nanoscale phase separation in the active layer of blend devices on resulting device characteristics and performance in more detail [114, 128].
It is worth mentioning here, that the photophysical properties of liquid crystalline materials (as discussed in Section 2.3.3) can be affected very significantly by post-production annealing treatments. In fact, the self-assembly of LC materials can be used to drive an alignment into macroscopically sized domains with high supramolecular order and outstanding bulk material properties [85].

2.7 Loss mechanisms and degradation of devices

2.7.1 Recombination mechanisms

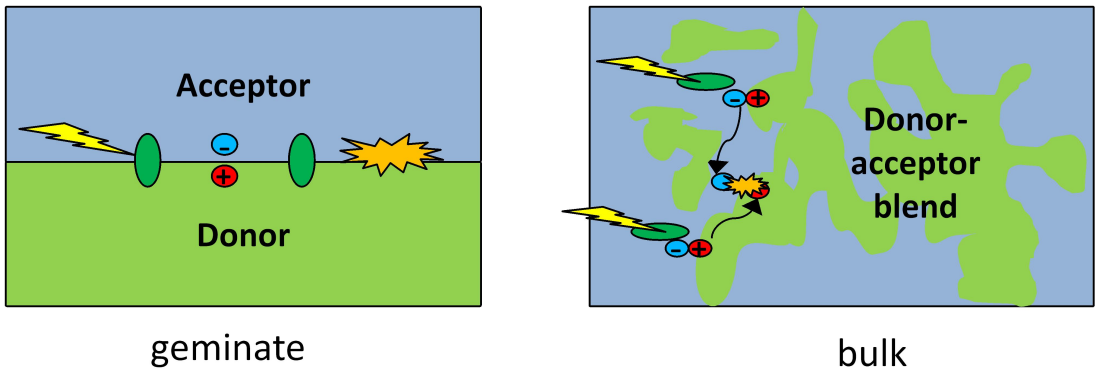

Figure 2.17: Recombination mechanisms for free charges in OPV devices. Mono-molecular and bi-molecular recombination of free charges are exemplarily shown for bi-layered and blend devices, respectively.

Analyzing and reducing recombination pathways present in organic photovoltaic devices can be very instructive to improving device efficiency: Not only the current generation but also fill factor and open circuit voltage may be strongly affected in devices where re-

combination loss plays a major role [58, 129]. As has been discussed previously (Section 2.2.2) the exciton binding energy can be overcome at the interface of organic donor and acceptor materials provided an appropriate offset in the energy levels. As a consequence exciton recombination can be minimized at the cost of a certain loss in maximum attainable open circuit potential.
After the formation of charged species at the interface of the donor and acceptor materials we can distinguish two distinct types of loss mechanisms: mono-molecular (geminate) and bi-molecular (bulk) recombination mechanisms may lead to charge carrier annihilation in the active layer of the photovoltaic device [58].
If mono-molecular recombination of electron-hole pairs is the only loss mechanism a strictly linear increase of current generation with increased incident light intensity is expected. This is commonly found to be the major loss mechanism in bi-layered and morphologically optimized blend devices at low to moderate light intensities [58]. On the contrary, free charges originating from different exciton separation processes may accumulate in the active layer of devices and subsequently recombine with one another. This non-geminate recombination occurs if charges are not efficiently extracted - a fact that can sometimes not be avoided in highly intermixed active layers, especially at high illumination intensities. A sub-linear increase in the current generation will be observed as a consequence. The common recombination routes are schematically shown in Figure 2.17.
When analyzing the continuous competition of charge separation and recombination in an OPV device under illumination it may be instructive to sketch a schematic energy level alignment as exemplarily shown in Figure 2.18: Possible charge carrier migration pathways after photo-excitation are indicated with arrows and termed in the figure caption. It is important to note, that the exact alignment of the energy levels which are shown only exemplarily in Figure 2.18 has a strong impact on the population of the individual states and thus the probability of charge separation at the interface after photo-excitation. A detailed analysis of this energy landscape has been conducted for several material combinations only recently and remains a hotly debated topic [51, 52, 130].
It is also important to mention here, that - besides the energetic landscape discussed - entropy plays an important role and helps to stabilize the charge separated state with two separated species (electron and hole) with respect to the single species of a charge transfer state (bound electron-hole pair).

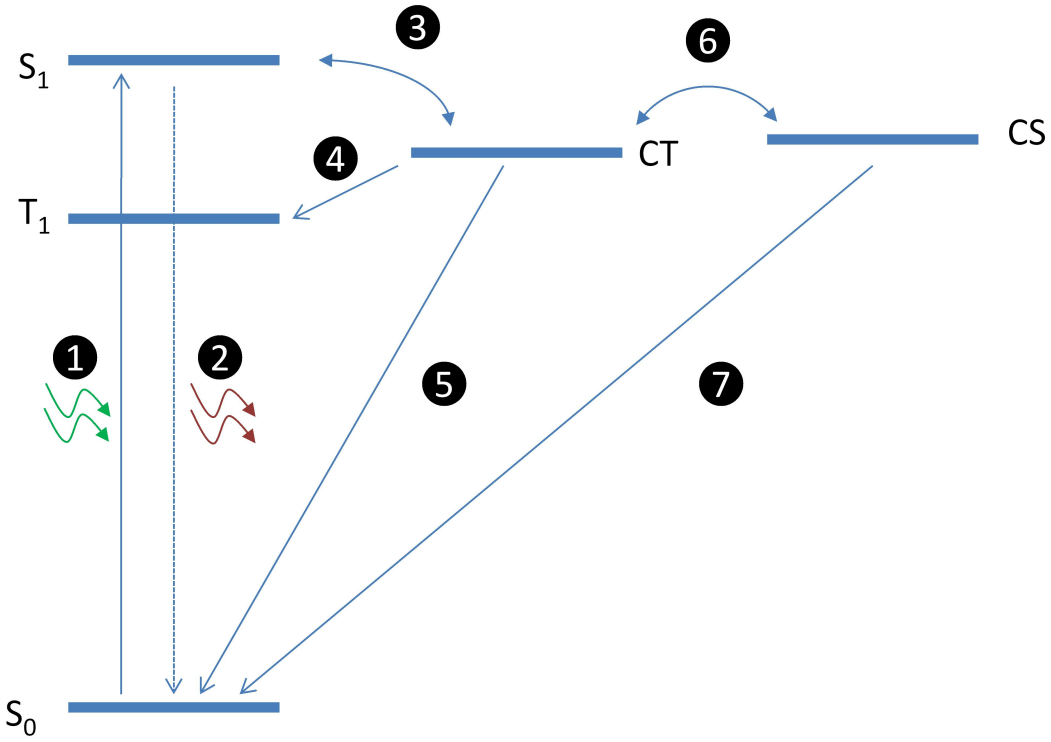

Figure 2.18: Schematic energy diagram of charge formation and recombination in organic donor-acceptor systems. After Photo-excitation (1) a singlet exciton (S_1) is formed. The singlet exciton can be transferred to a charge transfer (CT) state (2). Depending on the kinetics and energy level alignment the CT state may undergo geminate recombination to a triplet exciton (T_1) (3), relax to the singlet ground state (S_0) (4) or dissociate into separated charges (CS) (5). If charges are not extracted bimolecular recombination of separated charges may occur (6).

2.7.2 Up-scaling and stability of OPV devices

To allow commercial success of OPV devices not only the device efficiency but also applicability of fabrication processes for large scale production and lifetime of devices will have to be considered in greater detail in the future.
For solution processed devices deposition techniques such as spray coating and doctor-blading should therefore be chosen for the application of the organic materials rather than rotatory spin-coating. Time and cost intensive production steps involving high vacuum or even localized electron-beam lithography should be avoided, instead.
The device degradation is mainly caused by the exposure of organic compounds and contact materials to oxygen, water and strong illumination [131, 132]. However, temperature and mechanical stress can also significantly affect the device properties. Commonly devices are either fabricated and tested in an inert atmosphere or encapsulation

methods are used in order to avoid a direct exposure of the sensitive compounds to environmental conditions. On the other hand, resistivity of the organic compounds and contact materials to environmental conditions is of great importance to facilitate flexible and cost effective encapsulation methods and to improve the lifetime of devices. It is worth mentioning, that interfacial layers may also have a significant impact on the device lifetime [133]. For example, in "inverted devices" TiO_2 is used as transparent electrode with a low work function in combination with more noble metal top contacts. The reduced risk of contact oxidation allows the fabrication and storage of devices in ambient conditions even without device encapsulation [112, 134].

2.8 State of the art organic photovoltaic systems

In this section an overview to common donor-acceptor combinations for OPV deices is presented and individual advantages and drawbacks of the active material combinations are highlighted.

2.8.1 Polymer-fullerene blends

Solution processable blend mixtures of fullerenes with strongly absorbing polymers have repeatedly shown record efficiencies as active layer materials for OPV devices. For example, in the year 2001 a 2.5% power conversion efficiency was reported for a poly(para-phenylenevinylene) polymer (MDMO-PPV) in combination with the solubilized fullerene derivative [6,6]-penyl-C61 butyric acid methyl ester ($PC_{61}BM$) [135]. The blend mixtures of MDMO-PPV:$PC_{61}BM$ showed this high power conversion efficiency only when appropriate solvents were used for processing. A domain size in the order of several nanometers with bi-continuous pathways could be accomplished in these blend mixtures.
Similarly for blends of the polythiophene P3HT with $PC_{61}BM$ strongly morphology dependent efficiency values have been reported. In fact, highly optimized P3HT:$PC_{61}BM$ mixtures have shown certified efficiencies as high as 5% repeatedly [102, 136]. This material combination has dominated the sector of organic solar cell research during the last years [16]. Numerous studies have analyzed morphology, loss mechanisms, theoretical limitations and photophysical processes of these blend mixtures in great detail [16, 102].The theoretical maximum attainable current generation yield of a P3HT:$PC_{61}BM$ blend device has been calculated recently ($I_{SC}{}^{max}$=18.7 mA cm^{-2}); Instead, for a realistic layer thicknesses of $d \leq 400$ nm and assuming a realistic exciton separation efficiency

yield (IQE=80 %), the maximum attainable I_{SC} for these blend devices is significantly lower 11.5 mA cm^{-2} [16]. Experimental results have come very close to this theoretical value.

Several other types of polymers have been successfully used for the application in OPV devices in conjunction with $PC_{61}BM$. For example, polymers having donor-acceptor push-pull units like PCPDTBT show a lower HOMO-LUMO bandgap compared to P3HT resulting in an absorption onset shifted towards the near-IR region. As such, light absorption and photon harvesting can be accomplished over a wide spectral range and high short circuit currents of up to 15 mA/cm^2 have been shown in experimental studies [103].

Lately also other fullerene derivatives like $PC_{71}BM$ and Indene-$PC_{61}BM$ bisadducts have been studied in conjunction with several donor polymers [137, 138]. Better photon absorption and more suitable energy levels in conjunction with common polymers are believed to be the major reasons for improved device efficiencies using these molecules.

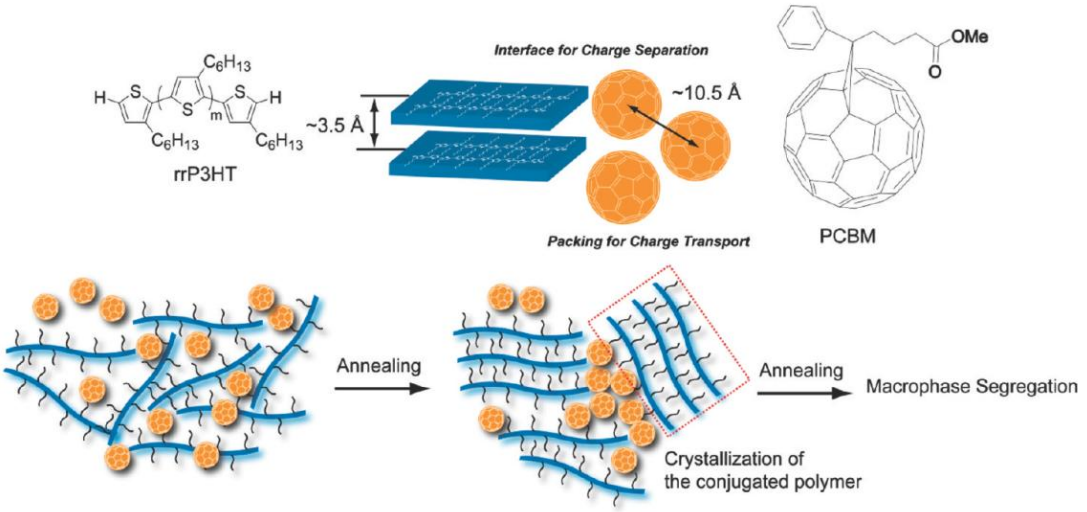

Figure 2.19: Schematic representation of a polymer-fullerene blend before and after annealing. The dimensions of fullerene molecules and the well studied donor-polymer P3HT are shown. Incompatibility in size allows the formation of bi-continuous networks after an annealing treatment. Reprinted with permission from [19] Copyright 2010 American Chemical Society.

Favorable properties of polymer-fullerene blends The common electron acceptor $PC_{61}BM$ shows outstanding electron conduction properties [110], suitable energy levels [11] and a long exciton diffusion length of about 40 nm [111]. Pristine and highly symmetric donor polymers like regio-regular P3HT (see Section 2.5.1) spun from so-

lution form crystalline phases and a layered stacking which allows high charge carrier mobility.
In fact, most important for the performance of the heterojunction device will be the interplay of both the polymer and the fullerene molecules in the active layer of the device. A high degree of intermixing of both donor and acceptor compounds is necessary for efficient exciton harvesting but has to be balanced by a certain degree of phase segregation between the materials to allow the extraction of the charges generated [128].
As cast films, obtained directly after solution deposition of the blended materials, are commonly not optimized for charge extraction. Charges may become trapped in the highly intermixed phases with no interconnection pathways.
However, post production treatments (e.g. thermal annealing, see Section 2.6.3) allow the formation of interconnected polymer networks within the blended material which may become filled with aggregates of the fullerene derivative. Figure 2.19 shows a schematic representation of the circular shaped fullerene molecules and the well studied donor polymer P3HT. A incompatibility in size and shape drives the formation of interconnected but well segregated domains throughout the annealing treatment. P3HT tends to assemble into highly ordered lamella sheets with a typical and characteristic layer spacing of $d = 3.5$ Å. Instead, the fullerene derivative tends to form clusters of nano-crystals with a molecular spacing of slightly more than 10 Å, which themselves are of appropriate size for exciton separation and exhibit high charge carrier mobility and good transport pathways [139].In summary, after annealing a high degree of donor-acceptor intermixing is maintained and percolation pathways are established allowing efficient extraction of charges [140].

Drawbacks and limitations of polymer-fullerene blends Record efficiency has been reported repeatedly for novel donor polymers blended with electron accepting fullerene derivatives. However, the material combination shows some intrinsic problems and some limitations apply for these photovoltaic devices.
Fullerenes, especially C_{60}-derivatives show only little absorbance in the visible wavelength range [141]. As such, best power conversion efficiency can commonly only be achieved when blending the fullerene with polymers showing a pronounced and wide-band photon absorption over the entire visible spectral range.
Furthermore, various polymers with appealing optical end electronic properties exhibit energy levels that are not ideal for a heterojunction with $PC_{61}BM$: in many cases a high offset of HOMO levels leads to a significant loss in the V_{OC} [11].
Another issue of several laboratory devices using polymer-fullerene blend mixtures con-

cerns the thickness of the devices. Peak efficiencies are reported frequently for an active layer thickness around or even below 100 nm [103, 142].Instead, an increased active layer thickness ($d \geq 200$ nm) is conductive for upscaling the device fabrication process2.7.2 and to reduce the risk of device shortening [143].
Furthermore, most known polymer-fullerene blends need post-processing treatments like thermal or solvent annealing in order to optimize the donor-acceptor morphology [103]. Long term stability and the operation under stress of differing environmental conditions might be critical for these devices. The morphology obtained after the specialized laboratory treatments used when high efficiency values are reported often differs from the entropically favored morphology. As such, decrease of device performance can often not be avoided when devices are used in ambient conditions. Furthermore, The influence on the exact blend morphology is only very limited - ideal inter-penetrating networks can often not be achieved and a certain degree of bi-molecular recombination can not be avoided [128].
After having seen tremendous improvements in the early years, the reports on new record efficiency values achieved for polymer-fullerene blends have become less frequent. Distinct concepts, e.g. using small molecular weight or oligomeric materials, vacuum processing techniques or more advanced processing techniques are drawing an increasing attention at present.

2.8.2 small-molecule and oligomer based devices

The use of oligomeric compounds or small molecular weight materials in the active layer of organic photovoltaic devices seems an appealing alternative to as an alternative to polymer-fullerene mixtures: Mono-dispersity, high purity and synthetic reproducibility can be guaranteed for the materials allowing deposition of thin films with undisturbed electronic properties [67]. Furthermore, the variability in material processing - both solution and evaporation deposition may be applied - provides an additional variability in device design and manufacture.

Solution processed small molecules A vast pool of small molecular weight donor and acceptor materials have been blended in the past to produce photovoltaic devices. Solution processable donor materials can be combined with fullerene derivatives or other other, commonly strongly absorbing acceptor materials [144]. For example, solution processable derivatives of the materials HBC and PDI (see Figure 2.16 and Figure 2.15) have been used in the active layer of OPV devices [22, 86]. More recently, diketopyropyroles [68] and squarine dyes have drawn much attention [145]: in conjunction with

a fullerene-based acceptor power conversion efficiencies of 4.4% and 5.2% have been obtained, respectively. Oligomeric and dendritic compounds have also been applied as active materials in blend devices with increasing success in the last years [125, 146].

Evaporated small molecules - bi-layers and mixed evaporation The first heterojunction photovoltaic device was based on a vacuum sublimated two layer system of small molecules [41]. Recent results have proven, that vacuum sublimation of small molecules and oligomers can very well compete with the performance obtained for solution processed polymer-fullerene bulk heterojunction solar cells: Using a strict bi-layered geometry the power conversion efficiency could be raised to over 4% [62] in the evaporated devices.
Co-evaporation and more advanced mixed evaporation techniques also seem appealing [147]. A record efficiency of over 5% and was achieved using co-evaporation of oligothiophenes and C_{60} [125]. Interestingly, a comparison using the same oligomeric merocyanine dyes in the active layer of either solution processed or evaporated devices shows a better performance for the sublimated devices [148].

2.8.3 Advanced heterojunction concepts - towards highly ordered and nanostructured devices

It has been shown only recently, that idealized interdigitated donor-acceptor structures could facilitate a significantly increased power conversion efficiency [74, 128]. Increased exciton separation, high charge carrier mobility and a reduced charge carrier recombination are expected for an optimum interdigitated heterojunction morphology as shown previously (Section 2.3.3).
Alternative and more sophisticated concepts to the solution processing of blends or the straightforward vacuum processing of bi-layered and co-evaporated devices are necessary to obtain these nanometer scaled and highly ordered architectures.
As an example, an interesting concept has been shown only recently by Matsuo et al.: a solution processed small molecule which can be in-solubilized and frozen into a desired morphology by thermal treatment is used as donor material [149]. A multi-step deposition process facilitates the formation of a three-layered structure with an intermixed phase sandwiched between pristine donor and acceptor materials at the respective electrodes.
More advanced concepts allow for the formation of highly ordered and precisely nanostructured organic layers. A method for the fabrication of such desirable interdigitated

structures relying on template assisted nano-imprinting will be shown herein (Chapter 6).

3 Experimental Concepts

This chapter gives a brief overview to both the materials and the experimental techniques used for the fabrication and subsequent analysis of organic films and photovoltaic devices.

3.1 Solar cell fabrication

3.1.1 Photoactive organic materials

HBC The hexa-*peri*-hexabenzocoronene (HBC) derivatives used in this thesis have been synthesized by Lukas Dössel and Akimitsu Narita at the Professor Müllen Group, Max Planck institute for polymer research, Mainz (MPIP). Synthesized compounds were analyzed by X-ray and differential scanning calorimetry (DSC) techniques. Chemical formula and specific properties of the HBC derivatives used herein will be presented along with the individual experiments.

PDI Perylene-diimide (PDI) has been obtained and used as recieved from Sensient technologies (ST 1/23) [150]. For transient absorption spectroscopy measurements the material has been purified by repetitive column chromatography.

PCPDTBT Poly [2,1,3-benzothiadiazole-4,7-diyl[4,4-bis(2-ethylhexyl) - 4H-cyclopenta-[2,1-b:3,4-b'] dithiophene-2,6-diyl]] - (PCPDTBT - ZZ50) has been obtained from Konarka technologies [6].

$PC_{61}BM$ Phenyl-C_{61}-butyric-methylester ($PC_{61}BM$) was obtained from Nano-C [151] and used as received.

CuPc Copper(II)-phthalocyanine (CuPc) was used as received from Sigma-Aldrich (purity 99.99%) [152] and sublimated onto devices.

3.1.2 Material processing

Solution processable molecules were commonly dissolved in chloroform and chlorobenzene solutions. Donor-acceptor blend solutions were stirred for several hours to allow a complete dissolution of the organic compounds. HBC:PDI blend mixtures were additionally filtered (PTFE, 45 µm pore) immediately before use to avoid the deposition of aggregated material. All solution processed organic layers were deposited by spin coating (using variable rotatory speed of $700 - 2000$ rpm), resulting in homogeneous organic thin films.

Vacuum deposition of organic compounds The vacuum sublimation of organic materials has been carried out by Christian Hundschell and Christoph Schaffer in the Dr Nickel group, LMU University Munich, using an organic thin film deposition chamber. Defined process parameters are set allowing the growth of high-purity layers ($p_0 \leq 1 * 10^{-7}$ mBar, sublimation rate $S < 1$ Å/min). For some experiments material was deposited on heated substrates ($T_{Substrate} \approx 70$ °C).

3.1.3 Device design

Organic photovoltaic devices were fabricated on indium tin oxide (ITO) coated glass substrates pre-cut to 14×14 mm^2 obtained from *Kintec technologies* [153] and *Präzisions Glas & Optik GmbH* [154]. A 3 mm thin stripe of ITO is removed at one side of the substrates. The ITO removal allows facial contacting of the individual photoactive pixels with spring loaded contact-pins and avoids shortening the devices in the contact area.
ITO substrates were cleaned by ultrasonication in detergent saturated water, acetone and subsequently isopropyl alcohol baths for 15 minutes each. In order to avoid contaminations caused by remaining carbon residues at the surface and to increase the hydrophilicity of the substrates an O_2 plasma cleaning step was carried out before the deposition of organic materials.
After deposition of the active layer via vacuum sublimation and/or solution processing metal top contacts are deposited by sputter coating or vacuum sublimation using a patterned shadow mask. Figure 3.1 shows a schematic representation of resulting devices. On each glass substrate three individual sub-cells are realized. In the following the three photoactive pixels will be referenced as: Pixel **L** (left), Pixel **M** (middle) and Pixel **R** (right).
The size of each pixel is defined by the dimensions of the patterned shadow mask

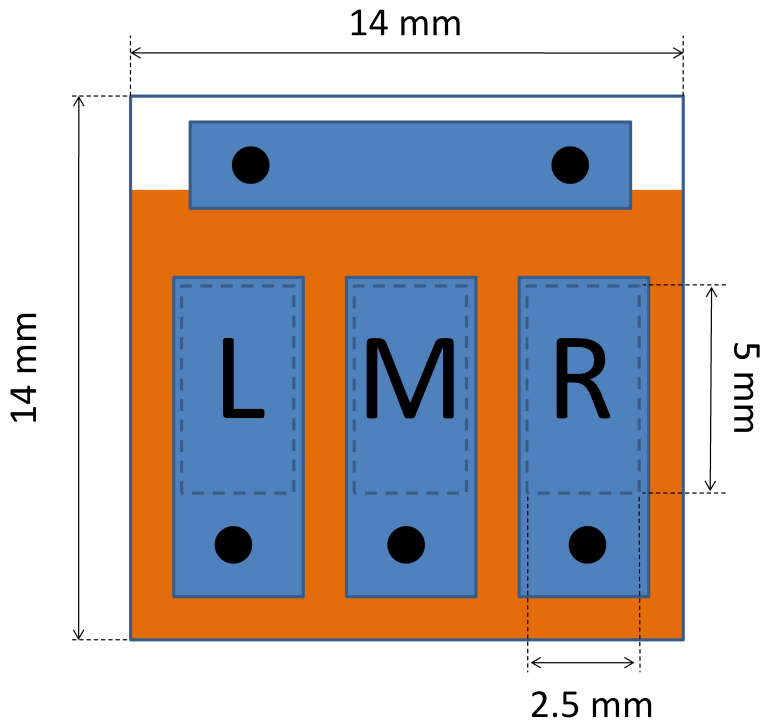

Figure 3.1: Layout used for the fabrication of OPV devices. Three individual pixels with an illuminated and photoactive area of $2.5 \times 5\ \mathrm{mm}^2$ are realized on each substrate as indicated with the dashed lines. The contacting of the ITO electrode is accomplished using a common metal contact for all three pixels.

$(3 \times 6\ \mathrm{mm}^2)$, resulting in an active cell area of about $A_{pixel} \approx 0.18\ \mathrm{cm}^2$; A slightly smaller shadow mask matching up with the individual pixels is used for all photoelectrical characterization experiments. This mask precisely defines the illuminated photoactive area of $A_{photoactive} = 2.5 \times 5\ \mathrm{mm}^2$. the exact dimensions of the resulting photoactive area was probed by optical microscopy measurements confirming $A_{photoactive} = 0.125 \pm 0.005\ \mathrm{cm}^2$.

3.1.4 Normal and inverted device geometry

Organic photovoltaic devices are based on an active layer (composed of donor and acceptor materials) sandwiched between bottom and top electrodes. The most straightforward method to achieve charge separation is using an ITO glass substrate serving as transparent bottom electrode and a metal contact with an appropriate work function as top contact. This geometry will be further referenced as *normal device geometry*.

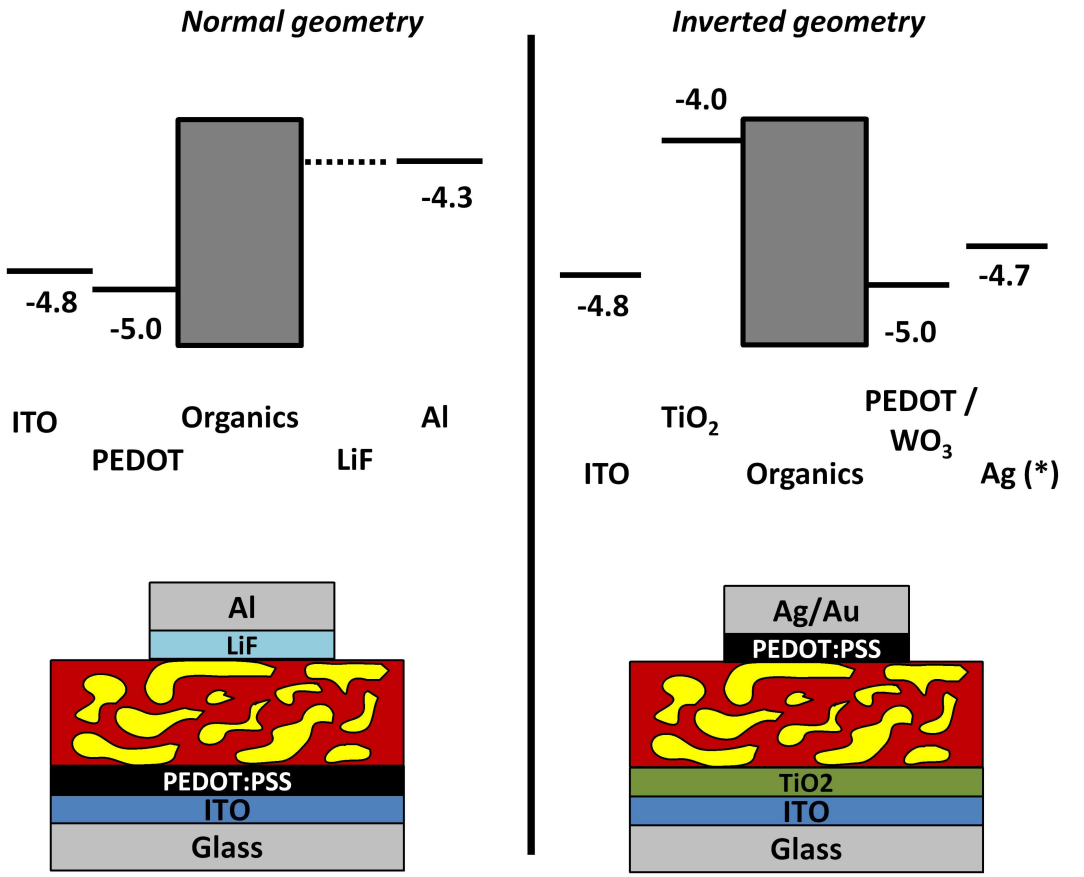

Figure 3.2: Normal and inverted device structure of OPV devices Energy level alignment and schematic view show both device geometries in comparison. Energy levels of interface and contact materials as further described in the text. (*) The energy level reported for Ag is based on measurements in ambient atmosphere.

Commonly aluminum is used as metal top contact making this layout highly sensitive to the exposure of oxygen. The rapid oxidation of aluminum causes a degradation of the contact.

An opposite direction of charge extraction is achieved for the *inverted device geometry*. In this case the transparent electrode serves as electron collector and holes are extracted at the reflecting back contact (see also Figure 3.2). The main advantage of the inverted geometry is a potentially higher air stability due to the usage of noble metals such as silver or gold as top contact. Several devices analyzed in the following chapters have been fabricated in the inverted device geometry and their performance other important parameters were monitored when exposed to air [112, 134]. The reduced degradation of the metal contacts upon air-exposure allows investigations on non-encapsulated devices

over periods of multiple days. As such, it became possible to conduct measurements of the device physics also outside of a glovebox compartment filled with an inert gas.
Another aspect speaking in favor of this device geometry is the possibility to allow for a vacuum free device production, when both top and bottom contacts are applied by printing techniques [9, 124, 155]. This is an important step towards upscaling and roll-to-roll processing of devices.
Different contact materials and/or interlayers are needed to provide ohmic contacts and a unhampered extraction of the charge carriers in the different geometries as will be further explained below (Section 3.1.5).
It is worth mentioning here, that vertical concentration gradients of material composition in the donor-acceptor blends should also be carefully considered as charge extraction pathways are altered when using different device geometries [22].

3.1.5 Contact and interface materials

Contact materials For all studies presented herein ITO was used as transparent conductive electrode. Metal top contacts Al, Ag and Au are evaporated at a rate of $S = 0.1 - 1$ Å/s and low process pressure ($P_0 \approx 10^{-6}$ mbar). For some studies Ag or Au electrodes were sputtered using a table top sputter deposition system (*Emitech K575X*).

Interface materials Interface materials are often used between the active layer and the external contacts of the devices. These additional layers serve for a number of properties and can severely influence the functionality and performance of the photovoltaic device [93, 156]. In summary, an interface material should:

- Allow for ohmic contacts between organics and electrode contact providing a suitable work function
- Show exciton blocking properties
- Exhibit selectively electron or hole blocking properties
- Serve as an optical spacer
- Reduce the surface roughness of the underlying layer

Table 3.1 gives an overview to the fermi levels of the contact materials as well as the conduction level of the interface modifiers used for the experimental studies of this thesis.

Material	Fermi level / conduction band [eV]	Reference
ITO	-4.8	[98]
PEDOT:PSS	-5.0	[98]
TiO_2	-4.0	[157]
WO_3	-4.8	[158]
Al	-4.3	[98]
Ag	-4.7 - -4.5	[159]

Table 3.1: Contact materials and interface modifiers used for the fabrication of organic photovoltaic devices.

TiO_2 layer deposition In order to modify the work function of the transparent electrode for the production of inverted devices a TiO_2 layer was deposited onto the ITO substrates.
Ideally the TiO_2 layer should provide a thin but dense layer showing only little light absorption but avoiding migration of excitons generated in the active layer to the cathode of the device. Furthermore, electron injecting and hole blocking properties are desired to minimize contact recombination. Last, a smooth and hydrophilic surface is wanted facilitating the application of subsequent solution deposited layers.
Several deposition methods of TiO_2 layers and their respective benefits and shortcomings have been analyzed in photovoltaic devices. In collaboration with the Professor Driscoll group, department of materials science and metallurgy, Cambridge, UK and the Professor Scheu group, department of chemistry, LMU Munich, Germany several different TiO_2 blocking layers were analyzed and their benefits and drawbacks for OPV devices tested: Layers processed by means of spray pyrolysis and sputter coating have been compared to other deposition methods, namely atomic layer deposition (ALD) and electro-deposition fabricated by the Driscoll group [160].
For the fabrication of spray deposited layers a diisopropoxytitanium bis(acetylacetonate) precursor solution diluted 1:10 in isopropyl alcohol is used. Spray deposition is performed at 450 °C yielding a final TiO_2 layer thickness of about 150 nm. Sputtering of TiO_2 was performed at 400 °C at precisely defined conditions (base pressure: $\approx 1 \cdot 10^{-8}$ mbar, argon flow $6.7 \cdot 10^{-3}$ mbar, 200 W DC sputtering). Substrates with a final TiO_2 layer thickness of $30 - 40$ nm were annealed (450 °C) on air for 30 minutes in order to heal oxygen defects.

PEDOT:PSS application The commercially available highly conductive doped aqueous polymer solution "PEDOT:PSS Al P 4083" [161] was applied in both normal and

inverted device geometries at the device anode. This solution processable material is applied by spin-coating and used to avoid contact recombination at the metal electrode. Furthermore this highly conductive hole blocking material may allow flattening the surface roughness of the underlying ITO or organic layers. For the application in an inverted device geometry - on top of the organic materials - a modification of the precursor solution and application via a dispersion head are mandatory as we have further summarized in a recent publication [112]. In brief, aqueous PEDOT:PSS is mixed 1:10 with isopropyl alcohol and applied onto the active layer. The sample is mounted on a spin coating device and abundantly sprayed with the diluted solution of PEDOT:PSS using a glass nozzle. Immediately after wetting the sample is spun at 600 rpm yielding a homogeneous layer of PEDOT:PSS. Resulting thickness of the PEDOT:PSS can thus be easily varied using different spin speeds. Deposition of PEDOT:PSS via spray-coating before spinning is necessary to yield homogeneous films [162]. The films are dried on air to guarantee ohmic contacts. It is worth mentioning, that in this geometry optical spacer effects of the PEDOT:PSS layer should be considered, also [156].

Lithium Fluoride (LiF) has been used widely as a contact interface material in organic light emitting devices [163]. The material has also proven to be beneficial for the application in OPV, especially at the interface of the organic and Al metal contact [164]. The extremely thin layers of LiF commonly used (0.7 nm) will not provide complete surface coverage. In fact, the beneficial effect of the LiF is believed to be related to dipole effects inducing changes in the work function of adjacent top contact materials and due to doping effects of Lithium cations of organic material [164]. Furthermore, it has been shown that LiF may limit oxygen diffusion into the organic layers [165] .

Tungsten oxide (WO_3) may be used as interfacial layer at the anode of the OPV device. Due to its high work function of -4.8 eV the blocking layer can be used to extract holes but suppress electron and exciton migration through the organic-metal interface in inverted photovoltaic devices [158].

3.2 Experimental characterization techniques

This section will give a short overview to the setups and analysis methods used for the characterization of OPV devices. Software modules have been developed for the automated data acquisition and graphical representation which allow the visualization

and real time analysis of the experimental data (snapshots of the programs are presented in Section 8 - Appendix A).

3.2.1 Diode characteristics

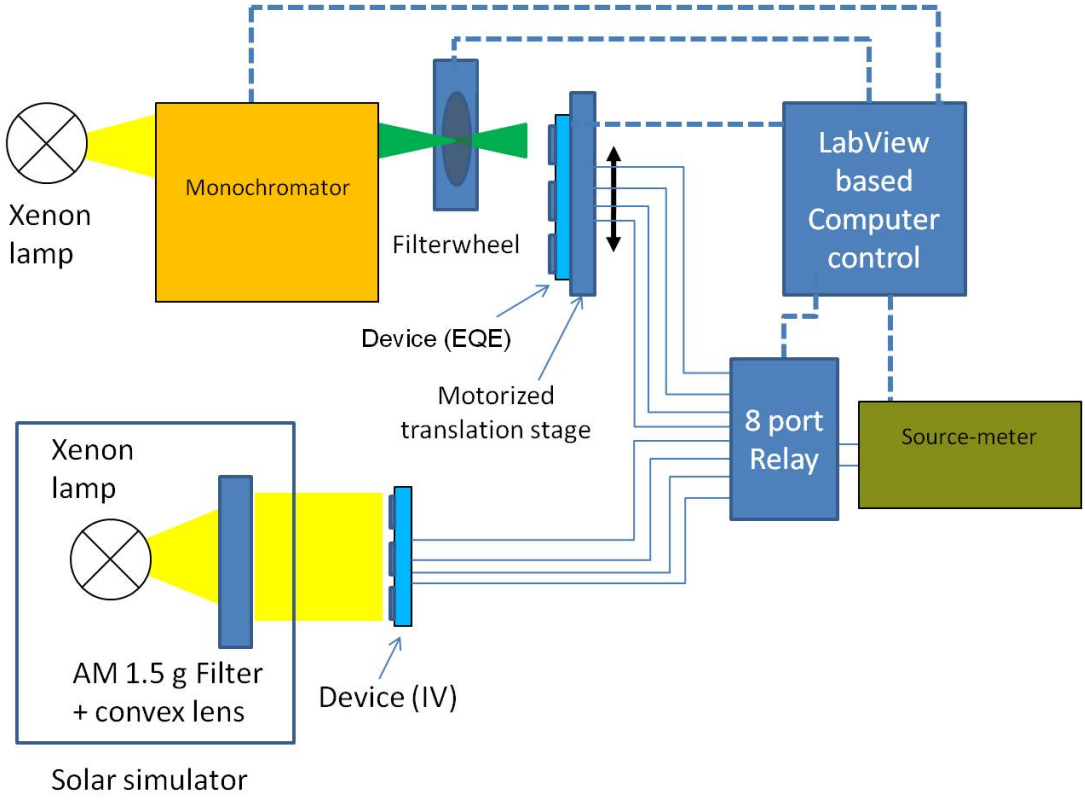

Figure 3.3: Combined IV- and EQE-measurement setup. Characterization of devices is accomplished using a fully computer controlled characterization setup.

The electrical characterization of the photovoltaic devices is performed using self-made characterization setup. A 150 W *LOT Oriel* solar simulator was used to illuminate the photovoltaic devices with continuous white-light well matching the $AM1.5g$ standard measurement conditions [45]. Voltage bias and current measurements are applied using a *Keithley* 2400 *Sourcemeter*. The setup is frequently re-calibrated using a certified silicon solar cell (*Fraunhofer ISE WPVS Cell*) equipped with a $KG5$ band-pass filter to minimize errors caused by the spectral mismatch of silicon and organic photovoltaic devices [45]. A secondary silicon diode equipped with a similar filter glass is used for everyday calibration purpose (Hamamatsu S1226-8BK).
A *LabView* program was developed to automatically sweep current-voltage curves of

the photovoltaic devices. The features of the program include a live-view function, automatic determination of solar cell characteristics and control of a relay hardware unit. The interface allows to switch the electrical connections and automatically record all pixels assembled on the specimen as is schematically visualized in Figure 3.3. A more detailed description of the program and its functionality can be found in the Appendix (Section 8.1.1).

Intensity dependent IV

A combination of two six-position filter-wheels was equipped with a series of ND filters and used to attenuate the incident simulated solar light radiation of a 150 W solar simulator. Using the silicon reference diode system described (see Section 3.2.1) the light intensity incident to the sample can be recorded for all filter combinations and automated device measurement cycles can be performed with up to 36 different illumination intensities. Automated control of the filter-wheels is also integrated to the program *"Solar Cell Test Station"* (Section 8.1.1). The intensity dependent IV curves may help to distinguish geminate and bulk recombination mechanisms (see Section 2.7.1).

Temperature dependent IV

An Oxford Instruments cryogenics setup (Cryogenic finger: *Optistat DN-V*, Controller: *ITC503S*) has been equipped with a device mounting stage and a software control panel integrated to the LabView based "Solar Cell Test Station" program to allow for acquisition of temperature dependent IV curves (see Section 8.1.1). The hardware allows to keep the sample at defined and constant temperatures in the range of $77 - 370$ K under inert atmosphere while performing (illumination intensity dependent) IV-curves. The temperature dependence of conductivity and mobility in organic molecular solids can give important insight to the hopping properties in OPV devices [166, p.219].

3.2.2 External quantum efficiency

The external quantum efficiency (EQE), often also referred to as incident photon to current efficiency (IPCE), gives insight to the spectral response of a photovoltaic device. As shown in equation 3.1 the EQE is the fraction of photons that are converted into electrons extracted from the device at a specific wavelength of incident illumination.
For the EQE measurements presented here a self-made setup was assembled (see Figure 3.3): A 150 W xenon lamp is focused into a 150 mm grating monochromator (*LOT*

omni 150) and the spectrally resolved light collimated onto the photo-active area of the devices. A motorized filter wheel equipped with a set of cut-off filters is mounted in the beam path to minimize sample radiation by second harmonics passing the grating monochromator. In order to determine the spectrally resolved lamp intensity incident to the sample a calibration scan is conducted using a photovoltaic cell with known spectral response (Fraunhofer ISE *WPVS Cell*). Using this lamp spectrum, the spectral response (SR_λ) of a sample device can be determined. For user friendly handling the setup is equipped with a motorized translation stage (Thorlabs PT1-Z7) allowing the computer controlled automated measurement of all three pixels realized on one device. The setup was calibrated to yield an illumination power of about $P_{incident} = 0.3\,\mathrm{mW/cm^2}$ at 490 nm with a slit with corresponding to a FWHM of circa 5 nm. The spectral response measurement system provides several additional features such as integrated SR_λ to EQE conversion and calculation of the estimated short circuit current yield at an $AM1.5g$ radiation profile.

$$EQE = \frac{Q/e}{P_\lambda/E_{Photon}} \tag{3.1}$$

$$EQE(\%) \approx 1240\frac{SR_\lambda}{\lambda}(\mathrm{Wnm/A}) \tag{3.2}$$

3.2.3 Time resolved charge extraction techniques

Transient photovoltage decay (PVD)

Transient photovoltage decay (PVD) measurements allow the time resolved analysis of charge carrier recombination in photovoltaic devices under working conditions [167, 168]: A white light source is used to bias the photovoltaic device generating a constant open circuit potential. Pulsed laser light is used to excite additional charge carriers in the device resulting in an increase in device potential (as is further explained in Section 2.4.2). After the laser stroke charge recombination results in a decay of the potential back to open ciruit conditions which is monitored using a digital oscilloscope. Figure 3.4 shows the assembly of the components including exemplary decay curves. Typical time scales for the voltage decay are in the order of multiple microseconds.
Sample irradiation is accomplished using a LOT-Oriel LS0106 solar simulator equipped with an *AM 1.5g* solar spectrum filter yielding an illumination intensity of approximately 50 $\mathrm{mW/cm^2}$. The illumination is superimposed with a pulsed laser (532 nm,

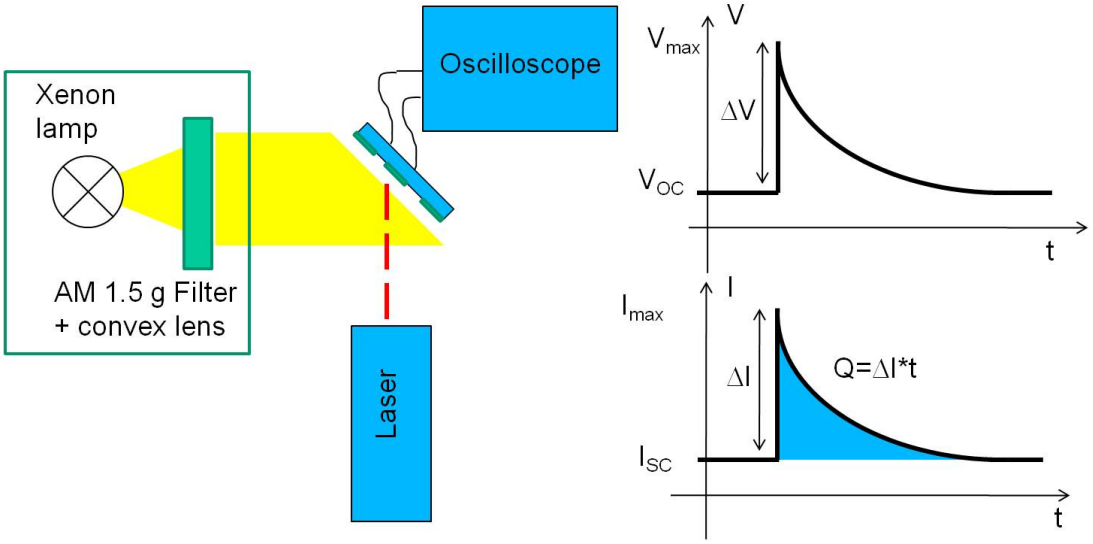

Figure 3.4: Transient photovoltage/photocurrent decay measurement setup. The schematic drawing shows the main components of the setup and an exemplary trajectory recorded.

pulse frequency 10 Hz, pulse energy $1 - 10$ µJ, pulse duration ≈ 4 ns). The changes in the potential between top and bottom contact of the photovoltaic devices caused by the additional laser pulses are monitored using a digital oscilloscope (Tekscope DPO 7254) with a termination resistance of 1 MΩ. Data obtained is commonly averaged over 100 transient decay events.

The decay process can be described using a bi-exponential function,

$$\mathrm{V_{Bias}} = \mathrm{A_{fast}} \mathrm{e}^{-\mathrm{k_{fast}} \mathrm{t}} + \mathrm{A_{slow}} \mathrm{e}^{-\mathrm{k_{slow}} \mathrm{t}} \tag{3.3}$$

with decay rates $\mathrm{k_{fast}}$ and $\mathrm{k_{slow}}$ differing by about one order of magnitude and respective constants A_{fast} and A_{slow}. Investigations at different laser pulse intensities have shown that $\mathrm{k_{fast}}$ strongly depends on the perturbing light intensity and does not reveal blend specific properties [169]. The slow decay rate instead gives insight to the material specific non-geminate recombination present in the photovoltaic devices: For solar cells under working conditions an e^{-1} lifetime of charges can be estimated from the decay rate as

$$\tau_{1/\mathrm{e}} = \mathrm{k}_{\mathrm{slow}}^{-1}. \tag{3.4}$$

Transient photocurrent decay (PCD)

Similar to PVD measurements for photocurrent decay (PCD) analysis solar cells are excited by pulsed laser irradiation. Time dependent current characteristics are recorded at an potential drop over the 50 Ω termination of the oscilloscope yielding quasi-short circuit conditions.
The amount of additionally generated charges induced by the laser pulse can be estimated at $\Delta Q = \Delta I \cdot \Delta t$ from the transient data obtained. Furthermore, using a combination of PVD and PCD measurements insight to the chemical capacitance C_{chem} may be obtained [167]:

$$C_{chem} = \frac{\Delta Q}{\Delta V}. \tag{3.5}$$

Transient photocurrents were calculated from the potential drop over the 50 Ω termination resistance of the oscilloscope. The RC constant of the system was estimated to be $\tau = RC \approx 150$ ns assuming a geometrical capacitance of $C_{geo} \approx 3$ nF. Photocurrent decay signals depend strongly on the laser intensity used. Furthermore, photocurrent generation induced by layer excitation and white light background illumination vary for different solar cells, especially in the case of non equal short circuit currents (I_{SC}). For the experimental studies presented herein two types of PCD measurements were conducted: In the first case the laser energy is kept constant resulting in the same perturbation intensity but in different photocurrent peak values. For the second type of PCD experiments the laser energy was adjusted each device to yield similar peak photocurrents for all samples. For all experiments the laser excitation energy was chosen to be low in order to minimize non-linear effects.

Charge carrier mobility analysis and the Photo-CELIV method

Improvement of charge carrier mobility μ in organic semiconducting films is of great importance for the development of more efficient OPV devices [58]. Several techniques are known to analyze both electron and hole mobility in organic thin films: Field effect transistors allow the determination of μ parallel to the substrate plane [12, 20]. Time of flight measurements give insight to the mobility obtained for organic films in the sandwich geometry [170]. However, this technique is limited to application in rather thick organic layers (necessity of strong photon absorption within a fraction of the sample thickness - commonly $d \geq 1$ µm).

Photo-CELIV is an analysis technique that allows to determine the transport properties

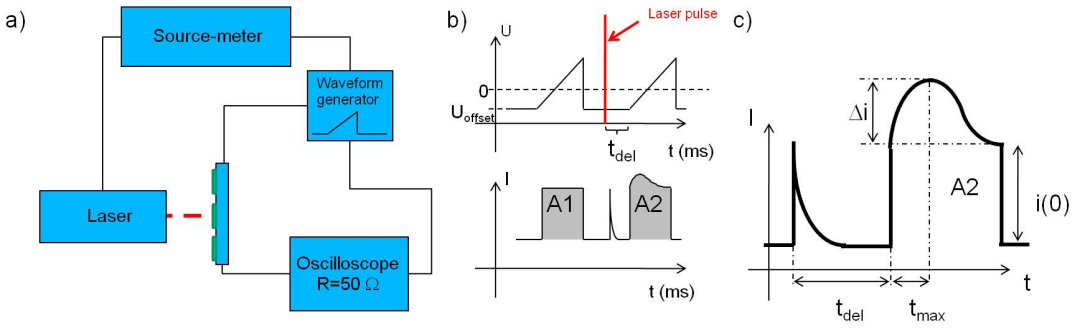

Figure 3.5: Photo-CELIV setup and signal analysis. a) A schematic representation of the components.**b)** Laser pulse, voltage sweep and current response of the photovoltaic device shown versus time axis. The shaded area (A1) reflects the initial capacitative response of the device. Additional charges are extracted upon voltage sweep after laser excitation (A2). The inset **c)** shows a magnification of the extraction signal after a laser excitation.

directly on photovoltaic devices: The solar cell is exposed to a short laser pulse prior to a voltage sweep allowing for the collection of photo-generated charges [171]. This charge extraction technique allows to investigate charge carrier mobility and gives valuable information on the recombination kinetics of the device [172].

A linear voltage sweep is applied in reverse bias to the photovoltaic devices [173] and charges generated by the laser light can be extracted at a defined delay time t_{del}. In Figure 3.5 both assembly of the components and the typical device response to laser pulse and voltage sweep are shown. In the steady state condition a compensation voltage is applied to the device using the waveform generator which prevents charges from exiting the device via the external contacts. The laser light generates free charge carriers in the device that may either recombine or become extracted through the subsequent voltage sweep. Using the characteristic parameters as shown in Figure 3.5 **c)** one can determine the mobility of the active layer of a photovoltaic device [171]:

$$\mu \approx \frac{2d^2}{3At_{max}^2\left[1+0.36\frac{\Delta i}{i(0)}\right]} \tag{3.6}$$

Furthermore, it is possible to calculate the charge carrier density in the device under investigation with respect to the laser delay time. As such, the recombination kinetics of the active layer can be analyzed based on the experimental data.

3.2.4 Morphological characterization

Both bulk (X-ray) and surface morphology (SEM, AFM) studies have been performed on several devices to investigate the morphology of various samples. The combination of these distinct morphology characterization tools allows to gain insight on both local and macroscopic features of the specimens.

Scanning electron microscopy

The surface morphology of several organic and metal-oxide films was analyzed using scanning electron microscopy (SEM) techniques: A beam of highly accelerated electrons is used to scan over the specimen and generates secondary electrons, light emission and characteristic x-rays upon interaction with the specimen. Back-scattered electrons or secondary electrons were recorded using a set of specialized detectors. Resulting images contain information on the topography and electrical conductivity of the specimen scanned. High magnifications and a large depth of field are characteristic features of state of the art SEM systems.
Both a *LEO FE-REM DSM 982* and a *Zeiss Ultra* scanning electron microscope were used for imaging. Cross section and top surface characterization were performed at $2-8$ kV acceleration voltage with a working distance of $1-10$ mm. For cross section imaging samples were perforated and cooled in a liquid N_2 bath to avoid disruption of the organic material near the break line. About 1 nm of Au was sputtered onto the specimens to reduce charging effects. Surfaces of organic material were commonly scanned with no further modification (no Au/Cr sputtering) in order to visualize the morphology of the organic layers only.

Atomic force microscopy

Scanning atomic force microscopy allows to raster the surface of a specimen using a cantilever needle and a piezo-electric stage. A laser is focused onto the rear side of the cantilever and the reflected signal is recorded using a four element photo-detector. In tapping mode atomic force microscopy the cantilever is oscillating at a certain drive frequency. Slight changes in the oscillation are recorded using the photo-diode reflecting an interaction of cantilever tip and specimen. Using this technique it is possible to obtain topographical images in the nanometer to micrometer length scale of the sample surface. The root mean square (RMS) is a characteristic measure for the surface

roughness of a sample being defined as:

$$RMS = \sqrt{\sum_i (x_i - \langle x \rangle)^2 / n}. \tag{3.7}$$

Where x_i indicates the height value obtained at data point i and n the number of points measured. AFM images were taken in tapping mode giving insight to topological features of both organic and metal oxide thin films. *Veeco instruments Inova* and *Veeco instruments Dimension 3100* scanning probe microscopes were used for the investigations and equipped with *Tap300Al* cantilever tips (resonance frequency f_R =200 − 500 kHz; force constant $40N/m$).
Image analysis including calculation of RMS roughness values were performed using the open source image analysis tools *Gwyddion* and *ImageJ*.

X-Ray investigations

X-ray scans were used to investigate packing of molecules and molecular alignment in several thin film samples and in extruded material. The high energy photons used for the x-ray investigations presented herein originate from a x-ray tube: Electrons are emitted from a hot cathode and accelerated in a vacuum tube to imping on a metal target where x-ray radiation is formed. The low wavelength radiation is scattered at the specimen and resulting interference patterns can be recoded by a photon detector. The scattering of x-ray on a crystal lattice can be described using Braggs law [174, p.12]:

$$m\lambda = 2dsin(\theta) \quad m = 1, 2, ... \tag{3.8}$$

Scattering patterns obtained contain information about the geometrical constants of the sample via Fourier transformation - For a more detailed analysis of scattering patterns and intensity it is therefore often useful to calculate expected scattering positions in reciprocal space.
For investigations on molecular packing and alignment of HBC molecules two dimensional wide angle x-ray (2D-WAXS) scans were performed on extruded samples in the group of Professor K. Müllen.
Further x-ray diffraction measurements were performed using a four-circle diffractometer in the group of PD Dr Nickel. A Ge (111) monochromatized MoK$_\alpha$ beam (λ = 0.71 Å) from a sealed-tube generator (900 W) was used as radiation source. The

diffraction curves were recorded by a scintillation detector. Exposure times were varied between 1 to 24 h.

3.2.5 Optical characterization

Spectroscopic measurements have been conducted on thin organic films deposited on quartz glass samples (ITOS, Suprasil, Grade II) and ITO coated substrates (pgo, $< 20\Omega/cm^2$) .

Absorption measurements

Absorption of thin organic layers was measured using an *Agilent Technologies 8453* UV-visible spectroscopy system. The transmission of CW-light (xenon and deuterium lamps) through thin films deposited on the substrates is spectrally resolved by a prism and recorded using a diode array. In a first approximation we can use Lambert-Beers law to correlate sample thickness with the wavelength dependent transmission of the sample:

$$\mathrm{I}(\lambda) = \mathrm{I}_0(\Lambda)\mathrm{e}^{-\mathrm{OD}} = \mathrm{I}_0(\lambda)\mathrm{e}^{-\alpha \mathrm{d}} \tag{3.9}$$

With OD as optical density and d being the thickness of the absorptive sample. As such, the absorption coefficient α gives an insight to how strong incident light will be absorbed by the media. It is worth mentioning here, that for the sample geometry used here attenuation of light can also occur due to scattering effects which might lead to an overestimation of the absorptivity of thin film samples. Furthermore, thin film interference effects might considerably influence absorption spectra, especially if sample absorption is low. Therefore, the UV-vis analysis method presented here shall not be used directly for quantitative comparison.

Polarized optical microscopy

Optical microscopy using polarized light allows to analyze the birefringence of a specimen: Linearly polarized light generated by a combination of a xenon lamp with a linear polarizer is incident to the sample (as shown in Figure 3.6. At the *analyzer* - a second polarizing film perpendicularly oriented to the first one all this light will be fully attenuated. However, if a birefringent film is placed between polarizer and analyzer with

its optical axis out-of-plane to the light propagation direction the polarization of the light is turned and light may pass the apparatus. For polaritzed optical microscopy investigation in this thesis samples were tilted ($\alpha \approx 30°$, as shown in Figure 3.6) and rotated under crossed polarizers and resulting images recorded using a digital camera. Figure 3.6 shows a simplified schematic of the radiation pathway between crossed polarizers as they are used for polarized optical microscopy (POM).

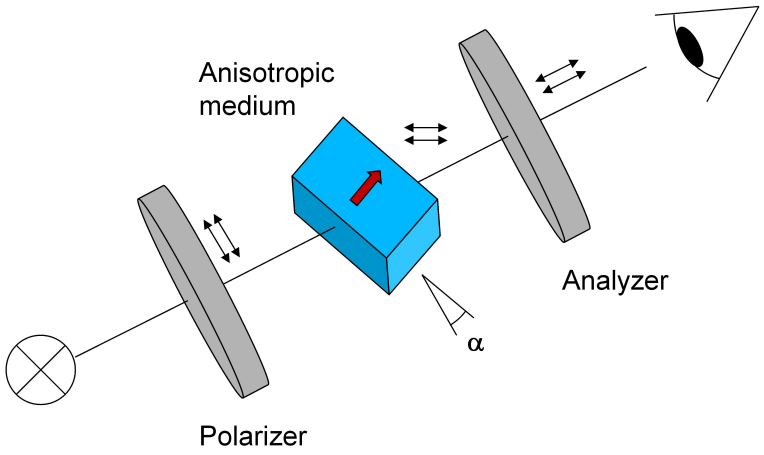

Figure 3.6: Schematic drawing of a birefringence analysis setup. Polarizer and Analyzer are kept perpendicular whilst the sample is turned and tilted on a rotatory stage. The

Photoluminescence analysis

Photons absorbed by organic material may become re-emitted with a certain time shift. Commonly this photoluminescence (PL) signal is found at a similar or lower wavelength (red shifted) compared to the sample radiation which indicates energy dissipation in the form of phonons.
When analyzing the active layer of photovoltaic devices *PL quenching* can often be observed: The radiation of a specific donor or acceptor material may become strongly reduced, when a heterojunction is formed by addition of an organic counterpart. Excitons diffusing to the interface become separated followed by other forms of energy dissipation rather than directly re-emitting their energy in form of a photon.
Steady-state PL measurements have been conducted on various samples using a *Horiba Yvon Fluorolog* PL spectrometer equipped with a 500 W halogen lamp (shown in Figure 3.7). Two grating monochromators allow to independently scan excitation (PLE) and emission (PL) wavelengths. Signals are detected using a water cooled Si detector.

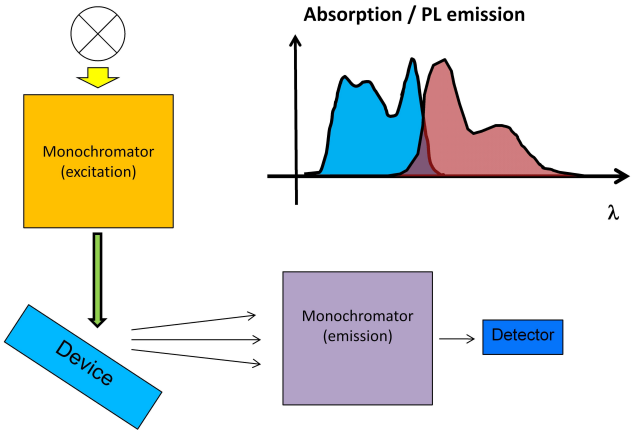

Figure 3.7: Steady-state photoluminescence setup. Photoluminescence excitation (PLE) and photoluminescence emission (PL) spectra are recorded using the two-monochromator setup. The inset graph shows a sketch of a red-shifted PL-spectrum along with an exemplary absorption spectrum.

3.2.6 Transient absorption spectroscopy

Transient absorption (TA), also referenced as photo-induced absorption (PIA), is a powerful pump-probe technique that allows to analyze excited states in organic semiconductors [52]. Using this technique it is possible to detect short lived (in the order of ps to ms) transient species which are formed after photo-excitation of the sample. Both time and wavelength resolved signals can be obtained and their analysis allows to gain insight to the charge separation and charge recombination processes occurring in the active layer of OPV devices [52, 175].
Figure 3.8 shows a schematic representation of the nanosecond TA setup which has been used for the analysis of organic materials. Both ground state bleaching (a decrease in absorption) and additional absorption generated by excited states after a laser excitation pulse have been analyzed for several organic thin films.
Pump light was generated by the second harmonics (532 nm) of a Q-switched Nd-YAG laser (*Spectra Physics, INDI-40-10*) producing 6 ns pulses with 10 Hz repetition rate. Laser intensity was attenuated using a set of reflective ND filters to the desired energy of $10 - 250\ \mu J/cm^2$pulse for kinetics data and to record the absorption spectra. A 500 W Xe lamp (Edinburgh Instruments) was used in combination with appropriate edge- or band-pass filters (Thorlabs) and focused on the sample. Changes of the transmitted light were spectrally resolved using a grating monochromator (Oriel 77200) and recorded by a 200 MHz amplified photo-diode (vis: Femto HCA-S-200M-SI; IR: Femto HCA-S-

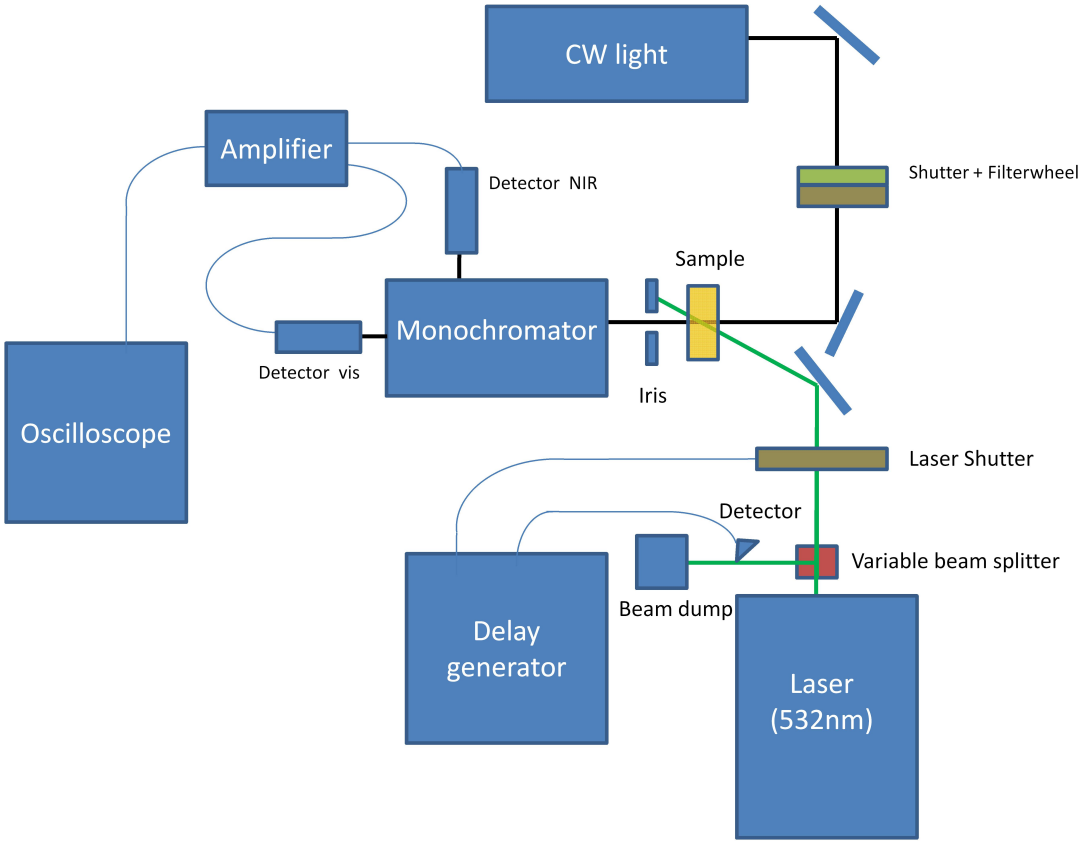

Figure 3.8: Schematic representation of a nanosecond transient absorption setup. The setup allows time and spectrally resolved investigations of excited species in thin films of organic materials.

200M-IN). The signals were amplified with a AC/DC pre-amplifier (Femto DHPV-200) and digitized with an oscilloscope. The transient signal incident to the monochromator was adjusted using an iris allowing to attenuate laser stray light.
All transient absorption measurements presented in this thesis have been recorded at the Intelligent Polymer Research Institute (IPRI) in Wollongong, Australia under the supervision of Dr Tracey Clarke and Dr Attila Mozer.

Spectra

A LabView based program-code for data acquisition, handling and representation ("TAS acquire data") was refurbished and several new features added (see Section 8.1.2). For the graphical representation of the data a second LabView data-evaluation tool was assembled as is shown in the Appendix (Section 8.1.3)

Kinetics

Kinetic data was acquired using multiple averaging cycles for each wavelength probed. Data acquisition is accomplished using the program TAS acquire data. Fits to the kinetic decay traces have been made using the fit function toolkit of Origin data analysis software. Fit functions used are described along with the experimental data.

3.2.7 Electrochemical analysis

Electrochemical measurements have been carried out for several organic compounds allowing to estimate HOMO and LUMO levels as well as giving insight to the optical properties of charged species formed at certain bias potentials.

Cyclic voltammetry

An *Autolab PGSTAT 302N* potentiostat/galvanostat was used for cyclic voltammetry analysis. Measurements were performed in a three electrode setup using a Pt counter electrode, a Ag/AgCl reference electrode and an 0.1 M solution of tetrabutylammoniumhexafluorophosphate in acetonitrile as electrolyte. As working electrode, thin organic films coated on ITO glass were used. HOMO and LUMO levels were calculated with respect to a reference measurement of a 0.01 M ferrocene solution.

Spectral electrochemistry

Spectral electrochemistry measurements were conducted using a quartz glass equipped sample chamber (*Autocell*). The chamber holds a three electrode setup and is equipped with quartz windows on both sides - a semi-transparent Pt mesh as counter electrode and a defined path length of the chamber facilitates detailed electrochemical measurements. Dicloromethan (DCM) containing 0.3 mg/mL tetrabutylammonim perchlorate (TBAP) was used as solvent for the experiments. The calibration of the Ag wire electrode against the vacuum potential has been obtained using a 5 mM ferrocene solution in acetonitrile. Potentials desired for the formation of charged species in solution are applied to the mesh grid electrode and uv-vis spectra are obtained using a Shimamadsu UV-vis-NIR absorption spectrometer.

4 Influencing the Supramolecular Assembly of Discotic Molecules

In this chapter the intermolecular packing and supramolecular organization of small molecule donor-acceptor heterojunction systems is analyzed. The influence of chemical substitutions and processing conditions on photophysical properties and performance of photovoltaic devices is analyzed and conclusions for an optimized donor-acceptor design allowing for increased charge generation and charge extraction are drawn. For all studies HBC molecules specifically synthesized by the Professor Müllen group were used as donor materials.
In a first study solution processable derivatives of the HBC donor molecules are blended with perylene-diimide (PDI) and bulk heterojunction solar cells are fabricated. Film morphology, supramolecular packing and photophysical properties are analyzed and correlated with the performance of photovoltaic devices. Possible recombination mechanisms are discussed based on studies analyzing the decay dynamics of charge carriers. Several results of this section have been published in the paper: "Discotic materials for organic solar cells: Effects of chemical structure on assembly and performance" [54]. The results are also correlated with a separate study on the supramolecular packing of HBC and PDI molecules based on X-ray analysis of thin blend films [53].
Separately, the properties of sublimated HBCs are investigated in bi-layered and co-evaporated photovoltaic devices. Appealing properties of the un-substituted HBC molecule include a long exciton diffusion length and high thermal stability. Different acceptor molecules - PDI and PCBM processed form solution and HBC-6F sublimated from the vapor phase - are compared as acceptor compounds in bi-layered devices.

4.1 HBC alkyl side chain modifications

HBC and PDI seem to be an appealing donor-acceptor couple for solar light harvesting, as the molecules show a complementary absorption spectrum and suitable energy levels. PDI as electron conducting acceptor is known for its strong absorbance and the donor

material HBC has the tendency to self assemble in a columnar fashion facilitating the formation of 1D molecular wires (as further described in Section 2.3.3). Exceptionally high charge carrier mobility values have been shown repeatedly for several derivatives of both classes of molecules when aligned in a suitable manner [20, 118]. In the year 2001 Schmidt-Mende and al. showed a remarkably high IPCE for bulk heterojunction devices based on the molecules HBC-Ph-C_{12} and PDI [22]. More recent studies on this donor-acceptor system have shown, that the supramolecular organization of the blend films plays a detrimental role and that slight changes in molecule design and processing conditions may strongly influence film morphology, charge carrier percolation pathways and thus also the photophysical properties of the blend films [86, 87].

The aim of this Chapter is to gain further insight to morphology as well as exciton separation and charge extraction mechanisms in the active layer of blended discotic molecules. The interplay of the donor and acceptor compounds and the influence of their supramolecular assembly on the photovoltaic performance is studied. HBC donor molecules are altered in shape by the attachment of a variety of residual groups. The impact of the structural changes are analyzed in blend devices with the common acceptor PDI. Similar approaches of residue modifications allowed to draw crucial conclusions on the structure-performance relationship in the past and helped severely for the conceptualization of novel and promising materials for OPV devices in several recent studies [79, 176]. This conceptual approach seems promising also for small molecules as has been shown recently [177].

Alkyl chains with different lengths (6, 8, 12 and 16 carbon atoms), a triple bond linker between HBC core and residual phenyl group and a swallow tailed dialkylphenyl chain are attached to the donor core molecule. Changes in both photophysical and electronic properties of the molecules and especially blend mixtures with PDI as acceptor are analyzed. Detailed insight to device physics and morphology is gained by analysis of photoluminescence quenching, transient photovoltage and photocurrent decay experiments and atomic force microscopy. The changes in blend morphology due to the variation of side chain length and structure are correlated to the solar cell performance of the resulting devices.

The investigations explain why using short alkyl side chains higher currents and consequently an increased device performance can be achieved. An external quantum efficiency of over 27% is reported for the photovoltaic devices. For the solar cell production an inverted structure with electron collecting TiO_2 bottom and Ag top electrode was chosen. This allows fabrication of long time air stable devices.

4.1.1 Experimental details

Material synthesis

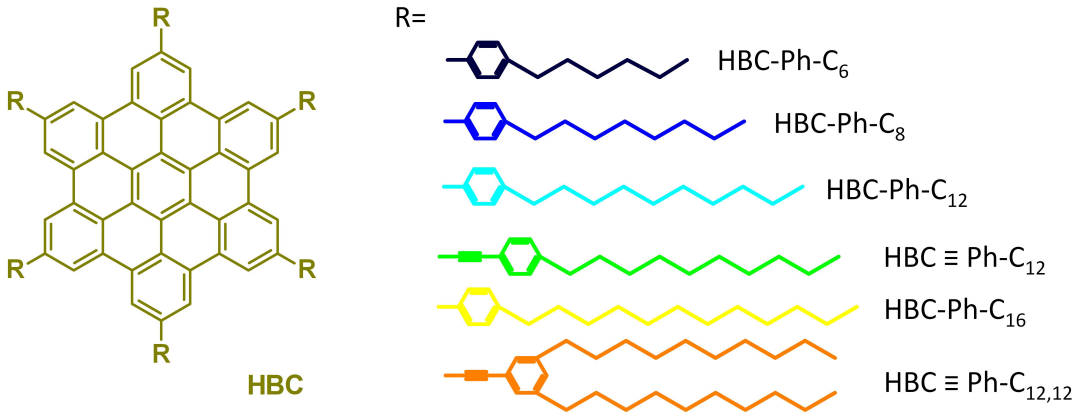

Figure 4.1: Solution processable HBC derivatives used in this study. All materials were cast from chloroform solution and blended with the electron acceptor perylene-diimide (PDI) at a ratio of 40:60 (HBC:PDI).

The chemical formula and abbreviation for all donor materials used in this study are summarized in Figure 4.1. The synthesis of the hexaphenyl-substituted HBCs (Fig. 4.1, HBC-Ph-C_6, HBC-Ph-C_8, HBC-Ph-C_{12}) with different alkyl chain lengths in the periphery was accomplished using a synthesis procedure reported elsewhere [178]. Due to the high sterical demand of the hexadecyl alkyl chain and its limited reactivity a more complex synthetic route was necessary to obtain the HBC-Ph-C_{16}. To introduce an additional triple bond between the HBC core and the substituents at the periphery, for compounds HBC≡Ph-C_{12} and HBC≡Ph-$C_{12,12}$ another synthetic route was used based on a six fold Sonogashira-Hagihara coupling reaction in the last synthetic step. After synthesis, all compounds were purified by repetitive re-precipitation and silica column chromatography to remove metal ions and impurities that would affect electronic properties and morphology [54].
Perylene tetracarboxdiimide (PDI) was used as received from Sensient technologies.

Device fabrication

Photovoltaic devices were fabricated as described in the experimental section 3.1. An inverted geometry was chosen for these solar cells allowing for high air stability of the devices with no further encapsulation. PEDOT:PSS was applied onto the active layer

and the devices were annealed for an extended period of 14 hours at 120 °C at ambient atmosphere prior to testing.

Surface morphology

Measurements were conducted on annealed devices (glass/ITO/TiO_2/blend/Ag). The metal top contacts were removed using a special foil (syrlon® foil, *Solaronics*) which was laminated onto the devices at elevated temperatures and subsequently removed at room temperature. Imaging was performed on areas previously covered by the metal top contacts.

4.1.2 Absorption analysis

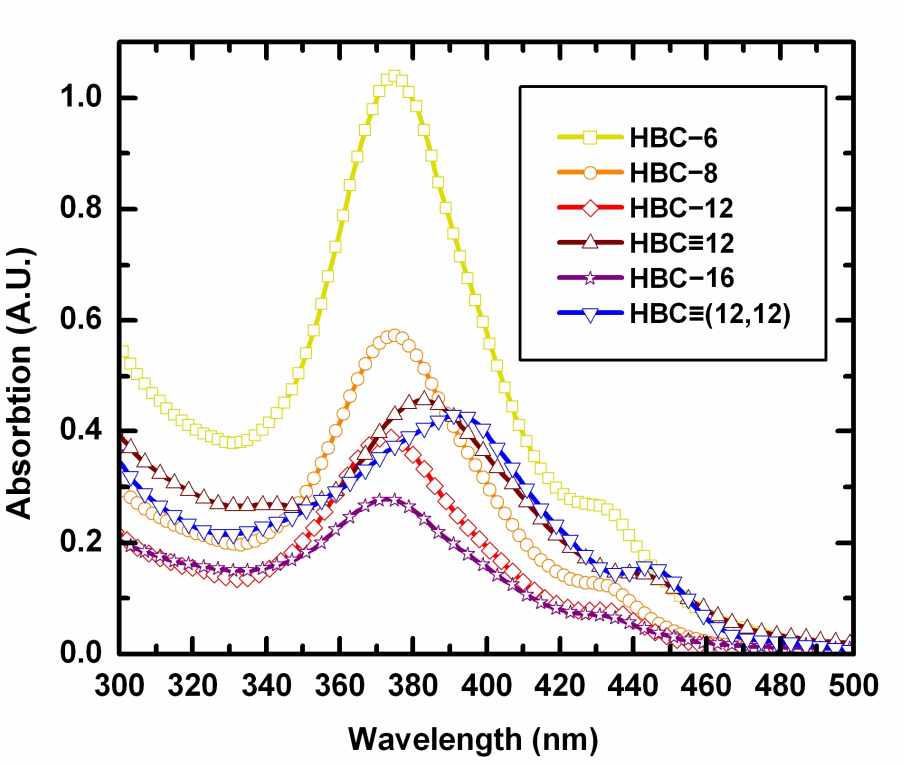

Figure 4.2: Thin film absorption spectra. Data is recorded for a thin layer of organic material deposited on quartz glass.

All organic compounds used in this study can be fully dissolved in chloroform, however long side chain derivatives dissolve more readily.

Material	core - core	d ($\pi - \pi$)	phase transitions
PDI	3.39 nm [180]	0.35 nm [22]	68 °C, Cr - I [87]
HBC-6	2.76 nm	0.35 nm	161 °C,LC-LC
HBC-8	2.97 nm	0.35 nm	153 °C, LC-LC
HBC-12	3.42 nm	0.35 nm	−22 °C,62 °C, LC-LC
HBC-16	3.70 nm	0.35 nm	9 °C, LC-LC
HBC≡Ph-C_{12}	3.37[1]-3.18[2] nm	0.35 nm	11 °C, 72 °C LC-LC
HBC≡Ph-$C_{12,12}$	3.63 nm	0.44[3] nm	59 °C, LC-LC

Table 4.1: Characteristic stacking parameters of extruded films. Characteristic distances and phase transitions have been derived by 2D-WAXS measurements and differential scanning calorimetry: Cr = crystalline, LC= liquid crystalline, I = isotropic. Packing structure: 1 = hexagonal, 2 = cubic, 3 = tilted herringbone.

Figure 4.2 shows absorption spectra obtained for thin films ($d \approx 100\,\text{nm}$) of the HBC derivatives under investigation. All derivatives show pronounced absorption in the wavelength region of $350 - 430\,\text{nm}$. PDI instead absorbs mostly in the range of $430 - 650\,\text{nm}$ [22]. At constant film thickness strongest absorption of the HBC derivatives is observed for short alkyl side chains. This is attributed to the increased number of chromophores per volume for small molecular weight HBCs. Both materials with triple bond liker unit, HBC≡Ph-C_{12} and HBC≡Ph-$C_{12,12}$, show bathochromically shifted absorption peaks when compared to the single bond HBCs. Fitting the absorption data to the Urbach model [179], we could derive a shift in E_{DA} of the single bonded to the triple bonded HBC from about 3.1 eV to about 2.9 eV.

4.1.3 Characterization of thermotropic behavior

The thermotropic properties of the chemical compounds synthesized were analyzed using differential scanning calorimetry (DSC) and 2D powder X-ray diffraction analysis. All HBC compounds show a liquid crystalline phase with at least one accessible phase transition as summarized in Table 4.1.

4.1.4 Solar cell performance

In order to compare the photovoltaic properties of the HBC derivatives blended with the acceptor PDI a set of bulk heterojunction solar cells was fabricated. All devices were assembled in an inverted geometry composed of ITO/TiO_2/blend/PEDOT/Ag. This inverted geometry was favored to the standard ITO/PEDOT/blend/Al design as strongly improved device lifetime of the cells can be achieved without encapsula-

tion [112, 181]. After solution deposition of the organic material yielding an active layer thickness of about 120 nm PEDOT was spun on all devices. As further described in the experimental chapter (Section 3.1.5) this interlayer shows hole selective and exciton blocking properties and serves as a protective layer for the subsequent application of the Ag top contact. Fully assembled devices were annealed at 120 °C for an extended period of 14 hours prior to device testing. Even though this long term annealing treatment results in a slightly decreased absorption for all blend materials (data not shown), drastically improved solar cell performance was recorded showing higher open circuit voltage and short circuit current. This is attributed to both a favorable realignment of HBC and PDI molecules and the formation of a better contact of the blend with the Ag electrode as further explained later in connection with AFM measurements.
When illuminated at standard conditions (AM 1.5 global, 100 mW/cm^2) all devices show a photovoltaic behavior.

Optimizing the blending ratio of donor and acceptor

The effect of donor to acceptor blending ratio on solar cell performance was screened for all derivatives as is summarized in Figure 4.3. For the HBC derivatives with increasing molecular weight a higher PDI content is necessary to achieve best power conversion efficiency: A mixing ratio of 30:70 wt% was found to perform best for HBC≡Ph-$C_{12,12}$:PDI. For short side chain HBCs instead equal weight ratio of donor and acceptor molecules yields best results (e.g. HBC-Ph-C_6:PDI with best blend ratio around 50:50 wt%). For best performance the content of HBC core molecules must thus be decreased significantly when increasing the alkyl chain length or introducing a branched tail.
We attribute this to differences in packing and morphology of the different blends. Bulky substituents on the periphery of HBC might hamper intermixing with PDI, as will be further explained later in connection with transient decay measurements and atomic force microscopy. As such, a higher PDI content is needed to provide sufficient interfacial area of donor and acceptor and yield maximum performance.

Device characterization

To compare the potential of the different HBCs in photovoltaic devices, all derivatives were blended with PDI at a constant mixing ratio of 40:60 wt% in the following experiments. Typical IV-curves at solar illumination (AM 1.5g, 100 mW/cm^2) are shown in Figure 4.4. Table 4.2 shows mean values and standard deviation of the solar cell

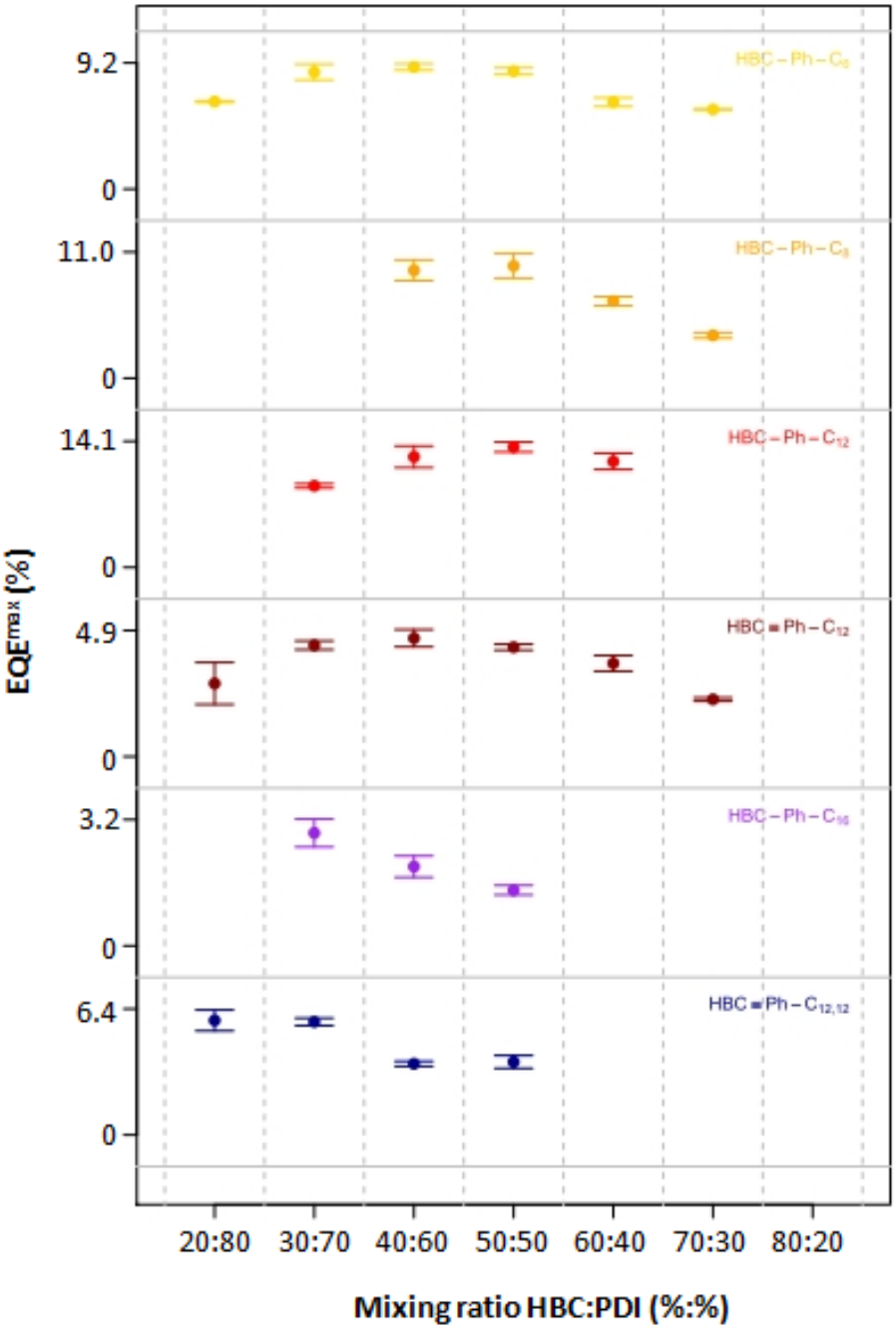

Figure 4.3: Determination of optimal blending ratio for different HBC:PDI blend mixtures The graph shows a relationship of donor molecular weight and acceptor content for optimal photovoltaic performance. Error bars show a confidence interval of one standard deviation (six individual pixels have been measured per data point)

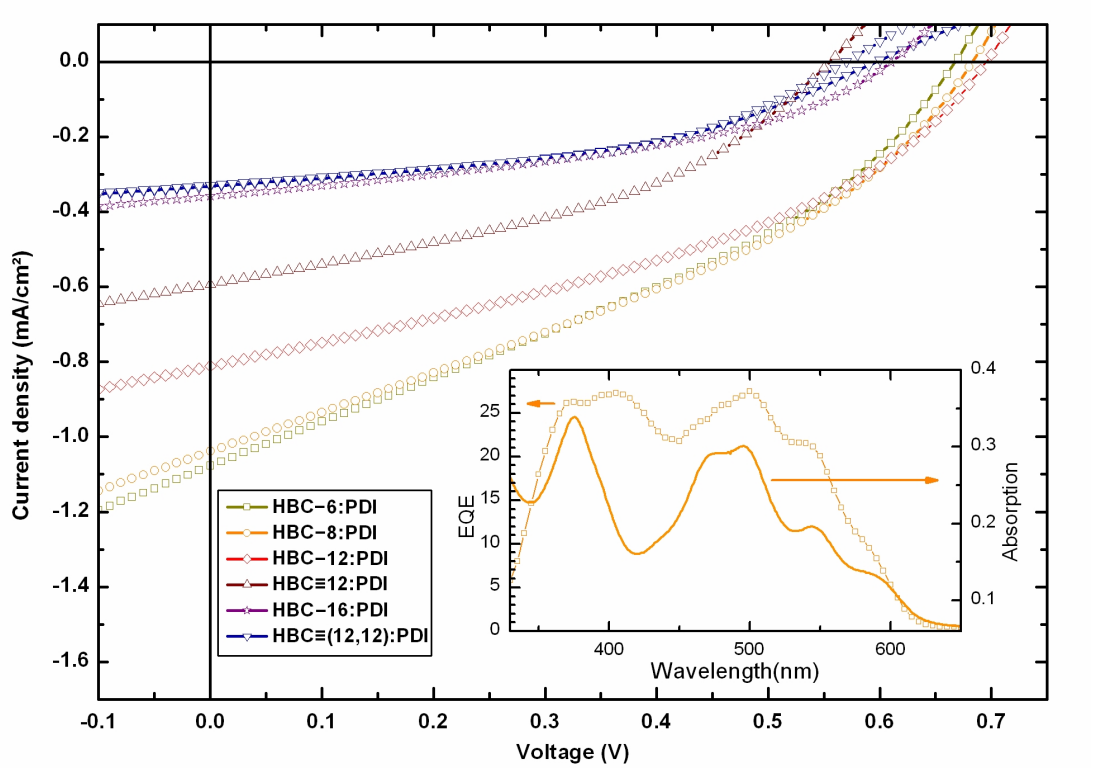

Figure 4.4: HBC:PDI blend IV-characteristics. Best photovoltaic devices are obtained for blends containing short side chain HBCs. The low fill factor of the devices is attributed to a strong bimolecular recombination.

characteristics based on six devices for each subset. Additionally, EQE measurements have been carried out on all devices. At balanced blend ratio the spectral response mainly follows the absorption of the thin films (exemplary shown for HBC-Ph-C_8:PDI, 40:60 wt%, inset Figure 4.4). An EQE of over 27% was recorded at 390 nm and 500 nm which is close to the peak absorption of HBC and PDI, respectively. For this blend composition the EQE remains above 20% ranging from $360 - 550$ nm.

The power conversion efficiency of the photovoltaic devices peaks at $\eta = 0.24\%$ upon simulated solar illumination at $100\,\mathrm{mW/cm^2}$ on air and found to be almost similar for all blends containing HBCs with short side chains (HBC-Ph-C_6, HBC-Ph-C_8 and HBC-Ph-C_{12}). Upon irradiation with monochromatic light at a low illumination intensity about eight times higher efficiencies have been already reported [22] and could be reproduced for the devices presented herein. However, at high illumination intensity the performance drops significantly. The sub-linear rise of currents with increasing illumination intensity is attributed to strong non-geminate charge carrier recombination (as

active material	I_{SC}[mA/cm^2]	V_{OC}[V]	FF [%]	IPCE [%]	R_s[Ωcm^2]	R_{sh}[Ωcm^2]
HBC-6:PDI	1.035 ± 0.042	0.643 ± 0.023	33.4 ± 0.2	0.22 ± 0.02	61 ± 9	820 ± 13
HBC-8:PDI	1.065 ± 0.035	0.665 ± 0.026	34.3 ± 0.6	0.24 ± 0.02	78 ± 6	906 ± 28
HBC-12:PDI	0.815 ± 0.050	0.690 ± 0.017	39.3 ± 0.7	0.22 ± 0.02	57 ± 12	1608 ± 127
HBC≡Ph-C_{12}:PDI	0.580 ± 0.030	0.542 ± 0.065	38.8 ± 1.4	0.12 ± 0.01	138 ± 69	1997 ± 215
HBC-16:PDI	0.340 ± 0.027	0.593 ± 0.065	39.2 ± 3.1	0.08 ± 0.02	76 ± 35	3729 ± 324
HBC≡Ph-$C_{12,12}$:PDI	0.306 ± 0.037	0.549 ± 0.041	44.5 ± 2.9	0.07 ± 0.02	321 ± 195	5091 ± 390

Table 4.2: Device characteristics of HBC:PDI blend solar cells. Mean values and standard deviations are given for a set of six solar cells each

will be further elucidated in Section 2.7.1) drastically limiting the device performance at 100 mW/cm^2 solar illumination [182].

The open circuit voltage ranges from $V_{OC} = 540 - 700$ mV and is highest for the HBC derivatives with single bond linked phenyl groups. Within this series of HBCs, the V_{OC} increases with the side chain length from HBC-Ph-$C_6$to HBC-Ph-C_{12}. A possible explanation are shielding effects of the alkylic residues decreasing the HOMO level with increasing side chain length as has been reported elsewhere [87]. Accordingly, the effective bandgap of donor and acceptor (E_{DA}=$E^D_{HOMO} - E^A_{LUMO}$) is increased, shifting also the V_{OC} to higher values [11]. As a different synthetic approach was used and purification appeared more challenging for HBC-Ph-C_{16}, the low V_{OC} in this blend may be determined by a higher content of impurities. However, also different molecular arrangement might be favored for this molecule due to the long side chains and could lead to a reduced V_{OC} [183]. For both HBCs with a triple bond linker unit about 200 mV lower open circuit voltages are recored. This can be attributed to a altered energy levels for these molecules. As already mentioned, the HOMO-LUMO gap of both HBC≡12 and HBC≡(12,12) is shifted by about 0.2 eV to lower values: Electrons can be partially delocalized to the triple-bond unit reducing the HOMO level of these molecules. The LUMO level instead is not expected to be influenced by the introduction of the triple bond - electrons remain confined to the unmodified HBC core unit [184].

A closer look to the short circuit current indicates differences in the exciton separation and charge carrier collection yield among the different blend materials. Short alkyl chains allow for highest currents and I_{SC} decreases with increasing side chain length of the HBC molecules. Differences in spacing between donor and acceptor are attributed to be the main reason for this finding as supported by PL measurements and transient photovoltage and photocurrent decay studies (see Section 4.1.5 and Section 4.1.6).

The fill factor of the devices ranges from FF = 33.5% for HBC-Ph-C_6:PDI to FF = 42.9% for HBC≡Ph-$C_{12,12}$:PDI blends. In a separate experiment I_{SC} of all cells was

regulated to an arbitrary but fixed value by adaption of solar illumination intensity. The FF does not considerably differ from that reported in Table 4.2, showing that FF and values for equivalent resistors strongly depend on material specific properties and are not governed by contact limitations.
Both shunt and series resistance for an equivalent diode model (see Section 2.4.1) are estimated from the IV curves: R_s values are based on the slope of the IV curves at a high forward bias (1.5 V) and R_{sh} determined at reverse bias (-1 V). R_{sh} ranges from 10^3 to 10^4 Ω/cm^2 which is comparable to values reported in solar cells based on other organic materials [185]. However, especially for the devices with short alkyl chain HBCs increasing the shunt resistance is of key importance for further device improvement. Instead, an exceptionally high series resistance of $R_s \approx 60 - 320$ Ω/cm^2 was recorded for all HBC:PDI blend devices. This value is at least one order of magnitude larger than numbers reported for morphologically optimized polymer:fullerene solar cells [107, 185]. High R_s values cause major limitations to both the FF and I_{SC} of our devices, especially for cells containing HBC≡Ph-C_{12} and particularly HBC≡Ph-$C_{12,12}$. Higher mobility in the blend material is needed to improve device characteristics as will be further motivated in connection with transient decay measurements. In an aligned, high purity film a record charge carrier mobility of up to 1 $cm^2V^{-1}s^{-1}$ has been obtained for both the discotic materials HBC and PDI [20, 70, 186]. However, this exceptionally high values may only be reached for pristine materials and only along the $\pi - \pi$ stacking axis. In the photovoltaic devices presented here homeotropic alignment (Section 2.3.3) and growth of crystalline domains consisting of pristine material are necessary to yield a maximum charge carrier mobility. At the same time direct percolation pathways to the electrodes are needed to allow unhampered charge extraction. It appears that this desired alignment and morphology is most likely not achieved in the devices studied. lateral charge carrier hopping between adjacent HBC cores appears to be necessary for current extraction. This is clearly favored for the hexagonally packed HBCs with short side chains and might be hindered for HBC≡Ph-C_{12} and HBC≡Ph-$C_{12,12}$ with their more space demanding cubic and herringbone packing (as reported in Table 4.1).

4.1.5 Photoluminescence analysis

Steady state photoluminescence measurements have been carried out on thin films of both pure PDI and HBC derivative films as well as on the blended compounds and quenching of the radiative loss mechanism analyzed. For the blends measurements were conducted on the fully assembled solar cell devices after annealing in reflection geometry. Thus direct insight to the spectral properties of the materials used in the

solar cells with the characteristics summarized in Table 4.2 was gained. Excitation was set to 375 nm and 490 nm, where prominent absorption takes place in the HBC and PDI molecules, respectively. PL signals were spectrally resolved as exemplary shown for excitation at 375 nm in Figure 4.5.

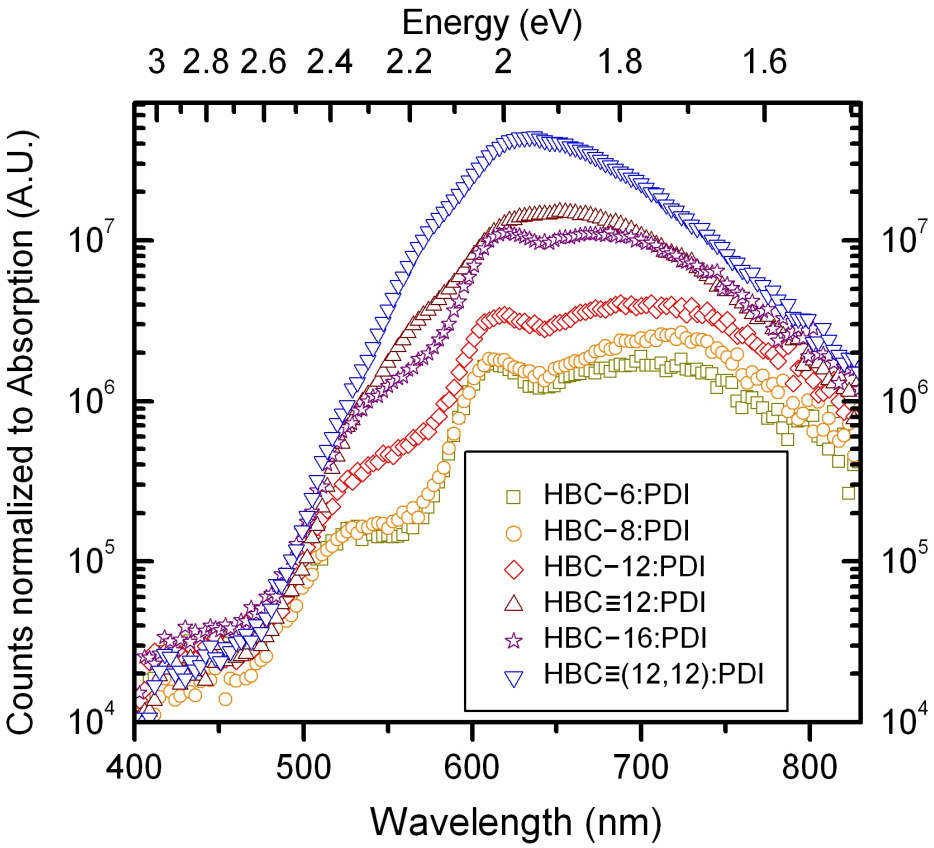

Figure 4.5: Steady state photoluminescence emission spectra of HBC:PDI blend films. Samples were excited at 375 nm in reflection geometry. The detector counts are normalized to the sample absorption.

Upon excitation of blend films at 375 nm, where mainly HBC absorbs broad emission features are visible at 525 nm and 610 nm matching well the emission of excited pure HBC and PDI films, respectively. Interestingly, the feature at around 725 nm (≈1.7 eV) is not visible for thin films prepared of either pristine HBC or PDI. The occurrence of this signal in the blend films is attributed to the emission via a photo induced charge

transfer state (CTS) [186]. In our experiments the feature could only be resolved for blends containing HBCs with a single bond linker unit. For both materials with a triple bond the altered energy gap is likely to induce a further red shifted CTS and could not be resolved with our experimental setup [186].
Upon excitation of PDI (490 nm) all emission curves of the blend films look very similar in shape varying only in the overall height with stronger quenching for short alkyl chains. Typical PDI related emission features are visible but no signal from HBC emission could be recognized. The signal at around 725 nm attributed to the CTS is still present for this excitation but decreased in intensity. Furthermore, photoluminescence excitation measurements have shown that the spectral contribution to this emission feature (725 nm) mainly follows the absorption of the blend films with higher yield upon HBC excitation.
Results of the PL measurements can be explained when looking at the energy levels of donor and acceptor molecules. As known from literature, the HOMO levels of HBC and PDI are very similar at around −5.3 eV [22]. When blend material is excited at 375 nm the offset in LUMO levels of about 0.65 eV may lead to both separation of excitons at the interface and energy transfer to the PDI [187]. Upon excitation at 490 nm instead most emission occurs directly from the PDI. Despite the low driving force due to the small offset in HOMO levels a significant number of excitons is separated at the interface resulting in a spectral contribution of the EQE at wavelengths above 450 nm. In addition, some radiative loss of CTS excitons can be detected upon PDI excitation. The overall radiative loss in the different blends can be estimated from the area under curve of the absorption normalized PL emission signals (Figure 4.5). At both excitation wavelengths probed, best quenching was observed for HBCs with short alkyl chains which is attributed to morphological differences in the thin films. As shown separately in Section 4.1.8 the spacing between PDI molecules and the HBC cores depends on the residue variations of the HBC molecules. It is worth mentioning that the area under curve increases dramatically for a side chain length of more than twelve carbon atoms, where disrupted non-ordered stacking was evidenced by X-ray investigations (as is shown in the following Section 4.1.8). Furthermore, better intermixing of donor and acceptor for short side chain HBCs is supported by AFM data. Intimate contact of HBC cores and the PDI is needed to efficiently separate excitons also allowing for higher photocurrents (as reported in Table 4.2 and Figure 4.4). For long and especially swallow tailed alkyl side chains, relaxation of excited molecules by charge separation becomes less probable. Instead, charge carriers recombine and emit their energy in terms of photoluminescence. In general the triple bond linker unit present in HBC≡Ph-C_{12} and HBC≡Ph-$C_{12,12}$ appears to widen the radiative loss channel of the blends. The overall

higher sterical demand of these HBCs is likely to be the reason: The phenyl group is located further away from the HBC core unit resulting in a less compact packing in HBC≡Ph-C_{12} (cubic lattice) and HBC≡Ph-$C_{12,12}$ (tilted herringbone structure) (see Table 4.1).

4.1.6 Transient decay measurements

Two types of transient decay measurements were performed on the solar cell devices in order to gain insight to charge carrier recombination and extraction.

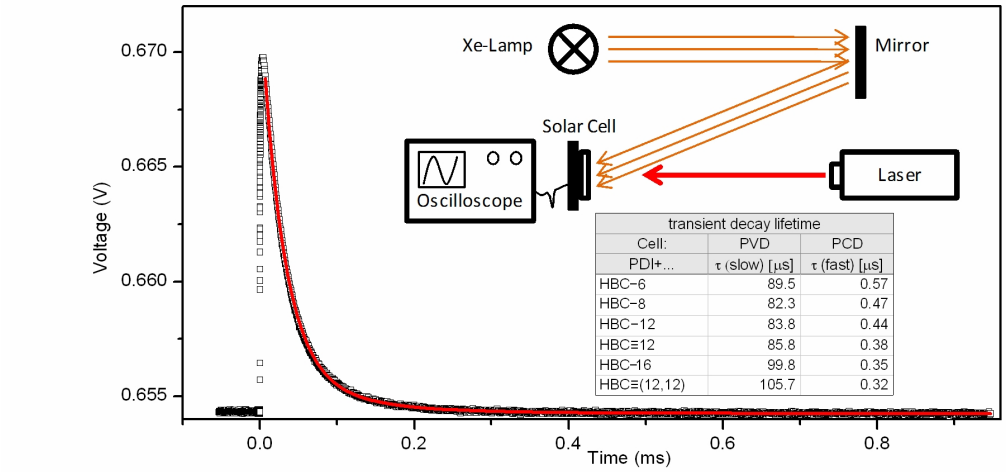

Figure 4.6: Photovoltage and photocurrent decay experiments. The graph shows an exemplary decay measurement (scattered) along with a bi-exponential fit to the data (red line). The inset image shows a schematic representation of the experimental setup and decay lifetimes obtained for the individual measurements.

Figure 4.6 shows a typical photovoltage decay (PVD) transient monitored with a digital high resolution oscilloscope. In addition to the steady state potential generated by white light illumination, supplementary charge carriers are created by short laser pulses (532 nm) raising also the open circuit potential of the cell temporarily. The voltage drops to the former level due to recombination of the additional charge carriers (see Section 3.2.3).

Annealed devices with blends of HBC:PDI (40:60 wt%) were analyzed and transients show lifetimes in the range of a few tens of microseconds which is comparable to common values found for other organic photovoltaic systems (inset Table, Figure 4.6) [188]. Charge recombination occurs faster in blends containing short side chain HBCs which further explains the differences observed in R_{sh} and FF as have been reported in Table

4.2: Both parameters are found to decrease gradually from long to short residues at the periphery of the HBCs, implying more pronounced recombination and increased leakage currents. Even though charge separation is not favored in the HBC≡Ph-$C_{12,12}$ containing blends manifested by the low I_{SC} and high PL loss, once excitons are separated in this blend, generated charges can efficiently be extracted and bi-molecular recombination is only a minor loss mechanism. For the cells containing HBC-Ph-C_6 instead, considerably more free carriers are produced yielding a higher short circuit current. However, devices suffer strong non-geminate recombination resulting in the low FF of these devices.

To further analyze the charge carrier generation and extraction, photocurrent decay measurements were also carried out on the solar cell devices. Contrary to the PVD experiments, measurements were conducted under short circuit conditions with no white light bias. Transients recorded are also subject to a bi-exponential decay and can be fitted with Equation 3.3. For PCD measurements, slow decay rates are strongly influenced by trap states and only the short lived state incorporates blend specific information [189]. An $1/e$ lifetime is extracted from the fast decay rates (Figure 4.6, inset Table). Reported charge extraction rates are two orders of magnitude faster than respective recombination rates determined by the PVD measurements - a prerequisite for efficient charge carrier extraction in the solar cell devices: Separated charges will rather exit the device via the external contacts than become annihilated within the active material.

All materials show a peak current response to the laser pulse of similar magnitude. However, the decay from this peak value occurs faster in the blends with long or branched side chain HBCs. The total amount of charge (Q) generated by one laser pulse on a specific cell is equal to the area under the decay curve (I vs. t). Q increases from HBC≡Ph-$C_{12,12}$ to HBC-Ph-C_6 which is consistent with the differences in short circuit currents of the IV measurements presented (Figure 4.4). Upon laser excitation at 532 nm, only PDI molecules become excited which can either contribute to charge carrier generation, or unwanted relaxation occurs. In the blends containing long residue HBCs prominent non-radiative and radiative relaxation of the excited PDI molecules are indicated by fast decay rates. For HBCs with short chain residues instead, where intimate contact of the HBC core to the excited PDI is provided, geminate recombination is suppressed and charges are generated over a longer period of time. This results in the slow decay rates recorded and is also in accordance with the PL signals quantifying the radiative recombination loss channel. It appears that the capability to extract more charges from the excited PDI outweighs the faster recombination for blends containing short alkyl chain HBCs as shown with PVD measurements and explains the significantly

higher short circuit currents of these materials [190].
The PCD decay rates reported for the HBC:PDI devices are comparable to those found in literature for high efficient polymer fullerene devices [190]. Nevertheless, peak current offset after perturbation and thus the overall extracted charge is found significantly lower for the small molecule devices presented here. Unfavorable molecular alignment seems to hamper the charge extraction in the blends of the discotic materials. This morphological limitation persists even after long time annealing treatments of the devices.

4.1.7 Surface morphology analysis

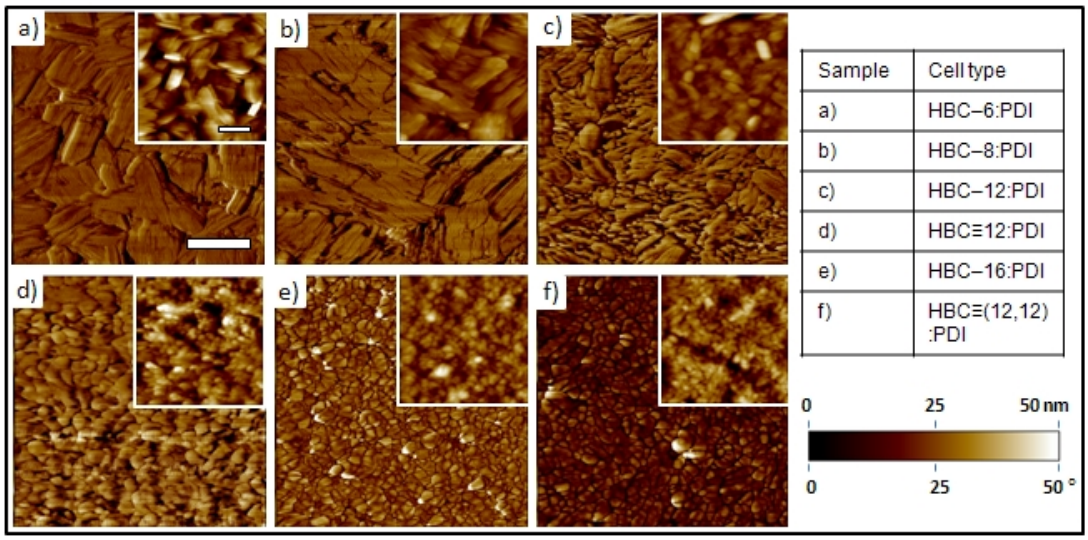

Figure 4.7: Tapping mode atomic force microscopy scans of the annealed HBC:PDI 40:60 wt% blend samples. The scale bar is 500 nm for both phase (large images) and height scans (insets). The images were taken after removal of the top contacts and give insight to the morphology obtained for annealed samples (120 C, 14 h) in confined geometry. Crystalline structures are observed mainly for short alkyl side chains at the periphery of HBC.

Tapping mode atomic force microscopy has been carried out on the different organic blend layers studied. Images were taken on the identical samples which yielded the above shown IV-characteristics after careful removal of the Ag top contact (as described in Section 4.1.1). As such, the surface morphology of the different blends could be analyzed exactly where the material was previously confined between bottom and top electrode. In open films, PDI forms long crystalline grains [117]. Pure HBC films exhibit rather smooth and almost featureless surface structures instead [22]. Throughout the annealing treatment at 120 °C PDI is in isotropic phase and also side chains of

the liquid crystalline HBCs are mobile (reference Table 4.1). As the blend material was kept in confinement - sandwiched between the TiO_2 and Ag electrode - the formation of PDI needles could be effectively suppressed yielding RMS roughness values of only $4-7$ nm for the different HBC:PDI blends studied. The confined annealing treatment leads to an improved morphology and is favorable for device performance. On the contrary, in the absence of a confinement layer PDI needles are likely to penetrate through the entire active layer establishing direct contact between both electrodes [86, 117]. Increased leakage currents and reduced shunt resistance are observed.
Furthermore, during thermal annealing also the nano-morphology of the blend material changes: realignment of the discotic molecules leads to increased ordering [139, 191]. An altered morphology showing larger grains becomes evident from AFM scans. The observed increase of device performance induced by the annealing treatment is attributed mainly to better percolation pathways.
After annealing in confined geometry the blend materials studied also show differences in surface topology as summarized in Figure 4.7: Flake like structures are visible for all derivatives, whereas the grain size decreases from about 500 nm (for HBC-Ph-C_6 and HBC-Ph-C_8) to 100 nm (for HBC-Ph-C_{16} and HBC≡Ph-$C_{12,12}$) in diameter. For longer side chain HBCs, the domains are interrupted by less ordered areas. This may also lead to a lower charge carrier mobility and could thus cause the lower currents observed for these materials. In contrast, the larger grains for the short side chain HBCs rather consist of better aligned material. X-ray experiments conducted on the devices show that most likely a mixed phase of HBC and PDI is present in these grains (see Section 4.1.8). Such strong intermixing of HBC and PDI allows efficient exciton separation upon illumination. These findings are consistent with both PL data and the device measurements under illumination indicating that the charge carrier generation yield is higher when incorporating short side chain molecules. The surface morphology of the active material indicates differences in cristallinity and quality of crystal growth. These parameters play an important role for the solar cell performance consisting of discotic molecules. Large and ordered domains incorporating intermixed donor and acceptor material allow better device performance than the disordered network structures obtained for the HBCs with longer side chains.

4.1.8 Blend morphology analysis

In order to investigate the effects of the supramolecular assembly on the device performance in more detail a series of X-ray diffraction studies were conducted by Dr Mahmoud al Hussein, a visiting researcher from University of Jordan, Amanon, as

summarized in a joint publication [53].
In brief, the X-ray diffraction studies were conducted on PDI, HBC-Ph-C_6, HBC-Ph-C_8, HBC-Ph-C_{12} and HBC-Ph-C_{16} pristine materials and blend films as used for the photovoltaic investigations. Packing and alignment of the molecules is analyzed in detail and a model for the supramolecular stacking established that is in accordance with the experimental findings.
We find a layered structure parallel to the substrate in both pristine HBC and PDI films: For the blend films the X-ray investigations provide a clear indication, that a micro-phase separated structure is formed as is schematically shown in Figure 4.8. This is especially the case for the short side chain HBCs (HBC-Ph-C_6 and HBC-Ph-C_8), where we observed crystalline domains in the AFM surface scans. The layered microstructure becomes more disordered when increasing the side chain length of the HBC molecules (e.g. HBC-Ph-C_{12}) and a predominantly disordered structure is formed for the HBC-Ph-C_{16}.
A similar alternating inter-columnar ordering has been reported previously for blend

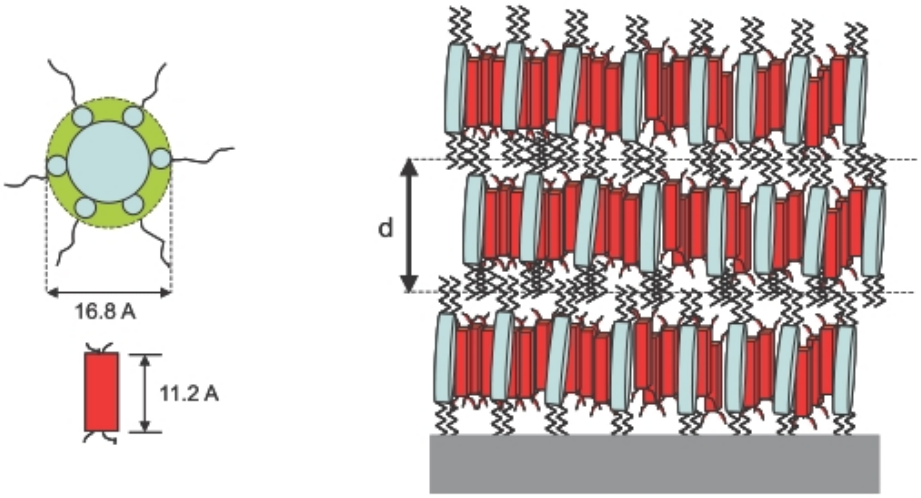

Figure 4.8: Schematic representation of the supramolecular stacking found for blends of PDI and HBC derivatives with short alkyl side chains. Snapshot taken from [53]

mixtures of HBC and PDI derivatives [18]. Enthalpic and entropic considerations may strongly favor this mixed stack motif when molecules of compatible size and shape are blended [19]. Apparently the gain in free energy due to the formation of donor-acceptor complexes overweights the entropic penalty of alternated stacking of PDI with with short side chain HBCs. On the contrary, for HBC-Ph-C_{12} and especially

HBC-Ph-C_{16} this highly ordered phase is disrupted as the long side chains cannot be incorporated into the tightly packed alternating inter-columnar ordering of HBC and PDI.
In order to compete with the high performance obtained for optimized polymer-fullerene blend devices a morphology allowing for strongly improved charge carrier extraction must be achieved in this small molecule blend systems: crystalline packing and a segregated motif with adjacent but pristine stacks of either donor or acceptor material is desired for unhampered charge carrier migration. Furthermore, face-on instead of the edge-on alignment observed here would be advantageous for charge carrier extraction [121]. Miscibility and compatibility of size and shape for the molecules studied will unavoidably lead to alternate stacking and strongly intermixed phases [19]. As such, peak performance in the blend devices can be achieved only when using short side chain HBCs and only at low illumination intensities [22]. Bi-molecular recombination will limit photovoltaic performance at standard testing conditions of 100 mW/cm^2

4.2 Alignment studies on soluble HBC derivatives

As shown in the previous Section blending of HBC and PDI molecules with compatible size and comparable thermotropic behavior will most commonly result in the formation of disordered or alternately stacked morphologies. Alternative approaches are necessary to achieve a desired homeotropic alignment of pristine material domains in thin film devices. In this section a short experimental study on a promising alternative concept is given.
As concluded from the previous study (Section 4.1) homeotropic stacking of the organic molecules is highly desired for the application in OPV devices. A face on alignment of the molecules will also facilitate a better charge extraction towards the external device contacts [183]. The alignment of pristine molecules exhibiting LC phases can be induced by external stimuli (see Section 2.3.3). However, a method to achieve *simultaneous* alignment into vertically segregated but adjacent columns of donor and acceptor molecules is not known at present.
As a first step towards this direction we are aiming to induce a horizontally segregated donor-acceptor morphology of homeotropic aligned molecules and investigate the applicability for OPV devices.
Surface interaction plays a great role when aligning thin films of LC molecules [192]. Well defined and controlled conditions facilitate the growth of large uniformly aligned domains. Melting of the organic material above the glass transition temperature fol-

Component name	T_i	Alignment properties	Additional comments	References
HBC-C(10,6)	93 °C	planar on surface; homeotropic in confinement	applied in solar cells EQE 6% at 490 nm	[87, 193]
HBC-C(14,10)	46 °C	no well defined LC phase	very low T_i	[87, 193]
HBC-C(6,2)	420 °C	planar and homeotrophic	very high T_i	[87, 193]
HBC-C3-O-C(10,6)	162 °C	homeotropic in open films	tilted 30° in Col_p phase	[121]

Table 4.3: Meltable derivatives of HBC. Literature survey on meltable HBC compounds, characteristic alignment properties and their applicability for solar cells.

lowed by slow cooling is a natural approach to achieving this goal. Table 4.3 summarizes a variety of HBC derivatives with reported melting points at accessible temperatures.

Most of these meltable HBC derivatives reported in literature can be aligned in a homeotropic fashion when kept in a confined geometry (e.g. sandwiched between two substrates) whilst cooling slowly from the isotropic to a columnar LC phase. In order to facilitate the application of the acceptor compound a direct access to the aligned HBC layer will be necessary. However, in open films where surface interactions are less dominant a disordered alignment is often favored due to the gain in entropy [121]. An exception is the HBC-C3-O-C(10,6) with elongated and bulky side chains showing pronounced homeotropic alignment also in the absence of a confinement [121]. However, electronic properties of this compound are believed to be limited by trapping of charges at the residual oxygen molecules [194]. As such, a reversible confinement approach as presented by Pouzet et al. appears extremely appealing [195]: A sacrificial layer of an inert polymer is applied from an orthogonal solvent capping the underlying spin cast donor material. Subsequently a temperature ramp is applied allowing the alignment of the material in the confined geometry. After removal of the capping layer with a suitable solvent subsequent layers can be applied on the aligned donor material. Figure 4.9 summarizes schematically the alignment procedure.

For the alignment studies presented here the molecule HBC-C(10,6) was used showing a melting point at slightly below 100 °C. The molecule has already been successfully tested in OPV devices [87, 193]. After solution deposition of the meltable HBC derivative ($d \approx$100 nm) from $CHCl_3$a poly-(4-vinylphenol) (P4VP) capping layer with a thickness of ≈0.5 µm was applied from an orthogonal solvent (methanol). Figure 4.10 **a)** shows a POM image of the organic film directly after spin coating. The image appears almost dark as the sample with non-oriented material does not change the polarization of the incoming light. The image does not change regardless of sample rotation or tilt on the microscope stage. After thermal annealing in confinement (120 °C, cooling rate

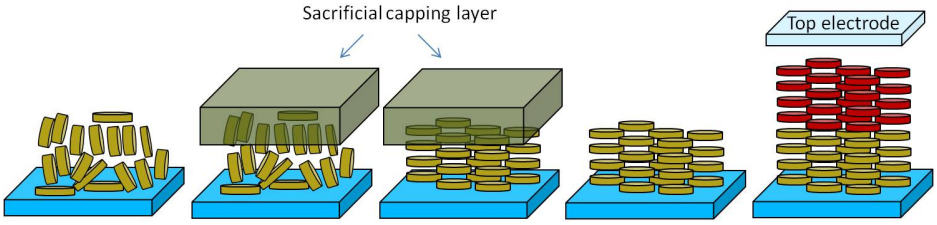

Figure 4.9: Cartoon showing the homeotropic alignment of molecules using a sacrificial capping layer. A sacrificial layer is used to allow confined alignment of the LC donor material as has been demonstrated by Pouzet et al. [195]. Subsequently an acceptor compound may be applied forming a heterojunction device.

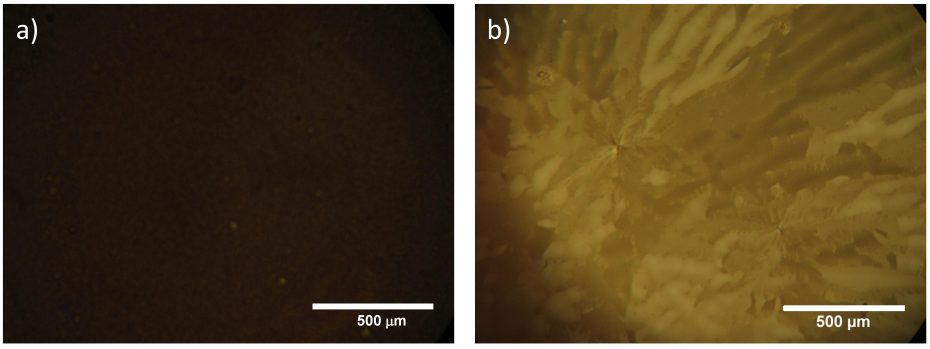

Figure 4.10: Polarized optical microscopy images of HBC-C(10,6) films on ITO substrate. (a) Non-oriented material obtained directly after solution deposition. **(b)** birefringence patterns observed on a tilted sample ($\alpha \approx 30°$f) or a film processed using the sacrificial layer method adopted from [195]. The image was obtained after annealing in confined geometry and removal of the capping layer.

≈1 °C/min) and subsequent removal of the sacrificial layer by careful rinsing of the sample in methanol, instead clearly different features may become visible (Figure 4.10 **b)**). The molecules in this sample which are lying homeotrophically oriented on the substrate plane will result in an optical axis pointing perpendicularly out of the substrate plane. From the POM image taken at a sample tilt of about 30° with respect to the optical pathway the formation of macroscopic, uni-axially oriented grains (in the order of several tens of µm) is evident. This highly aligned organic layer seems promising for the fabrication of a photovoltaic device with an enhanced molecular order.

In a next step the acceptor material - in our case PDI - is applied onto the pre-oriented donor molecules. However, a straightforward deposition of PDI from solution is not feasible without dissolution of the underlying HBC layer.

In a brief separate study we were not able to find orthogonal solvents for the donor and

acceptor compounds, respectively. As an alternative route, vacuum sublimation of PDI onto the solution processed donor material has also been tested. Slow and controlled layer growth at low temperatures of PDI is a prerequisite for the assembly of photovoltaic devices: Bombardment of the soft to viscous HBC with impinging molecules can easily lead to the formation of pinholes in the thin layer of aligned donor material. On the other hand, PDI is known to grow large crystallites (up to several micrometer long) when deposited at low to moderate sublimation rates [196]. The growth of such large crystallites should be avoided in OPV devices [86, 117] The challenges described for the applications of a dense but uniform layer of PDI onto the meltable HBC could not be overcome at present and therefore the production of photovoltaic devices using this approach did not show reproducible results. Furthermore, it remains to be clarified, weather the capping material will be fully dissolved and removed by the methanol rinsing procedure used here.

4.3 Evaporation of discotic small molecules

In the previous Sections several solution processing techniques have been discussed in detail for the deposition of discotic materials. An entirely different approach to realize thin films of small molecules is based on sublimation techniques providing also a distinct tool to influence the supramolecular assembly of the molecules. In the following section bi-layered and co-evaporated morphologies cast from the vapor phase are investigated. Furthermore, a combined approach using both sublimation and solution processing techniques for the application of donor and acceptor material, respectively, is tested. Several devices discussed in the following Chapter are also based on this "hybrid" approach (see Chapter 5).

4.3.1 Materials and methods

Unsubstituted HBC (HBC_{parent})

Unsubstituted HBC molecules (HBC_{parent}) can grow in highly crystalline phases and have shown attractive electronic properties when evaporated [197]. The synthesis of this molecule has been accomplished by the Prof. Müllen group and is described in detail elsewhere [198].
In a first experiment the exciton diffusion length L_D of thin films of HBC_{parent} is analyzed. A steady state photoluminescence quenching study and thickness dependent

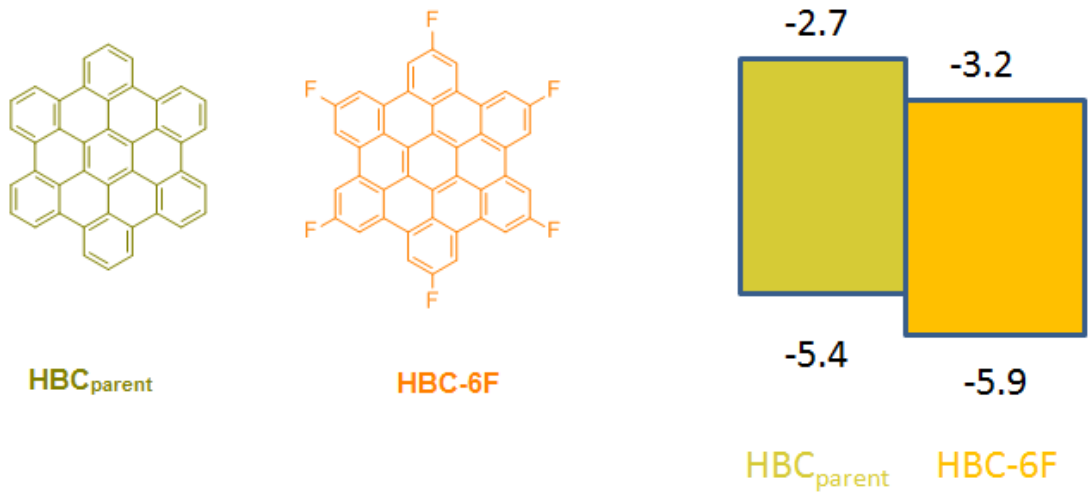

Figure 4.11: HBC derivatives used for vacuum sublimation. Unmodified HBC (HBC_{parent}) and hexa-fluorinated HBC (HBC-6F) are used as donor and acceptor molecules, respectively.

quantum efficiency measurements are performed and reveal an exceptionally long L_D underlyning the potential of HBC as a donor material in OPV devices.
For a sharply defined bi-layer system with a donor material of layer thickness L the application of a suitable acceptor molecule will induce a PL quenching ratio Q [199]:

$$Q = \frac{\left[a^2{L_D}^2 + aL_D \tanh(L/L_D)\right] \exp(-aL) - a^2{L_D}^2(\cosh(L/L_D))^{-1}}{(1 - a^2{L_D}^2)(1 - \exp(-aL))} \tag{4.1}$$

Figure 4.12 shows the quenching rate obtained for a number of different HBC layer thicknesses upon addition of PDI from the solution phase. The colored lines show the estimated quenching rate using the formula 4.1 at a donor material thickness as is shown in the legend. The experimentally obtained data points suggest a value of $L_D = (25 \pm 5$ nm). It is worth mentioning, that the calculation and estimation of L_D may only give a rough estimate: As can be seen from the inset image, the controlled evaporation of HBC yields smooth but not perfectly flat layers with a RMS surface roughness of below 1 nm. A flat heterojunction topology is a prerequisite for the correct application of equation 4.1. In fact, a separate study analyzing the photovoltaic performance of bi-layered heterojunction cells with differing HBC_{parent} layer thicknesses d_{HBC} yields highest performance at $d_{HBC} \approx 25nm$. The performance of devices with higher d_{HBC} is found to be decreased - Excitons generated in the first nanometers of the HBC_{parent} cannot reach the interface before recombination occurs and the filtering effects of this material reduces the current yield.

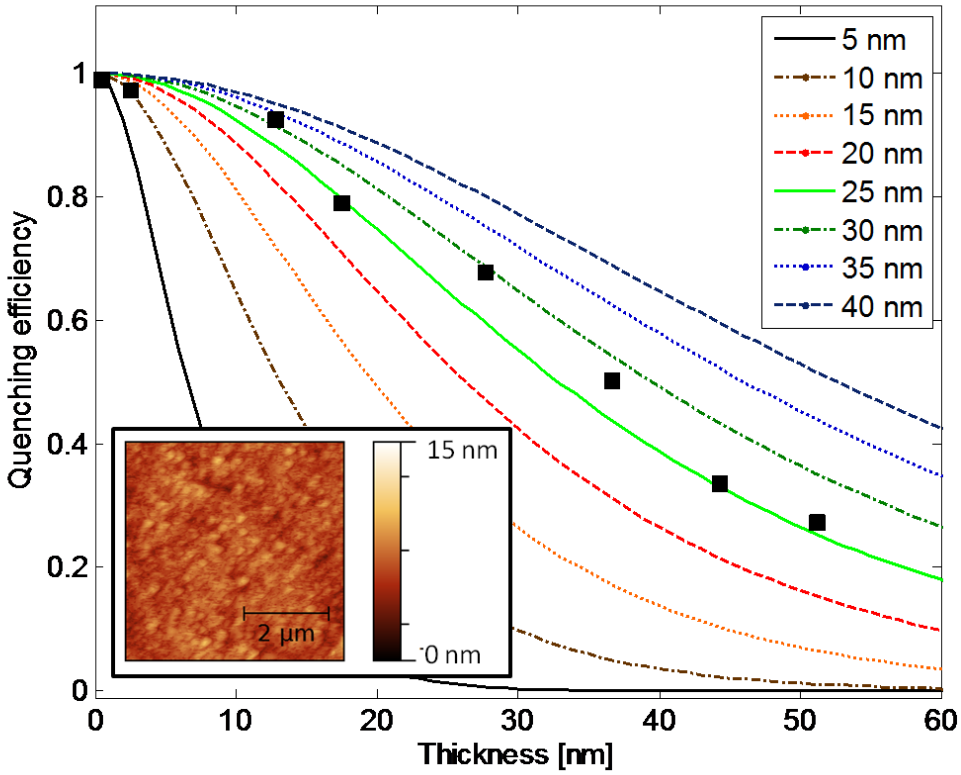

Figure 4.12: Quenching rate analysis for the vacuum processed donor material HBC_{parent}. Data points (black squares) indicate quenching rates obtained depending on the thicknesses of HBC_{parent}. Colored lines are derived using equation 4.1 at an L_D as is indicated in the figure legend. The AFM inset image shows the surface topology of an HBC_{parent} film with a RMS roughness of ≤ 1 nm

It can be concluded, that HBC_{parent} shows very promising properties as a donor material in OPV devices showing an exceptionally high L_D in the order of $20 - 30$ nm.

Fluorinated HBC (HBC-6F)

A fluorinated HBC derivative has been synthesized at the Professor Müllen group as has been described previously [200]. Recent studies using this fluorinated graphene-like molecule have shown p-type semiconducting properties and revealed HOMO and LUMO levels of the organic compound [201, 202]: The electron withdrawing fluorine atoms attached to the six residual positions lower the electronic levels by circa 0.5 eV as is schematically shown in Figure 4.11. The optical absorption of this molecule is very

similar to the spectrum obtained for the unsubstituted HBC_{parent}: peak absorption is centered at around 360 nm strongly decaying towards higher wavelengths with an onset at below 500 nm. The suitable energy level alignment (as shown in Figure 4.11) combined with the similar processing conditions facilitate the investigation of HBC_{parent} and HBC-6F donor-acceptor photovoltaic devices.

4.3.2 Sublimated bi-layer and co-evaporated devices

Two different morphologies cast from the vapor phase are compared for heterojunction devices: Fist a strict bilayer geometry is established by subsequent deposition of HBC_{parent} and HBC-6F. Second, we analyze a structure composed of HBC_{parent} (pristine) / HBC_{parent}:HBC-6F (co-evaporated, blending ratio $\approx$ 1:1) / HBC-6F (pristine). The device geometry is chosen as follows: ITO/PEDOT/active layer/LiF/Al. Metal contacts are evaporated in a N_2 filled glovebox and encapsulated for measurements to avoid contact degradation in ambient atmosphere. Figure 4.13 shows the current voltage characteristics of exemplary devices with an approximate organic layer thicknesses of 30 nm $\|$ 20 nm (HBC_{parent} $\|$ HBC-6F) and 25 nm $\|$ 10 nm $\|$ 15 nm (HBC_{parent} $\|$ HBC_{parent}:HBC-6F $\|$ HBC-6F).
Under AM 1.5 global, 100 mW/cm^2 illumination the devices exhibit a remarkably high V_{OC} of $1.3 - 1.4$ V which can be attributed to the high ΔE_{DA} of the molecules used (see Figure 4.11). On the other hand the current density of the devices remains comparably low. As mentioned above the relatively large bandgap of about 2.7 eV for both HBC derivatives does not allow photon harvesting in the visible to near-IR spectral region.
Interestingly the photovoltaic performance of the bi-layered devices is superior to the co-evaporated sample. In the devices with the intermixed layer structure an increased exciton harvesting yield is expected due to the increased surface area between donor and acceptor. However, it appears, that the morphology obtained in this co-evaporated mixed phase is not suitable for efficient extraction of the photo-generated charges: the diode characteristics in the absence of light suggests that the current flow at both forward and reverse bias is reduced by almost one order of magnitude in the co-evaporated sample. The formation of space charge may also cause the higher V_{OC} observed for the co-evaporated device. Very similar observations have been made for sublimated devices composed of phthalocyanines, where an alternate stacking of the donor and acceptor molecules was observed [203]. An optimization of the film deposition conditions might facilitate the growth of segregated domains of donor and acceptor stacks in the mixed phase [19]. However, the evaporation setup used here for the application of the organic material does not allow an individual control of the deposition rates for co-evaporation.

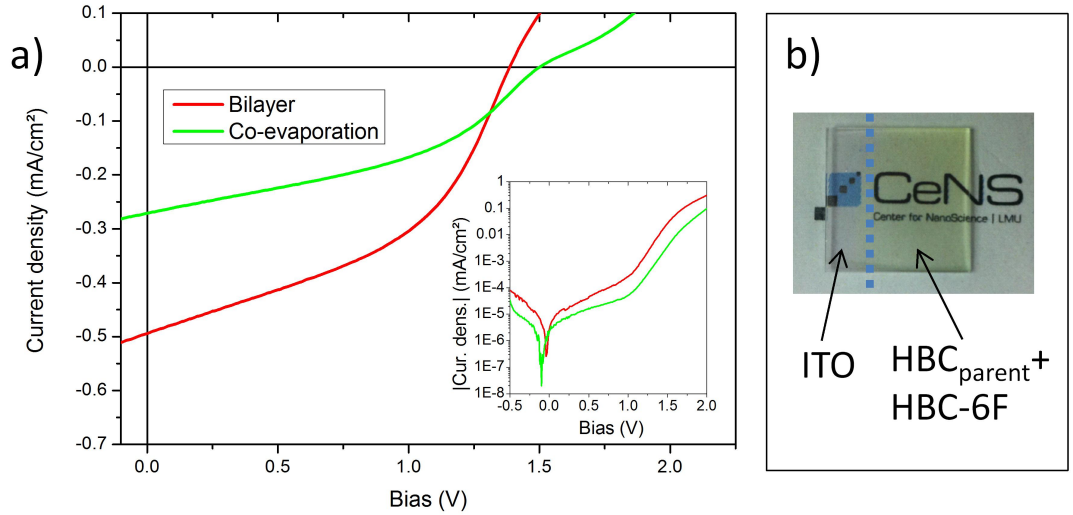

Figure 4.13: IV characteristics and photograph of evaporated HBC$_{parent}$- HBC-6F devices. a) The photovoltaic characteristics of bi-layered and co-evaporated (pristine-mixed-pristine layer sandwich) devices is compared under illumination (large figure) and in the dark (inset figure). **b)** The photograph shows an ITO covered with the two UV-light absorbing active materials as used for manufacturing OPV devices.

In summary a photovoltaic performance of $\eta \approx 0.35\%$ has been shown for sublimated devices with a strict interface between HBC$_{\text{parent}}$ and HBC-6F. We conclude, that sublimation of organic materials can be seen as a powerful method to grow highly ordered layers of a discotic molecule. The pronounced supramolecular assembly in this pristine HBC layer exhibits appealing properties such as a very high exciton diffusion length. Further work will be necessary to optimize the photovoltaic performance achieved for mixed evaporated devices. A favorable stacking of donor and acceptor molecules is most likely not obtained for the mixed evaporated phase. Instead, a comparative study with the bi-layered devices suggests that highly intermixed phases and possibly an alternated stacking is formed for the co-evaporation of HBC$_{\text{parent}}$ and HBC-6F reducing the current generation in these samples despite the large interfacial area. These morphological limitations might be overcome by precisely tuning the film growth conditions, especially in the co-sublimation phase.

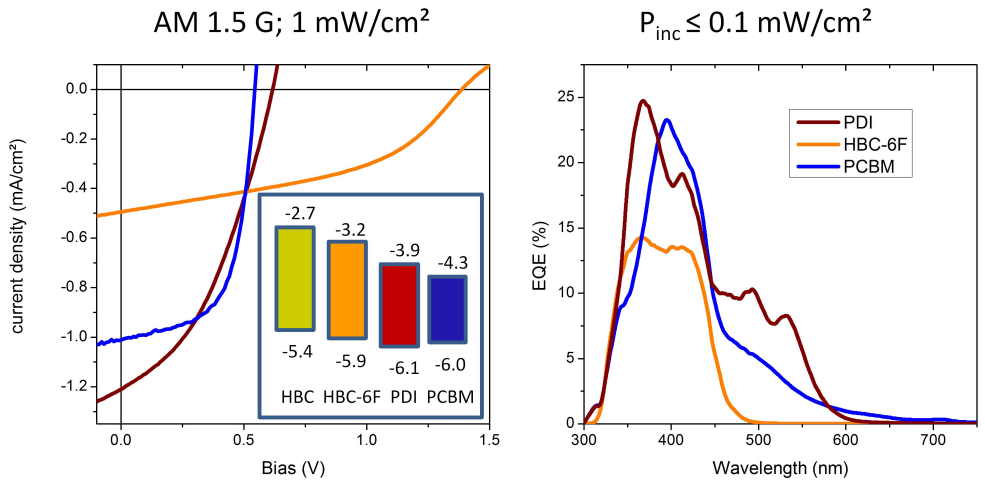

Figure 4.14: A comparison of photovoltaic devices using HBC_{parent} as a common donor molecule. V_{OC} and I_{SC} strongly deviate for the acceptor molecules PDI (red), PCBM (blue) and HBC-6F (orange) as further explained in the text. The inset image shows a schematic of the energy level alignment of the active materials. The EQE spectrum shows the photon harvesting yield in the different spectral regions for the devices under investigation. Data has been obtained at low illumination intensities reducing parasitic geminate recombination.

4.3.3 A Hybrid approach: combining vacuum sublimation and solution processing

Using sublimation processes for the active layer deposition seems attractive: as shown in the previous Section (4.3.2) vacuum processed bi-layered devices show comparable efficiency to the best solution processed blend devices investigated (see Section 4.1). This is especially noteworthy, as the HBC derivatives used for the bi-layers allow photon harvesting in the UV spectral region only. Furthermore, the interface area is strongly confined in the bi-layered geometry.

Combining the evaporated HBC_{parent} with other acceptor materials showing photon absorption in the visible spectral region as well as favorable properties for electron conduction seems appealing. Devices using PDI as well a the common fullerene derivative, PCBM have been tested. In both cases a "hybrid" approach is used: acceptor molecules are processed form solution onto the evaporated donor material. Figure 4.14 shows a comparison of the photovoltaic characteristics for the devices with a planar interface. Highest currents can be harvested when PDI is used as acceptor and current generation remains low for the devices using HBC-6F as acceptor. This can be directly correlated to the photon absorption under simulated solar irradiation for the different acceptor

molecules. For the devices using $PC_{61}BM$ as acceptor best rectification and fill factor is observed. Despite a significantly lower absorption of these devices in the visible spectral region when compared to the $HBC_{parent} \parallel PDI$ couple an almost similar current generation is observed at short circuit conditions. In fact, a superior device efficiency is obtained for the devices with $PC_{61}BM$ as acceptor at the maximum power point. This finding is attributed to a high exciton separation yield as well as favorable electron accepting and transport properties of fullerenes. Instead, for PDI as n-type semiconductor strong limitations apply as will be further discussed in the following Chapter.
In summary the results show that the combined vacuum and solution processing of organic materials holds promise for the the fabrication of efficient photovoltaic devices. Despite little absorption in the visible spectral region, devices using $PC_{61}BM$ as acceptor show the highest fill factor, lowest shunt resistance and best power conversion efficiency.

4.4 Summary

We have studied the application of discotic molecules for photovoltaic applications. The supramolecular assembly of donor and acceptor molecules was varied and the impact on photocurrent generation intensively studied.
The influence of alkyl side chain modifications at the donor molecule on molecular assembly with a common acceptor molecule has been investigated in a first series of experimental studies. Short alkyl chains at the periphery allow for an intimate contact of the HBC cores to a PDI acceptor molecule. PCD and PL measurements indicate that radiative and non-radiative loss mechanisms of excited molecules can be efficiently suppressed when using HBCs with shorter side chains, where consequently best exciton separation and highest current generation yields are found. For these blends an external quantum efficiency of over 27% was achieved at low illumination intensities.
AFM measurements explain the significance of annealing in confinement and reveal differences in cristallinity of the blends under investigation. In conjunction with the X-ray studies performed by Dr Hussein the findings clearly support the formation of an intermixed donor-acceptor phase for short chain HBCs and a disordered phase for long and bulky residues attached to the HBC core. Consequently, increased interfacial area between donor and acceptor as well as a higher charge carrier mobility are achieved for devices where PDI is blended short side chain HBCs. On the other hand, the alternate stacking evidenced in the intermixed donor-acceptor phase especially for the devices using HBCs with short side chains leads to strong bi-molecular recombination as is

supported by the PCD measurements and reflected in a reduced fill factor.
In summary, an increased influence on the morphology of the donor-acceptor interface is crucial to further improve the performance of the devices. A homeotropic alignment consisting of segregated donor and acceptor stacks is believed to allow for strongly reducing the non-geminate recombination present for the best devices investigated here. Face on aligned molecules will facilitate faster charge transport towards the electrodes leading to improved charge extraction.
Several pathways to directly influence the packing of the donor and acceptor molecules have been investigated: A layer-by-layer solution deposition approach using a sacrificial polymer allows to strongly influence the alignment of a meltable HBC derivative. A subsequent deposition of an acceptor from an orthogonal solvent might allow the fabrication of efficient devices.
The molecular assembly and photovoltaic performance of disc shaped donor and acceptor compounds was studied also using sublimation techniques. Co-evaporation of the small molecules results in unfavorable donor-acceptor morphologies, similar to the stacking observed for materials cast from the solution phase. Instead, experiments conducted on bi-layered devices using the unmodified HBC as donor compound reveal the potential of the discotic molecules: A crystalline growth with high supramolecular order can be achieved on the conductive substrate for the HBC donor molecules. Consequently, a long exciton diffusion length is evidenced for this layer. Resulting devices yield a similar power conversion efficiency as is obtained for the best blend mixtures despite the strongly reduced interfacial area of donor and acceptor materials in this device architecture.
Initial experiments show the potential of this pristine HBC layer with high supramolecular order in conjunction with solution processed acceptor layers - an approach that is further optimized in the devices presented in the following Chapter.

5 Perylene Sensitization of Fullerenes

In this Chapter an advanced light harvesting concept for the application in OPV devices is presented and analyzed in detail. The addition of an energy relay dye (PDI) to a fullerene derivative ($PC_{61}BM$) is shown resulting in increased light harvesting and significantly improved power conversion efficiency in various devices.
As mentioned already in the previous Chapter, fullerenes are excellent electron acceptors, but show only limited light absorption. On the other hand, the strong absorbing dye molecule PDI allows only limited performance as an acceptor in photovoltaic devices - possibly due to a lower exciton diffusion length, an inferior electron affinity and morphological limitations [13, 204]. It is shown here, that a combination of both these small molecules within one devices allows to combine their favorable properties: Strongly increased current generation can be achieved in heterojunction devices using a common donor molecule and sensitizing PCBM with PDI.
To demonstrate the potential of the perylene sensitization mechanism on $PC_{61}BM$ we investigate OPV devices using two distinct donor materials: vacuum sublimated HBC is used as small molecular weight donor material with a long exciton diffusion length (see Section 4.3. As mentioned before, the large bandgap of this discotic molecule ($E_g \geq 2.5$ eV) allows photon harvesting only in the UV spectral region (absorption onset at ≈ 500 nm). In a separate device study the donor polymer PCPDTBT is tested in conjunction with dye and fullerene molecules: PCPDTBT absorbs strongly in the near-IR spectral region ($600 - 850$ nm) and has proven its potential in high-efficiency OPV devices previously [98, 103].
Solar cells using either of the above donor materials and $PC_{61}BM$ as electron acceptor absorb strongly in the UV and in the near-IR, respectively, but show limited absorption in the visible. Upon sensitization of the fullerene light harvesting can be significantly improved at a constant device thickness resulting in increased current generation and improved solar cell efficiency. For the photovoltaic devices presented here an overall performance enhancement of up to 160% is achieved via this sensitization method. Using a combination of several experimental techniques, the charge carrier separation and extraction pathways are analyzed in detail and a model for possible energy and charge

transfer process developed for the sensitized devices.
Some of the findings presented in this Chapter have also been published in "Perylene Sensitization of Fullerenes for Improved Performance in Organic Photovoltaics" [99].

5.1 Motivation and concept

Fullerenes are frequently used in organic photovoltaics due to their high electron mobility [110], suitable energy levels [11] and high exciton diffusion length [111]. However, visible light absorption of fullerenes, especially of the most common C_{60} derivatives, is limited. Therefore strongly light absorbing donor materials are needed for efficient light harvesting in the thin active layer of OPV devices. Photocurrent generation and thus power conversion efficiency of this type of solar cell is confined by the spectral overlap of the relatively narrow absorption band of commonly used donor molecules with the solar spectrum. Herein we present the concept of fullerene dye sensitization which allows increased light harvesting on the electron acceptor side of the heterojunction. The concept is exemplarily shown for unsubstituted HBC, an UV absorbing small molecule and PCPDTBT, a near infrared absorbing donor polymer (Chemical names and structure formula are summarized in Section 3.1.1).
In both systems a remarkably higher power conversion efficiency is achieved *via* perylene sensitization of the fullerene acceptor. Steady-state photoluminescence and transient photocurrent decay studies suggest energy and charge transfer routes for sensitized devices. Transient absorption studies combined with spectral electrochemistry measurements reveal the possible pathways of the additionally generated excited states at the sensitizer molecule.

5.2 A dye sensitization mechanism for increased photon harvesting

Maximizing photon harvesting yield while maintaining high open circuit voltage is of fundamental importance for OPV devices. Remarkable current generation and efficiency have been shown for bulk heterojunction devices using a mixture of conjugated polymers as electron donors and fullerene derivatives as acceptors [103, 205, 206]. In recent, further improvements to current yields could be achieved by using low bandgap polymers, shifting the absorption band towards the near-IR allowing for a better spectral overlap with the solar radiation [103, 104]. However, this concept alone does not

allow wide-ranging photon harvesting over the solar spectrum due to the limited absorption bandwidth of most common polymers: Additional light harvesting in the visible to near-IR spectral region of the donor polymers is usually accompanied by a reduction in the UV and visible region.
Tandem cells are one possibility to achieve a wide-band absorption in the active layer and thus strongly enhance the current generation as has been shown both in theoretical and experimental studies [98, 207]. However, fabrication of tandem devices implies more elaborate fabrication processes.
As mentioned already in Section 2.8.1 the common electron acceptor $PC_{61}BM$ shows only little absorption in the visible wavelength region. For this reason, best efficiency in solution processed single junction OPV devices has been reported using $PC_{71}BM$ fullerene derivatives as acceptor molecules which show enhanced light absorption at longer wavelengths [137, 208, 209]. However, C_{70} derivatives are scarce and will remain expensive due to lack of a selective synthesis route. This hinders cost effective, large scale application in roll-to-roll fabricated devices [210]. Furthermore, the molar extinction coefficient of most fullerenes is comparably low and is difficult to be tuned for an ideal solar photon harvesting.
In the previous studies we have shown results using an alternative electron acceptor, PDI, with an increased light absorption. Potential benefits of non-fullerene electron acceptors (e.g. vinazene, perylene and quinine) have drawn much attention in recent [22, 144, 211, 212]. However, in accordance to literature the findings presented herein (Chapter 4) suggest that at present a non-ideal nano-morphology leads to strong bi-molecular recombination using these small molecule acceptors and thus only limited charge collection efficiencies can be achieved at moderate to high illumination intensities [19, 204].
In this Chapter improved light harvesting and current generation in OPV devices is shown *via* perylene sensitization of $PC_{61}BM$ fullerenes. Perylene is an excellent sensitizer molecule due to its suitable energy levels, high molecular extinction in the visible region ($\epsilon \approx 80000\,M^{-1}cm^{-1}$) and its exceptionally high fluorescence yield of close to unity [115, 213]. The devices benefit from both the strong light absorption by the dye molecule and the exceptional charge extraction properties of fullerene molecules.
Data presented in this study suggests that photo-excited sensitizer dye molecules may transfer the excitation energy via fluorescent resonant energy transfer (FRET) towards the fullerene followed by charge separation at the interface to the donor molecule. When in direct contact with both electron donor and acceptor, excitons generated at the dye molecules may also be separated by a direct hole transfer to the donor, which can be followed by dye regeneration via charge transfer to the fullerene.

Only recently similar sensitization concepts have proven to be beneficial for dye sensitized and hybrid solar cells [214–218]. Using highly specialized dyes and acceptor molecules theoretical and experimental sensitization studies have been reported also for OPV devices [219–223]. However, to our knowledge this is the first experimental demonstration of bulk-heterojunction solar cells showing significantly improved performance upon sensitization.
Recently "ternary blends" with a cascaded alignment of HOMO and LUMO levels have also shown to allow for increased current generation [224]. However, introducing a third compound to the active layer also creates additional heterojunction interfaces. Charge generation and recombination has to be addressed for each interface individually.
We propose that the energy transfer process occurring predominantly at low dye loading ratio has a distinct advantage: The sensitizer dye remains electrically neutral when energy transfer occurs from the photo-excited dye to the fullerene. As such, this process is not expected to significantly influence the charge recombination and transport kinetics of the electron donor and acceptor components. Studies performed on a three component mixtures give additional insight to the charge migration pathways at all heterojunction interfaces.
In summary, the additional charge generation via dye excitation allows a decoupling of light absorption and charge transport in the OPV devices. Using this method we can show a versatile and very cost effective way for increased current generation in heterojunction photovoltaic devices.

5.3 Materials and Methods

5.3.1 Organic compounds

The chemical structures and energy levels of the molecules used are listed in Chapter 2. Absorption spectra of the optically active components are summarized in Figure 5.1. $PC_{61}BM$ light absorption is strongest in the UV-region and extends with a narrow tail to over 800 nm. Despite the low HOMO-LUMO bandgap of around 1.7 eV the absorption of $PC_{61}BM$ in the visible is strongly suppressed due to a symmetry forbidden optical excitation [223, 225]. Instead, PDI shows pronounced absorption in the visible with two characteristic features centered at around 495 nm and 540 nm as has been discussed earlier (Chapter 4). The molar extinction coefficient and fluorescence yield of PDI are exceptionally high, which renders this molecule to be an ideal candidate for increased light harvesting in thin film devices [213]. The absorption of HBC peaks at 355 nm

and decreases strongly towards longer wavelengths. PCPDTBT has a low bandgap of approximately 1.4 eV. It shows a low extinction coefficient between 450 – 600 nm, but a pronounced absorption at higher wavelengths extending well over 800 nm.
Incomplete light harvesting in the visible part of the spectrum (between 450 nm and 600 nm) by both the electron acceptor $PC_{61}BM$ and either of the donor materials HBC and PCPDTBT, respectively, motivate the acceptor sensitization. PDI shows a very pronounced absorption in the above mentioned spectral region and has well suited energy levels for energy transfer to the fullerene (see also Figure 5.7).

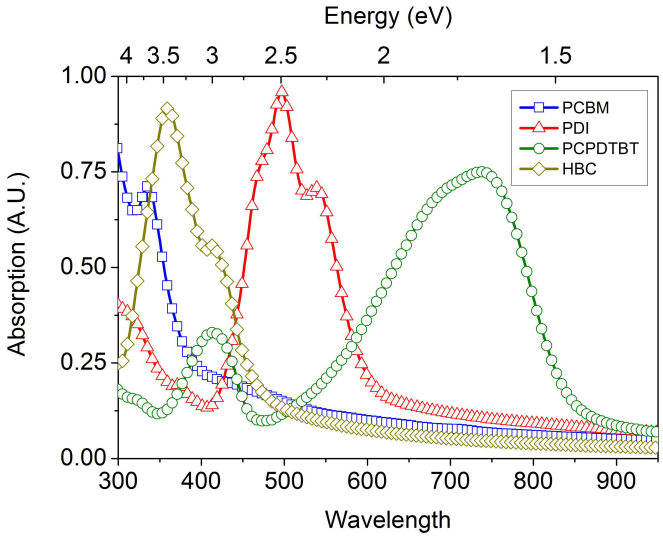

Figure 5.1: Ground state absorption spectra obtained for thin films of the organic materials under investigation

5.3.2 Experimental methods

Photovoltaic devices shown in this Chapter have been prepared according to the methods presented in Chapter 3. For inverted devices TiO_2 was deposited by spray deposition at 450 °C. $PC_{61}BM$ and PDI were solution cast from chloroform solution. In order to guarantee a strict bi-layered interface of the acceptor with the donor polymer PCPDTBT (Konarka) a lamination technique was used as described elsewhere [27, 222]. In brief, thin films of PCPDTBT were spun on freshly cleaved mica from chlorobenzene, floated on deionized water and transferred onto the substrates. PEDOT:PSS was deposited onto the organic layer of inverted devices using the spray deposition method

described before (Section 3.1.5). For the non-inverted devices PEDOT:PSS was solution deposited as bought on the freshly cleaned ITO substrates. After annealing for 5 minutes at 145 °C the samples were transferred to a vacuum sublimation chamber. Vacuum sublimation of HBC_{parent} is performed as described in Chapter 4.3. $PC_{61}BM$ and PDI were spun onto the HBC from chloroform solution. LiF and Al were evaporated onto the photoactive material.

5.4 Photovoltaic device analysis

As mentioned above we will investigate two model systems that show a distinct absorption to the sensitizer dye. HBC-$PC_{61}BM$ and PCPDTBT-$PC_{61}BM$ bi-layered solar cells were fabricated using different techniques to assure well defined donor-acceptor heterojunction interfaces. HBC is deposited via vacuum sublimation and the resulting films are insoluble in common solvents. Therefore, $PC_{61}BM$ and PDI can be spin cast from solution on top of HBC films. For PCPDTBT devices instead an inverted geometry is used and thin films of the polymer are transferred on top of $PC_{61}BM$:PDI using a floating technique. Besides, the potential of PDI-sensitization of $PC_{61}BM$ is also shown in ternary blends using either of the donor materials, $PC_{61}BM$ and PDI.

5.4.1 Device studies using an UV absorbing small molecular donor

As shown in Figure 5.2 bi-layered solar cells with HBC as donor show a clear device improvement if $PC_{61}BM$ is sensitized with PDI: under AM 1.5 global, 100 mW/cm^2 illumination both I_{SC} and V_{OC} increase significantly upon blending PDI with the fullerene. At the optimal dye loading ratio of 50% I_{SC} is enhanced by a factor of 1.8 and the overall efficiency by 160%. We note that at 50 % PDI content in the acceptor mixture the FF is slightly decreased when compared to solar cells without PDI sensitization and performance drops significantly for devices with PDI (*vide infra*).
To our knowledge, the efficiency of over 0.4 % under simulated solar light achieved for ideally sensitized devices presented here is the highest performance reported so far using pristine HBCs as a donor material. This is especially noteworthy since the donor-acceptor interface is intrinsically small in a bi-layered device.
EQE measurements (Figure 5.2) clearly reveal the origin of the additionally generated charge carriers for the sensitized device: Devices without PDI show the highest peak photon-to-current conversion efficiency ($EQE_{max} = 22\%$) but the contribution at higher wavelengths to the photocurrent is minimal. At a PDI content of 50 % the peak

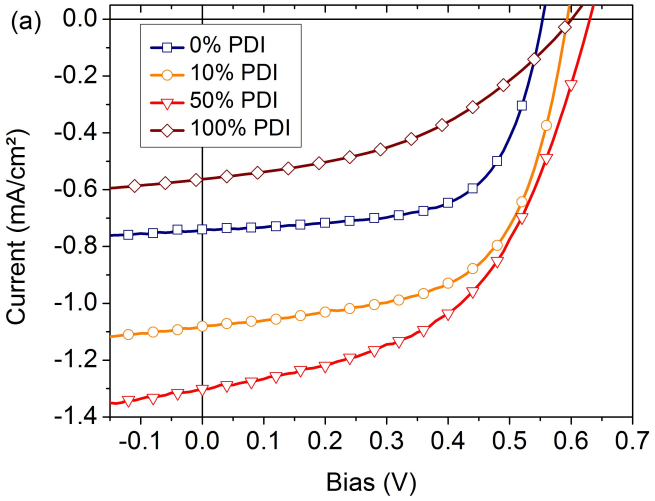

Figure 5.2: IV-curves of bi-layer solar cells using HBC as donor material. PCBM is used as acceptor molecule. The dye loading ratio in the acceptor phase is indicated in the figure legend. For comparison a the device characteristics for a device using pristine PDI (100% PDI) is shown also.

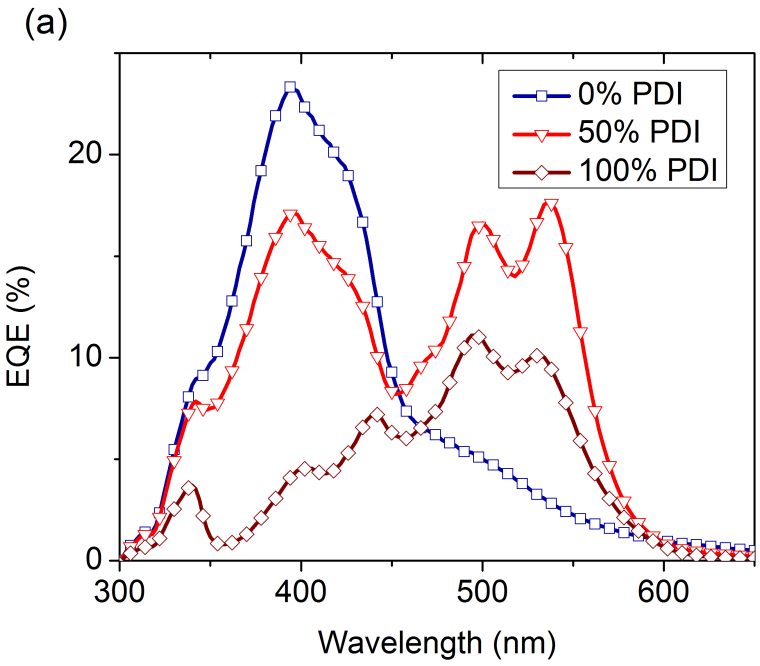

Figure 5.3: EQE spectra of HBC bi-layer solar cells. Devices using pristine PCBM, pristine PDI and an ideally sensitized acceptor mixture (50 wt%:50 wt%) PDI:PCBM are compared.

around 400 nm, which is attributed to current generation via excitation of both HBC and $PC_{61}BM$, slightly decreases but the EQE is significantly enhanced in the spectral region of strong PDI absorption ($450 - 650$ nm). Due to a better overlap with the solar spectrum the overall photocurrent is dramatically increased in this case. For PDI-only devices the EQE in the PDI is found to be lower than at 50 % PDI content, probably due to transport limitations as further analyzed along with the photocurrent decay data (Section 5.5.1). This reduced EQE is in good accordance with the lower I_{SC} measured at 1 sun illumination (Figure 5.2).
As supported by PL and TAS experiments (Section 5.5.2 and Section 5.5.3), resonance energy transfer is likely to occur in sensitized devices from photo-excited PDI to $PC_{61}BM$. With increasing PDI content more photons in the visible are absorbed by the acceptor blend, excitons are transferred to $PC_{61}BM$ and separated at the HBC-$PC_{61}BM$ interface. This results in significantly improved photocurrents for PDI containing devices and facilitates photon harvesting in the visible. Interestingly we also observe a slightly higher V_{OC} for the sensitized devices ($\Delta V_{OC} \approx 100$ mV) at optimal dye loading ratio. We note that an improved V_{OC} may be resulting from increased charge carrier density and reduced bimolecular recombination [226]. Charge extraction experiments presented in the following section shed some light into the possible extraction pathways.

5.4.2 Sensitized devices studies using a near-IR absorbing polymer

The promise of the sensitization concept is supported further by experiments with PCPDTBT as donor material. Bi-layered devices are realized in an inverted geometry, i.e. with TiO_2 as hole-blocking bottom contact and lamination of the donor polymer onto solution processed acceptors as further described in the experimental part (Section 5.3.2). Solar cell performance was found to be improved upon addition of PDI to the acceptor similar to the results obtained using HBC as donor material. However, for this system best efficiencies were obtained at a PDI content of only 25 % (Figure 5.4). At higher sensitizer loading ratio the power conversion efficiency was found to be decreased. EQE spectra reveal mechanisms similar to the case of HBC devices. Upon addition of 25 % PDI a pronounced EQE feature in the PDI absorption region around 500 nm arises without significantly affecting current generation in other spectral regions. At further increased PDI content the EQE drops at all wavelengths resulting in decreased photocurrent generation at simulated solar light illumination.
The differences in optimized PDI content are attributed mainly to a competition of PDI and PCPDTBT absorption (Figure 5.1). In contrast to HBC, the PCPDTBT absorp-

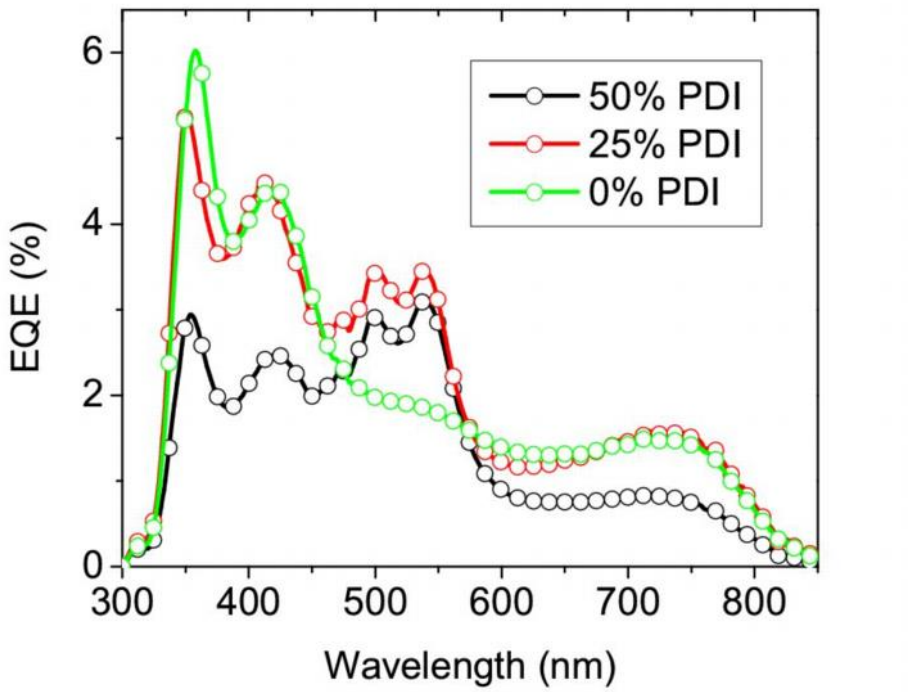

Figure 5.4: EQE spectra of bi-layer solar cells using PCPDTBT as donor polymer. The polymer is laminated onto the solution processed PDI and $PC_{61}BM$ layers to ensure a strict interface.

tion at $450 - 650$ nm cannot be neglected. Therefore, a lower amount of perylene is needed for optimized photon harvesting in the visible spectral region.

Morphological limitations are apparent from experiments with blend devices using PCPDTBT, $PC_{61}BM$ and PDI as a ternary mixture. Only small amounts (approximately 2%) of sensitizer may be added for increased current generation and device performance as evident from the IV curves and EQE spectra shown in Figure 5.5. An addition of 5 % PDI results in decreased current generation at all wavelengths. The morphology and consequently power conversion efficiency of PCPDTBT:$PC_{61}BM$ solar cells is very sensitive to processing conditions, e.g. use of solvent additives [103]. We propose that even small amounts of PDI disturb the formation of an efficient donor-acceptor network in PCPDTBT:$PC_{61}BM$ blends. Thus, non-ideal phase separation of PCPDTBT, $PC_{61}BM$ and the added PDI lead to incomplete charge carrier percolation pathways and a modification of the donor-acceptor interfacial area which are crucial for high-efficiency excitonic solar cells. Nevertheless, the addition of the perylene sensitizer PDI directly contributes to photocurrent generation in PCPDTBT:$PC_{61}BM$ blend so-

lar cells which intrinsically absorb only weakly in the visible (450 – 600 nm) as can be observed in the EQE spectra.

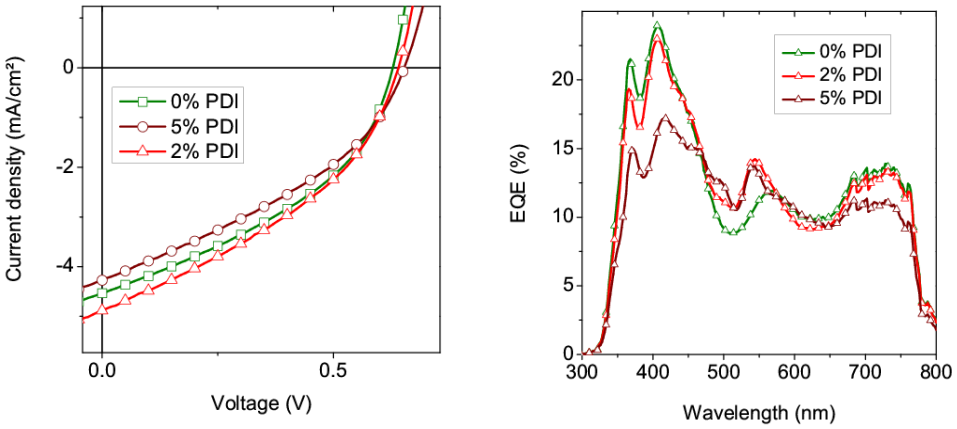

Figure 5.5: IV characteristics (a) and EQE spectra (b) of sensitized PCPDTBT blend devices. The addition of low amounts of sensitizer molecules allows increased current generation in the devices..

5.5 Energy and charge transfer mechanisms

In the following section it is our aim to shed some light into the photophysical mechanisms present in the sensitized devices, that allow increased current generation and performance in the photovoltaic devices upon sensitization. We will limit ourselves to devices using HBC as donor material, as for this wide bandgap material a simultaneous excitation of sensitizer dye and donor material can be avoided using an excitation wavelength of 532 nm.

5.5.1 Photocurrent decay studies

Charge carrier transport and extraction can be analyzed in photovoltaic devices using transient photocurrent decay (PCD) measurements as has been shown already in the previous Chapter (Section 4.1.6).
The photocurrent of HBC-$PC_{61}BM$ (+PDI) bi-layer solar cells is monitored on short timescales (200 ns - 20 µs) after laser excitation under a constant white light background illumination. Additional charge carriers are generated in the devices upon laser

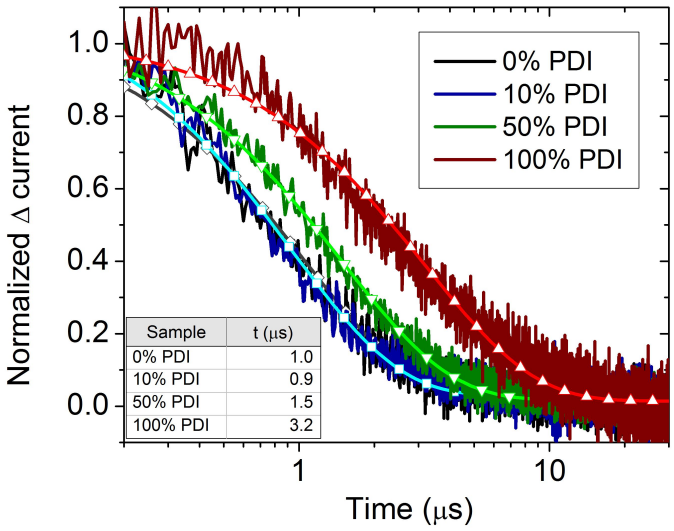

Figure 5.6: Photocurrent decay analysis of sensitized photovoltaic devices HBC as donor material and PDI/PCBM as acceptors

pulse excitation and cause an additional photocurrent [189, 227].
Normalized current decay curves are shown in Figure 5.6. At the pump wavelength of 532 nm exciton generation is favored in the sensitizer dye but only limited excitation of $PC_{61}BM$ molecules will be achieved (see Figure 5.1). Fastest decay is monitored for non sensitized HBC:PCBM devices or devices with a low dye loading ratio. For devices using PDI as the sole acceptor a strongly delayed charge extraction signal is observed, instead. We tentatively assign this delayed charge extraction to trapping of charges on perylene grain boundaries. The existence of long lived trap states and extended photo-excitation lifetimes has been reported previously for perylene [228–230]. Mono-exponential fits ($\Delta I = I_0 * e^{-t/\tau}$) to the decay data reveal a time constant of $\tau_{PCBM} = 1.0$ µs for devices using $PC_{61}BM$as sole acceptor. A similar decay constant of $\tau_{sens1} = 0.9$ µs is obtained when fitting data obtained from devices with 10% PDI content (the deviation to the pristine $PC_{61}BM$ device is within the measurement error). Using pristine PDI as acceptor a time constant of $\tau_{PDI} = 3.2$ µs was extracted from the decay data. Upon addition of 50% PDI a fit reveals a lifetime of τ_{sens2} =1.5 µs. A simple superposition of PDI and $PC_{61}BM$ extraction lifetimes would instead suggest a significantly longer lifetime (τ_{super}=$(A * \tau_{PDI} + B * \tau_{PCBM})/2 > 2.1$ µs for $A > B$ [molar extinction of PDI > molar extinction of PCBM at the excitation wavelength of 532 nm]).

The experimental data obtained suggests that for the sensitized devices also in case of photo-excitation of the PDI the charge extraction of the electrons occurs predominantly via the fullerene. This is in accordance with the IV curves shown: FF and rectification of sensitized devices mimic closely the curve shape obtained when using $PC_{61}BM$ as sole acceptor.
We propose two mechanisms which can explain the experimental findings: As summa-

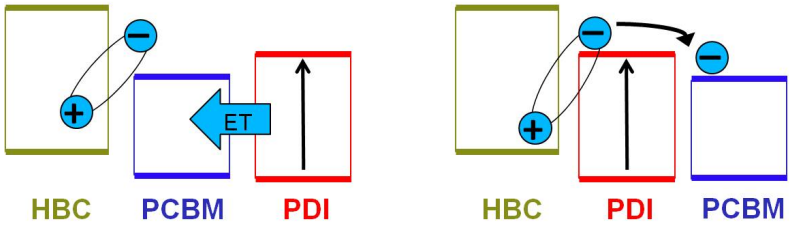

Figure 5.7: Energy level alignment of HBC_{parent}, PDI and $PC_{61}BM$. Possible charge generation and extraction pathways after photo-excitation of the sensitizer molecule are depicted.

rized in Figure 5.7 resonance energy transfer may occour from the photo-excited PDI to the fullerene followed by a charge separation at the interface to the donor material. However, considering the energy levels as summarized in Figure 5.7, charge separation at the HBC-PDI interface should also be considered, especially at high dye loading ratio. This charge generation process might be followed by electron transfer from the charged PDI to $PC_{61}BM$. As visible in the photocurrent decay transients a delayed charge extraction is observed for devices containing PDI only in the acceptor phase. Both excitation transport to the donor-acceptor junction and mobility of electrons after charge separation are significantly slower in PDI when compared to $PC_{61}BM$. However, using PCD experiments alone, we can not distinguish the two plausible pathways for charge generation upon sensitizer excitation. Further experiments are necessary to elucidate the process in more detail.

5.5.2 Photoluminescence studies

Steady state photoluminescence (PL) measurements have been conducted on sensitized $PC_{61}BM$ thin films. PDI and $PC_{61}BM$ have been blended to the desired composition and deposited on quartz glass at an equal film thickness ($d \approx$100 nm). At the excitation wavelength of 532 nm PDI absorbs strongly, but $PC_{61}BM$ absorption is found to be very weak. We account for the photo-absorption differences at the excitation wavelength by normalizing the PL spectra. The peak emission of PDI and $PC_{61}BM$ is centered at 650

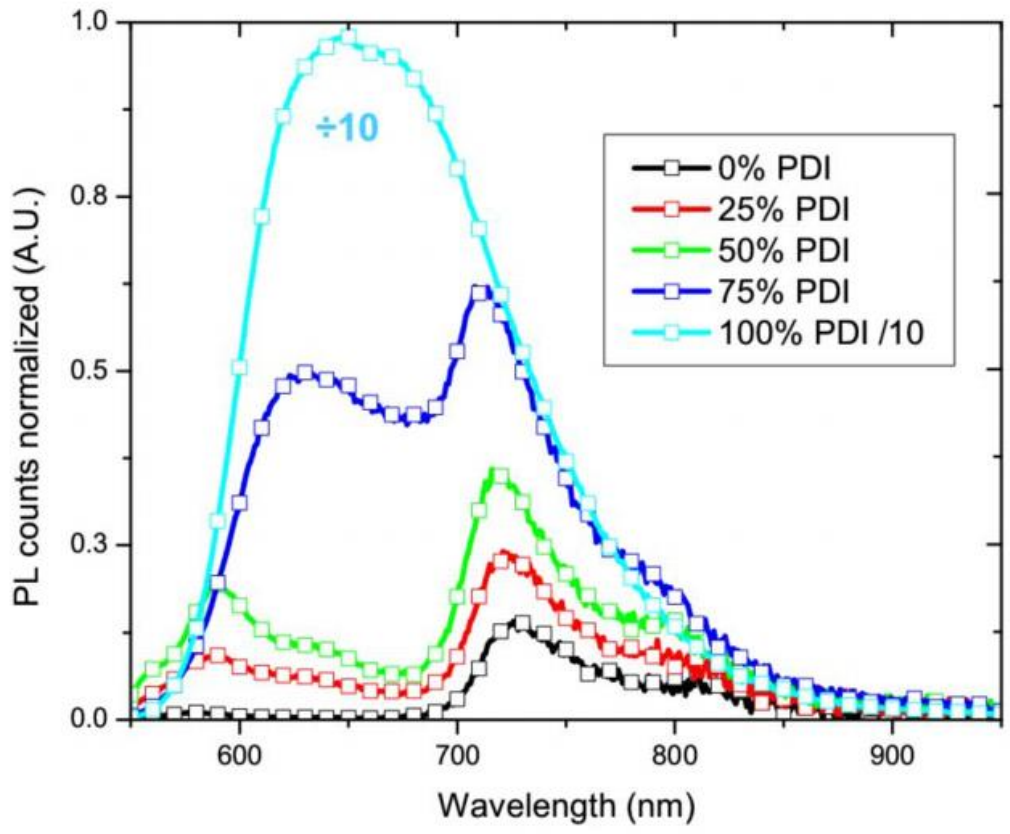

Figure 5.8: Steady state photoluminescence emission spectra of sensitized $PC_{61}BM$ films. Excitation was set to 532 nm and emission recorded for samples of comparable thickness. Signals are normalized to the film absorption at the excitation wavelength.

nm and 725 nm, respectively (Figure 5.8). In blend films of the two small molecules the observed peaks can be attributed to PDI and $PC_{61}BM$ fluorescence. However, the peak heights obtained cannot be explained by the fraction of light absorbed in the two compounds: The addition of small amounts of the perylene dye to $PC_{61}BM$ yields an increased emission from the fullerene. Despite reduced $PC_{61}BM$ content in a 25:75 (PDI:$PC_{61}BM$ wt%) blend film we observe a twofold increased emission at around 725 nm when compared to a pristine $PC_{61}BM$ film. At the same time perylene emission in the blend films is strongly suppressed and blue shifted. Similar trends can be observed at higher dye loading ratios: the emission feature at 725 nm (assigned to $PC_{61}BM$) is enhanced while perylene emission (600 nm) is strongly suppressed and shifted towards shorter wavelengths. Aggregation effects frequently observed for PDI may affect the perylene PL emission peak position as observed here, but cannot explain the observed

PDI: $PC_{61}BM$ [wt%:wt%]	Rel. PDI PL (%)	Rel. $PC_{61}BM$ PL (%)	$PC_{61}BM$ PL norm to $PC_{61}BM$ content
100:0	100.0	0.0	—
90:10	11.9	59.8	18.0
75:25	4.9	100.0	12.0
50:50	0.9	64.6	3.9
25:75	0.5	49.8	2.0
5:95	0.2	40.3	1.3
0:100	0.0	33.2	1.0

Table 5.1: Peak analysis of photoluminescence spectra for pristine and blended films of PDI and PCBM. The relative PL emission yield of PDI was calculated by normalizing the emission of the blend films recorded at 650 nm to the emission of the pristine film. Relative $PC_{61}BM$ PL was determined subtracting the PDI emission signature from each film individually. PL rates are subsequently normalized to 100%

increase in $PC_{61}BM$ emission upon blending PDI to the fullerene [116, 117].
In order to determine the contribution of the sensitizer to the $PC_{61}BM$ emission, the signature of the PDI emission is subtracted for each spectrum individually (Table 5.1). The subtracted signal at 725 nm, attributed to the emission of $PC_{61}BM$, is found to be highest at a blending ratio of 75:25 (PDI:$PC_{61}BM$ wt%). Normalizing the $PC_{61}BM$ emission in the blend films to the $PC_{61}BM$ content in the respective layers reveals an 18 fold increase of the $PC_{61}BM$ emission for a 90:10 (PDI:$PC_{61}BM$ wt%) film. These findings are attributed to an energy transfer from the strongly absorbing perylene dye to the $PC_{61}BM$.

Calculating the förster-radius of the PDI:PCBM system Despite little ground state absorption of $PC_{61}BM$ in the visible (Figure 5.1) resonance energy transfer can still be very effective when using strongly fluorescent dye molecules. Perylenes are known to show an exceptionally high fluorescence quantum yield of close to unity [213]. Liu et al. reported a Förster resonance radius of 2.7 nm using nile red as fluorescence donor and $PC_{61}BM$ as acceptor [231].

$$R_0^6 = \frac{9000 \ln 10 \kappa^2 Q_D}{128 \pi^5 n^4 N_A} \int F_D(\lambda) \epsilon_A(\lambda) \lambda^4 d\Lambda \tag{5.1}$$

Using formula 5.1 and assuming a fluorescence yield of $Q_D = 0.96$ [213] and a refractive index of $n = 1.5$ [232, 233] we estimate a Förster radius of $R_0 = 2.8\,\mathrm{nm}$ for the PDI:$PC_{61}BM$ system.

5.5.3 Analysis of photo-excited states

Transient Absorption on PDI:PCBM samples

In order gain insight to the photophysics of PDI and $PC_{61}BM$, nanosecond transient absorption spectroscopy (TAS) measurements were performed at the Intelligent Polymer Research Institute at Wollongong, Australia under the supervision of Dr Attila Mozer. This pump probe techniques is a powerful method for the analysis of photo-excited states in organic compounds [52]. Pristine $PC_{61}BM$ and (50:50 wt%) PDI:$PC_{61}BM$ blend films were measured both in the presence and in the absence of oxygen. A pump wavelength of 532 nm (strong PDI and weak $PC_{61}BM$ light absorption) was used and changes in transmission of the samples were monitored in the visible to near-IR spectral region (500 – 1200 nm) at various pump beam intensities. For the transient absorption measurements re-purified PDI was used.
Energy transfer from photo-excited PDI molecules to $PC_{61}BM$ is expected to result in strongly increased $PC_{61}BM$ triplet yield as will be shown below. Based on the scematic energy diagram in Figure 5.7 electron transfer from PDI to $PC_{61}BM$ is also possible, although with a relatively small thermodynamic driving force of 0.4 eV. This electron transfer process would yield PDI cations and $PC_{61}BM$ electrons. A subsequent recombination of these charged species could also result in $PC_{61}BM$ triplet formation – however, this process should occur on time scale of this recombination process, typically in the range of µs to ms [52].
The spectroscopic features of charged and triplet states of $PC_{61}BM$ and PDI can be well distinguished using TAS: PDI cations are expected to show a narrow absorption band centered at 590 nm [213] and $PC_{61}BM$ electrons strongly absorb at 1040 nm [234]. PDI triplets show two absorption features at around 480 and 510 nm, whereas $PC_{61}BM$ triplets have a very distinct transient absorption spectrum showing a peak at 710 nm and a broad shoulder at around 825 nm [213, 235]. The lifetime of the $PC_{61}BM$ triplet has been reported to be on the order of 10-20 µs [236]. However, the triplet lifetime is highly sensitive to the presence of oxygen: effective triplet energy transfer to ground state triplet oxygen leads to a quenching of $PC_{61}BM$ triplets [223]. Instead, the lifetime of charged photo-excitations is not expected to be strongly influenced by the presence of oxygen. Furthermore, the recombination kinetics of charges is typically bi-molecular and therefore depends on the pump light intensity, whereas triplets decay mono-exponentially with no obvious excitation energy dependence (at low excitation energies where triplet-triplet interactions can be neglected).
Transient absorption experiments were carried out either in ambient atmosphere or en-

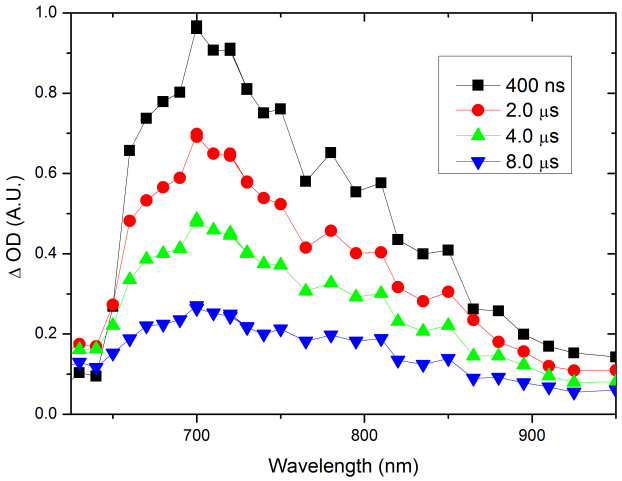

Figure 5.9: TAS on PDI:PCBM blend sample. Spectrum shows features well matching the characteristic features of $PC_{61}BM$ triplets.

capsulated in a nitrogen-filled capillary. Figure 5.9 shows a spectrum recorded for the blend film encapsulated in nitrogen showing the strongest absorption at 710 nm and a broad shoulder in the 800 nm region, in accordance with the $PC_{61}BM$ triplet signal reported in literature [236]. Kinetic traces recorded at the peak wavelength of 710 nm can be fitted to a mono-exponential decay $y = A * e^{-t/\tau}$ as visualized in Figure 5.10: A linear dependence of the signal amplitude with excitation energies is observed. Moreover, fits to the kinetic traces at 710 nm in the absence of oxygen reveal an excitation energy independent lifetime of $\tau \approx 9$ µs, which is slightly shorter but of similar magnitude as reported in literature [236].

We propose that the $PC_{61}BM$ triplet lifetime observed here is affected by small amounts of impurities in the PDI, or remaining oxygen trapped in the films during fabrication. More importantly, we observe a strong reduction of both the magnitude and lifetime of the signal at 710 nmin the presence of oxygen. We also note that at this wavelength (710 nm) a contribution by PDI triplets to the signal (centered at 500nm) can be excluded [224].

The $PC_{61}BM$ triplets observed in the blend films could be formed via direct photo-excitation of $PC_{61}BM$ or by energy transfer from photo-excited PDI singlets (at 532 nm) and subsequent inter-system crossing from singlet to triplet $PC_{61}BM$, analogous to the mechanisms observed for polyfluorene:$PC_{61}BM$ blend films [236].

A pristine $PC_{61}BM$ sample with similar thickness was measured using the same en-

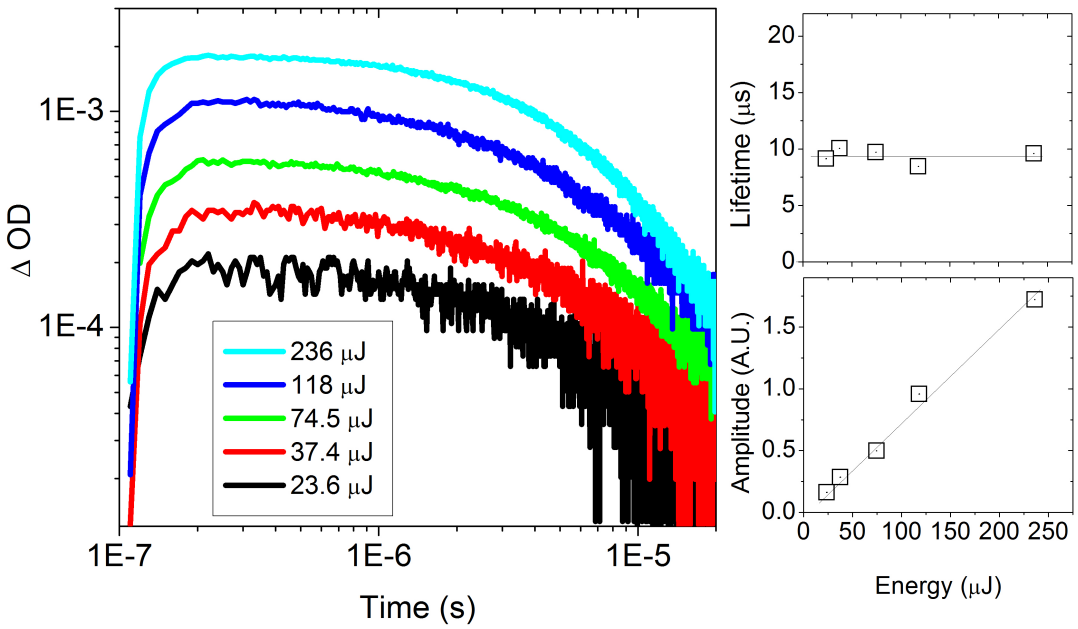

Figure 5.10: Transient absorption kinetics acquired at 710 nm for PDI:$PC_{61}BM$ blend films under air exclusion. Pump laser was set to 532 nm and sample excitation energy was adjusted (23.5 – 235 $\mu Jcm^{-2}pulse^{-1}$) using a set of reflective ND filters. Inset figures show lifetime and amplitude derived from mono-exponential fits ($y = A * e^{-t/\tau}$) to the kinetics data.

capsulation method. A scan of the probe over wavelengths in the range of 500 nm to 1200 nm revealed only very weak signals and no distinct shape of the spectrum for this reference sample. We attribute this finding to the weak photo-excitation of $PC_{61}BM$ at 532 nm, and therefore low triplet yields beyond the detection limit of our setup ($\Delta OD \leq 5 - 10\ \mu OD$). This comparison shows a significantly improved triplet yield in the PDI:PCBM blend at a similar film thickness of 100 nm. While delayed PCBM triplet generation through recombination, faster than the 50 ns time-resolution of our setup, cannot be excluded, all our findings strongly suggest that energy transfer is likely to be the dominant mechanism for PDI:$PC_{61}BM$ blends upon PDI excitation.

Photo-excited states in ternary blend mixtures

The transient absorption studies performed on PDI:PCBM samples (Section 5.5.3) have evidenced an energy transfer from the photo-excited sensitizer molecule to the fullerene.

However, it is not known at this stage, weather other mechanisms, e.g. the charge transfer route proposed in section 5.5.1, will also contribute to the charge generation upon PDI excitation. In order to elucidate this energetically possible route it is necessary to investigate samples containing sensitizer, fullerenes and donor molecules.
A solution processed HBC derivative (HBC-Ph-C_{12}) has been chosen for these studies allowing a strongly increased interfacial area of the three components when compared to the bi-layered devices shown above. The investigations performed here should be seen as a qualitative approach rather than a quantitative disambiguation of possible charge carrier migration pathways in sensitized devices.

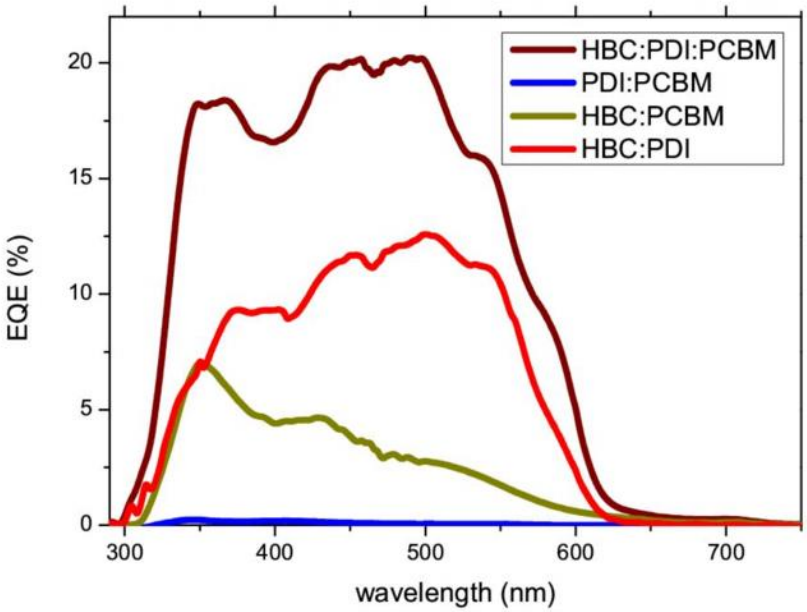

Figure 5.11: External quantum efficiency of donor-acceptor blends and ternary mixtures. HBC-Ph-C_{12} was used as donor material. The blending ratio is 1:1 (HBC:PDI, HBC:PCBM, PDI:PCBM) and 2:1:1 (HBC:PDI:PCBM) for the ternary blend device, respectively.

External quantum efficiency of small molecular weight blend mixtures In a first experiment inverted photovoltaic blend devices (layer structure: ITO/Sputtered TiO_2/ organic/Ag) were assembled with all material combinations of the three compounds HBC-Ph-C_{12}, PDI and $PC_{61}BM$. Figure 5.11 shows the EQE obtained for the four different material combinations as stated in the figure legend. The blending ratio is 1:1 (HBC:PDI, HBC:PCBM, PDI:PCBM) and 2:1:1 (HBC:PDI:PCBM) for the ternary blend device, respectively. At this very low illumination intensity best photon to current

conversion efficiency is obtained for the ternary blend followed by the HBC:PDI and HBC:PCBM blends.
It is important to note here, that the mixture of the two electron acceptor compounds PDI and PCBM yields only negligible current generation at all wavelengths. This finding is consistent with the energy band level alignment and the energy transfer mechanism evidenced from photo-excited PDI to PCBM. As such, charge separation at this organic-organic interface is not possible. In fact, the very low currents generated under illumination (EQE $< 1\%$) are attributed to an exciton separation at the interface of the organic materials with the TiO_2 layers.
It is worth mentioning, that at a standard illumination of $100\,mW/cm^2$ the current density and efficiency of the ternary blend device presented here is in fact lower than the values obtained for the blend devices consisting of HBC and PDI and also lower than those obtained for best sensitized devices realized on vacuum deposited HBC_{parent}. Strongly enhanced bimolecular recombination is apparent for ternary blend devices which is attributed to missing percolation pathways in the complex system of a three component mixture. However, at this point our focus is to determine which energy and charge transfer routes are apparent in the different blend mixtures.

Spectral electrochemistry Cyclic voltammetry scans reveal oxidation and reduction onsets for the three photoactive materials $PC_{61}BM$, PDI and HBC-Ph-C_{12} under investigation (as described in the experimental Section 3.2.7).
Spectral electrochemistry measurements shown in Figure 5.12 reveal the changes in absorption obtained for the organic compounds in DCM solution upon applying an appropriate bias voltage for each compound.
For the formation of HBC cation (HBC-Ph-$C_{12}^{\bullet+}$), PDI anion ($PDI^{\bullet-}$) and PCBM anionic species ($PC_{61}BM^{\bullet-}$) the voltage was set to -5.4 V (HBC-Ph-C_{12}), -3.9 V (PDI) and -3.6 V ($PC_{61}BM$) versus vacuum level. The charged species formed at the bias potentials applied reproducibly show a distinctive band structure as summarized in Figure 5.12. The $PDI^{\bullet-}$ absorption spectrum shows a series of distinct features at 710 nm, 800 nm and 950 nm very well in accordance to literature [213]. Spectra obtained for HBC-Ph-$C_{12}^{\bullet+}$ and $PC_{61}BM^{\bullet-}$ show strongest absorption at 1200 nm and 1050 nm respectively [141, 235].

Transient absorption studies Transient absorption spectra have been recorded for thin blend films, namely PDI:PCBM, HBC:PDI and HBC:PDI:PCBM. It is our intention to determine the formation and recombination of charged species generated after

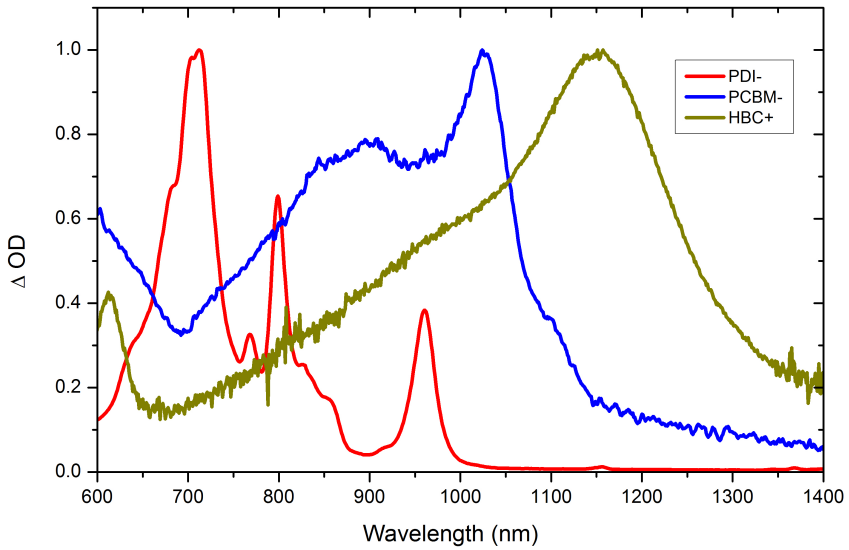

Figure 5.12: Spectral electrochemistry data obtained for charged species of the molecules under investigation. HBC cation ($HBC^{\bullet+}$), PDI anion ($PDI^{\bullet-}$) and PCBM anionic species ($PC_{61}BM^{\bullet-}$) show distinctive absorption spectra.

laser excitation. The measurements have been performed on air. As such, $PC_{61}BM$ triplet signals generated *via* energy transfer from the photo-excited PDI to the $PC_{61}BM$ will be strongly suppressed (as has been shown in Section 5.5.3) and are most likely not visible in the transients recorded at the timescale shown here (100 ns - 10 µs). However, if charged species are formed upon laser excitation a change in the sample transmission should become evident also in the presence of oxygen.

As already mentioned in the previous section for the PDI:PCBM sample no transient absorption signals could be observed on air. Either no charged species are generated in this blend or generated species recombine at timescales faster than the detection limit of our setup ($50 - 100$ ns). This is also in accordance to studies on photovoltaic devices based on the two materials yielding a good diode shape but no photocurrent upon illumination. These findings support energy transfer rather than charge transfer. Instead, HBC:PDI blend films show strong transient absorption signals with multiple bands as visualized in Figure 5.13 (upper panel). The pronounced signal centered at 710 nm and a set of signal spikes at higher wavelengths (800 nm, 950 nm) can be attributed to the PDI radical anion ($PDI^{\bullet-}$) in accordance with the SEC experiments (Figure 5.12) and also with literature [213]. We observe a slight red shift for all peak

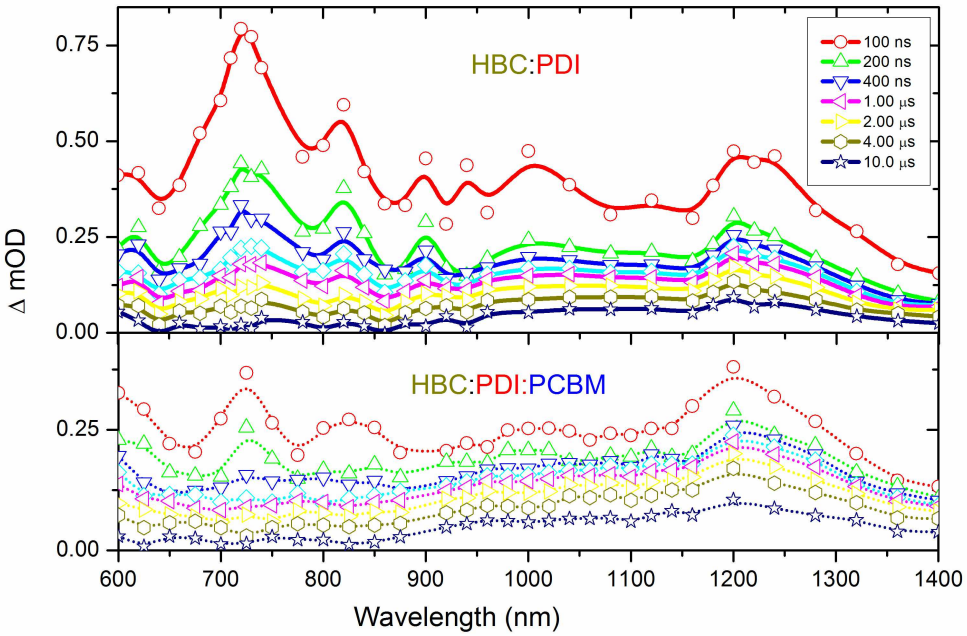

Figure 5.13: Transient absorption spectra of HBC:PDI and HBC:PDI:$PC_{61}BM$ samples. Different colors show changes in transmission upon laser excitation at 532 nm at the times specified in the figure legend.

positions of the $PDI^{\bullet-}$ in the solid phase for the TAS samples compared to the SEC data. This can be well explained by aggregation effects occurring for the TAS measurements conducted on thin films and not in the solution phase in contrast to the SEC spectra [116]. The signal located at 1200 nm is attributed to the cationic species of HBC ($HBC^{\bullet+}$), again slightly red shifted compared to the SEC data. The time evolution of the spectrally resolved data reveals that both $HBC^{\bullet+}$ and $PDI^{\bullet-}$ decay on an equal time scale indicating that $HBC^{\bullet+}$ and $PDI^{\bullet-}$ recombine with each other.
TAS data obtained for HBC:PDI:$PC_{61}BM$ at the same excitation energy yield the spectra presented in Figure 5.13 (lower panel). Similarly to the HBC:PDI blend pronounced signals at 710 nm, 800 nm and 1200 nm can be observed which are attributed to $PDI^{\bullet-}$ (710nm, 800 nm) and $HBC^{\bullet+}$ (1200nm). The signal observed at around $950 - 1050$ nm appears to be slightly broadened extending well over 1000 nm. When using the same laser excitation energy in both systems analyzed (HBC:PDI and HBC:PDI:PCBM) a similarly pronounced $HBC^{\bullet+}$ absorption is evident 100 ns after excitation. However,

the relative peak height at 710 nm ($PDI^{\bullet-}$) of the two samples varies significantly: The $PDI^{\bullet-}$ absorption yield is about a factor of two lower in the ternary blend.
Analyzing the kinetic decays of the transient data reveals further differences in the two systems. After about 400 ns the peak located at 710 nm ($PDI^{\bullet-}$) has almost completely vanished for the ternary system in striking contrast to the persistent signal observed for the HBC:PDI mixture. However, at 1200 nm a more pronounced absorption band can be detected for the ternary system at long times after the laser excitation ($1 - 10$ µs). HBC cations seem to be stabilized in the films containing $PC_{61}BM$.
The spectrally resolved transient absorption data strongly suggests the presence of charge separation at the HBC-Ph-C_{12}:PDI interface followed by the formation of $PDI^{\bullet-}$ and HBC-Ph-$C_{12}{}^{\bullet+}$ in both sensitized and non-sensitized films. The deviations in the kinetic evolution of the spectral data for the two samples might be explained as follows: A charge transfer process might occur in the ternary mixture from the charged PDI to $PC_{61}BM$ at a timescale in the order of nanoseconds to microseconds (as schematically shown in Figure 5.7 (right panel)). This could explain both the lower $PDI^{\bullet-}$ signal 100 ns after laser excitation and signal decay back to the noise level after shorter time scales in the ternary sample. The slight broadening observed for the ternary sample at around $950 - 1050$ nm might tentatively be attributed to an absorption of $PC_{61}BM^{\bullet-}$ species in the sample formed after charge transfer. The signal obtained form the $HBC^{\bullet+}$ (1200 nm) appears pronounced and remains visible also long times after the laser excitation (t >10 µs) which might be attributed to a reduced recombination of the $HBC^{\bullet+}$ with $PC_{61}BM^{\bullet-}$ formed after charge transfer.
Summarizing the above findings the transient absorption studies performed on the ternary system support a charge transfer from photo-excited PDI to $PC_{61}BM$. A significant fraction of $PDI^{\bullet-}$ generated is already transferred to surrounding PCBM 100 ns after the laser excitation resulting in lower signal at 710 nm. This could also explain the broadened signal around 1000 nm matching well the absorption of PCBM anions. 400 ns after excitation the $PDI^{\bullet-}$ signal cannot be clearly located in this system indicating almost complete charge transfer of $PDI^{\bullet-}$ to PCBM. $PDI^{\bullet-}$ – $HBC^{\bullet+}$ recombination is suppressed due to the relaxation of $PDI^{\bullet-}$ via charging of PCBM. The spectra show that $HBC^{\bullet+}$ is stabilized in the ternary system allowing for an increased charge carrier extraction in photovoltaic devices. As evidenced by the TAS experiment for devices with a ternary mixture (HBC:PDI:PCBM) anionic species formed at the PDI can directly be transferred to PCBM which allows for fast charge carrier extraction and reduced recombination at the HBC:PCI interface - similar to the energy transfer mechanism elucidated in the previous experiments. It is worth mentioning here, that both energy and charge transfer processes have been evidenced in near equal proportions on cova-

lently linked perylene-fullerenes in a recent study [237].

5.6 Summary

Although dye sensitization for increased photon harvesting has generally been proposed earlier, this is the first time demonstration in fullerene based organic devices allowing for strongly improved performance. Having outstanding properties as electron acceptor $PC_{61}BM$ shows only little absorption in the visible. In conjunction with low or wide bandgap donor materials a significant fraction of light cannot be harvested in thin film devices. This study shows that significantly improved absorption in the visible can be achieved using a sensitization mechanism of $PC_{61}BM$ with high extinction dye molecules. Energy from excited PDI can be transferred to $PC_{61}BM$ followed by charge separation at the interface to the donor molecule thus combining the strong absorption of PDI in the visible light and the outstanding properties of $PC_{61}BM$ as electron acceptor. In HBC-based bi-layered devices, the addition of large amounts of PDI to $PC_{61}BM$ leads to a slight increase in V_{OC}. However, the more pronounced effect is a significant increase in photocurrent which can be attributed to an energy transfer from PDI to $PC_{61}BM$ as supported by EQE, PL and TA measurements. The positive effect of PDI sensitization is further shown in solar cell experiments with the near-IR absorbing polymer PCPDTBT: The addition of PDI leads to increased current generation and thus superior performance in both bi-layered and blend devices. However, limitations apply for the sensitization method used in this study. This is especially the case for blend devices where only little amounts of PDI may be added to yield an increase in current generation. A wavelength independent reduced quantum yield at higher PDI contents is attributed to unfavorable changes of the blend morphology. Furthermore, the tendency of PDI to crystallize may result in exciton trapping and renders PDI non-ideal for $PC_{61}BM$ sensitization. Design of other dyes, especially PDI derivatives with less pronounced crystallinity might be a route towards further improved photovoltaic performance. Dye molecules covalently linked to fullerenes appear especially appealing in this context - highly efficient energy transfer between absorber moiety and fullerene and reduced morphological issues are expected.
Detailed photophysical studies on ternary blends of donor, acceptor and sensitizer further elucidate the charge carrier generation process in the sensitized devices. The findings support, that both energy and charge transfer occur in the three component systems under investigation. It is worth mentioning, that energy transfer can occur over

a distance of several nanometers, whereas charge transfer requires intimate contact and direct overlap of wavefunctions. As such, the nano-morphology of the films plays an important role for the charge generation pathways in the sensitized devices: In the absence of a donor molecule energy transfer appears to be a very efficient process, also at high dye loading rates of 75 % PDI and more as shown by PL measurements and TA studies on PDI:PCBM samples. When HBC is added to the system charge separation between the donor and PDI and energy transfer from sensitizer to $PC_{61}BM$ followed by a charge separation at the donor interface are competing processes.
Our findings strongly support resonance energy transfer from the dye to the fullerene enabling decoupling of light absorption and charge transport. On the other hand, a transient absorption study on ternary blends of HBC, PDI and PCBM reveals, that after exciton separation at the interface of PDI with HBC charge transfer may occur from the dye anion to $PC_{61}BM$ followed by charge extraction *via* the fullerene. Both charge and energy transfer mechanisms elucidated here may lead to increased photon harvesting in the devices under investigation.
It is worth mentioning, that sensitization concepts as presented herein play an increasing role in the filed of organic photovoltaic devices and can be seen as a viable new concept for performance enhancement in organic photovoltaic devices. Only recently a closely related approach was presented by Schenker et al [238]. In these multi-layered OPV devices energy transfer allows minimizing recombination losses and increasing power conversion efficiency.

6 Nanostructured Organic Interfaces

This Chapter deals with template assisted nanostructuring of organic molecules. Precisely defined control over the donor-acceptor interfacial area and geometry can be obtained.
In a first Section a short motivation is given for the use of a nanostructured heterojunction. The ordered interface geometry may promote exciton separation and reduce charge recombination rendering this approach superior to the bi-layered and intermixed interface designs presented in the previous Chapters. As such, patterning of organic compounds on a nanometer length scale is of great interest for application in the OPV devices.
A nano-imprinting techniques is presented that allows to precisely pattern the organic materials with high precision. Hexagonally ordered anodized aluminum oxide templates fabricated by colleges in the Hybrid Nanostructures research group are used as stamps to structure the organic material. Using the imprinting techniques the fabrication of interdigitated geometries at organic-organic interfaces is shown and individual advantages discussed for different organic materials.
Free standing nanowires of a crosslinkable HBC molecule are realized on ITO support using an in situ polymerization techniques. The experimental findings presented here are also summarized in the publication "Nanostructuring Discotic Molecules on ITO support" [239].
A slightly modified imprinting procedure is applied to pattern the well studied electron acceptor material $PC_{61}BM$. Using these nanostructured organic layers Dunbar et al. reported recently plasmonic effects at the interface to a metal electrode allowing increased light harvesting [240].

6.1 Morphology concepts in comparison

In the previous Chapters intermixed and segregated (bi-layered) heterojunction geometries have been analyzed and optimized with respect to the photovoltaic performance of

the resulting devices. For the blend mixtures of the discotic molecules best performance is obtained when using short HBC side chains allowing an intimate packing of the donor and acceptor materials (Section 4.1).
For sensitized devices highest performance can be reached at standard conditions (AM 1.5 global, 100 mW/cm^2), when the acceptor-dye mixture is applied onto a vapor deposited pristine layer of HBC_{parent} (Section 5.4.1 and Section 5.5.3).
A short comparison of these devices at varying illumination intensities underlines the advantages and drawbacks of the different morphology concepts investigated in the previous Chapters. Nanostructured interfaces at the donor-acceptor heterojunction are expected to combine the individual advantages within one device and allow for an increased performance.

6.1.1 Charge recombination in bi-layer and blend devices

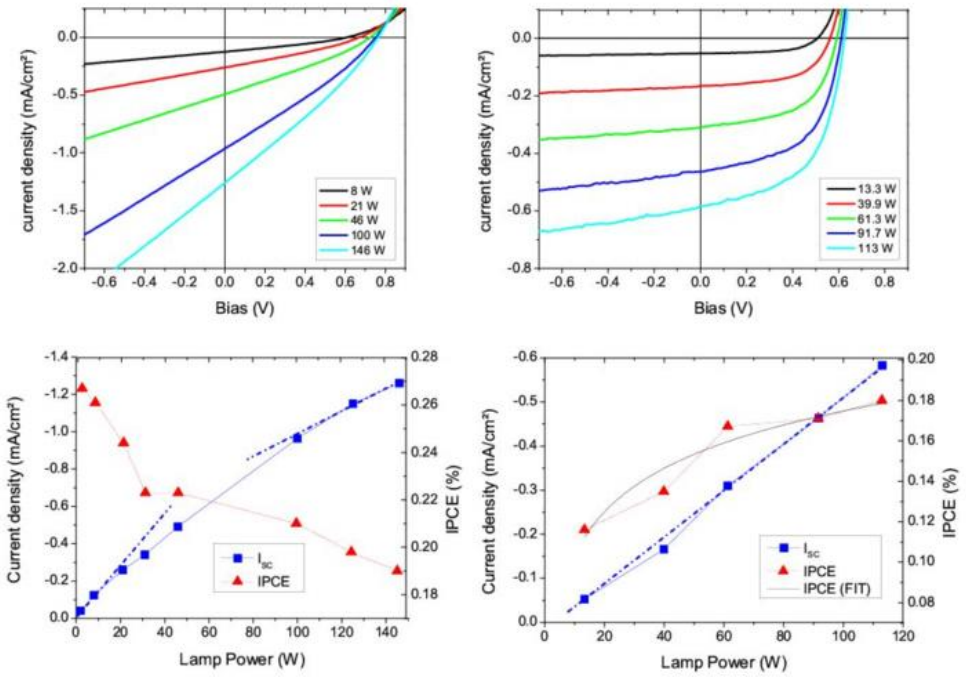

Figure 6.1: Illumination intensity dependent characterization of a HBC-Ph-C_8:PDI device. The data points have been obtained for measurements at different illumination intensities.

Figure 6.1 shows a comparison of the photovoltaic properties obtained for devices using blended active materials (HBC-Ph-C_8:PDI) and devices with a strict bi-layered donor-acceptor interface (HBC_{parent} ‖ PDI+PCBM). Device fabrication and the morphology

concepts have been investigated in detail in the previous Chapters (Section 4.1 and Section 5.4.1, respectively).
Varying the illumination intensity (P_{inc}) alters the exciton generation rate in the photoactive layer of the organic materials. Provided a mono-exponential decay process a strictly linear increase in I_{SC} and a logarithmic dependence of V_{OC} is expected (Section 2.4.4). If the fill factor of the device remains unchanged, combining Equation 2.4 and Equation 2.7 we obtain

$$\eta \propto \ln P_{inc} \tag{6.1}$$

Instead, if non-geminate recombination occurs, a sub-linear rise of current density with increasing illumination density will be be obtained affecting also the power conversion efficiency of the devices (Section 2.7.1).
Despite a relatively similar power conversion efficiency is obtained for the two devices under investigation at standard conditions (100 mW/cm^2) striking differences are observed for the characteristic parameters under varying illumination intensity.
For blend devices based on the discotic materials (Figure 6.1, left side) a sub-linear increase in current density and an inverse dependence of the device performance on irradiation intensity is observed. The measurements indicate the built-up of significant space charge and bi-molecular recombination losses under normal working conditions. A significant amount of non-geminate recombination limits the fill factor and performance especially at higher illumination intensities.
This is not the case for the sensitized bi-layered device shown in (Figure 6.1, right side) where excitons generated can be extracted from the device efficiently even at high illumination intensities. A linear rise in I_{SC} is observed with increasing illumination intensity. A fit of the power conversion efficiency to equation 6.1 is in good agreement with the experimental data.
We conclude, that for the sensitized bi-layered device excitons generated can be extracted from the device efficiently at all illumination intensities probed (up to 1.5 sun) which is not the case for the blend geometry. On the other hand, the exciton separation yield is strongly limited in the sandwich geometry due to the intrinsically small interfacial area of donor and acceptor also reflected in the comparably lower current generation obtained at a negative or low extraction bias.

6.1.2 Nanostructured interfaces for optimized photovoltaic devices

Nanostructured interfaces should allow to combine the benefits of both bi-layer and blend architectures: As shown earlier (Section 4.3.2), a suitable supramolecular assem-

bly of a pristine material can be obtained exhibiting attractive properties such as a high charge carrier mobility and long exciton diffusion length. At the same time the large interfacial area allows promoting exciton separation and charge recombination is minimized due to the direct percolation pathways for generated charges to the respective electrodes.
Precise control of both nano-morphology and molecular alignment are necessary to obtain optimized charge carrier mobility and reduced recombination loss in the OPV device [19, 58, 128, 241]. However, as discussed previously (Chapter 4) it remains an unsolved challenge to achieve the desired morphology of stacks consisting of segregated but adjacent donor and acceptor materials by self assembly processes alone.
An appealing approach to gain increased influence on the morphology is the formation of concentration gradients or interdigitated interfaces of donor and acceptor molecules e.g. by subsequent deposition and controlled inter-diffusion of the compounds. Reduced recombination and high charge carrier mobility have been shown for such devices [211, 242, 243]. Precise control of the interfacial architecture on the nanometer length scale will allow to further reduce the recombination losses while maintaining comprehensive exciton harvesting. Furthermore, using the interdigitated geometry at the donor-acceptor heterojunction superior material properties can be accessed due to unperturbed supramolecular stacking of the pristine and separated organic layers similar to the observations in the pristine HBC layers (Section 4.3.2). In fact, it is known from literature, that material alignment can also be induced by the template assisted confinement into nanometer sized pillars [23, 244]. As such, template induced patterning might not only help to achieve interdigitated interfaces between donor and acceptor but also an increased supramolecular organization in the pristine material phases.

6.2 Anodized alumina oxide template fabrication

Various methods have shown to hold promise for the controlled nano-patterning of organic materials. Bottom up approaches are often based on the self-assembly of block-copolymers or polymer brushes [245, 246]. More independent control of nanostructure dimensions and molecular packing can be gained by top down methods, e.g. hard template production and a transfer of this structure into the organic material [23]. Nanostructured templates can be subsequently filled with organic material by various techniques: e.g. spin coating or electrophoretic deposition [24, 25].
Furthermore, in contrast to direct patterning of the organic material using lithographic techniques, a large throughput and cost effective production might be feasible for tem-

plate assisted methods [82]: The structuring of the template can be achieved within reasonable time (minutes to hours) and templates might be reused for repetitive structuring of organic films. The production of anodized alumina oxide (AAO) membranes relies on an electrical field assisted self organization process. As such, highly ordered structures may be obtained and plasmonic effects can be observed.
AAO templates used here have been fabricated by Dominik Lembke on high purity Al foil by two-step anodization as has been shown elsewhere [247, 248]. In brief, the aluminum foil is electro-polished to remove oxide and subsequently anodized in an acidic electrolyte solution. Pore depth, inter-pore distance and diameter can be controlled independently by proper choice of electrolyte solution, anodization voltage and time and subsequent pore widening procedures [248, 249]. In this study both sulfuric acid and oxalic acid were used as electrolyte solutions with anodization voltages of 25 V and 40 V, respectively. Pore widening was conducted in a H_3PO_4 bath (5 wt%) for $5 - 60$ minutes yielding different pore diameters.

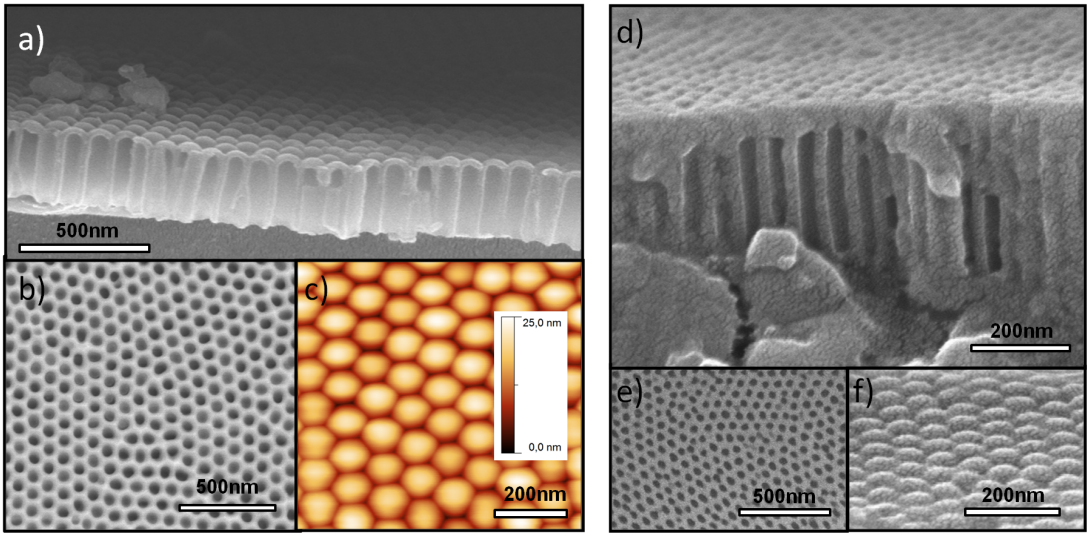

Figure 6.2: AFM and SEM images of AAO templates fabricated for organic layer imprinting. a-c) Anodization in oxalic acid at 40 V for 150 seconds, 30 minutes pore widening. **d-f)** Anodization in sulfuric acid at 25 V for 300 seconds, pore widening 10 minutes.

Pore dimensions and quality of the AAO templates used for organic imprinting have been monitored by multiple SEM and AFM scans (Figure 6.2). Clear differences are apparent for samples produced at low and high anodization voltages in sulphuric acid (Figure 6.2, **d-f**) and oxalic acid (Figure 6.2, **a-c**), respectively. Bottom views of the AAO membranes (Figure 6.2 **b, e**) show the typical hexagonal ordering and reveal

pore diameter and inter-pore distance. Top views (Figure 6.2 **c, f**) and cross sections (Figure 6.2 **a, d**) have been conducted on the membranes after removal of the Al support and subsequent transfer onto an ITO support. The scans are also used to probe the exact pore depth, diameter and quality of the hexagonal ordering: Image analysis reveals an inter-pore distance (d_{pore}) of $d_{pore} \approx 60$ nm (sulphuric acid) and $d_{pore} \approx 100$ nm (oxalic acid) for the samples shown in good accordance with literature [248, 249].

6.3 Nanostructuring discotic molecules on ITO support

In this Section an imprinting technique using AAO hard templates as stamps is shown for a solution processable HBC derivative. An exact pattern transfer of the AAO structures into the organic layer is accomplished via the imprinting techniques. Acrylate moieties at the residues of the discotic molecule allow the polymerization of the organic compound at elevated temperatures stabilizing the compound irreversibly. The template can be fully removed after the structure transfer and subsequent solution deposition of an organic acceptor without dissolution of the donor material becomes feasible. The production of nano-patterned films is realized for a variety of nanowire dimensions on square centimeter areas. The fabrication directly on conductive glass support and control over the formation of a dense barrier layer underneath the pillar structure renders this approach very instructive for the fabrication of a new generation of OPV devices with nanostructured and highly interdigitated donor-acceptor interface.

6.3.1 Materials and methods

The synthesis and chemical properties of the crosslinkable discotic material $HBC_{acrylate}$ used for this study have been studied previously [250, 251]. Figure 6.3 shows the chemical formula of the HBC with six acrylate moieties at the peripheral positions. Differential scanning calorimetry and x-ray studies revealed a crystalline order at room temperature, a phase transition to a liquid crystalline state at 112 °C and an irreversible polymerization reaction of the acrylate moieties starting at approximately 150 °C [250].
Thin films of the compound solubilized in chloroform were directly deposited on ITO coated glass substrates or quartz glass using spin coating techniques.
The pattern of the AAO membranes produced was transferred into the organic material by an imprinting step using a temperature and pressure controlled bench press. The crosslinkable material is polymerized in the confinement of the AAO template by slowly ramping both the substrate temperature and the applied pressure to 170 °C and 100

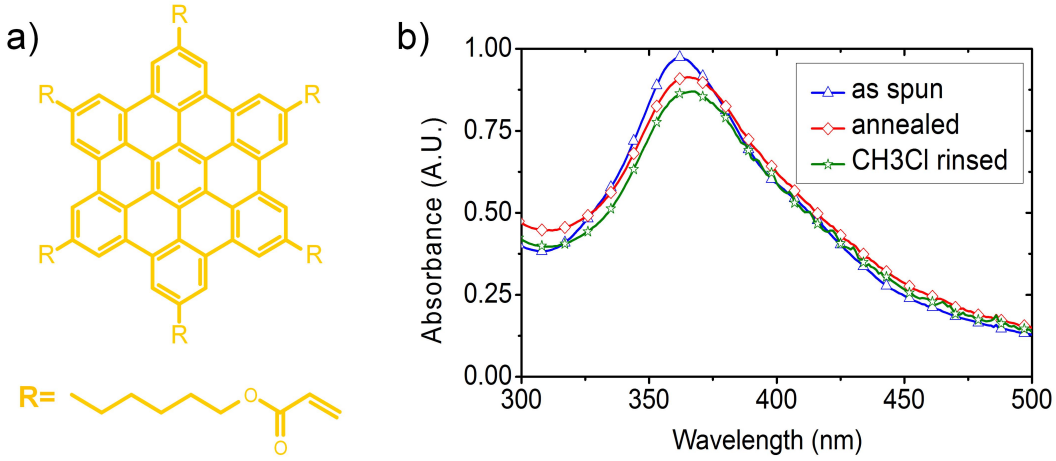

Figure 6.3: Molecular structure and absorption spectra of the $HBC_{acrylate}$, a crosslinkable HBC derivative. a) $HBC_{acrylate}$ chemical formula. **b)** Thin film absorption spectra for $HBC_{acrylate}$ on quartz glass as spun, after annealing (170 °C and after subsequent solvent rinse.

bar, respectively. After maintaining the sample for 2 h at this elevated temperature the pressure is released and samples are cooled back to room temperature at a rate of 1 °C/min. Subsequently aluminum support and AAO membrane are carefully removed by immersion of the sample in dilute $CuCl_2$ solution (0.2 M) and phosphoric acid bath (5 wt%).

6.3.2 Optical absorption of imprinted films

In a first experiment homogeneous thin films of the organic compound were deposited on quartz substrates. Annealing of the films above the polymerization temperature renders the material insoluble in organic solvents. Consequently absorption spectra recorded from a film as spun, after an annealing treatment at 170 °C and after subsequent rinsing in chloroform show an almost negligible deviation (Figure 6.3 **b**) . Instead, a significant change in the thin film absorption is evident for the organic material before and after imprinting (Figure 6.4 **b)**). The change in absorption is attributed to a reallocation of the material and can be explained using Lambert-Beers law (Equation 3.9). In the following an estimation of the extinction for flat and structured films is presented (calculations presented here have been performed in collaboration with Christian Hundschell):
The distance of two neighboring pillars can be calculated as twice the radius of the inner circle r_i of a hexagon. As such the area of the hexagon $A_{Hexagon}$ can be written

as

$$\mathrm{A_{Hexagon}} = 2\sqrt{3}\mathrm{r_i^2} = \frac{\sqrt{3}}{2}\mathrm{a^2} \tag{6.2}$$

The gain in surface area using an idealized imprinting pattern as depicted in Figure 6.4 **c)** can be calculated as follows:

$$\frac{\mathrm{A_{imprint}}}{\mathrm{A_{Hexagon}}} = \frac{\mathrm{A_{Hexagon}} + \mathrm{A_{cylinder_{mantle}}}}{\mathrm{A_{Hexagon}}} = 1 + \frac{2\pi \mathrm{d_s h}}{\sqrt{3}\mathrm{a^2}} \tag{6.3}$$

For a flat film of organic material Lambert Beers law (Equation 3.9) can be applied to calculate the wavelength dependent transmission. After the imprint procedure a certain fraction (C_1) of the sample (the cylinders) exhibit increased material thickness d_1 and thus increased absorption surrounded by areas (C_2) with a lower film thickness d_2 and reduced film absorption. As such, the transmission of the sample can be seen as a superposition of both areas $I(\lambda) = C_1 I_1 + C_2 I_2$ with $C_1 + C_2 = 1$. We calculate C_1 as:

$$\mathrm{C_1} = \frac{\mathrm{A_{cylinder_{top}}}}{\mathrm{A_{Hexagon}}} = \frac{1/4\mathrm{d_s^2}\pi}{\sqrt{3}/2\mathrm{a^2}} = \frac{\pi}{2\sqrt{3}\mathrm{R^2}} \tag{6.4}$$

.

With $R = \frac{a}{d_s}$. The transmission of the imprinted sample is estimated as:

$$\mathrm{I}(\lambda) = \frac{\pi}{2\sqrt{3}\mathrm{R^2}}\mathrm{I_0}(\lambda)\mathrm{e}^{-\alpha(\mathrm{d_1+h})} + \left(1 - \frac{\pi}{2\sqrt{3}\mathrm{R^2}}\mathrm{I_0}\lambda\mathrm{e}^{-\alpha\mathrm{d_1}}\right) \tag{6.5}$$

.

For the absorption of the film we derive:

$$\mathrm{OD_{Nano}} = \alpha \mathrm{d_1} \ln\left(1 - \frac{\pi}{2\sqrt{3}\mathrm{R^2}}(1 - \mathrm{e}^{\alpha \mathrm{h}})\right) \tag{6.6}$$

Assuming the volume of the organic material to be constant before and after the imprint:

$$\mathrm{dA_{hexagon}} = \mathrm{hA_{cylinder_{top}}} + \mathrm{d_1 A_{hexagon}} \tag{6.7}$$

Where d denotes the thickness of the film prior to imprinting. Taking these formulas we derive:

$$\mathrm{OD_{Nano}} = \frac{\mathrm{OD_{flat}} d_1 2\sqrt{3}\mathrm{R}^2}{\mathrm{h}\pi + 2\sqrt{3}\mathrm{R}^2 d_1} - \ln\left\{1 - \frac{\pi}{2\sqrt{3}\mathrm{R}^2}\left(1 - \exp\left[-\frac{\mathrm{OD_{flat}} 2\sqrt{3}\mathrm{hR}^2}{\mathrm{h}\pi + 2\sqrt{3}\mathrm{R}^2 d_1}\right]\right)\right\} \quad (6.8)$$

For an illumination incident perpendicular to the substrate plane formula 6.8 can be used to estimate the absorption of an imprinted film. When assuming an imprint down to the substrate plane ($d_1 = 0$) the formula 6.8 can be simplified to:

$$\mathrm{OD_{Nano}} = -\ln\left\{1 - \frac{\pi}{2\sqrt{3}\mathrm{R}^2}\left(1 - \exp\left[-\frac{\mathrm{OD_{flat}} 2\sqrt{3}\mathrm{R}^2}{\pi}\right]\right)\right\} \quad (6.9)$$

The dashed line in Figure 6.4 **b)** shows the calculated absorption assuming an imprint down to the substrate and a 3/4 quotient for pillar height/pillar spacing as derived from SEM scans on this specific sample. The slight deviation from the measured spectrum after imprint is attributed to light scattering effects, material realignment due to the imprinting as well as a marginal surface roughness of the spin coated film.

6.3.3 Production of imprinted films on ITO support

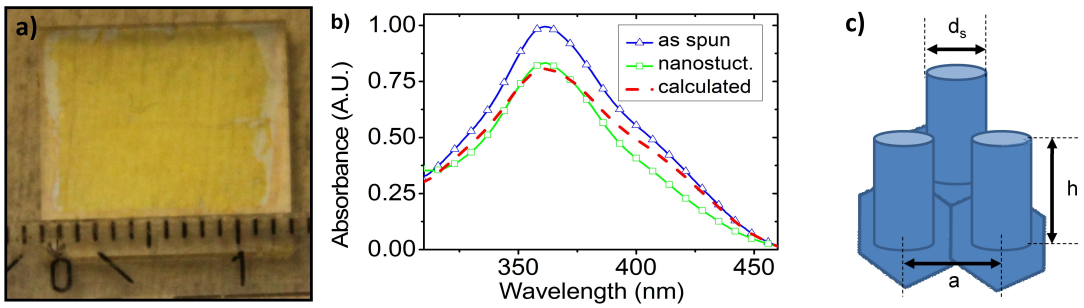

Figure 6.4: Imprinted and polymerized $\mathrm{HBC_{acrylate}}$ films on ITO support a) Photograph showing uniformly imprinted film with a substrate area of $14 \times 14\ \mathrm{mm}^2$ **b)** Absorption of $\mathrm{HBC_{acrylate}}$ on ITO support as spun and after nanostructuring. The dashed line shows the calculated absorption (pore diameter 75 nm, inter-pore distance 100 nm, imprint down to the substrate) **c)** Schematic drawing of an idealized hexagonal pillar structure.

In order to produce nanostructured and polymerized $\mathrm{HBC_{acrylate}}$ films about 100 nm thick layers of the organic material are spun onto ITO coated glass and immediately transferred to the press. High pressure and a stepwise increase of the temperature are applied to the sandwich of substrate and AAO on aluminum support in order to

induce both an area-wide template filling and subsequent polymerization of the organic material. After slow cooling back to room temperature the AAO is found to adhere to the substrate. The sandwich structures are then transferred into a self-made holder equipped with gaskets which is used to selectively immerse the aluminum top surface of the stack to the $CuCl_2$ solution. The gasket system provides protection of the ITO layer from exposure to the acidic and basic solutions. Figure 6.4 **a)** shows a photograph of a nanostructured film after template removal. The HBC film is recovered after the imprinting process with no visible defects. Only to the edges, where the gasket system did not prevent the exposure to the acidic and basic solutions the ITO is dissolved and subsequently the organic film starts to de-laminate.

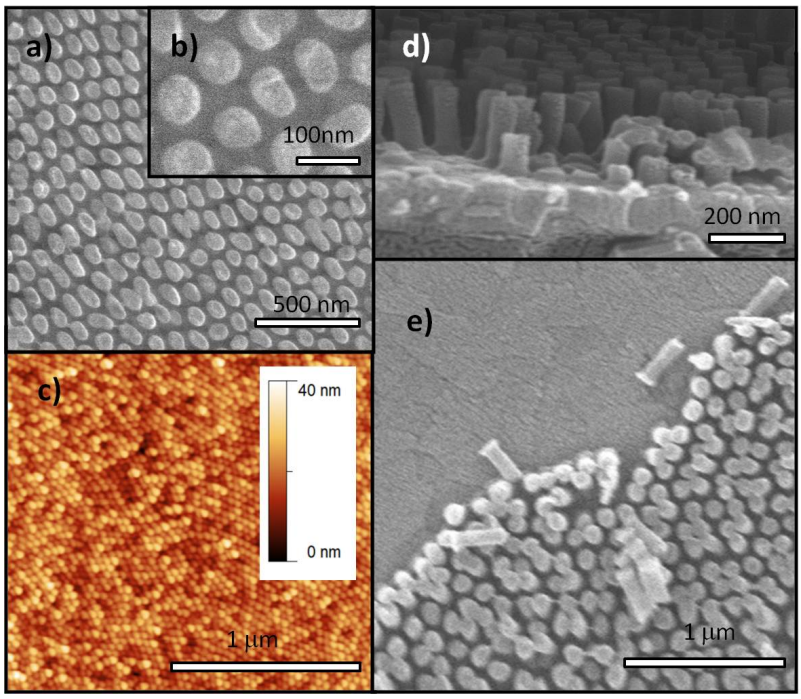

Figure 6.5: Nanostructured HBC films realized on ITO support. SEM and AFM images show the surface of the nanostructures realized in the organic material on a substrate support after imprinting and AAO template removal.

Resulting nanostructured films have been analyzed by atomic force microscopy (AFM) and scanning electron microscopy (SEM) techniques (Figure 6.5). SEM top views (Figure 6.5 **a**) and **b**) show hexagonally ordered pillars of the polymerized organic material. The pattern is an exact replica of the imprinted AAO structure showing identical ordering and dimensions. An AFM scan visualizes the top surface of the wires (Figure 6.5 **c**) and reveals that the resulting pillars show only little deviations in height. As such,

the structures are suitable for the fabrication of photovoltaic devices. It should be mentioned that due to tip convolution effects of the high aspect ratio structures the topology scan does not cover valuable information on the height of individual pillars. Figure 6.5 **d**) shows a SEM cross-section at a viewing angle of approximately 15 deg. The free standing wires can be seen directly attached to the ITO support. Furthermore, we also analyzed the edge of a sample (Figure 6.5 **e**). On the left hand side the pure ITO surface is visible and to the lower right the organic nanowires are attached. At the borderline some wires have been ripped off allowing visualizing both aspect ratio and ordering within one SEM micro-graph. For the structures visualized in Figure 6.5 **e**) we find nanowires of 300 nm length and a diameter of 90 nm (aspect ratio of 3.3). To further analyze the structure transfer from inorganic hard template

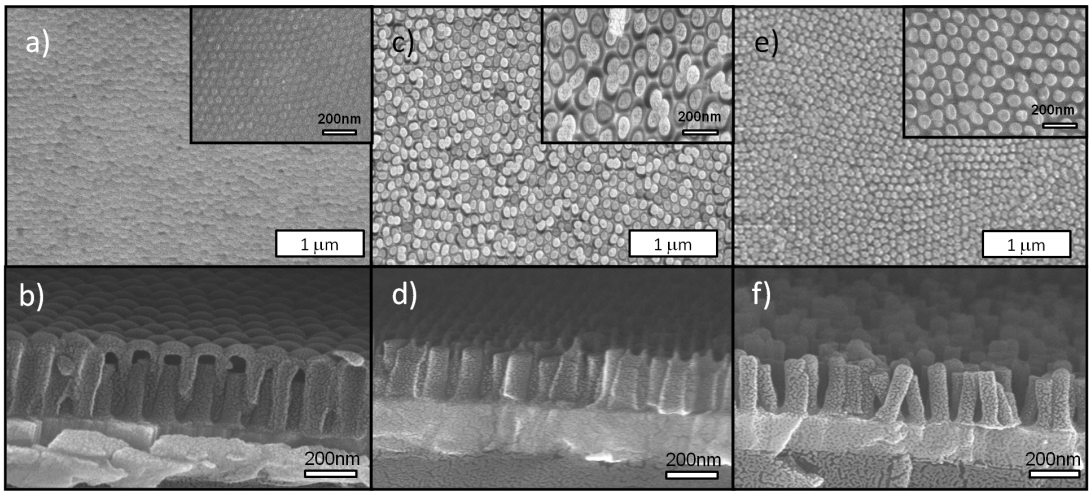

Figure 6.6: Analysis of the HBC filling level and AAO etching evolution by SEM images. Top views **a) c) e)** and cross sections **b) d) f)** show the evolution of the AAO etching process.

into the organic material we also monitored the structures through the AAO etching processes (Figure 6.6). Interestingly we can precisely determine the level of filling for individual membrane pores (Figure 6.6 **a**, **b**): for the aspect ratio shown the organic material reaches up to about 4/5 of the AAO template depth. Enclosed air inside the membrane pores is compressed throughout the imprinting process and due to increasing temperature polymerization of the initially soft organic material takes place rendering it more viscous and finally immobile. Simple calculations applying the ideal gas law reveal that at about 12 bar air pressure of the enclosed air the material flow into the pores is stopped for the sample shown. It should be mentioned that the pore filling is apparently also stopped if the AAO reaches down to the ITO support regardless of

the pressure and temperatures applied. An easier and more precise control over the formation of a barrier layer can be gained by using a two-step polymerization as will be described below. Images taken after etching only a few nanometers of AAO (Figure 6.6 **c**, **d**) reveal a complete removal of the barrier layer and demonstrate that almost all pores are filled with the organic material. Figure 6.6 **e**) and **f**) show the same sample after a complete removal of the AAO template.

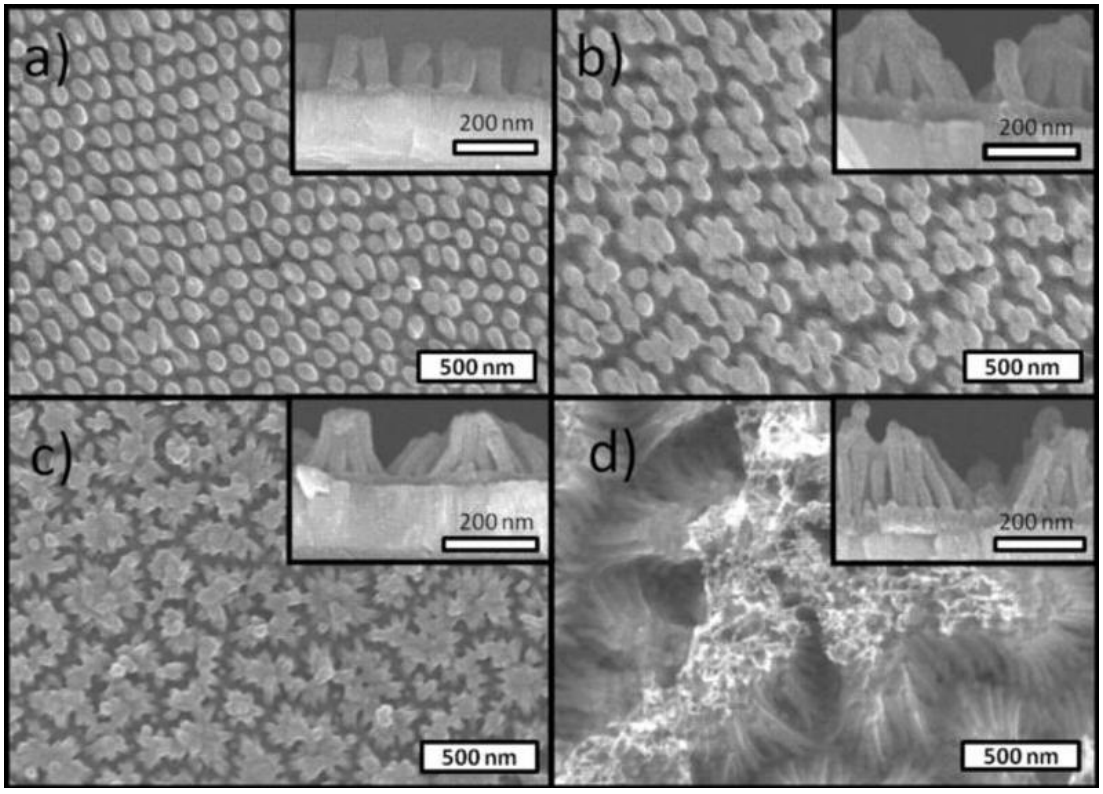

Figure 6.7: SEM top views and cross sections of HBC nanowires on ITO support with various aspect ratios. a) Free standing organic nanowires are obtained aligned in a honeycomb pattern. For higher aspect ratio the wires start to bend **b**) and finally form bundles **c**), **d**) still remaining grafted to the conducting substrate support.

Using a selection of different AAO templates organic nanowire arrays with various dimensions were fabricated. Figure 6.7 shows a selection of the polymerized wires in SEM top and side views. Fully free standing wires have been achieved with an aspect ratio of 2.2 using an AAO anodized at 40 V in oxalic acid for 60 seconds and a pore widening for 20 minutes (Figure 6.7 **a**). When increasing the nanowire length the structures start to bend (Figure 6.7 (**b**), oxalic acid at 40 V for 80 seconds, pore

widening 20 minutes; aspect ratio: 2.7). Further increase in length and reduction of diameter leads to aggregation of the wires upon drying in air (Figure 6.7 (**c**), sulfuric acid at 25 V for 150 seconds, pore widening 10 minutes; aspect ratio of 5.5). Bundles of several wires can be found when imprinting with very small pores (Figure 6.7 (**d**), sulfuric acid at 25 V for 300 seconds, 5 minutes pore widening). The resulting nanowires have a length of 180 nm and a diameter of only 22 nm (aspect ratio of 8.1). Even at the highest aspect ratio of over eight the wires are still bound tightly to the ITO surface and form big bundles rather than to collapse. Critical point drying might help to yield free standing structures also at higher aspect ratio [252, 253].

6.3.4 Application of nanostructured HBC layers for photovoltaic devices

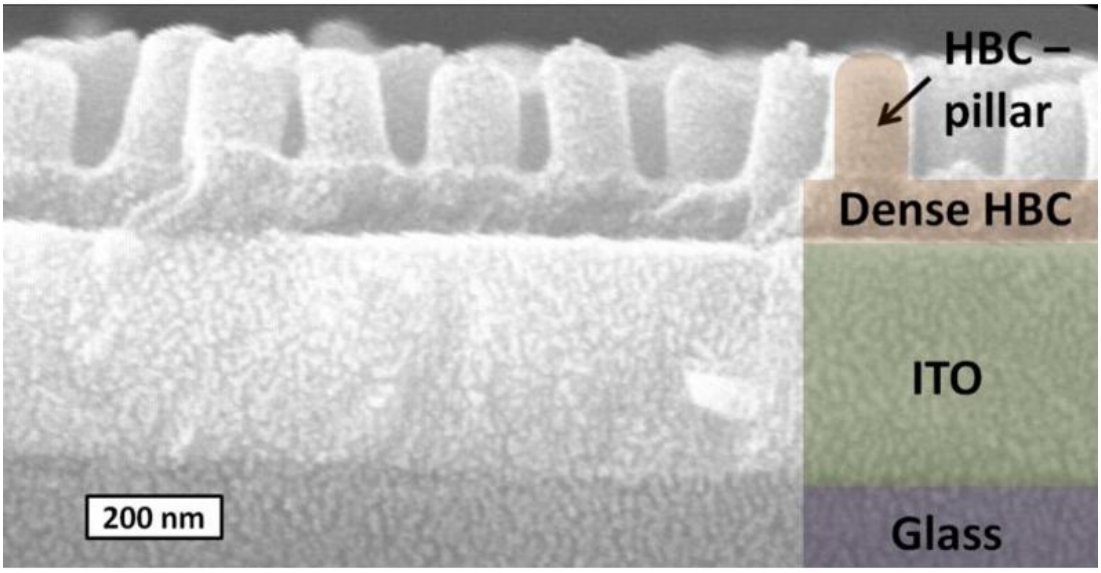

Figure 6.8: SEM cross-section micro-graph showing HBC nanowires and dense supporting HBC barrier layer. The sample was fabricated by a two-step polymerization as described in the text.

A little modification in the fabrication process facilitates a precise control over the formation of a dense HBC layer underneath the patterned film (Figure 6.8). In a first step a thin layer of the organic material is deposited by spin coating on the ITO support. This flat film is polymerized and immobilized by thermal annealing at 170 °C resulting in the formation of a dense barrier layer. Subsequently, a second layer of the organic material was deposited from solution followed by an imprinting step as described previously (Section 6.3.1). Only the material in the second layer consisting of monomeric

$HBC_{acrylate}$ molecules can be reallocated by the imprinting step. Varying the spin coating parameters for the two deposition steps allows to individually and precisely control the thickness of the non-structured dense barrier layer and the formation of the nanopillars. Figure 6.8 shows a sample with an array of 180 nm long wires grafted on a 30 nm thick barrier layer produced using the two-step imprinting procedure described above.

Accurate control over the growth of a barrier layer is very instructive for the assembly of efficient photovoltaic devices; the thin and compact layer at the bottom in combination with a uniform pillar height as shown in Figure 6.5 **c)** ensure that donor and acceptor compounds will be only in contact with their respective electrodes. As such, exciton and charge carrier recombination at the device contacts can be suppressed effectively.

Upon polymerization the molecules can be frozen in crystalline or liquid crystalline state depending on the cross-linking procedure: If acrylate moieties are polymerized at elevated temperatures as reported here the resulting films show liquid crystalline order [250]. This allows minimizing grain boundaries while maintaining the $\pi - \pi$ stacking of neighboring discotic molecules [17]. On the other hand the polymerization of the molecule could also be induced by UV-curing at lower temperatures resulting in amorphous or crystalline films which might be advantageous for some applications [250].

Nanostructured organic films have been produced previously with other organic donor materials yielding a comparable aspect ratio as presented herein [24, 254]. However, in these studies the nanowires are produced by direct (over)-filling of commercial AAO templates and a subsequent lamination step on ITO via special silanes, e.g. vinyl-$Si(OMe)_3$ [24], or directly on the ITO support using siloxane-derivatized organic materials [254]. In contrast, the technique presented here allows for a production of fully organic nanowires directly on the ITO support with precise control of a barrier layer. Intimate contact and complete grafting to the ITO substrate with no air encapsulation is ensured. Furthermore, no siloxane is necessary for ITO grafting which might alter the electronic properties of the organic compound or introduce traps in the bulk material.

After cross-linking of the donor material an acceptor compound can be directly processed onto the imprinted layer from the solution phase while maintaining the interfacial patterns. Furthermore, the cross-linking assisted patterning does not rely on distinct melting temperatures of the two organic materials as it is the case for the so called double imprinting presented recently [255].

Photovoltaic devices have been fabricated using the nanostructured $HBC_{acrylate}$ films and PDI or $PC_{61}BM$ as an acceptor. For all devices using the thermally polymerized HBC material as a donor compound only very low conductivity and almost negligible current generation was observed.

On the contrary, very high charge carrier mobility has been shown for other HBC derivatives [20]. Despite careful processing and subsequent rinsing of the HBC layers a decrease in conductivity could result from adhesion of siloxane used for the AAO surface modification or other solvents used throughout the AAO removal procedure. Furthermore, optimization of the AAO surface treatment, the nanowire diameter and the polymerization procedure might be necessary to yield an improved molecular alignment [241, 244, 256, 257]. However, in the present study the low conductivity of the polymerized $HBC_{acrylate}$ films is attributed mainly to charge trapping in the residual groups attached to the HBC core. In previous studies a strong dependence of the residues attached to HBC on conductivity and charge extraction yield was observed (Chapter 4), well in accordance with literature [194]. Furthermore, it has been shown, that on average only four out of the six acrylate moieties of the monomer will be cross-linked during the polymerization procedure [250]. Non-linked acrylate moieties present in the polymerized films will most likely act as traps, hinder defect free face-to-face stacking of the HBC cores and strongly limit charge carrier transport through the organic layer. A reduction of cross-linker binding sites per molecule and conjugated linkage units will certainly help reduce this conductivity issue.
It is worth mentioning here, that nitrene mediated cross-linking of polymers allows the formation of highly stabilized structures and does not negatively affect the conductivity of the conducting polymers. In fact, a remarkably high performance has been achieved using the cross-linked polymers as donor materials in OPV devices [258] as will be discussed in more detail in the outlook of this thesis (Section 7.3).

6.4 Nanostructuring solution processable fullerenes

The imprinting techniques shown in the previous Section appears suitable for the patterning of other organic semiconducting materials also. $PC_{61}BM$ is an especially attractive candidate which has been very well studied for application in OPV devices [110]. The molecule can be processed from the solution phase and does not tend to crystallize, unlike PDI [117]. As such, nanometer-sized patterning of the material seems feasible using the AAO template approach presented (Section 6.2).
However, in contrast to the polymerization based structuring method presented for the cross-linkable HBC derivative a selective etching of the AAO template cannot be accomplished without dissolution of the fullerene molecules. Great care must be taken when mechanically removing the AAO template form the soft organic material.

$PC_{61}BM$ molecules are not grafted to the substrate support making delamination and disruption of the nanometer sized structures very likely.
After carefully adapting the imprinting parameters and by using a suitable silanization techniques we succeeded to fabricate nano-patterned films of $PC_{61}BM$ on a substrate support.

6.4.1 Light trapping in Plasmonic nanovoid arrays

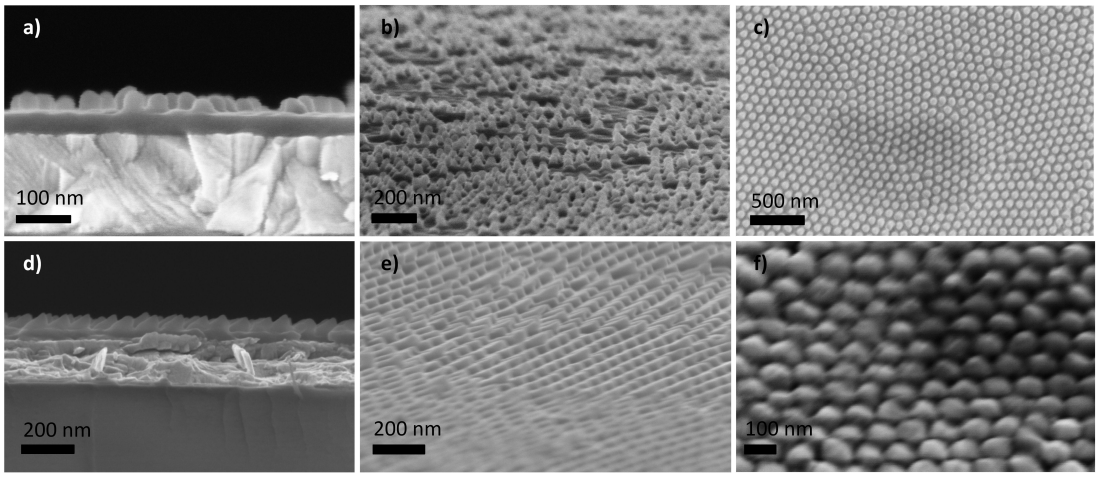

Figure 6.9: Nanopatterned films of $PC_{61}BM$ on ITO support. The SEM images show the structures obtained in the $PC_{61}BM$ after imprinting. Different shapes of patterns are obtained in the $PC_{61}BM$ after imprinting with AAO templates showing smaller **a)-c)** and larger **d)-f)** pore distances as is described in the text. The micrographs show the samples in cross section, at 45° viewing angle and in planar configuration, respectively.

Thin films of $PC_{61}BM$ were spun from chloroform solution directly on quartz glass and ITO coated substrates. A fluorinated silane was covalently bound to the AAO templates in order to reduce adhesion with the organic material [259]. Samples were transferred to a bench press and imprinting conducted at a temperature of 120 °C. At this elevated temperature the $PC_{61}BM$ is in a molten and viscous state allowing infiltration into the nanometer-sized pore structure of the AAO template [260]. A poly-dimethyl siloxane (PDMS) rubber gasket is used to uniformly distribute the applied pressure of approximately 100 bar over the entire sample area of 14×14 mm. After a short cooling of the stack on air the sample is quickly mechanically demolded from the AAO membrane.
Figure 6.9 shows a selection of SEM images obtained for the patterned organic layers. For imaging purpose the samples were fabricated on conductive ITO support facilitating high electron microscope resolution with no metal surface coating. As such, direct

insight to the morphology of the organic layers is obtained.
Clear differences can be seen for the organic layers depending on the pore size of the AAO stamps used. Organic material processed using *stamp A* (sulfuric acid, 40 nm pore diameter, 60 nm pore-pore distance) shows regular cylindrical stubs of about 40 nm length and 40 nm height with rounded edges (Figure 6.9 **a)-c)**). For the samples processed with *stamp B* (oxalic acid, 60 nm pore diameter, 100 nm pore-pore distance) we obtain slightly irregular cone shaped patterns as visualized in (Figure 6.9 **d)-f)**). The formation of these slanted structures is attributed to a slight deformation of the imprinted pattern in $PC_{61}BM$, which is in a molten and viscous state at 120 °C upon demolding [260].
An identical imprint process was used for $PC_{61}BM$ deposited on quartz glass and silver was carefully evaporated onto the structured organic layers. Subsequently Ricky Dunbar studied the optical effects occurring at the resulting highly ordered metal-organic interface. Absorption measurements conducted in reflection geometry are well in accordance to simulations performed and show that the patterned layers facilitate an increased light absorption in the organic material when compared to flat films [240]. The light trapping effect is attributed to surface bound plasmonic modes excited near the patterned and highly ordered metal-organic interface. The use of highly ordered nano-patterned electrodes as investigated here may be beneficial for an increased light harvesting in thin film organic solar cells.
It is worth mentioning, that a careful optimization of the imprinting procedure was necessary to facilitate the production of patterned $PC_{61}BM$ layers with an area wide imprint and only low amounts of defects. However, the aspect ratio and imprint quality as has been obtained using the polymerized $HBC_{acrylate}$cannot be reproduced using the $PC_{61}BM$ which lacks a cross-linking moiety.

6.4.2 Production of photovoltaic devices using nanostructured $PC_{61}BM$

Initial experiments have been conducted using nano-patterned $PC_{61}BM$ as presented in the previous study in heterojunction photovoltaic devices with an interdigitated interface.
An *inverted device geometry* was chosen using sputter deposited TiO_2 as an electron conducting bottom contact showing a very low intrinsic surface roughness. $PC_{61}BM$ was spun onto the smooth TiO_2 layer support and structured using AAO templates as described in Section 6.4.1. In order to both maintain a strict donor-acceptor interface and to retain the fragile structures of the imprinted film donor material was deposited from the vapor phase. Both CuPc and HBC_{parent} have been tested in this context showing

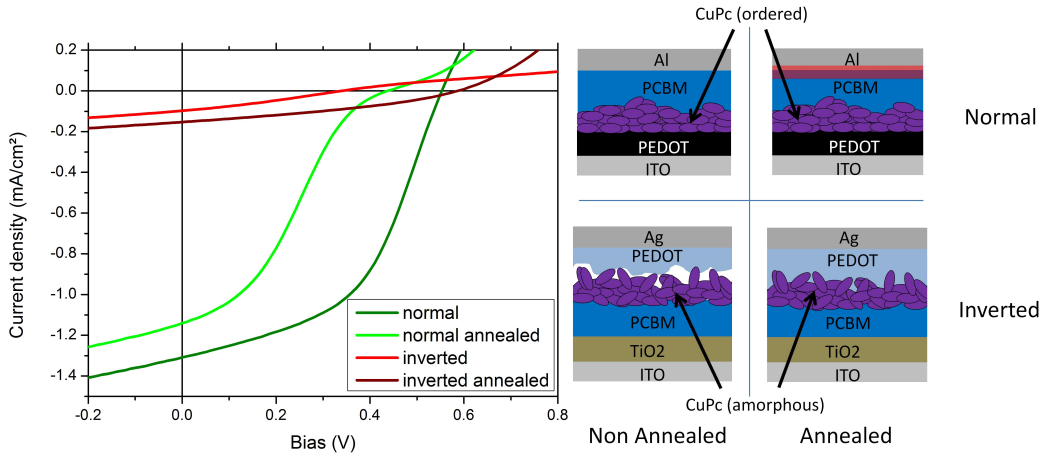

Figure 6.10: $PC_{61}BM$-CuPc photovoltaic bi-layered devices. The IV characteristics under illumination is shown for devices assembled in normal (green colors) and inverted (red colors) device geometries. Dark colors indicate the device characteristics obtained after an annealing treatment. A schematic representation of the assumed cross-section morphology is given in the cartoon images.

individual advantages but also some drawbacks.

CuPc is an appealing donor material showing a wide band absorption and the highest power conversion efficiency achieved to date using a bi-layered device geometry in conjunction with C_{60}(IPCE $\approx$ 4%) [62]. The impact of the interface morphology for CuPc-C_{60} solar cells (planar, mixed and ideally nanostructured interfaces) on the resulting device characteristics has been modeled and intensively studied in the past [128]. Nano-patterned interface architectures are believed to allow further increasing the device performance in this donor acceptor system.

From an energetic point of view replacing the electron acceptor C_{60} with the solution processable $PC_{61}BM$ as is desired for our studies is expected to have an only negligible impact on the device characteristics. In fact, a recent study shows superior efficiency for the soluble fullerene derivative at the heterojunction to CuPc [100].

Device studies conducted in our laboratories in collaboration with Claudia Palumbiny and Sarah Lindner instead reveal very strong limitations for the applicability of this donor-acceptor system for imprinting experiments: Figure 6.10 shows bi-layered devices in *normal* and *inverted geometry* (see Section 3.1.4) with no further interface modification (no imprint). Striking differences are observed for the devices depending on the stacking of the active layers. This is clearly contrast to observations typically made using other active materials [93]. Furthermore, the performance of the devices is strongly affected when applying an annealing treatment, similar to the conditions applied com-

monly during the imprint procedure (120 °C).
A possible and plausible explanation for the entirely different IV-characteristics observed despite using the same active materials is illustrated using the schematic cross-section images shown in Figure 6.10. Generally devices in an *inverted geometry* show a drastically lower performance than it is the case for the devices assembled in *normal geometry*. This finding is attributed to surface dependent alignment effects of the evaporated CuPc well in accordance with literature [261]. The growth of crystalline, ordered and homogeneous layers as obtained on the substrate support might not be accomplished for the CuPc layers grown on $PC_{61}BM$ (as is further supported by AFM measurements). This may result in a non-ideal interface contact between the rough CuPc surface and the interface material PEDOT and cause generally lower performance for the inverted devices. The annealing treatment has an entirely different effect for the different device geometries. Degradation of the Al contact and the surface exposed $PC_{61}BM$ might cause the "s"-shape formation in the *normal device geometry*. Instead, better infiltration of the interface material PEDOT into the coarsely structured CuPc layer is believed to allow an improved fill factor and performance in the inverted devices. Taking these findings into account it is concluded, that possible effects originating from template assisted nano-patterning of the $PC_{61}BM$ layer will be overwhelmed by alignment, degradation and infiltration issues occouring in this material combination. Other sublimated donor materials yielding less textured films might be more suitable to clarify effects originating from a nanostructured donor-acceptor interface.
Unsubstituted HBC is an alternative donor material processed from the vapor phase showing high exciton diffusion length as well as suitable energy levels and has been shown to grow in rather smooth and flat layers (see Section 4.3). On the other hand, the large HOMO-LUMO bandgap of the material confines the photon absorption to wavelengths well below 500 nm (shown in Figure 4.11). Nevertheless, the photovoltaic performance obtained for flat-junction $PC_{61}BM$-HBC devices might directly reflect changes in the interface geometry obtained via imprinting of $PC_{61}BM$.
Typical IV-characteristics obtained for photovoltaic devices assembled using these compounds (device architecture $ITO/TiO_2/PC_{61}BM/HBC_{parent}/WO_3/Ag$) are shown in Figure 6.11. Planar and nanostructured $PC_{61}BM$ layers have been used as electron acceptors and HBC_{parent} was evaporated as donor material.
The photovoltaic performance is found to be clearly superior for the non-structured bi-layer devices. A lower shunt resistance causes a reduced V_{OC}, I_{SC} and FF for all nano-patterned devices shown. The increased leakage currents and a strong deviation of the curve shape for the individual nano-patterned devices is attributed to a (partly) shunting of the sandwich stack. In fact extensive SEM scans conducted on the surface

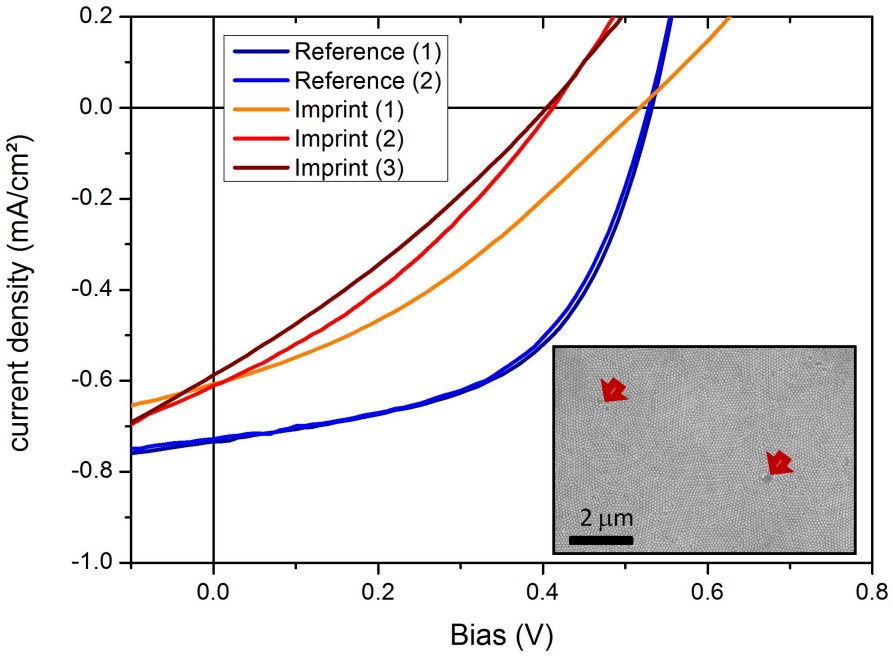

Figure 6.11: $PC_{61}BM$-HBC_{parent} photovoltaic devices with planar and nanostructured interfaces. The IV characteristics under illumination is shown for a planar (blue colors) and nano-patterned (red colors) donor-acceptor interface. The inset images show defects fond on the surface of typical nano-structured $PC_{61}BM$ layers.

of nano-patterned $PC_{61}BM$ layers reveal low amounts of small defects as is exemplarily shown in the inset image of Figure 6.11, indicated with the red arrows.
Further optimization of the imprinting procedure or the use of a barrier layer underneath the nanostructured $PC_{61}BM$ might help to minimize the shunting of devices with interdigitated interfaces and allow a more valuable comparison of nanostructured and planar interface geometries in these bi-layered photovoltaic devices.

6.5 Summary

In this Chapter a method for the nano-patterning of organic semiconducting materials is demonstrated. Precise control over the imprinted pattern is achieved by using AAO templates as stamps with individual control over nanowire length, spacing and diameter. It is demonstrated that the highly ordered hexagonal structure of the AAOs can be fully

transferred into cross-linkable organic materials.

Free-standing organic nanowires directly grafted to ITO support are realized using a HBC derivative with cross-linkable acrylate side chains. The resulting structures show an aspect ratio of up to 8.1 (22 nm in diameter, 180 nm long). Nanostructured samples have been produced on square centimeters and the process presented here is easily scalable to even larger sample areas. We also demonstrate the deposition of a dense barrier layer with tunable thickness underneath the structured films by a two step polymerization. No additional grafting material is necessary for the attachment to the ITO support rendering this approach very instructive towards the fabrication of nanostructured OPV devices with precise morphology control. After polymerization the patterned organic material is insoluble in common organic solvents allowing for simple and cost effective application of an acceptor compound. However, the cross-linking moiety used here does not seem appropriate for the fabrication of photovoltaic devices: the low conductivity observed for initial device studies is attributed mainly to charge carrier trapping in the abundant acrylate moieties at the periphery of the $HBC_{acrylate}$ molecules.

A similar AAO template assisted approach allows to structure thin films of $PC_{61}BM$. Using these highly ordered nano-patterned layers light trapping effects can be evidenced at the interface with a subsequently evaporated metal. Furthermore, the nano-patterned layers of $PC_{61}BM$ appear instructive for the fabrication of photovoltaic devices. Initial experiments show, that conductivity issues are not apparent. On the other hand, at present it remains a challenge to achieve a high aspect ratio and an area-wide defect free imprint for this small molecule lacking a cross-linking side group.

7 Conclusion and Outlook

In this thesis both supramolecular assembly and nanoscale interface morphologies are investigated for organic donor and acceptor materials used in photovoltaic devices. The morphology of the organic compounds as well as their photophysical behavior has been studied in detail and related to the photovoltaic performance obtained in the heterojunction devices.

7.1 Supramolecular assembly

A variety of solution processable discotic molecules have been applied as donor and acceptor molecules for blend devices. It is shown that the molecular packing has a significant impact on the photophysical behavior of resulting devices. Both exciton separation probability and current generation are found to increase with shorter side chains attached to the HBC-donor molecules under investigation. On the other hand, increased recombination and therefore reduced fill factors are observed, when a more intimate packing is allowed for the donor and acceptor molecules limiting the overall performance of the devices. For all solution processable discotic molecules investigated here we observe a rather unfavorable intermixing of donor and acceptor compounds. Both edge-on stacking and an alternate stapling have been evidenced for the HBC molecules with short side chains in conjunction with PDI. Instead, for longer side chain HBCs rather disrupted and non-ordered morphologies are obtained. The lack of the formation of interdigitated network structures with direct percolation pathways to the respective device electrodes hinders a more efficient charge carrier extraction from the device and thus limits the power conversion efficiency.
In an alternative approach the deposition of small molecular weight donor and acceptor molecules is accomplished using vacuum sublimation techniques. Pristine layers of unsubstituted HBC are grown in crystalline layers with increased supramolecular order resulting in a remarkably high exciton diffusion length. In conjunction with the hexafluorinated analogue for the first time devices relying solely on large polycyclic aromatic hydrocarbons are presented.

Strongly improved fill factor and rectification of devices can be obtained when using the solution processable buckminsterfullerene $PC_{61}BM$ as electron acceptor instead of a discotic molecule. A finding, that can be attributed to strongly reduced recombination losses at the interface due to the excellent electron conduction properties of the fullerene derivative. On the other hand, charge generation of this type of devices is strongly limited due to the narrow spectral overlap of the organic materials HBC and $PC_{61}BM$ with the solar radiation spectrum.
A sensitizing method is presented herein which allows to combine the photon absorption of a dye molecule with the outstanding electron collection and charge extraction capabilities of fullerene derivatives. Several photophysical studies underline the importance of an energy transfer mechanism from photo-excited dye molecules to the fullerene derivative. As a result, strongly increased current generation and photovoltaic performance can be obtained for the dye sensitized OPV devices investigated here.
In summary, supramolecular assemblies of pristine HBC layers show very suitable properties for efficient OPV devices. Best performance can be obtained at the heterojunction with a dye sensitized fullerene. Further performance increase is expected when increasing the interfacial area of the donor and acceptor compounds. A great challenge remains to *simultaneously* orient and organize the donor and acceptor molecules in mixed phases. The formation of unfavorable morphologies hinders the efficient extraction of charge carriers generated in the organic semiconductor blend.

7.2 Nanoscale morphologies

Interdigitated interfaces on the nanometer length scale between the donor and acceptor materials hold great promise to allow the desired decoupling of photon absorption and charge extraction while maintaining influence over the assembly and supramolecular organization of the pristine materials.
A template assisted and easily scalable method is applied to precisely pattern organic materials on a nanometer length scale. It is shown how an imprinting procedure can be used to transfer the patterns of highly ordered aluminum oxide membranes into structured organic thin films on a substrate support.
A large aspect ratio of over 8:1 is achieved for a HBC derivative with thermally crosslinkable residual groups. The controlled formation of a barrier layer and the defect free production on square centimeter areas renders this approach appealing towards the formation of OPV devices with interdigitated donor-acceptor interfaces.
Unfortunately, the electronic properties of the polymerized HBC network are not suit-

able for the incorporation as donor layer in OPV devices. Acrylate side chains are believed to act as traps hindering charge transport in this organic layer.
In general the template assisted imprint method shown here is very versatile. The patterning technique is not limited to the cross-linkable HBC but also thin films of $PC_{61}BM$ have been successfully structured. Highly ordered patterned layers of $PC_{61}BM$ can be applied for plasmon enhanced absorption and show great potential for manufacturing OPV devices with interdigitated interfaces.

7.3 Outlook

A variety of studies shown in this thesis reveal the importance of the supramolecular assembly and nanoscale morphologies at the interface of the organic compounds for an improved photovoltaic performance.
The findings presented here strongly motivate a combination of both the bottom-up approach relying on the self assembly of individual molecules and a template assisted top-down method using a nano-imprinting technique. The self organization of the molecules into aligned stacks combined with the confinement into the highly ordered interdigitated structures of separated donor and acceptor phases holds great promise to allow for OPV devices with superior power conversion efficiency.
The experimental findings presented herein also help to define directions for further research. A short overview to a selection of ongoing research activities and possible future directions is given below.

Device characterization tools Several experimental characterization tools have been developed to gain an increased understanding of the photophysical behavior of OPV devices. A variety of setups was assembled and used to record the data presented in this thesis.
Initial results on photovoltaic devices have been obtained using an integrated IV-measurement system with a temperature control unit. A continuation of these studies may help to reveal detailed information on the exciton binding properties in OPV devices [90, 97, 262]. This technique might be especially interesting when comparing properties of devices relying on different interfacial architectures as are studied in this thesis.
Determining charge carrier density, lifetime and mobility in the photoactive materials is also of great interest. Both the charge extraction in a linearly increasing voltage techniques (CELIV) [123, 171, 263] and charge extraction experiments using a MOSFET

switch which have been assembled, initially tested and prepared for future measurements will allow detailed insight to the charge carrier dynamics.

Liquid crystalline materials and supramolecular order It has been shown herein, that liquid crystalline materials have a high potential to allow self organization of molecules into appealing morphologies for OPV applications. The use of a sacrificial capping layer [195] combined with specially functionalized molecules [17] facilitate the supramolecular assembly of the molecules in homeotrophically aligned stacks of pristine material on transparent electrode support as has been shown herein (Section 4.2).
Only recently and for the first time a study has proven the orientation of *both* LC donor and acceptor molecules within one device [264]. A confinement based method is used similar to the approach presented herein (Section 4.2). Instead of using a sacrificial capping layer the researchers realize a subsequent freezing of the organic materials in a bi-layered geometry facilitated by clearly distinct phase transition temperatures of the two compounds. This proof of principle seems very instructive for the development of a heterojunction device using strongly oriented liquid crystalline materials in the active layer. The high supramolecular order achieved solely using self-assembly processes and might allow for an increased device efficiency if LC materials with suitable electronic properties are found.
Gorodetsky et al. show a different approach to benefit from supramolecular assembly [265]. A combination of solution processing and evaporation techniques is used to fabricate OPV devices (similar as has been investigated in Section 4.3.3). A hexabenzocoronene derivative is pre-oriented in the LC phase on an ITO glass support and subsequently covered with vacuum sublimated fullerenes (C_{60}) forming the acceptor material of the heterojunction. The appealing properties of the strongly oriented pristine HBC material may be retained in the heterojunction device.
Both approaches relying on well separated material phases show the potential of supramolecular assembly of LC materials for the fabrication of photovoltaic devices. Clearly superior device efficiency is expected for a simultaneous assembly of donor and acceptor compounds into segregated but highly ordered domains but has yet to be realized.

Cross-linkable materials The template assisted imprinting of cross-linkable organic materials as shown herein (Section 6.3) allows to fabricate ideally structured organic layers with nanometer precision and barrier layer formation for the direct use in OPV devices with interdigitated interfaces. Patterning the organic donor material with AAO templates followed by polymerization and subsequent filling with an organic counterpart

is a versatile method and not intrinsically limited to the electronically not suitable molecule used here.

A new class of cross-linkers for polymeric materials was synthesized and presented recently by the Professor Ho group, National University of Singapore. Cross-linking of polymer strands into extended networks allows similar structure manipulations as have been realized using $HBC_{acrylate}$. In fact, the combination of polymer strands with low amounts of fluorinated phenyl azides as cross linking material shows several advantages when compared to the $HBC_{acrylate}$. It has been proven that the charge carrier mobility and photophysical properties of the polymer material is not significantly affected by the cross-linking procedure [258] and only ow amount of cross-linkage units is necessary to induce the gelation of the individual polymer strands. Efficient heterojunction OPV devices have been realized already using the novel combination of polymer and phenyl-azide.

Experiments using materials synthesized by the Professor Ho group in combination with an advanced nano-patterning technique as shown in Chapter 6 are currently underway and will be continued by colleges at the Hybrid Nanostructures research group. The precise control over the nano-morphology as shown herein is expected to allow for a superior device efficiency.

8 Appendix A: Computer programs

This chapter gives an overview to the computer programs that have been designed and developed for data acquisition, management and handling. Program code generated by the author may not be distributed without further permission.
Great thanks to Andreas Jakowetz especially for implementing several new functions into the data acquisition program "Solar Test Station". Many thanks also to all my co-workers and users of the programs for consequently helping to find errors and suggestions on how to improve the programs.

8.1 LabView Programs

8.1.1 Solar Cell Test Station

Module: IV-curve monitor

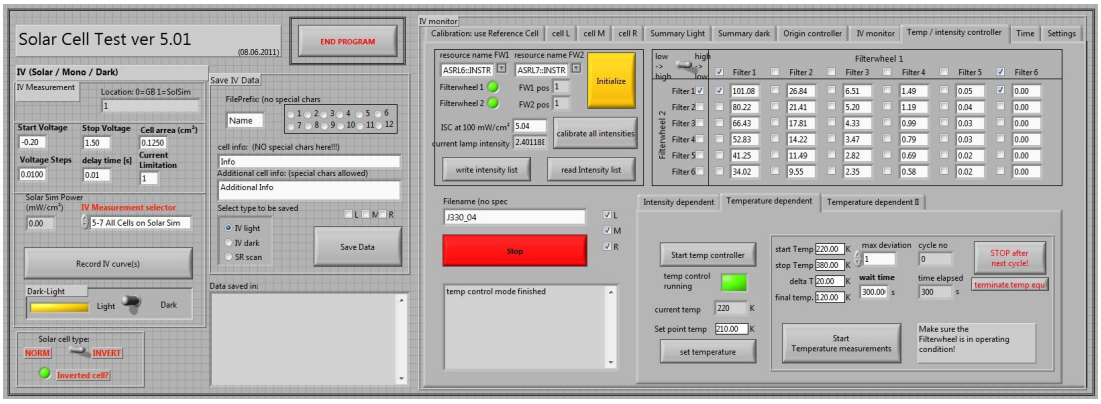

Figure 8.1: Snapshot from the graphical user interface designed for the automated acquisition of diode characteristics.

"Solar cell Test station" has been designed to simultaneously control several hardware units and visualize their results via a graphical user interface. The program code is

designed to allow real time visualization of current-voltage measurements and spectrally resolved response analysis.

Module: EQE determination

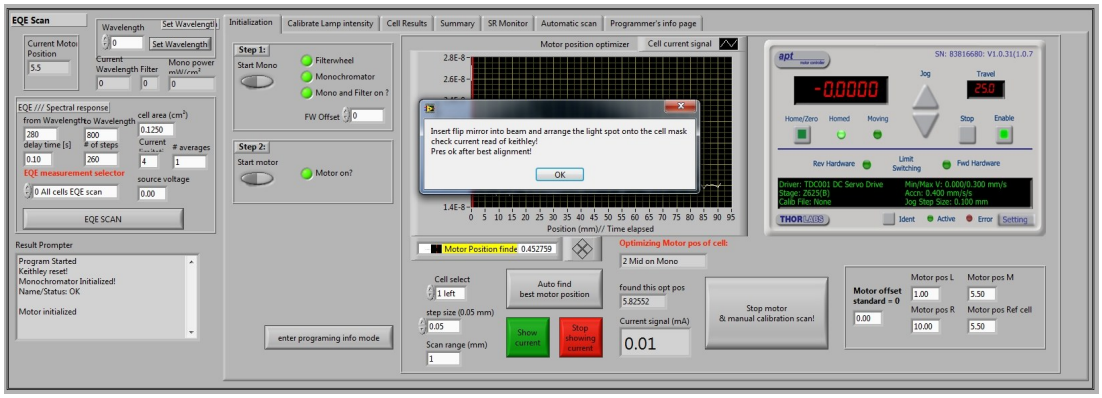

Figure 8.2: Snapshot from the graphical user interface designed for the automated acquisition of the external quantum efficiency.

Module: Temperature and Intensity dependent measurements

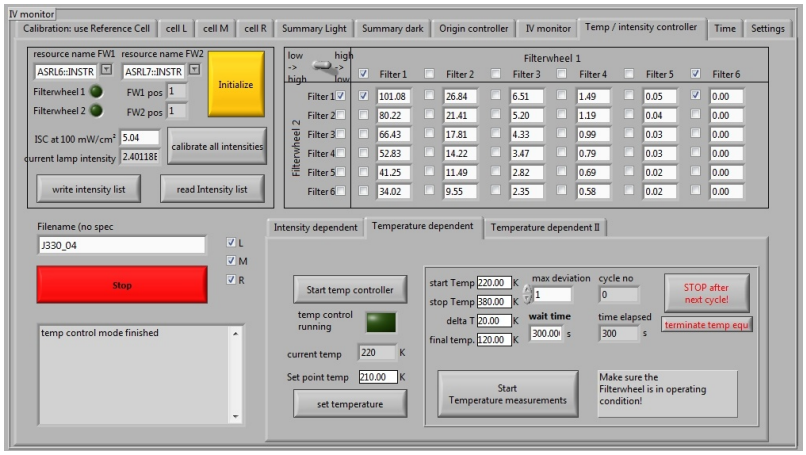

Figure 8.3: Snapshot from the graphical user interface designed for the automated acquisition of temperature and intensity dependent diode characteristics.

The control panel allows to sweep a pre-defined series of temperatures in the range of 77...377 K and 36 intensities for each photovoltaic device. The IV cuves are recorded

automatically and saved for a separate data analysis commonly performed using the program "SolarPlotGUI" (section 8.2.1)

8.1.2 TAS data acquisition

The program "TAS data acquisition" was refurbished and complemented with additional functions in order to allow straightforward acquisition and handling of transient absorption data.

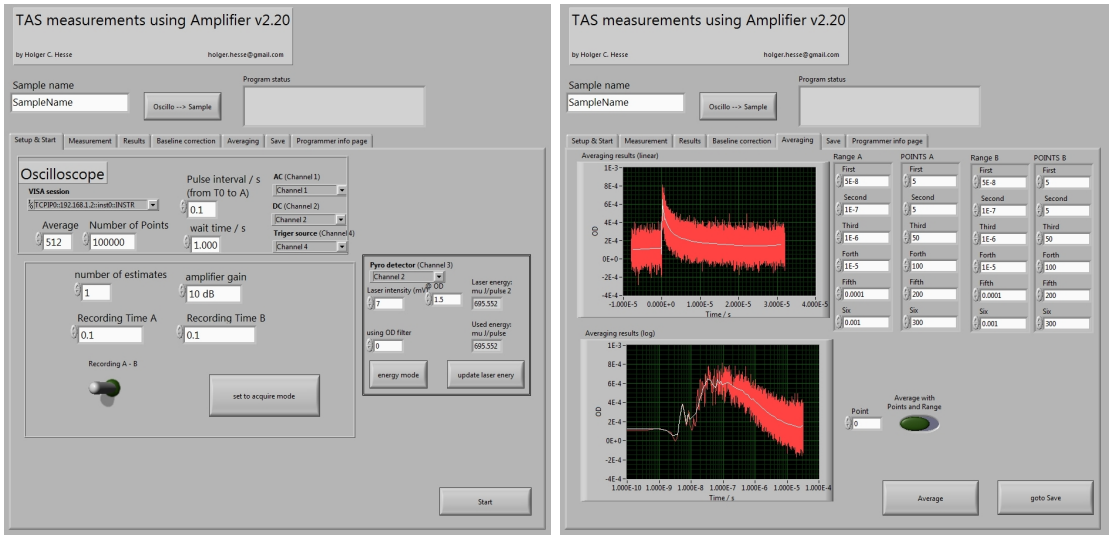

Figure 8.4: Snapshots taken from the transient absorption data acquisition program.

8.1.3 TAS spectrum calculator

8.1.4 Charge extraction using switch

A LabView program has been developed to allow the fully automated control of delay generator, oscilloscope, laser shutter and a MOSFET based automated switch unit. Program features include the recording and handling of V_{OC} decay and switch controlled I_{SC} delay curves at variable delay times. Furthermore charge and charge density values are calculated using the program and data obtained is graphically represented.

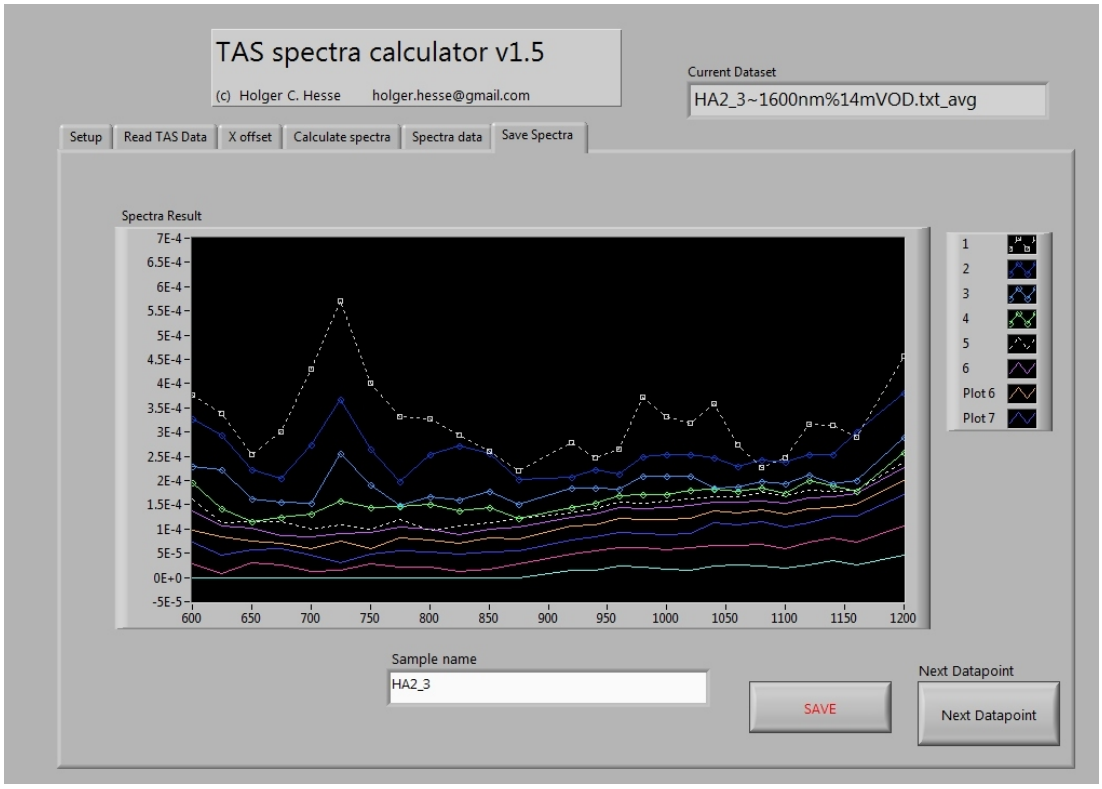

Figure 8.5: Transient absorption spectrum generator. The program facilitates the combination of TA data gathered for a spectrum.

8.2 Mathlab data evaluation Programs

8.2.1 SolarPlotGUI

SolarPlotGUI is a "Mathlab" based program developed for an on-the-fly analysis and evaluation of Solar cell measurements. The graphical user interface allows to handle, group and organize various datasets. The tool can be used to handle color graphs of several kinds of datasets including:

- absorption
- dark and light IV curves
- comparison of characteristic device parameters (V_{OC}, I_{SC},η, ...)
- temperature and intensity dependent device characteristics
- External quantum efficiency

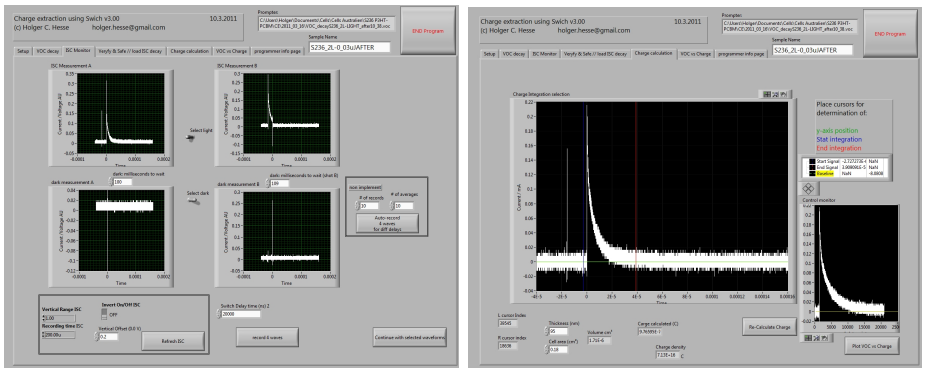

Figure 8.6: Snapshots taken from the charge extraction LabView program.

- photo-CELIV

Figure 8.7 and Figure 8.8 show the graphical user interface and some exemplary data plots generated using the program. Furthermore data tables containing all characteristic parameters can be generated and used for further in-depth analysis.

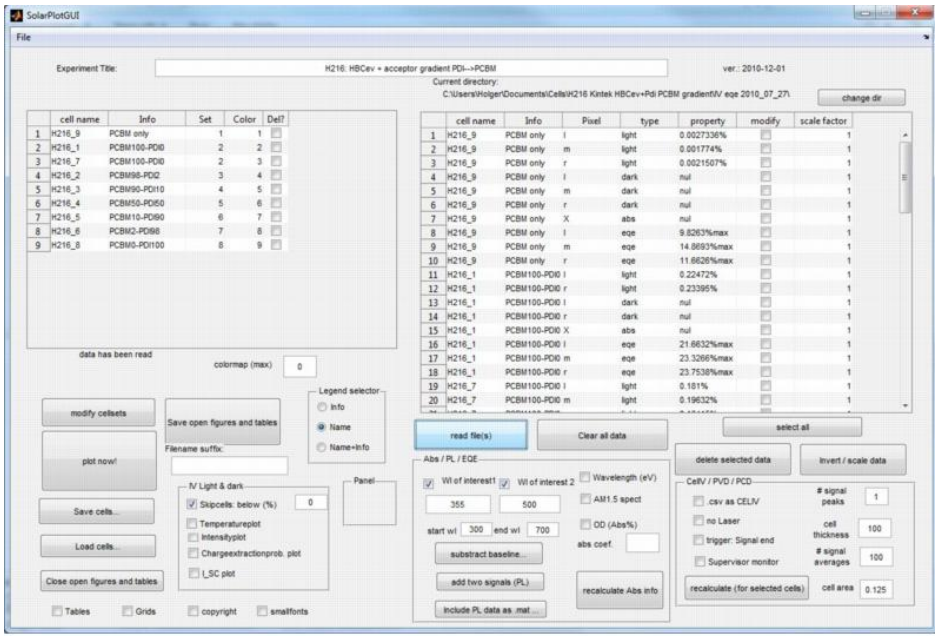

Figure 8.7: Snapshot from graphical user interface of SolarPlotGUI. Data handling as well as automated generation of summary plots and data tables is controlled via the user interface

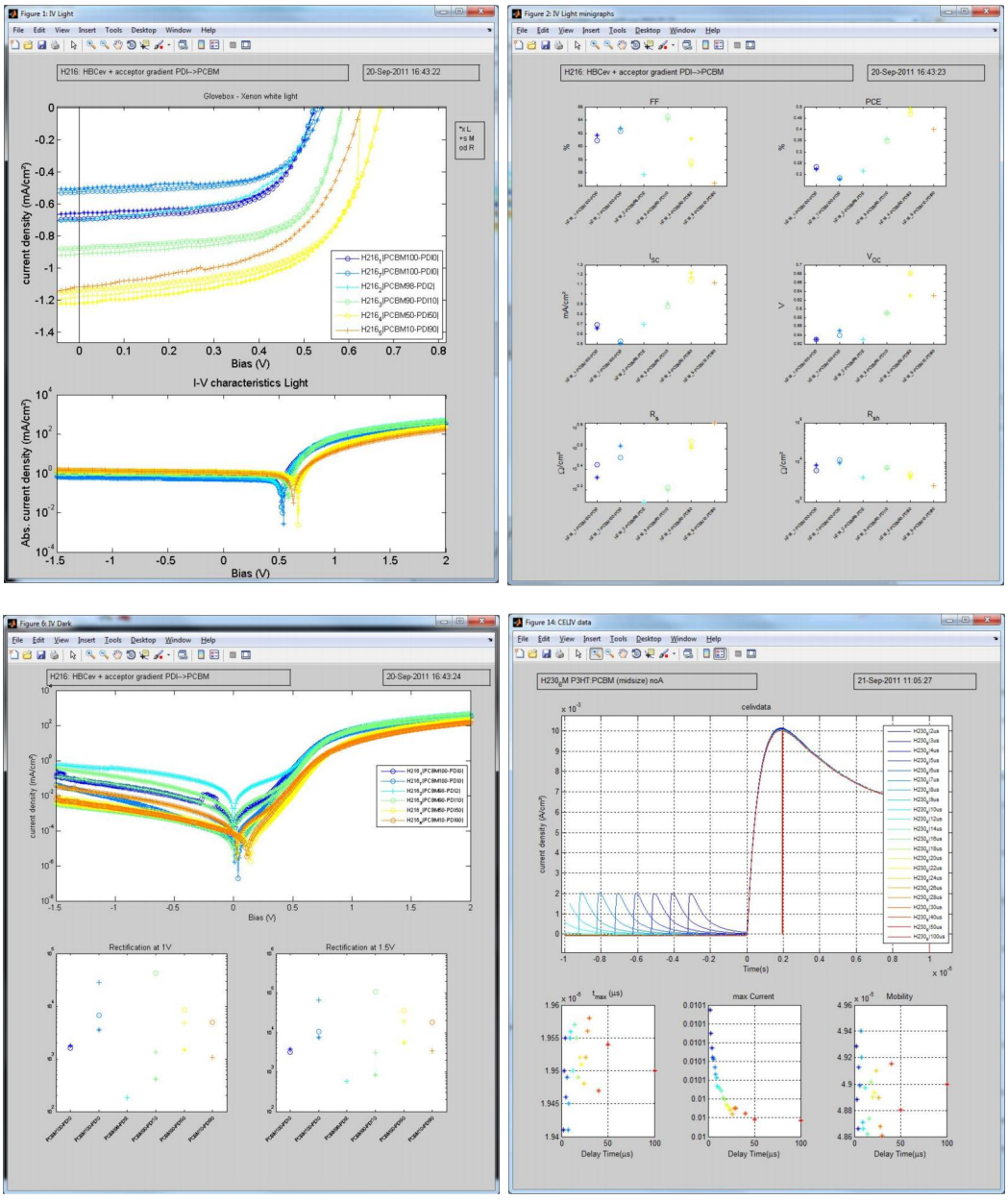

Figure 8.8: Snapshots from the program SolarPlotGUI. a) A set of IV curves under standard illumination **b)** An automatically generated summary of the characteristic device data. **c)** IV-curve data obtained in the dark and **d)** Photo-CELIV charge extraction cures plotted for different laser pulse delay times.

Appendix B: Related Author Publications

Holger C. Hesse, Jonas Weickert, Mahmoud Al-Hussein, Lukas Doessel, Xinliang Feng, Klaus Müllen, and Lukas Schmidt-Mende. Discotic materials for organic solar cells: Effects of chemical structure on assembly and performance. *Solar Energy Materials and Solar Cells*, 94(3):560–567, 2010.

Holger. C. Hesse, Dominik Lebmbke, Lukas Dössel, Xingliang Feng, Klaus Müllen, and Lukas Schmidt-Mende. Nanostructuring discotic molecules on ito support. *Nanotechnology*, 22(5):055303, 2011.

Holger C. Hesse, Jonas Weickert, Christian Hundschell, Xinliang Feng, Klaus Müllen, Bert Nickel, Attila J. Mozer, and Lukas Schmidt-Mende. Perylene sensitization of fullerenes for improved performance in organic photovoltaics. *Advanced Energy Materials*, 1(5):861–869, 2011.

Holger C. Hesse, Christoph Schaffer, Christian Hundschell, Akimitsu Narita, Xinliang Feng, Klaus Müllen, Bert Nickel, and Lukas Schmidt-Mende. Large polycyclic aromatic hydrocarbons for application in donor-acceptor photovoltaics. *physica status solidi a*, accepted, 2011.

Mahmoud al Hussein, Holger C. Hesse, Jonas Weickert, and Lukas Schmidt-Mende. Structural properties of discotic hexabenzocoronene/perylene diimide active layer of bulk heterojunction photovoltaic devices. *Thin Solid Films*, 520(1):307–313, 2011.

R Dunbar, H. C. Hesse, D Lembke, and L Schmidt Mende. Light trapping plasmonic nanovoid arrays. *Phys Rev B*, accepted, 2011.

Sun Haiyan, Jonas Weickert, Holger C. Hesse, and Lukas Schmidt-Mende. Uv light protection through tio2 blocking layers for inverted organic solar cells. *Solar Energy Materials and Solar Cells*, 95(12):3450–3454, 2011.

Jonas Weickert, Ricky B. Dunbar, Holger C. Hesse, Wolfgang Wiedemann, and Lukas Schmidt-Mende. Nanostructured organic and hybrid solar cells. *Advanced Materials*, 23(16):1810–1828, 2011.

Kevin P. Musselman, Andreas Wisnet, Diana C. Iza, Holger C. Hesse, Christina Scheu, Judith L. MacManus-Driscoll, and Lukas Schmidt-Mende. Strong efficiency improvements in ultra-low-cost inorganic nanowire solar cells. *Advanced Materials*, 22(35):E254–E258, 2010.

Jonas Weickert, Haiyan Sun, Claudia Palumbiny, Holger Christian Hesse, and Lukas Schmidt-Mende. Spray-deposited pedot:pss for inverted organic solar cells. *Solar Energy Materials and Solar Cells*, 94(12):2371–2374, 2010.

Appendix C: Conference List

H.C. Hesse, D. Lembke, L. Dössel, C.Hundschell B. Nickel, K.Müllen, and L.Schmidt-Mende. Nanostructured interfaces and supramolecular assembly of discotic molecules. In *Plastic electronics*, Dresden, Germany, 2011.

H.C. Hesse, D. Lembke, X. Feng, C. Hundschell, B. Nickel, K. Müllen, and L. Schmidt-Mende. Perylene sensitization of fullerenes for enhanced performance in organic photovoltaics. In *MRS Spring Meeting*, San Francico, USA, 2011.

H. C. Hesse, C. Palumbiny, D. Lembke, X. Feng, C. Hundschell, B. Nickel, K. Müllen, and L. Schmidt-Mende. Perylene sensitization of fullerenes and nanostructured device architectures for enhanced performance in organic photovoltaics. In *EMRS Spring Meeting*, Nice, France, 2011.

H.C. Hesse, L. Dössel, C. Hundschell, K. Müllen, B.Nickel, and L. Schmidt-Mende:. Supramolecular assembly and nanostructured interfaces in opv,. In *Ordered 1D Nanostructures for Photovoltaics*, Mallorca, Spain, 2010.

Bibliography

[1] Godfrey Boyle. *Renewable Energy*, volume second edition. Oxford University press, 2004.

[2] wikipedia.org. Fukushima daiichi nuclear disaster. *www.en.wikipedia.org /wiki/Fukushima_ Daiichi_ nuclear_ disaster*, 2011.

[3] nobelprze.org. The nobel prize in chemistry 2000. *www.nobelprize.org /nobel_ prizes/ chemistry/ laureates/ 2000/*, 2011(13 Feb), 2000.

[4] Plastic Electronics Conference Dresdenm 2010. www.plastic-electronics2010.com/. *InnovationFab*, 2011(13 Feb), 2010.

[5] Heliatek. Heliatek gmbh. *www.heliatek.com*, 2011.

[6] Konarka Technologies Inc. Konarka technologies. *www.konarka.com*, 2011.

[7] Richard R. Lunt and Vladimir Bulovic. Transparent, near-infrared organic photovoltaic solar cells for window and energy-scavenging applications. *Applied Physics Letters*, 98(11):113305, 2011.

[8] Gary P. Kushto, Woohong Kim, and Zakya H. Kafafi. Flexible organic photovoltaics using conducting polymer electrodes. *Applied Physics Letters*, 86(9):093502, 2005.

[9] FC Krebs. All solution roll-to-roll processed polymer solar cells free from indium-tin-oxide and vacuum coating steps. *Organic Electronics*, 2009.

[10] Robert F. Service. Outlook brightens for plastic solar cells. *Science*, 332(6027):293, 2011.

[11] MC Scharber, D Mühlbacher, M Koppe, P Denk, C Waldauf, AJ Heeger, and CJ Brabec. Design rules for donors in bulk-heterojunction solar cells-towards 10 *Advanced Materials*, 18(6):789–794, 2006.

[12] C.D. Dimitrakopoulos and P.R.L. Malenfant. Organic thin film transistors for large area electronics. *Advanced Materials*, 14(2):99, 2002.

[13] RR Lunt, NC Giebink, AA Belak, JB Benziger, and SR Forrest. Exciton diffusion lengths of organic semiconductor thin films measured by spectrally resolved photoluminescence quenching. *Journal of Applied Physics*, 105(5):3711, 2009.

[14] G. Dennler, M.C. Scharber, and C.J. Brabec. Polymer fullerene bulk heterojunction solar cells. *Advanced Materials*, 21(13):1323–1338, 2009.

[15] S.R. Forrest. The limits to organic photovoltaic cell efficiency. *MRS bulletin*, 30(01):28–32, 2005.

[16] T. Ameri, G. Dennler, C. Waldauf, H. Azimi, A. Seemann, K. Forberich, J. Hauch, M. Scharber, K. Hingerl, and C. J. Brabec. Fabrication, optical modeling, and color characterization of semitransparent bulk-heterojunction organic solar cells in an inverted structure. *Advanced Functional Materials*, 20(10):1592–1598, 2010.

[17] W. Pisula, M. Zorn, J. Y. Chang, K. Mullen, and R. Zentel. Liquid crystalline ordering and charge transport in semiconducting materials. *Macromolecular Rapid Communications*, 30(14):1179–1202, 2009.

[18] W. Pisula, M. Kastler, D. Wasserfallen, J. W. F. Robertson, F. Nolde, C. Kohl, and K. Mullen. Pronounced supramolecular order in discotic donor-acceptor mixtures. *Angewandte Chemie-International Edition*, 45(5):819–823, 2006.

[19] D. Venkataraman, Serkan Yurt, B. Harihara Venkatraman, and Nagarjuna Gavvalapalli. Role of molecular architecture in organic photovoltaic cells. *The Journal of Physical Chemistry Letters*, 1(6):947–958, 2010.

[20] A. M. van de Craats, J. M. Warman, A. Fechtenkotter, J. D. Brand, M. A. Harbison, and K. Mullen. Record charge carrier mobility in a room-temperature discotic liquid-crystalline derivative of hexabenzocoronene. *Advanced Materials*, 11(17):1469–1472, 1999.

[21] C. Y. Liu, A. Fechtenkotter, M. D. Watson, K. Mullen, and A. J. Bard. Room temperature discotic liquid crystalline thin films of hexa-peri-hexabenzocoronene: Synthesis and optoelectronic properties. *Chemistry of Materials*, 15(1):124–130, 2003.

[22] L. Schmidt-Mende, A. Fechtenkotter, K. Mullen, E. Moons, R. H. Friend, and J. D. MacKenzie. Self-organized discotic liquid crystals for high-efficiency organic photovoltaics. *Science*, 293(5532):1119–1122, 2001.

[23] M. Steinhart. Supramolecular organization of polymeric materials in nanoporous hard templates. *Self-Assembled Nanomaterials Ii: Nanotubes*, 220:123–187, 2008.

[24] N. Haberkorn, J. S. Gutmann, and P. Theato. Template-assisted fabrication of free-standing nanorod arrays of a hole-conducting cross-linked triphenylamine derivative: Toward ordered bulk-heterojunction solar cells. *Acs Nano*, 3(6):1415–1422, 2009.

[25] R. Bai, M. Ouyang, R. J. Zhou, M. M. Shi, M. Wang, and H. Z. Chen. Well-defined nanoarrays from an n-type organic perylene-diimide derivative for photoconductive devices. *Nanotechnology*, 19(5):–, 2008.

[26] Mukti Aryal, Fatih Buyukserin, Kamil Mielczarek, Xiao-Mei Zhao, Jinming Gao, Anvar Zakhidov, and Wenchuang Hu. Imprinted large-scale high density polymer nanopillars for organic solar cells. *J. Vac. Sci. Technol. B*, 26:2562–2566, 2008.

[27] W Wiedemann, L Sims, A Abdellah, A Exner, R Meier, KP Musselman, JL MacManus-Driscoll, P Muller-Buschbaum, G Scarpa, and P Lugli. Nanostructured interfaces in polymer solar cells. *Applied Physics Letters*, 96(26):263109, 2010.

[28] H Hoppe, M Niggemann, C Winder, J Kraut, R Hiesgen, A Hinsch, D Meissner, and NS Sariciftci. Nanoscale morphology of conjugated polymer/fullerene-based bulk-heterojunction solar cells. *Advanced Functional Materials*, 14(10):1005–1011, 2004.

[29] HJ Snaith and L Schmidt-Mende. Advances in liquid-electrolyte and solid-state dye-sensitized solar cells. *Advanced Materials*, 19(20):3187–3200, 2007.

[30] Dyesol. Dyesol. *www.dyesol.com*, 2011.

[31] Kazmerski. www.nrel.gov. *National Renewable Energy Laboratory*, 2011.

[32] B. O'regan and M. Grätzel. A low-cost, high-efficiency solar cell based on dye-sensitized colloidal tio2 films. *Nature*, 353:737–740, 1991.

[33] M. Graetzel. Solar energy conversion by dye-sensitized photovoltaic cells. *Inorg. Chem*, 44(20):6841–6851, 2005.

[34] M. K. Nazeeruddin, Peter PÃ©chy, Thierry Renouard, Shaik M. Zakeeruddin, Robin Humphry-Baker, Pascal Comte, Paul Liska, Le Cevey, Emiliana Costa, Valery Shklover, Leone Spiccia, Glen B. Deacon, Carlo A. Bignozzi, and Michael Grätzel. Engineering of efficient panchromatic sensitizers for nanocrystalline tio2-based solar cells. *Journal of the American Chemical Society*, 123(8):1613–1624, 2001.

[35] M. Law, L.E. Greene, J.C. Johnson, R. Saykally, and P. Yang. Nanowire dye-sensitized solar cells. *Nature Materials*, 4(6):455–459, 2005.

[36] B. Li, L. Wang, B. Kang, P. Wang, and Y. Qiu. Review of recent progress in solid-state dye-sensitized solar cells. *Solar Energy Materials and Solar Cells*, 90(5):549–573, 2006.

[37] Jonas Weickert, Ricky B. Dunbar, Holger C. Hesse, Wolfgang Wiedemann, and Lukas Schmidt-Mende. Nanostructured organic and hybrid solar cells. *Advanced Materials*, 23(16):1810–1828, 2011.

[38] Y.Y. Lin, C.W. Chen, T.H. Chu, W.F. Su, C.C. Lin, C.H. Ku, J.J. Wu, and C.H. Chen. Nanostructured metal oxide/conjugated polymer hybrid solar cells by low temperature solution processes. *Journal of Materials Chemistry*, 17(43):4571–4576, 2007.

[39] G.K. Mor, K. Shankar, M. Paulose, O.K. Varghese, and C.A. Grimes. High efficiency double heterojunction polymer photovoltaic cells using highly ordered tio nanotube arrays. *Applied Physics Letters*, 91:152111, 2007.

[40] Jonas Weickert, Florian Auras, Thomas Bein, and Lukas Schmidt-Mende. Characterization of interfacial modifiers for hybrid solar cells. *The Journal of Physical Chemistry C*, pages null–null, 2011.

[41] CW Tang. Two layer organic photovoltaic cell. *Applied Physics Letters*, 48:183, 1986.

[42] Thomson Reuthers. Isi web of knowledge. *www.isiknowledge.com/*, 2011(18 Juli), 2011.

[43] H. Hoppe and N. S. Sariciftci. Polymer solar cells. In *Photoresponsive Polymers Ii*, volume 214 of *Advances in Polymer Science*, pages 1–86. Springer-Verlag Berlin, Berlin, 2008.

[44] Slawomir Braun, William R. Salaneck, and Mats Fahlman. Energy-level alignment at organic/metal and organic/organic interfaces. *Advanced Materials*, 21(14-15):1450–1472, 2009.

[45] National Renewable Energy Laboratory. Reference solar spectral irradiance: Air mass 1.5. *www.rredc.nrel.gov/solar/spectra/am1.5/*, 2011.

[46] PE Shaw, A Ruseckas, and IDW Samuel. Exciton diffusion measurements in poly (3-hexylthiophene). *Advanced Materials*, 20(18):3516–3520, 2008.

[47] H. Sirringhaus. Device physics of solution-processed organic field-effect transistors. *Advanced Materials*, 17(20):2411–2425, 2005.

[48] Richard R. Lunt, Jay B. Benziger, and Stephen R. Forrest. Relationship between crystalline order and exciton diffusion length in molecular organic semiconductors. *Advanced Materials*, 22(11):1233–1236, 2010.

[49] L. Onsager. Initial recombination of ions. *Physical Review*, 54(8):554, 1938.

[50] V. D. Mihailetchi, L. J. A. Koster, J. C. Hummelen, and P. W. M. Blom. Photocurrent generation in polymer-fullerene bulk heterojunctions. *Physical Review Letters*, 93(21):216601, 2004.

[51] Jiye Lee, Koen Vandewal, Shane R. Yost, Matthias E. Bahlke, Ludwig Goris, Marc A. Baldo, Jean V. Manca, and Troy Van Voorhis. Charge transfer state versus hot exciton dissociation in polymerâ^'fullerene blended solar cells. *Journal of the American Chemical Society*, 132(34):11878–11880, 2010.

[52] TM Clarke and JR Durrant. Charge photogeneration in organic solar cells. *Chemical Reviews*, 110(11):6736–6767, 2010.

[53] Mahmoud al Hussein, Holger C. Hesse, Jonas Weickert, and Lukas Schmidt-Mende. Structural properties of discotic hexabenzocoronene/perylene diimide active layer of bulk heterojunction photovoltaic devices. *Thin Solid Films*, 520(1):307–313, 2011.

[54] Holger C. Hesse, Jonas Weickert, Mahmoud Al-Hussein, Lukas Doessel, Xinliang Feng, Klaus Müllen, and Lukas Schmidt-Mende. Discotic materials for organic solar cells: Effects of chemical structure on assembly and performance. *Solar Energy Materials and Solar Cells*, 94(3):560–567, 2010.

[55] H Hoppe and NS Sariciftci. Morphology of polymer/fullerene bulk heterojunction solar cells. *Journal of Materials Chemistry*, 16(1):45–61, 2006.

[56] J. Liu, Y. Shi, and Y. Yang. Solvation-induced morphology effects on the performance of polymer-based photovoltaic devices. *Advanced Functional Materials*, 11(6):420, 2001.

[57] A. Geiser, B. Fan, H. Benmansour, F. Castro, J. Heier, B. Keller, K.E. Mayerhofer, F. Nüesch, and R. Hany. Poly (3-hexylthiophene)/c60 heterojunction solar cells:

Implication of morphology on performance and ambipolar charge collection. *Solar Energy Materials and Solar Cells*, 92(4):464–473, 2008.

[58] R. A. Street and M. Schoendorf. Interface state recombination in organic solar cells. *Physical Review B*, 81(20):–, 2010.

[59] Y. Kim, S. Cook, S. M. Tuladhar, S. A. Choulis, J. Nelson, J. R. Durrant, D. D. C. Bradley, M. Giles, I. Mcculloch, C. S. Ha, and M. Ree. A strong regioregularity effect in self-organizing conjugated polymer films and high-efficiency polythiophene: fullerene solar cells. *Nature Materials*, 5(3):197–203, 2006.

[60] Sam-Shajing Sun. Design of a block copolymer solar cell. *Solar Energy Materials and Solar Cells*, 79(2):257–264, 2003.

[61] K. Schulze, C. Uhrich, R. Schüppel, K. Leo, M. Pfeiffer, E. Brier, E. Reinold, and P. Bäuerle. Efficient vacuum-deposited organic solar cells based on a new low-bandgap oligothiophene and fullerene c60. *Advanced Materials*, 18(21):2872–2875, 2006.

[62] Jiangeng Xue, Soichi Uchida, Barry P. Rand, and Stephen R. Forrest. 4.2resistances. *Applied Physics Letters*, 84(16):3013–3015, 2004.

[63] Jenny Nelson. Organic photovoltaic films. *Current Opinion in Solid State and Materials Science*, 6(1):87–95, 2002.

[64] A. Yakimov and S. R. Forrest. High photovoltage multiple-heterojunction organic solar cells incorporating interfacial metallic nanoclusters. *Applied Physics Letters*, 80(9):1667–1669, 2002.

[65] T. Ameri, G. Dennler, C. Lungenschmied, and C.J. Brabec. Organic tandem solar cells: a review. *Energy & Environmental Science*, 2(4):347–363, 2009.

[66] G. Yu, J. Gao, JC Hummelen, F. Wudl, and AJ Heeger. Polymer photovoltaic cells: enhanced efficiencies via a network of internal donor-acceptor heterojunctions. *Science*, 270(5243):1789, 1995.

[67] B. Rand, J. Genoe, P. Heremans, and J. Poortmans. Solar cells utilizing small molecular weight organic semiconductor. *Progress in Photovoltaics*, 15:659–676, 2007.

[68] Bright Walker, Arnold B. Tamayo, Xuan-Dung Dang, Peter Zalar, Jung Hwa Seo, Andres Garcia, Mananya Tantiwiwat, and Thuc-Quyen Nguyen. Nanoscale phase

separation and high photovoltaic efficiency in solution-processed, small-molecule bulk heterojunction solar cells. *Advanced Functional Materials*, 19(19):3063–3069, 2009.

[69] K. Walzer, B. Maennig, M. Pfeiffer, and K. Leo. Highly efficient organic devices based on electrically doped transport layers. *Chem. Rev*, 107(4):1233–1271, 2007.

[70] S. Sergeyev, W. Pisula, and Y. H. Geerts. Discotic liquid crystals: A new generation of organic semiconductors. *Chemical Society Reviews*, 36(12):1902–1929, 2007.

[71] W. S. Shin, H. H. Jeong, M. K. Kim, S. H. Jin, M. R. Kim, J. K. Lee, J. W. Lee, and Y. S. Gal. Effects of functional groups at perylene diimide derivatives on organic photovoltaic device application. *Journal of Materials Chemistry*, 16(4):384–390, 2006.

[72] Z. J. Chen, M. G. Debije, T. Debaerdemaeker, P. Osswald, and F. Wurthner. Tetrachloro-substituted perylene bisimide dyes as promising n-type organic semiconductors: Studies on structural, electrochemical and charge transport properties. *Chemphyschem*, 5(1):137–140, 2004.

[73] Mukti Aryal, Krutarth Trivedi, and Wenchuang Hu. Nano-confinement induced chain alignment in ordered p3ht nanostructures defined by nanoimprint lithography. *Acs Nano*, 3(10):3085–3090, 2009.

[74] R. A. Marsh, C. Groves, and N. C. Greenham. A microscopic model for the behavior of nanostructured organic photovoltaic devices. *Journal of applied Physics*, 101(8):083509, 2007.

[75] M Sommer, SM Lindner, and M Thelakkat. Microphase-separated donor-acceptor diblock copolymers: Influence of homo energy levels and morphology on polymer solar cells. *Advanced Functional Materials*, 17(9):1493–1500, 2007.

[76] I. W. Hamley. Ordering in thin films of block copolymers: Fundamentals to potential applications. *Progress in Polymer Science*, 34(11):1161–1210, 2009.

[77] W. Warta, R. Stehle, and N. Karl. Ultrapure, high mobility organic photoconductors. *Applied Physics A: Materials Science and Processing*, 36(3):163–170, 1985.

[78] RJ Bushby and OR Lozman. Discotic liquid crystals 25 years on. *Current Opinion in Colloid & Interface Science*, 7(5-6):343–354, 2002.

[79] Falk May, Valentina Marcon, Michael Ryan Hansen, Ferdinand Grozema, and Denis Andrienko. Relationship between supramolecular assembly and charge-carrier mobility in perylenediimide derivatives: The impact of side chains. *Journal of Materials Chemistry*, 2011.

[80] A. Cristadoro, M. Ai, H.J. Räder, J.P. Rabe, and K. Müllen. Electrical field-induced alignment of nonpolar hexabenzocoronene molecules into columnar structures on highly oriented pyrolitic graphite investigated by stm and sfm. *The Journal of Physical Chemistry C*, 112(14):5563–5566, 2008.

[81] HS Kim, SM Choi, JH Lee, P Busch, SJ Koza, EA Verploegen, and BD Pate. Uniaxially oriented, highly ordered, large area columnar superstructures of discotic supramolecules using magnetic field and surface interactions. *Advanced Materials*, 20(6):1105–1109, 2008.

[82] Felix Sunjoo Kim, Guoqiang Ren, and Samson A. Jenekhe. One-dimensional nanostructures of π-conjugated molecular systems: Assembly, properties, and applications from photovoltaics, sensors, and nanophotonics to nanoelectronics. *Chemistry of Materials*, 23(3):682–732, 2010.

[83] Russell A. Cormier and Brian A. Gregg. Self-organization in thin films of liquid crystalline perylene diimides. *The Journal of Physical Chemistry B*, 101(51):11004–11006, 1997.

[84] Trirup Dutta Choudhury, Nandiraju V. S. Rao, Robert Tenent, Jeffrey Blackburn, Brian Gregg, and Ivan I. Smalyukh. Homeotropic alignment and director structures in thin films of triphenylamine-based discotic liquid crystals controlled by supporting nanostructured substrates and surface confinement. *The Journal of Physical Chemistry B*, 115(4):609–617, 2011.

[85] C. J. Brinker, Y. Lu, A. Sellinger, and H. Fan. Evaporation-induced self-assembly: Nanostructures made easy. *Advanced Materials*, 11(7):579–585, 1999.

[86] J. P. Schmidtke, R. H. Friend, M. Kastler, and K. Mullen. Control of morphology in efficient photovoltaic diodes from discotic liquid crystals. *Journal of Chemical Physics*, 124(17):–, 2006.

[87] J. Li, M. Kastler, W. Pisula, J. W. F. Robertson, D. Wasserfallen, A. C. Grimsdale, J. Wu, and K. Mullen. Organic bulk-heterojunction photovoltaics based on alkyl substituted discotics. *Advanced Functional Materials*, 17(14):2528–2533, 2007.

[88] D. Cheyns and et al. Nanoimprinted semiconducting polymer films with 50Â nm features and their application to organic heterojunction solar cells. *Nanotechnology*, 19(42):424016, 2008.

[89] X. He, F. Gao, G. Tu, D. Hasko, S. Hu ttner, U. Steiner, N.C. Greenham, R.H. Friend, and W.T.S. Huck. Formation of nanopatterned polymer blends in photovoltaic devices. *Nano Letters*, 10(4):1302–1307, 2010.

[90] Barry P. Rand, Diana P. Burk, and Stephen R. Forrest. Offset energies at organic semiconductor heterojunctions and their influence on the open-circuit voltage of thin-film solar cells. *Physical Review B*, 75(11):115327, 2007.

[91] A. Fahrenbruch and R.H. Bube. *Fundamentals of solar cells.* Academic Press,Orlando, FL, USA, 1983.

[92] N. C. Giebink, G. P. Wiederrecht, M. R. Wasielewski, and S. R. Forrest. Ideal diode equation for organic heterojunctions. i. derivation and application. *Physical Review B*, 82(15):155305, 2010.

[93] Roland Steim, F. Rene Kogler, and Christoph J. Brabec. Interface materials for organic solar cells. *Journal of Materials Chemistry*, pages –, 2010.

[94] M. Dolores Perez, Carsten Borek, Stephen R. Forrest, and Mark E. Thompson. Molecular and morphological influences on the open circuit voltages of organic photovoltaic devices. *Journal of the American Chemical Society*, 131(26):9281–9286, 2009.

[95] Selyan Price and Robert Margolis. *2008 Solar Technologies Market Report 2008.* NREL Energy Labs, 2010.

[96] EA Katz, D. Faiman, SM Tuladhar, JM Kroon, MM Wienk, T. Fromherz, F. Padinger, CJ Brabec, and NS Sariciftci. Temperature dependence for the photovoltaic device parameters of polymer-fullerene solar cells under operating conditions. *Journal of Applied Physics*, 90:5343, 2001.

[97] I. Riedel, J. Parisi, V. Dyakonov, L. Lutsen, D. Vanderzande, and J. C. Hummelen. Effect of temperature and illumination on the electrical characteristics of polymer-fullerene bulk-heterojunction solar cells. *Advanced Functional Materials*, 14(1):38–44, 2004.

[98] Jin Young Kim, Kwanghee Lee, Nelson E. Coates, Daniel Moses, Thuc-Quyen Nguyen, Mark Dante, and Alan J. Heeger. Efficient tandem polymer solar cells fabricated by all-solution processing. *Science*, 317(5835):222–225, 2007.

[99] Holger C. Hesse, Jonas Weickert, Christian Hundschell, Xinliang Feng, Klaus Müllen, Bert Nickel, Attila J. Mozer, and Lukas Schmidt-Mende. Perylene sensitization of fullerenes for improved performance in organic photovoltaics. *Advanced Energy Materials*, 1(5):861–869, 2011.

[100] C.W. Chu, V. Shrotriya, G. Li, and Y. Yang. Tuning acceptor energy level for efficient charge collection in copper-phthalocyanine-based organic solar cells. *Applied Physics Letters*, 88:153504, 2006.

[101] Juan Luis Delgado, Pierre-Antoine Bouit, Salvatore Filippone, Ma Angeles Herranz, and Nazario Martin. Organic photovoltaics: a chemical approach. *Chemical Communications*, 46(27):4853–4865, 2010.

[102] W. Ma, C. Yang, X. Gong, K. Lee, and A. J Heeger. Thermally stable, efficient polymer solar cells with nanoscale control of the interpenetrating network morphology. *Advanced Functional Materials*, 15(10):1617–1622, 2005.

[103] J Peet, JY Kim, NE Coates, WL Ma, D Moses, AJ Heeger, and GC Bazan. Efficiency enhancement in low-bandgap polymer solar cells by processing with alkane dithiols. *Nature Materials*, 6(7):497–500, 2007.

[104] D Mühlbacher, M Scharber, M Morana, Z Zhu, D Waller, R Gaudiana, and C Brabec. High photovoltaic performance of a low-bandgap polymer. *Advanced Materials*, 18(21):2884–2889, 2006.

[105] S. H. Park, A. Roy, S. Beaupre, S. Cho, N. Coates, J. S. Moon, D. Moses, M. Leclerc, K. Lee, and A. J. Heeger. Bulk heterojunction solar cells with internal quantum efficiency approaching 100 *Nature Photonics*, 3(5):297–U5, 2009.

[106] X. Yang and J. Loos. Toward high-performance polymer solar cells: The importance of morphology control. *Macromolecules*, 40(5):1353–1362, 2007.

[107] G. Li, V. Shrotriya, Y. Yao, and Y. Yang. Investigation of annealing effects and film thickness dependence of polymer solar cells based on poly(3-hexylthio-phene),. *Journal of Applied Physics*, 98:43704-43705, 2005.

[108] N. Karl. Charge carrier transport in organic semiconductors. *Synthetic Metals*, 133-134:649–657, 2003.

[109] D. Kurrle and J. Pflaum. Exciton diffusion length in the organic semiconductor diindenoperylene. *Applied Physics Letters*, 92:133306, 2008.

[110] VD Mihailetchi, JKJ van Duren, PWM Blom, JC Hummelen, RAJ Janssen, JM Kroon, MT Rispens, WJH Verhees, and MM Wienk. Electron transport in a methanofullerene. *Advanced Functional Materials*, 13(1):43–46, 2003.

[111] P Peumans, A Yakimov, and SR Forrest. Small molecular weight organic thin-film photodetectors and solar cells. *Journal of Applied Physics*, 93:3693, 2003.

[112] Jonas Weickert, Haiyan Sun, Claudia Palumbiny, Holger Christian Hesse, and Lukas Schmidt-Mende. Spray-deposited pedot:pss for inverted organic solar cells. *Solar Energy Materials and Solar Cells*, 94(12):2371–2374, 2010.

[113] Suzanne Ferrere, Arie Zaban, and Brian A. Gregg. Dye sensitization of nanocrystalline tin oxide by perylene derivatives. *The Journal of Physical Chemistry B*, 101(23):4490–4493, 1997.

[114] P. E. Keivanidis, I. A. Howard, and R. H. Friend. Intermolecular interactions of perylene diimides in photovoltaic blends of fluorene copolymers: Disorder effects on photophysical properties, film morphology and device efficiency. *Advanced Functional Materials*, 18(20):3189–3202, 2008.

[115] Safa Shoaee, Tracey M. Clarke, Chun Huang, Stephen Barlow, Seth R. Marder, Martin Heeney, Iain McCulloch, and James R. Durrant. Acceptor energy level control of charge photogeneration in organic donor/acceptor blends. *Journal of the American Chemical Society*, 132(37):12919–12926, 2010.

[116] E.H.A. Beckers, S.C.J. Meskers, A.P.H.J. Schenning, Z. Chen, F. Würthner, P. Marsal, D. Beljonne, J. Cornil, and R.A.J. Janssen. Influence of intermolecular orientation on the photoinduced charge transfer kinetics in self-assembled aggregates of donor-acceptor arrays. *Journal of the American Chemical Society*, 128(2):649–657, 2006.

[117] P. Peumans, S. Uchida, and S. R. Forrest. Efficient bulk heterojunction photovoltaic cells using small-molecular-weight organic thin films. *Nature*, 425(6954):158–162, 2003.

[118] C.W. Struijk, A.B. Sieval, J.E.J. Dakhorst, M. van Dijk, P. Kimkes, R.B.M. Koehorst, H. Donker, T.J. Schaafsma, S.J. Picken, and A.M. van de Craats. Liquid crystalline perylene diimides: Architecture and charge carrier mobilities. *Journal of the American Chemical Society*, 122(45):11057–11066, 2000.

[119] Shunji Ito, Mike Wehmeier, J. Diedrich Brand, Christian Kübel, Rebekka Epsch, Jürgen P. Rabe, and Klaus Müllen. Synthesis and self-assembly of functionalized hexa-peri-hexabenzocoronenes. *Chemistry - A European Journal*, 6(23):4327–4342, 2000.

[120] J. M. Warman, J. Piris, W. Pisula, M. Kastler, D. Wasserfallen, and K. Mullen. Charge recombination via intercolumnar electron tunneling through the lipid-like mantle of discotic hexa-alkyl-hexa-peri-hexabenzocoronenes. *Journal of the American Chemical Society*, 127(41):14257–14262, 2005.

[121] W. Pisula, Z. Tomovic, B. El Hamaoui, M. D. Watson, T. Pakula, and K. Mullen. Control of the homeotropic order of discotic hexa-peri-hexabenzocoronenes. *Advanced Functional Materials*, 15(6):893–904, 2005.

[122] Max Shtein, Peter Peumans, Jay B. Benziger, and Stephen R. Forrest. *Micropatterning of small molecular weight organic semiconductor thin films using organic vapor phase deposition*, volume 93. AIP, 2003.

[123] M Schubert, R Steyrleuthner, S Bange, A Sellinger, and D Neher. Charge transport and recombination in bulk heterojunction solar cells containing a dicyanoimidazole-based molecular acceptor. *Pphysica status solidi a*, 206(12):2743–2749, 2009.

[124] G. Li, V. Shrotriya, J. S. Huang, Y. Yao, T. Moriarty, K. Emery, and Y. Yang. High-efficiency solution processable polymer photovoltaic cells by self-organization of polymer blends. *Nature Materials*, 4(11):864–868, 2005.

[125] Roland Fitzner, Egon Reinold, Amaresh Mishra, Elena Mena-Osteritz, Hannah Ziehlke, Christian Körner, Karl Leo, Moritz Riede, Matthias Weil, Olga Tsaryova, AndrÃ© Weiss, Christian Uhrich, Martin Pfeiffer, and Peter Bäuerle. Dicyanovinyl-substituted oligothiophenes: Structure-property relationships and application in vacuum-processed small molecule organic solar cells. *Advanced Functional Materials*, 21(5):897–910, 2011.

[126] Steve Miller, Giovanni Fanchini, Yun-Yue Lin, Cheng Li, Chun-Wei Chen, Wei-Fang Su, and Manish Chhowalla. Investigation of nanoscale morphological changes in organic photovoltaics during solvent vapor annealing. *Journal of Materials Chemistry*, 18(3):306–312, 2008.

[127] G. Li, Y. Yao, H. Yang, V. Shrotriya, G. Yang, and Y. Yang. solvent annealing effect in polymer solar cells based on poly(3-hexylthiophene) and methanofullerenes. *Advanced Functional Materials*, 17(10):1636–1644, 2007.

[128] Fan Yang and Stephen R. Forrest. Photocurrent generation in nanostructured organic solar cells. *Acs Nano*, 2(5):1022–1032, 2008.

[129] Andrea Maurano, Rick Hamilton, Chris G. Shuttle, Amy M. Ballantyne, Jenny Nelson, Brian O Regan, Weimin Zhang, Iain McCulloch, Hamed Azimi, Mauro Morana, Christoph J. Brabec, and James R. Durrant. Recombination dynamics as a key determinant of open circuit voltage in organic bulk heterojunction solar cells: A comparison of four different donor polymers. *Advanced Materials*, 22(44):4987–4992, 2010.

[130] Y.W. Soon, T.M. Clarke, W. Zhang, T. Agostinelli, J. Kirkpatrick, C. Dyer-Smith, I. McCulloch, J. Nelson, and J.R. Durrant. Energy versus electron transfer in organic solar cells: a comparison of the photophysics of two indenofluorene: fullerene blend films. *Chem. Sci.*, 2:1111–1120, 2011.

[131] M. Jorgensen, K. Norrman, and F. C. Krebs. Stability/degradation of polymer solar cells. *Solar Energy Materials and Solar Cells*, 92(7):686–714, 2008.

[132] Kenji Kawano, Roberto Pacios, Dmitry Poplavskyy, Jenny Nelson, Donal D. C. Bradley, and James R. Durrant. Degradation of organic solar cells due to air exposure. *Solar Energy Materials and Solar Cells*, 90(20):3520–3530, 2006.

[133] QL Song, ML Wang, EG Obbard, XY Sun, XM Ding, XY Hou, and CM Li. Degradation of small-molecule organic solar cells. *Applied Physics Letters*, 89(25):251118–251118–3, 2006.

[134] Sun Haiyan, Jonas Weickert, Holger C. Hesse, and Lukas Schmidt-Mende. Uv light protection through tio2 blocking layers for inverted organic solar cells. *Solar Energy Materials and Solar Cells*, 95(12):3450–3454, 2011.

[135] Sean E. Shaheen, Christoph J. Brabec, N. Serdar Sariciftci, Franz Padinger, Thomas Fromherz, and Jan C. Hummelen. 2.5 *Applied Physics Letters*, 78(6):841–843, 2001.

[136] MS White, DC Olson, SE Shaheen, N. Kopidakis, and D.S. Ginley. Inverted bulk-heterojunction organic photovoltaic device using a solution-derived zno underlayer. *Applied Physics Letters*, 89(14):143517–143517–3, 2006.

[137] M. M. Wienk, M. Turbiez, J. Gilot, and R. A. J. Janssen. Narrow-bandgap diketo-pyrrolo-pyrrole polymer solar cells: The effect of processing on the performance. *Advanced Materials*, 20(13):2556–2560, 2008.

[138] G. Zhao, Y. He, and Y. Li. 6.5hexylthiophene) and indene c60 bisadduct by device optimization. *Advanced Materials*, 2010.

[139] Xiaoniu Yang, Joachim Loos, Sjoerd C. Veenstra, Wiljan J. H. Verhees, Martijn M. Wienk, Jan M. Kroon, Matthias A. J. Michels, and Rene A. J. Janssen. Nanoscale morphology of high-performance polymer solar cells. *Nano Letters*, 5(4):579–583, 2005.

[140] Neil D. Treat, Michael A. Brady, Gordon Smith, Michael F. Toney, Edward J. Kramer, Craig J. Hawker, and Michael L. Chabinyc. Interdiffusion of pcbm and p3ht reveals miscibility in a photovoltaically active blend. *Advanced Energy Materials*, 1(1):82–89, 2011.

[141] James W. Arbogast, Aleksander P. Darmanyan, Christopher S. Foote, F. N. Diederich, R. L. Whetten, Y. Rubin, Marcos M. Alvarez, and Samir J. Anz. Photophysical properties of sixty atom carbon molecule (c60). *The Journal of Physical Chemistry*, 95(1):11–12, 1991.

[142] Y. Kim, S.A. Choulis, J. Nelson, D.D.C. Bradley, S. Cook, and J.R. Durrant. Device annealing effect in organic solar cells with blends of regioregular poly (3-hexylthiophene) and soluble fullerene. *Applied Physics Letters*, 86(6):063502–063502–3, 2005.

[143] J. Peet, L. Wen, P. Byrne, S. Rodman, K. Forberich, Y. Shao, N. Drolet, R. Gaudiana, G. Dennler, and D. Waller. *Bulk heterojunction solar cells with thick active layers and high fill factors enabled by a bithiophene-co-thiazolothiazole push-pull copolymer*, volume 98. AIP, 2011.

[144] Prashant Sonar, Jacelyn Pui Fong Lim, and Khai Leok Chan. Organic non-fullerene acceptors for organic photovoltaics. *Energy & Environmental Science*, 4:1558–1574, 2011.

[145] Guodan Wei, Siyi Wang, Kai Sun, Mark E. Thompson, and Stephen R. Forrest. Solvent-annealed crystalline squaraine: Pc70bm (1:6) solar cells. *Advanced Energy Materials*, 1(2):184–187, 2011.

[146] Chang-Qi Ma, Marta Fonrodona, Martin C. Schikora, Martijn M. Wienk, RenÃ© A. J. Janssen, and Peter Bäuerle. Solution-processed bulk-heterojunction solar cells based on monodisperse dendritic oligothiophenes. *Advanced Functional Materials*, 18(20):3323–3331, 2008.

[147] F. Yang, K. Sun, and S. R Forrest. Efficient solar cells using all-organic nanocrystalline networks. *Advanced Materials*, 19(23):4166–4171, 2007.

[148] Nils M. Kronenberg, Vera Steinmann, Hannah Bürckstümmer, Jaehyung Hwang, Dirk Hertel, Frank Würthner, and Klaus Meerholz. Direct comparison of highly efficient solution- and vacuum-processed organic solar cells based on merocyanine dyes. *Advanced Materials*, 22(37):4193–4197, 2010.

[149] Yutaka Matsuo, Yoshiharu Sato, Takaaki Niinomi, Iwao Soga, Hideyuki Tanaka, and Eiichi Nakamura. Columnar structure in bulk heterojunction in solution-processable three-layered p-i-n organic photovoltaic devices using tetrabenzoporphyrin precursor and silylmethyl[60]fullerene. *Journal of the American Chemical Society*, 131(44):16048–16050, 2009.

[150] Sensient Imaging Technologies. Sensient st1/23. *www.syntec-sensient.com*, 2011.

[151] Nano-C. Nano-c pc[60]bm. *www.Nano-C.com*, 2011.

[152] Sigma-Aldrich. Sigma-aldrich. *www.sigmaaldrich.com*, 2011.

[153] Kintec. www.kintec.hk/. *Kintec Company*, 2011.

[154] Präzisions Glas & Optik. Produktcode cec010s. *www.pgo-online.com/*, 2011.

[155] R. Schueppel, K. Schmidt, C. Uhrich, K. Schulze, D. Wynands, J.L. Bredas, E. Brier, E. Reinold, H.B. Bu, P. Baeuerle, B. Maennig, M. Pfeiffer, and K. Leo. Optimizing organic photovoltaics using tailored heterojunctions: a photo-induced absorption study of oligothiophenes with low band gaps. *Physical Review B*, 77:085311, 2008.

[156] J.Y. Kim, S.H. Kim, H.H. Lee, K. Lee, W. Ma, X. Gong, and A.J. Heeger. New architecture for high-efficiency polymer photovoltaic cells using solution-based titanium oxide as an optical spacer. *Advanced Materials*, 18(5):572–576, 2006.

[157] Yu Bang-Ying and et al. Efficient inverted solar cells using tio2 nanotube arrays. *Nanotechnology*, 19(25):255202, 2008.

[158] Chen Tao, Shengping Ruan, Guohua Xie, Xiangzi Kong, Liang Shen, Fanxu Meng, Caixia Liu, Xindong Zhang, Wei Dong, and Weiyou Chen. Role of tungsten oxide in inverted polymer solar cells. *Applied Physics Letters*, 94(4):043311–3, 2009.

[159] David R. Lide. *CRC Handbook of Chemistry and Physics vol. 90*, volume 90 of *CRC Handbook of Chemistry and Physics vol. 90*. CRC Press, 2009.

[160] David Munoz-Rojas, Diana C. Iza, Jonas Weickert, and Holger C. Hesse. Effect of tio2 hole-blocking layer deposition for inverted bulk heterojunction solar cells. *Solar energy materials and solar cells*, submission in Progress.

[161] Heraeus Clevios GmbH. Clevios conducting polymer p al 4083. *www.clevios.com*, 2011.

[162] Yee-Fun Lim, Sungsoo Lee, David J. Herman, Matthew T. Lloyd, John E. Anthony, and George G. Malliaras. *Spray-deposited poly(3,4-ethylenedioxythiophene):poly(styrenesulfonate) top electrode for organic solar cells*, volume 93. AIP, 2008.

[163] H. Heil, J. Steiger, S. Karg, M. Gastel, H. Ortner, H. Von Seggern, and M. Stössel. Mechanisms of injection enhancement in organic light-emitting diodes through an al/lif electrode. *Journal of Applied Physics*, 89:420, 2001.

[164] Christoph J. Brabec, Sean E. Shaheen, Christoph Winder, N. Serdar Sariciftci, and Patrick Denk. Effect of lif/metal electrodes on the performance of plastic solar cells. *Applied Physics Letters*, 80(7):1288–1290, 2002.

[165] D. Grozea, A. Turak, X. D. Feng, Z. H. Lu, D. Johnson, and R. Wood. Chemical structure of al/lif/alq interfaces in organic light-emitting diodes. *Applied Physics Letters*, 81(17):3173–3175, 2002.

[166] M. Schwoerer and H.C. Wolf. *Organic molecular solids*. Wiley Online Library, 2007.

[167] Liyang Luo, Chia-Jung Lin, Chen-Shiung Hung, Chen-Fu Lo, Ching-Yao Lin, and Eric Wei-Guang Diau. Effects of potential shift and efficiency of charge collection on nanotube-based porphyrin-sensitized solar cells with conjugated links of varied length. *Physical Chemistry Chemical Physics*, 2010.

[168] R. Salach-Bielecki, T. Pisarkiewicz, T. Stapinski, and P. Wojcik. Influence of junction parameters on the open circuit voltage decay in solar cells. *Opto-Electronics Review*, 12(1):79–83, 2004.

[169] N. W. Duffy, L. M. Peter, and K. G. U. Wijayantha. Characterisation of electron transport and back reaction in dye-sensitised nanocrystalline solar cells by small amplitude laser pulse excitation. *Electrochemistry Communications*, 2(4):262–266, 2000.

[170] S. Grabtchak and M. Cocivera. Analysis of the transition from dispersive to non-dispersive transport for photoconductivity transients. *Philosophical Magazine B-Physics of Condensed Matter Statistical Mechanics Electronic Optical and Magnetic Properties*, 79(6):881–895, 1999.

[171] AJ Mozer, NS Sariciftci, L Lutsen, D Vanderzande, R österbacka, M Westerling, and G JuÅ¡ka. Charge transport and recombination in bulk heterojunction solar cells studied by the photoinduced charge extraction in linearly increasing voltage technique. *Applied Physics Letters*, 86:112104, 2005.

[172] G. Dennler, A. J. Mozer, G. Juska, A. Pivrikas, R. österbacka, A. Fuchsbauer, and N. S. Sariciftci. Charge carrier mobility and lifetime versus composition of conjugated polymer/fullerene bulk-heterojunction solar cells. *Organic Electronics*, 7(4):229–234, 2006.

[173] G JuÅ¡ka, K Arlauskas, M Vili nas, K Genevi ius, R österbacka, and H Stubb. Charge transport in -conjugated polymers from extraction current transients. *Physical Review B*, 62(24):16235–16238, 2000.

[174] J. Als-Nielsen. *Elements of modern X-ray physics*. Wiley, 2011.

[175] M.P. Eng, P.R.F. Barnes, and J.R. Durrant. Concentration-dependent hole mobility and recombination coefficient in bulk heterojunctions determined from transient absorption spectroscopy. *The Journal of Physical Chemistry Letters*, 1:3096–3100, 2010.

[176] L. H Nguyen, H. Hoppe, T. Erb, S. Günes, G. Gobsch, and N. S Sariciftci. Effects of annealing on the nanomorphology and performance of poly(alkylthiophene):fullerene bulk-heterojunction solar cells. *Advanced Functional Materials*, 17(7):1071–1078, 2007.

[177] W. Pisula, Z. Tomovic, C. Simpson, M. Kastler, T. Pakula, and K. Müllen. Relationship between core size, side chain length, and the supramolecular organization of polycyclic aromatic hydrocarbons. *Chemistry of Materials*, 17(17):4296–4303, 2005.

[178] A. Fechtenkotter, K. Saalwachter, M. A. Harbison, K. Mullen, and H. W. Spiess. Highly ordered columnar structures from hexa-peri-hexabenzocoronenes - synthesis, x-ray diffraction, and solid-state heteronuclear multiple-quantum nmr investigations. *Angewandte Chemie-International Edition*, 38(20):3039–3042, 1999.

[179] D. C. Olson, S. E. Shaheen, M. S. White, W. J. Mitchell, M. F. A. M. van Hest, R. T. Collins, and D. S. Ginley. Band-offset engineering for enhanced open-circuit voltage in polymer-oxide hybrid solar cells. *Advanced Functional Materials*, 17(2):264–269, 2007.

[180] FranÃ§oise Provencher, Jean-FrÃ©dÃ©ric Laprade, Michel CÃ´tÃ©, and Carlos Silva. Excitons in perylene tetracarboxdiimide crystals for optoelectronics. *physica status solidi (c)*, 6(1):93–96, 2009.

[181] C. S. Kim, S. S. Lee, E. D. Gomez, J. B. Kim, and Y. L. Loo. Transient photovoltaic behavior of air-stable, inverted organic solar cells with solution-processed electron transport layer. *Applied Physics Letters*, 94(11):–, 2009.

[182] VD Mihailetchi, J Wildeman, and PWM Blom. Space-charge limited photocurrent. *Physical Review Letters*, 94(12):126602, 2005.

[183] C. Videlot and D. Fichou. Influence of molecular orientation on the photovoltaic properties of octithiophene. *Synthetic Metals*, 102(1-3):885–888, 1999.

[184] Ivan Gutman, Zeljko Tomovic, Klaus Müllen, and Jürgen P. Rabe. On the distribution of [pi]-electrons in large polycyclic aromatic hydrocarbons. *Chemical Physics Letters*, 397(4-6):412–416, 2004.

[185] M. S. Kim, B. G. Kim, and J. Kim. Effective variables to control the fill factor of organic photovoltaic cells. *Acs Applied Materials & Interfaces*, 1(6):1264–1269, 2009.

[186] D. Veldman, S. C. J. Meskers, and R. A. J. Janssen. The energy of charge-transfer states in electron donor-acceptor blends: Insight into the energy losses in organic solar cells. *Advanced Functional Materials*, 19(12):1939–1948, 2009.

[187] Ignacio B. Martini, Bin Ma, Tatiana Da Ros, Roger Helgeson, Fred Wudl, and Benjamin J. Schwartz. Ultrafast competition between energy and charge transfer in a functionalized electron donor/fullerene derivative. *Chemical Physics Letters*, 327(5-6):253–262, 2000.

[188] L. J. A. Koster, V. D. Mihailetchi, and P. W. M. Blom. Bimolecular recombination in polymer/fullerene bulk heterojunction solar cells. *Applied Physics Letters*, 88(5):–, 2006.

[189] M. A. Fox, H. L. Pan, W. E. Jones, and D. Melamed. Spectroscopy and time-resolved photocurrent response in ordered porphyrin thin-films. *Journal of Physical Chemistry*, 99(29):11523–11530, 1995.

[190] C. G. Shuttle, A. Maurano, R. Hamilton, B. O'Regan, J. C. de Mello, and J. R. Durrant. Charge extraction analysis of charge carrier densities in a polythiophene/fullerene solar cell: Analysis of the origin of the device dark current. *Applied Physics Letters*, 93(18):–, 2008.

[191] W. Pisula, M. Kastler, B. El Hamaoui, M. C. Garcia-Gutierrez, R. J. Davies, C. Riekel, and K. Mullen. Dendritic morphology in homeotropically aligned discotic films. *Chemphyschem*, 8(7):1025–1028, 2007.

[192] W. Pisula, A. Menon, M. Stepputat, I. Lieberwirth, U. Kolb, A. Tracz, H. Sirringhaus, T. Pakula, and K. Mullen. A zone-casting technique for device fabrication of field-effect transistors based on discotic hexa-peri-hexabenzoeoronene. *Advanced Materials*, 17(6):684–+, 2005.

[193] M. Kastler, W. Pisula, F. Laquai, A. Kumar, R. J. Davies, S. Baluschev, M. C. Garcia-Gutierrez, D. Wasserfallen, H. J. Butt, C. Riekel, G. Wegner, and K. Mullen. Organization of charge-carrier pathways for organic electronics. *Advanced Materials*, 18(17):2255–+, 2006.

[194] X. Feng, V. Marcon, W. Pisula, M. R. Hansen, J. Kirkpatrick, F. Grozema, D. Andrienko, K. Kremer, and K. Mullen. Towards high charge-carrier mobilities by rational design of the shape and periphery of discotics. *Nat Mater*, 8(5):421–6, 2009.

[195] E. Pouzet, V. De Cupere, C. Heintz, J. W. Andreasen, D. W. Breiby, M. M. Nielsen, P. Viville, R. Lazzaroni, G. Gbabode, and Y. H. Geerts. Homeotropic alignment of a discotic liquid crystal induced by a sacrificial layer. *Journal of Physical Chemistry C*, 113(32):14398–14406, 2009.

[196] Laura N. Serkovic Loli, Hicham Hamoudi, J. Esteban Gayone, M. Luz Martiarena, Esteban A. Sanchez, Oscar Grizzi, Luca Pasquali, Stefano Nannarone,

Bryan P. Doyle, Celine Dablemont, and Vladimir A. Esaulov. Growth of n,n'-bis(1-ethylpropyl)perylene-3,4,9,10-tetracarboxdiimide films on ag (111). *The Journal of Physical Chemistry C*, 113(41):17866–17875, 2009.

[197] H. Glowatzki, G. N. Gavrila, S. Seifert, R. L. Johnson, J. Rader, K. Mullen, D. R. T. Zahn, J. P. Rabe, and N. Koch. Hexa-peri-hexabenzocoronene on ag(111): Monolayer/multilayer transition of molecular orientation and electronic structure. *The Journal of Physical Chemistry C*, 112(5):1570–1574, 2008.

[198] P Rempala, J KroulÃk, and BT King. A slippery slope: mechanistic analysis of the intramolecular scholl reaction of hexaphenylbenzene. *J. Am. Chem. Soc*, 126(46):15002–15003, 2004.

[199] P. W M Blom, V. D Mihailetchi, L. J A Koster, and D. E Markov. Device physics of polymer:fullerene bulk heterojunction solar cells. *Advanced Materials*, 19(12):1551–1566, 2007.

[200] Y. Kikuzawa, T. Mori, and H. Takeuchi. Synthesis of 2,5,8,11,14,17-hexafluoro-hexa-perihexabenzocoronene for n-type organic field-effect transistors. *Organic Letters*, 9(23):4817–4820, 2007.

[201] T Mori, Y Kikuzawa, and H Takeuchi. N-type field-effect transistor based on a fluorinated-graphene. *Organic Electronics*, 9(3):328–332, 2008.

[202] S. Entani, T. Kaji, S. Ikeda, T. Mori, Y. Kikuzawa, H. Takeuchi, and K. Saiki. Fluorine substitution of hexa-peri-hexabenzocoronene: Change in growth mode and electronic structure. *Journal of Physical Chemistry C*, 113(15):6202–6207, 2009.

[203] A Opitz, B Ecker, J Wagner, A Hinderhofer, F Schreiber, J Manara, J Pflaum, and W Brütting. Mixed crystalline films of co-evaporated hydrogen-and fluorine-terminated phthalocyanines and their application in photovoltaic devices. *Organic Electronics*, 10(7):1259–1267, 2009.

[204] Safa Shoaee, Zesheng An, Xuan Zhang, Stephen Barlow, Seth R. Marder, Warren Duffy, Martin Heeney, Iain McCulloch, and James R. Durrant. Charge photogeneration in polythiophene-perylene diimide blend films. *Chemical Communications*, 45(36):5445–5447, 2009.

[205] Yongye Liang, Zheng Xu, Jiangbin Xia, Szu-Ting Tsai, Yue Wu, Gang Li, Claire Ray, and Luping Yu. For the bright future - bulk heterojunction polymer solar cells with power conversion efficiency of 7.4*Advanced Materials*, 22(20):E135–E138, 2010.

[206] Sung Heum Park, Anshuman Roy, Serge Beaupre, Shinuk Cho, Nelson Coates, Ji Sun Moon, Daniel Moses, Mario Leclerc, Kwanghee Lee, and Alan J. Heeger. Bulk heterojunction solar cells with internal quantum efficiency approaching 100 *Nature Photonics*, 3(5):297–302, 2009.

[207] G. Dennler, M. C Scharber, T. Ameri, P. Denk, K. Forberich, C. Waldauf, and C. J Brabec. Design rules for donors in bulk-heterojunction tandem solar cells: Towards 15 % energy-conversion efficiency. *Advanced Materials*, 20(3):579–583, 2008.

[208] Yongye Liang, Yue Wu, Danqin Feng, Szu-Ting Tsai, Hae-Jung Son, Gang Li, and Luping Yu. Development of new semiconducting polymers for high performance solar cells. *Journal of the American Chemical Society*, 131(1):56–57, 2008.

[209] M. M. Wienk, J. M. Kroon, W. J. H. Verhees, J. Knol, J. C. Hummelen, P. A. van Hal, and R. A. J. Janssen. Efficient methano[70]fullerene/mdmo-ppv bulk heterojunction photovoltaic cells. *Angewandte Chemie International Edition*, 42(29):3371–3375, 2003.

[210] Youjun He, Hsiang-Yu Chen, Jianhui Hou, and Yongfang Li. Indeneâ^'c60 bisadduct: A new acceptor for high-performance polymer solar cells. *Journal of the American Chemical Society*, 132(4):1377–1382, 2010.

[211] M Schubert, C Yin, M Castellani, S Bange, TL Tam, A Sellinger, HH Hörhold, T Kietzke, and D Neher. Heterojunction topology versus fill factor correlations in novel hybrid small-molecular/polymeric solar cells. *The Journal of Chemical Physics*, 130:094703, 2009.

[212] John E. Anthony. Small-molecule, nonfullerene acceptors for polymer bulk heterojunction organic photovoltaics. *Chemistry of Materials*, pages 583–590, 2010.

[213] T. Kircher and H.G. Löhmannsröben. Photoinduced charge recombination reactions of a perylene dye in acetonitrile. *Phys. Chem. Chem. Phys.*, 1(17):3987–3992, 1999.

[214] B. E. Hardin, E. T. Hoke, P. B. Armstrong, J. H. Yum, P. Comte, T. Torres, J. M. J. Frechet, M. K. Nazeeruddin, M. Gratzel, and M. D. McGehee. Increased light harvesting in dye-sensitized solar cells with energy relay dyes. *Nature Photonics*, 3(7):406–411, 2009.

[215] G. K. Mor, J. Basham, M. Paulose, S. Kim, O. K. Varghese, A. Vaish, S. Yoriya, and C. A. Grimes. High-efficiency forster resonance energy transfer in solid-state dye sensitized solar cells. *Nano Letters*, 10(7):2387–2394, 2010.

[216] Kristina Driscoll, Junfeng Fang, Nicola Humphry-Baker, Tomas Torres, Wilhelm T. S. Huck, Henry J. Snaith, and Richard H. Friend. Enhanced photoresponse in solid-state excitonic solar cells via resonant energy transfer and cascaded charge transfer from a secondary absorber. *Nano Letters*, 10(12):4981-4988, 2010.

[217] Y.R. Park, Y.J. Lee, C.J. Yu, and J.H. Kim. Investigations of the polymer alignment, the nonradiative resonant energy transfer, and the photovoltaic response of poly (3-hexylthiophene)/tio hybrid solar cells. *Journal of Applied Physics*, 108:044508, 2010.

[218] K. Shankar, X. Feng, and C.A. Grimes. Enhanced harvesting of red photons in nanowire solar cells: Evidence of resonance energy transfer. *Acs Nano*, 3(4):788–794, 2009.

[219] C. Winder, G. Matt, J. C. Hummelen, R. A. J. Janssen, N. S. Sariciftci, and C. J. Brabec. Sensitization of low bandgap polymer bulk heterojunction solar cells. *Thin Solid Films*, 403-404:373–379, 2002.

[220] Theodulf Rousseau, Antonio Cravino, Thomas Bura, Gilles Ulrich, Raymond Ziessel, and Jean Roncali. Multi-donor molecular bulk heterojunction solar cells: improving conversion efficiency by synergistic dye combinations. *Journal of Materials Chemistry*, 19(16):2298–2300, 2009.

[221] R. Koeppe, O. Bossart, G. Calzaferri, and N. S. Sariciftci. Advanced photon-harvesting concepts for low-energy gap organic solar cells. *Solar Energy Materials and Solar Cells*, 91(11):986–995, 2007.

[222] L. C. Chen, D. Godovsky, O. Inganäs, J. C. Hummelen, R. A. J. Janssens, M. Svensson, and M. R. Andersson. Polymer photovoltaic devices from stratified multilayers of donor acceptor blends. *Advanced Materials*, 12(18):1367–1370, 2000.

[223] David C. Coffey, Andrew J. Ferguson, Nikos Kopidakis, and Garry Rumbles. Photovoltaic charge generation in organic semiconductors based on long-range energy transfer. *Acs Nano*, 4(9):5437–5445, 2010.

[224] M. Koppe, H. J. Egelhaaf, G. Dennler, M. C. Scharber, C. J. Brabec, P. Schilinsky, and C. N. Hoth. Near ir sensitization of organic bulk heterojunction solar

cells: Towards optimization of the spectral response of organic solar cells. *Advanced Functional Materials*, 20(2):338–346, 2010.

[225] Z. Shuai and JL Bredas. Electronic structure and nonlinear optical properties of the fullerenes c_{60} and c_{70}: A valence-effective-hamiltonian study. *Physical Review B*, 46(24):16135, 1992.

[226] CG Shuttle, B. O Regan, AM Ballantyne, J. Nelson, DDC Bradley, and JR Durrant. Bimolecular recombination losses in polythiophene: Fullerene solar cells. *Physical Review B*, 78(11):113201, 2008.

[227] A. Rybak, W. Pisula, J. Jung, and J. Ulanski. Influence of molecular order on charge carrier photogeneration in perylene derivative layer. *Thin Solid Films*, 516(12):4201–4207, 2008.

[228] J. J. Dittmer, E. A. Marseglia, and R. H. Friend. Electron trapping in dye/polymer blend photovoltaic cells. *Advanced Materials*, 12(17):1270–1274, 2000.

[229] R. F. Fink, J. Seibt, V. Engel, M. Renz, M. Kaupp, S. Lochbrunner, H. M. Zhao, J. Pfister, F. Wurthner, and B. Engels. Exciton trapping in pi-conjugated materials: A quantum-chemistry-based protocol applied to perylene bisimide dye aggregates. *Journal of the American Chemical Society*, 130(39):12858–+, 2008.

[230] J. Seibt, P. Marquetand, V. Engel, Z. Chen, V. Dehrn, and F. Wurthner. On the geometry dependence of molecular dimer spectra with an application to aggregates of perylene bisimide. *Chemical Physics*, 328(1-3):354–362, 2006.

[231] Y.X. Liu, M.A. Summers, S.R. Scully, and M.D. McGehee. Resonance energy transfer from organic chromophores to fullerene molecules. *Journal of Applied Physics*, 99:093521, 2006.

[232] O. Stenzel, AN Lebedev, M. Schreiber, and DRT Zahn. Simulation of linear optical losses of absorbing heterogeneous thin solid films. *Thin Solid Films*, 372(1-2):200–208, 2000.

[233] AMC Ng, KY Cheung, MK Fung, AB Djurisic, and WK Chan. Spectroscopic ellipsometry characterization of polymer-fullerene blend films. *Thin Solid Films*, 517(3):1047–1052, 2008.

[234] Hideo Ohkita, Steffan Cook, Yeni Astuti, Warren Duffy, Steve Tierney, Weimin Zhang, Martin Heeney, Iain McCulloch, Jenny Nelson, Donal D. C. Bradley, and

James R. Durrant. Charge carrier formation in polythiophene/fullerene blend films studied by transient absorption spectroscopy. *Journal of the American Chemical Society*, 130(10):3030–3042, 2008.

[235] Dirk M. Guldi, Hartmut Hungerbuehler, Eberhard Janata, and Klaus Dieter Asmus. Redox processes and alkylation reactions of fullerene c60 as studied by pulse radiolysis. *The Journal of Physical Chemistry*, 97(43):11258–11264, 1993.

[236] R.V. Bensasson and E. Bienvenüe. Photophysical properties of three methanofullerene derivatives. *Chemistry A European Journal*, 4(2):270–278, 1998.

[237] R. Koeppe and N. S. Sariciftci. Photoinduced charge and energy transfer involving fullerene derivatives. *Photochemical & Photobiological Sciences*, 5(12):1122–1131, 2006.

[238] Cody W. Schlenker, Vincent S. Barlier, Stephanie W. Chin, Matthew T. Whited, R. Eric McAnally, Stephen R. Forrest, and Mark E. Thompson. Cascade organic solar cells. *Chemistry of Materials*, pages null–null, 2011.

[239] Holger. C. Hesse, Dominik Lebmbke, Lukas Dössel, Xingliang Feng, Klaus Müllen, and Lukas Schmidt-Mende. Nanostructuring discotic molecules on ito support. *Nanotechnology*, 22(5):055303, 2011.

[240] R Dunbar, H. C. Hesse, D Lembke, and L Schmidt Mende. Light trapping plasmonic nanovoid arrays. *Phys Rev B*, accepted, 2011.

[241] Wojciech Pisula, Xinliang Feng, and Klaus Müllen. Tuning the columnar organization of discotic polycyclic aromatic hydrocarbons. *Advanced Materials*, 9999(9999):NA, 2010.

[242] LC Chen, D Godovsky, O Inganäs, JC Hummelen, RAJ Janssens, M Svensson, and MR Andersson. Polymer photovoltaic devices from stratified multilayers of donor-acceptor blends. *Advanced Materials*, 12(18):1367–1370, 2000.

[243] M Drees, K Premaratne, W Graupner, JR Heflin, RM Davis, D Marciu, and M Miller. Creation of a gradient polymer-fullerene interface in photovoltaic devices by thermally controlled interdiffusion. *Applied Physics Letters*, 81:4607, 2002.

[244] M. Steinhart, S. Zimmermann, P. Goring, A. K. Schaper, U. Gosele, C. Weder, and J. H. Wendorff. Liquid crystalline nanowires in porous alumina: Geometric confinement versus influence of pore walls (vol 5, pg 432, 2005). *Nano Letters*, 5(5):995–995, 2005.

[245] J. I. Lee, S. H. Cho, S. M. Park, J. K. Kim, J. K. Kim, J. W. Yu, Y. C. Kim, and T. P. Russell. Highly aligned ultrahigh density arrays of conducting polymer nanorods using block copolymer templates. *Nano Letters*, 8(8):2315–2320, 2008.

[246] Henry J. Snaith, Gregory L. Whiting, Baoquan Sun, Neil C. Greenham, Wilhelm T. S. Huck, and Richard H. Friend. Self-organization of nanocrystals in polymer brushes. application in heterojunction photovoltaic diodes. *Nano Letters*, 5(9):1653–1657, 2005.

[247] W. Lee, R. Ji, U. Gosele, and K. Nielsch. Fast fabrication of long-range ordered porous alumina membranes by hard anodization. *Nature Materials*, 5(9):741–747, 2006.

[248] A. P. Li, F. Muller, A. Birner, K. Nielsch, and U. Gosele. Hexagonal pore arrays with a 50-420 nm interpore distance formed by self-organization in anodic alumina. *Journal of Applied Physics*, 84(11):6023–6026, 1998.

[249] K. P. Musselman, G. J. Mulholland, A. P. Robinson, L. Schmidt-Mende, and J. L. MacManus-Driscoll. Low-temperature synthesis of large-area, free-standing nanorod arrays on ito/glass and other conducting substrates. *Advanced Materials*, 20(23):4470–4475, 2008.

[250] M. Kastler, W. Pisula, R. J. Davies, T. Gorelik, U. Kolb, and K. Mullen. Nanostructuring with a crosslinkable discotic material. *Small*, 3(8):1438–1444, 2007.

[251] L. J. Zhi, J. S. Wu, J. X. Li, U. Kolb, and K. Mullen. Carbonization of disclike molecules in porous alumina membranes: Toward carbon nanotubes with controlled graphene-layer orientation. *Angewandte Chemie-International Edition*, 44(14):2120–2123, 2005.

[252] Kai Zhu, Todd B. Vinzant, Nathan R. Neale, and Arthur J. Frank. Removing structural disorder from oriented tio2 nanotube arrays: reducing the dimensionality of transport and recombination in dye-sensitized solar cells. *Nano Letters*, 7(12):3739–3746, 2007.

[253] Ioan Botiz, Alex B. F. Martinson, and Seth B. Darling. Minimizing lateral domain collapse in etched poly(3-hexylthiophene)-block-polylactide thin films for improved optoelectronic performance. *Langmuir*, 26(11):8756–8761, 2010.

[254] Niko Haberkorn, Stefan A. L. Weber, Rüdiger Berger, and Patrick Theato. Template-based preparation of free-standing semiconducting polymeric nanorod ar-

rays on conductive substrates. *Acs Applied Materials & Interfaces*, 2(6):1573–1580, 2010.

[255] X He, F Gao, G Tu, D Hasko, S Hu ttner, U Steiner, NC Greenham, RH Friend, and WTS Huck. Formation of nanopatterned polymer blends in photovoltaic devices. *Nano Lett*, 10(4):1302–1307, 2010.

[256] K. Akagi, G. Piao, S. Kaneko, K. Sakamaki, H. Shirakawa, and M. Kyotani. Helical polyacetylene synthesized with a chiral nematic reaction field. *Science*, 282(5394):1683–1686, 1998.

[257] Sadaki Samitsu, Yoichi Takanishi, and Jun Yamamoto. Self-assembly and one-dimensional alignment of a conducting polymer nanofiber in a nematic liquid crystal. *Macromolecules*, 42(13):4366–4368, 2009.

[258] R.Q. Png, P.J. Chia, J.C. Tang, B. Liu, S. Sivaramakrishnan, M. Zhou, S.H. Khong, H.S.O. Chan, J.H. Burroughes, and L.L. Chua. High-performance polymer semiconducting heterostructure devices by nitrene-mediated photocrosslinking of alkyl side chains. *Nature Materials*, 9(2):152–158, 2009.

[259] M. Beck, M. Graczyk, I. Maximov, E. L. Sarwe, T. G. I. Ling, M. Keil, and L. Montelius. Improving stamps for 10 nm level wafer scale nanoimprint lithography. *Microelectronic Engineering*, 61-2:441–448, 2002.

[260] J. Zhao, A. Swinnen, G. Van Assche, J. Manca, D. Vanderzande, and B.V. Mele. Phase diagram of p3ht/pcbm blends and its implication for the stability of morphology. *The Journal of Physical Chemistry B*, 113(6):1587–1591, 2009.

[261] P. Sullivan, T. S. Jones, A. J. Ferguson, and S. Heutz. *Structural templating as a route to improved photovoltaic performance in copper phthalocyanine/fullerene (C60) heterojunctions*, volume 91. AIP, 2007.

[262] H. Kumar, P. Kumar, N. Chaudhary, R. Bhardwaj, S. Chand, S. C. Jain, and V. Kumar. Effect of temperature on the performance of cupc/c60 photovoltaic device. *Journal of Physics D: Applied Physics*, 42:015102–015102, 2009.

[263] B Homa, M Andersson, and O Inganäs. Photogenerated charge carrier transport and recombination in polyfluorene/fullerene bilayer and blend photovoltaic devices. *Organic Electronics*, 10(3):501–505, 2009.

[264] O. Thiebaut, H. Bock, and E. Grelet. Face-on oriented bilayer of two discotic columnar liquid crystals for organic donor-acceptor heterojunction. *Journal of the American Chemical Society*, 132(20):6886–+, 2010.

[265] Alon A. Gorodetsky, Chien-Yang Chiu, Theanne Schiros, Matteo Palma, Marshall Cox, Zhang Jia, Wesley Sattler, Ioannis Kymissis, Michael Steigerwald, and Colin Nuckolls. Reticulated heterojunctions for photovoltaic devices. *Angewandte Chemie International Edition*, 49(43):7909–7912, 2010.

List of Figures

Acknowledgment

I would like to thank Professor Lukas Schmidt-Mende for his plenary support and continuous feedback on my work. I highly appreciate his encouragement and open discussions about possible directions for my research projects. I also thank his support for facilitate my exchange programs with the Professor Driscoll Group and the group of Dr Attila Mozer. I strongly acknowledge the fruitful discussions with Dr Bert Nickel and his support as a second advisor of my PhD thesis. I would also like to acknowledge Lukas Dössel, Xinliang Feng, Chen Li and Professor Müllen at the Max Planck Institute for Polymer Research for their supply with organic materials and fruitful discussions about chemistry related questions. I strongly acknowledge the support by Dr Attila Mozer and Dr Tracey Clarke at the Intelligent Polymer Research Institute, Wollongong, Australia during my research visit. I would like to thank Dr Kevin Musselman at the Professor Driscoll group and Dr Andrew Nattestad at the Intelligent Polymer Research Institute in Wollongong for their help with my experiments. I also thank Christian Hundschell and Christoph Schaffer at the research group of Dr Bert Nickel at the LMU for performing several organic evaporation x-ray experiments Thanks to all the co-workers in the Hybrid Nanostructures Group: Claudia, Dominik, Feng, Jacek, Jinhu, Lothar, Ricky, Sun and Wolfgang. I had a very nice time with you guys in the lab and also during our spare time. Special thanks goes to Jonas, whom I really enjoyed working with at all times.